Copyright © and Moral Rights for this thesis and, where applicable, any accompanying data are retained by the author and/or other copyright owners. A copy can be downloaded for personal non-commercial research or study, without prior permission or charge. This thesis and the accompanying data cannot be reproduced or quoted extensively from without first obtaining permission in writing from the copyright holder/s. The content of the thesis and accompanying research data (where applicable) must not be changed in any way or sold commercially in any format or medium without the formal permission of the copyright holder/s.

When referring to this thesis and any accompanying data, full bibliographic details must be given, e.g.

Thesis: Author (Year of Submission) "Full thesis title", University of Southampton, name of the University Faculty or School or Department, PhD Thesis, pagination.

Data: Author (Year) Title. URI [dataset]

University of Southampton

Faculty of Environmental and Life Science

School of Ocean and Earth Science

Characterising NADPH oxidase in marine diatoms

by

Jack Edward Dickenson

ORCID: 0000-0002-2781-2450

Thesis for the degree of Doctor of Philosophy

September 2020

University of Southampton

Abstract

Faculty of Environmental and Life Science

School of Ocean and Earth Science

Thesis for the degree of Doctor of Philosophy

Characterising NADPH oxidase in marine diatoms

by

Jack Edward Dickenson

NADPH oxidase (NOX) is a widespread enzyme that catalyses the transmembrane reduction of oxygen, generating extracellular reactive oxygen species (ROS). NOX-derived production of ROS is best characterised as a defence mechanism, but a number of functions have been ascribed across eukaryotes, including intercellular signalling, facilitating cell-wall development and nutrient acquisition. Though extracellular ROS (eROS) production in unicellular algae is increasingly researched, characterisation of an enzyme source is relatively limited. This thesis addressed this by examining NOX distribution and function in marine diatoms, reporting several key findings. Firstly, a detailed screen of diatoms was carried out to identify NOX protein distribution. Compared to established NOX proteins in plants and animals, diatom NOX proteins are shown to be unusually diverse, with three structurally and phylogenetically distinct Classes of NOX protein and an atypical NOX-like Class. Secondly, the dynamics of eROS production and transmembrane electron transport were examined in three ecologically distinct marine diatoms. Baseline production rates differed significantly between species and changes to light intensity generated species-specific effects. NOX activity was inferred to be responsible for ROS production in two of the species tested. Finally, the function for NOX in the model diatom *Phaeodactylum tricornutum* was investigated. Following chemical inhibition of NOX, significant reductions to growth and photophysiology were observed, alongside an increase in cytosolic H_2O_2 (detected using a genetically encoded biosensor roGFP2-Orp1). This thesis proposes that NOX acts as a photoprotective mechanism by dissipating excess electrons and preventing over-reduction of chloroplast photosystems. Together, this study greatly improves understanding of NOX proteins in diatoms. By focusing on an understudied group, compared to animals or plants, knowledge of NOX distribution is expanded, with implications for NOX evolution. Furthermore, active eROS production can be beneficial to marine algae, and an electron dissipation function may explain the widespread use of eROS production by phytoplankton. While enzymatic sources of eROS are surprisingly diverse in diatoms, NOX likely represents the most common source. Thus, greater understanding of NOX function and distribution in diatoms may provide insights into understanding unique diatom photoprotection mechanisms, helping explain how diatoms can respond to changing environmental conditions.

Table of Contents

Table of Contents ..... **i**

Table of Tables ..... **vii**

Table of Figures ..... **ix**

Research Thesis: Declaration of Authorship ..... **xiii**

Acknowledgements ..... **xvii**

Definitions and Abbreviations ..... **xix**

Chapter 1 Introduction **1**

1.1 An introduction to diatoms 2

1.1.1 Diatom biology, ecology, and evolution 2

1.1.2 Diatom signalling pathways 4

1.2 Reactive oxygen species (ROS) 5

1.3 Intracellular ROS signalling in diatoms 7

1.4 NADPH oxidase (NOX) 8

1.4.1 NOX structure 8

1.4.2 NOX identification 9

1.4.3 NOX activity in humans 10

1.5 NOX and eROS functions in different lineages 11

1.5.1 eROS production and NOX proteins in animals 12

1.5.2 eROS production and NOX proteins in plants (Embryophytes) 13

1.5.3 eROS production and NOX proteins in fungi 14

1.5.4 eROS production and NOX proteins in brown algae (Phaeophyceae) 15

1.5.5 eROS production and NOX proteins in red algae (Rhodophyceae) 15

1.5.6 eROS production and NOX proteins in green algae (Chlorophyceae) 16

1.5.7 eROS production and NOX proteins in marine phytoplankton 16

1.5.8 eROS production and NOX proteins in prokaryotes 18

1.5.9 eROS production and NOX proteins in marine diatoms 18

1.6 The link between eROS production and light intensity 21

1.6.1 The diatom chloroplast and photosynthetic electron transport chain structure 21

1.6.2 Strategies to prevent photosystem over-reduction 22

1.7 General conclusions and aims of the thesis 23

Chapter 2 The unusual phylogeny and structure of diatom NOX proteins 25

2.1 Introduction 26

2.2 Methods 29

2.2.1 Confirmation of *P. tricornutum* NOX 29

2.2.2 Screening of diatom NOX and glutathione reductase (GR) sequences 29

2.2.3 Phylogenetic analysis 30

2.3 Results 31

2.3.1 Identification of NOX proteins in *P. tricornutum* 31

2.3.2 Distribution of NOX proteins 32

2.3.3 Types of NOX protein 33

2.3.3.1 Class 1 NOX proteins composition and structure 36

2.3.3.2 Class 2 NOX proteins composition and structure 36

2.3.3.3 Class 3 NOX proteins composition and structure 36

2.3.3.4 NOX-like and FRE proteins composition and structure 38

2.3.4 NOX protein conserved motifs and residues 38

2.3.5 GR phylogeny 42

2.4 Discussion 48

2.4.1 Diatom NOX diversity is unusually high 48

2.4.2 *T. oceanica*-like GR proteins are uncommon in marine diatoms 49

2.4.3 An evolutionary explanation for diatom NOX diversity 50

2.4.4 Strategies for identifying future NOX proteins 51

2.4.5 Conclusions 52

Chapter 3 Extracellular ROS production and plasma membrane electron transport in three marine diatoms 53

3.1 Introduction 54

3.2 Methods 56

3.2.1 Cell culture and physiology measurements 56

3.2.2 Chemical preparation 56

3.2.3 Potassium ferricyanide reduction assay for TMET 57
3.2.4 OxyBURST Green assay for eROS production 58
3.2.5 Light intensity 58
3.2.6 Statistical analysis 58
3.3 Results 60
3.3.1 Validation of FCR assay 60
3.3.2 Comparison of baseline FCR activity and eROS production 61
3.3.3 Effect of NOX inhibition on FCR activity and eROS production 62
3.3.4 Effect of light intensity on FCR 67
3.3.5 Effect of light intensity on eROS production 69
3.4 Discussion 72
3.4.1 Diatom species differences in TMET and eROS production 72
3.4.2 NOX involvement in TMET and eROS production 72
3.4.3 Light intensity effects on TMET and eROS production 73
3.4.4 Conclusions 76
Chapter 4 **Using the fluorescent biosensor roGFP2-Orp1 to explore H_2O_2 dynamics in *Phaeodactylum tricornutum* 77**
4.1 Introduction 78
4.2 Methods 82
4.2.1 Cell culture 82
4.2.2 Biolistic transformation of biosensor proteins into *P. tricornutum* 82
4.2.3 Detection and characterisation of intracellular H_2O_2 using a plate reader assay 83
4.2.4 Screening and measurement of chloroplast-targeted roGFP2-Orp1 84
4.2.5 Detection of intracellular H_2O_2 using epifluorescence microscopy 85
4.2.6 Monitoring intracellular Ca^{2+} and H_2O_2 through perfusion experiments 85
4.2.7 Long term changes in cellular parameters following H_2O_2 addition 86
4.2.8 Statistical analysis 86
4.3 Results 87
4.3.1 Screening and transformation with roGFP2-Orp1 87
4.3.2 Characterisation of roGFP2-Orp1 89

4.3.3 Transformation and screening of roGFP2-ChlOrp1 90
4.3.4 Effects of H_2O_2 on roGFP2-ChlOrp1 92
4.3.5 Effects of H_2O_2 on *P. tricornutum* cell physiology 94
4.3.5.1 Long term effect (days) of exogenous H_2O_2 addition to *P. tricornutum* 94
4.3.5.2 Medium term (min to hour) effects of exogenous H_2O_2 addition to P. tricornutum 96
4.3.5.3 Short term effects of H_2O_2 on *P. tricornutum* 97
4.3.6 High light triggers a reversible increase in cytosolic H_2O_2 99
4.4 Discussion 102
4.4.1 Successful expression of roGFP2-Orp1 in *P. tricornutum* 102
4.4.2 How tolerant is *P. tricornutum* to H_2O_2? 102
4.4.3 H_2O_2 addition affects *P. tricornutum* photophysiology 103
4.4.4 Heterogenous responses to H_2O_2 in *P. tricornutum* 104
4.4.5 Through what action does H_2O_2 addition reduce cell growth? 104
4.4.6 Are the quantities of exogenous H_2O_2 environmentally relevant? 105
4.4.7 Conclusions 106
Chapter 5 Characterisation of the function of NOX proteins in *Phaeodactylum tricornutum* 107
5.1 Introduction 108
5.2 Methods 111
5.2.1 Cell culture 111
5.2.2 Chemical preparation 111
5.2.3 Measurements of eROS production, photosynthetic parameters and cytosolic H_2O_2 111
5.2.4 Effect of DPI on photosynthetic parameters 112
5.2.5 Oxygen evolution measurements 112
5.2.6 Statistical analysis 113
5.2.7 Cloning of PtNOX1 & PtNOX2 113
5.2.8 Genetic transformation of *P. tricornutum* 114
5.2.9 Screening of *P. tricornutum* colonies for NOX localisation 114

5.3 Results 117

5.3.1 Localisation of PtNOX1 117

5.3.2 Chemical inhibition of NOX triggers dose-dependent effects on cellular physiology 118

5.3.3 Interactions of light intensity and NOX inhibition on cellular physiology 122

5.3.4 Differing effects of NOX inhibition in *A. glacialis* and *T. weissflogii.* 130

5.3.5 GSSG has no effect on *P. tricornutum* eROS production. 130

5.3.6 Redox state-altering chemicals affect iROS and eROS production in *P. tricornutum* 131

5.4 Discussion 135

5.4.1 NOX activity can affect *P. tricornutum* redox state 135

5.4.2 Is DPI a suitable inhibitor for *P. tricornutum* NOX proteins? 135

5.4.3 NOX activity in *P. tricornutum* is coupled with photosynthesis 136

5.4.4 NOX interactions with non-photosynthetic pathways 137

5.4.5 Evidence for NOX interactions with other metabolic pathways: AOX and PSII 138

5.4.6 Enzymatic and functional differences in eROS production between diatoms 140

5.4.7 Conclusions 141

Chapter 6 General Discussion 143

6.1 Summary of key findings 144

6.2 The structural diversity of diatom NOX proteins 145

6.2.1 What processes may have led to the diversity of diatom NOX proteins? 145

6.2.2 A functional explanation for diatom NOX diversity? 146

6.2.3 Why are there alternative enzymatic sources in diatoms? 146

6.2.4 Future steps to identify NOX proteins 147

6.3 The importance of H_2O_2 in diatom tolerance and signalling 148

6.3.1 How does H_2O_2 affect *P. tricornutum* signalling? 148

6.3.2 How do diatom tolerances to H_2O_2 compare? 148

6.3.3 What sources of H_2O_2 could initiate redox signalling in diatoms? 149

6.3.4 What steps should be taken to further understand H_2O_2 signalling in *P. tricornutum*? 150

6.4 NOX proteins as an electron dissipation mechanism in *P. tricornutum* 150

6.4.1 How do NOX proteins enhance diatom fitness? 150

6.4.2 eROS production for electron dissipation is a common microalgal strategy 151

6.4.3 How can the risk of DPI toxicity be minimised in future NOX characterisation experiments? 151

6.4.4 What other conditions may affect NOX activity in diatoms? 152

6.5 Concluding Remarks 153

Appendix A Chapter 1 Supplementary information 155

A.1 List of diatoms screened and distribution of NOX protein hits. 155

Appendix B Chapter 4 Supplementary information 161

B.1 Biosensor sequences cloned into plasmid. 161

B.2 Plasmid map for shuttle vector pPhat-T1. 164

Appendix C Chapter 5 Supplementary information 165

C.1 Plasmid map for pPha-T1-Venus shuttle vector. 165

List of Accompanying Materials 166

List of References 167

Table of Tables

Table 1.1 Literature reporting extracellular ROS production in diatoms......19

Table 1.2 Summary of the range of functions of NOX-derived eROS......21

Table 2.1 Comparison of transcript expression levels of *PtFRE1-3* and *PtNOX1-2* in *P. tricornutum*. 31

Table 2.2 The abundance of NOX proteins differs between the four taxonomic groups......33

Table 2.3 The distribution of each Class of diatom NOX protein differs between the four diatom taxonomic groups. 34

Table 2.4 Comparison of conserved motifs between NOX and FRE sequences......40

Table 2.5 Comparison of presence and absence of NOX and GR proteins within selected diatom species. 45

Table 3.1 Comparison of the responses of each species to different treatments in each assay.74

Table 4.1 Comparison of growth rate between the different H_2O_2 treatments. 94

Table 5.1 Primers used for extraction of NOX genes and screening of Venus tagged NOX sequences......114

Table 5.2 Summary of the effects of 1 µM DPI on photosynthetic parameters under different light intensities......126

Table 5.3 Comparison of diatom eROS production and potential enzymatic sources. 141

Table of Figures

Figure 1.1 The typical diatom cell structure. 3

Figure 1.2 Structure of the most common ROS and equations for creation of superoxide, hydrogen peroxide and hydroxyl radicals. 6

Figure 1.3 . The detailed structural components of NOX2. 9

Figure 1.4 A simple comparison of ROS production between human NOX2 and plant NOX (Rboh). 11

Figure 1.5 eROS production is widespread in eukaryotes. 12

Figure 2.1 Frequency of *P. tricornutum FRE* and *NOX* genes under different environmental conditions in EST libraries. 32

Figure 2.2 Phylogenetic tree of NOX proteins in eukaryotes. 35

Figure 2.3 Comparison of conserved structural domains between NOX Classes and FRE proteins. 37

Figure 2.4 Comparison of the conserved motifs between different NOX and FRE proteins. ... 39

Figure 2.5 Phylogeny of GR proteins across different lineages. 43

Figure 2.6 Possible scenarios explaining the unusual diversity of NOX proteins in diatoms. .. 51

Figure 3.1 A standard curve of 420 nm absorbance vs potassium ferricyanide concentration. 57

Figure 3.2 Comparison of 420 nm absorbance in the presence of potassium ferricyanide or potassium ferrocyanide. 60

Figure 3.3 Baseline comparison of (A) FCR activity and (B) eROS production between three test species. 61

Figure 3.4 The effect of DPI on FCR activity. 63

Figure 3.5 The effect of DPI on eROS production. 64

Figure 3.6 The effect of solvents on FCR activity and eROS production in *P. tricornutum.* 66

Figure 3.7 Effect of light intensity and the photosynthesis inhibitor DCMU on FCR activity. .. 68

Figure 3.8 Effect of light intensity and the photosynthesis inhibitor DCMU on eROS production. 70

Figure 3.9 . A generalised model for how light intensity may affect marine diatom TMET and eROS production. 75

Figure 4.1 Comparison of the differing methods of action for H_2O_2 sensing in HyPer and roGFP2-Orp1. 80

Figure 4.2 Excitation spectra of roGFP2. 84

Figure 4.3 roGFP2-Orp1 is expressed in the cytosol of *Phaeodactylum tricornutum*. 88

Figure 4.4 Responses of roGFP2-Orp1 in *P. tricornutum*. 90

Figure 4.5 Expression of roGFP2-ChlOrp1 in *P. tricornutum*. 91

Figure 4.6 Characterising the response of roGFP2-ChlOrp1 to addition of 100 µM H_2O_2. 93

Figure 4.7 H_2O_2 concentration affects growth and photosynthetic efficiency of *P. tricornutum*. 95

Figure 4.8 H_2O_2 concentration affects physiological parameters in roGFP2-Orp1 cells. 97

Figure 4.9 Rapid changes in roGFP2-Orp1 fluorescence following perfusions of different concentrations of H_2O_2. 98

Figure 4.10 Elevations of cytosolic Ca^{2+} detected with R-GECO following different treatments of hydrogen peroxide. 99

Figure 4.11 High light intensities trigger cytosolic H_2O_2 production. 100

Figure 4.12 Breakdown of individual cell maximum 400:475 nm values under the different light regimes. 101

Figure 5.1 A simplified model of some of the main mechanisms for diatoms to dissipate excess electrons, or for balancing the ATP:NADPH ratio. 110

Figure 5.2 Primer positions used for colony PCR screening of potential NOX-Venus constructs. 115

Figure 5.3 Gel screening of successfully transformed *E. coli* colonies with Venus tagged PtNOX1 and PtNOX2. 116

Figure 5.4 PtNOX1 localises to *P. tricornutum* plasma membrane. 117

Figure 5.5 Pilot study demonstrating a dose dependent increase in cytosolic H_2O_2 with DPI.118

Figure 5.6 DPI concentration affects cytosolic H_2O_2 and photosynthetic efficiency. 119

Figure 5.7 DPI reduces long-term cell viability in wild-type *P. tricornutum*. 121

Figure 5.8 Light intensity in conjunction with DPI addition affects cellular parameters. 123

Figure 5.9 DPI in conjunction with light affects chlorophyll fluorescence during NPQ induction curves. 124

Figure 5.10 DPI and DCMU affect O_2 evolution and consumption in *P. tricornutum*. 129

Figure 5.11 DPI has contrasting effects on Fv/Fm in *T. weissflogii* and *A. glacialis*. 130

Figure 5.12 GSSG has no effect on *P. tricornutum* eROS production. 131

Figure 5.13 Metabolic inhibitors affect *P. tricornutum* cytosolic H_2O_2 levels. 132

Figure 5.14 AOX inhibition increases *P. tricornutum* eROS production but does not affect Fv/Fm. 133

Figure 5.15 PSII inhibition increases eROS production and reduces Fv/Fm in *P. tricornutum.* 134

Figure 5.16 Comparing the different effects of different metabolic inhibitors on cellular parameters in *P. tricornutum*. 139

Figure 6.1 NOX as an electron dissipation mechanism. 145

Research Thesis: Declaration of Authorship

Print name: JACK EDWARD DICKENSON

Title of thesis: Characterising NADPH oxidase in marine diatoms

I declare that this thesis and the work presented in it are my own and has been generated by me as the result of my own original research.

I confirm that:

1. This work was done wholly or mainly while in candidature for a research degree at this University;
2. Where any part of this thesis has previously been submitted for a degree or any other qualification at this University or any other institution, this has been clearly stated;
3. Where I have consulted the published work of others, this is always clearly attributed;
4. Where I have quoted from the work of others, the source is always given. With the exception of such quotations, this thesis is entirely my own work;
5. I have acknowledged all main sources of help;
6. Where the thesis is based on work done by myself jointly with others, I have made clear exactly what was done by others and what I have contributed myself;
7. None of this work has been published before submission

Signature: ..... Date: 11/09/2020.....

Declaration of authorship continued: outline of work conducted jointly with or by others presented in this thesis (information pertaining to point 6 on previous page).

Chapter 4: Using the fluorescent biosensor roGFP2-Orp1 to explore H2O2 dynamics in Phaeodactylum tricornutum

The majority of experimental work was carried out by Jack Dickenson with the following exception:

Dr G. Wheeler designed the redox biosensor sequences, described in Section 4.2.2 and Appendix B1.

Chapter 5: Characterisation of the function of NOX proteins in Phaeodactylum tricornutum

The majority of experimental work was carried out by Jack Dickenson with the following exception:

Ms C. Hopkins generated *P. tricornutum* genomic DNA used for cloning PtNOX1 and PtNOX2, described in Section 5.2.7.

University of Southampton Research Repository

Copyright © and Moral Rights for this thesis and, where applicable, any accompanying data are retained by the author and/or other copyright owners. A copy can be downloaded for personal non-commercial research or study, without prior permission or charge. This thesis and the accompanying data cannot be reproduced or quoted extensively from without first obtaining permission in writing from the copyright holder/s. The content of the thesis and accompanying research data (where applicable) must not be changed in any way or sold commercially in any format or medium without the formal permission of the copyright holder/s.

When referring to this thesis and any accompanying data, full bibliographic details must be given, e.g.

Thesis: Author (Year of Submission) "Full thesis title", University of Southampton, name of the University Faculty or School or Department, PhD Thesis, pagination.

Data: Author (Year) Title. URI [dataset]

Acknowledgements

I would like to formally thank the European Research Council for funding my PhD through the SeaCells project and to thank the University of Southampton and the Marine Biological Association for hosting and supporting me through my PhD.

There certainly were moments where I wasn't sure if I'd make it to this point, and the global pandemic certainly added to the challenge. So this is dedicated to everyone who helped me achieve this.

A huge thanks go towards my primary supervisors for their many hours of patience, support, honesty and guidance throughout my PhD. Thank you, Dr Glen Wheeler, for engaging me with enthusiasm regardless of the triviality of my enquires, redirecting me when required, expanding my knowledge of molecular biology, and being an excellent footballing opponent. Thank you to Professor Colin Brownlee for helping me think bigger and consider the wider implications of my work, how best to articulate it, for educating me on the scope of microscopy and chlorophyll fluorescence and for several excellent boat trips, which sadly did not include one to the Southern Ocean. Maybe next time.

Thank you to the University of Southampton staff for aiding my PhD. Thank you to my Southampton supervisor Professor Mark Moore and my panel chair Professor Duncan Purdie for always providing excellent outside insight for my project. Thank you to Ms Mary Smith for exceptional helpfulness in dealing with my questions with poise and grace.

There have been some exceptional scientists at the MBA who have guided me through the different aspects of my PhD. The Cell and Molecular team have been immensely important by ensuring access to equipment, chemicals, cells, and my questioning so thank you to Angela Ward, Claire Hopkins, Shae Bailey, and Tyrone Roberts. I couldn't have developed my enthusiasm for microalgae without Charlotte Walker, Serena Flori and Doro Kottmeier guiding me through algae culturing, microscopy, photophysiology and cell chemistry. And of course, thank you to the MBA Sepia team for providing regular access to seawater for me to peruse for phytoplankton, and to Gerald Boalch for guiding my attempts at diatom taxonomy. The exciting and slightly terrifying world of molecular biology was made much easier to digest thanks to Katherine Helliwell, Kim Bird and Susie Wharam. And thanks to Gerald Langer who has advised me on a whole manner of topics since my MRes project with foraminifera and has always been able to offer new perspectives.

Together, my extended family have played a critical role in ensuring I didn't fall into the rabbit hole of an all-consuming PhD. Their continual support in my marine biology journey has been vital. In particular, I'm very grateful for them coping with me talking to/at them about algae signalling for four years. My mum Mags and my dad Mark kept reminding me I could, and I would 'get PhD done'. It turns out they were right.

Throughout my PhD, I've experienced a plethora of wonderful experiences/distractions with my friends. So while I can't thank everyone by name, thanks for the many hours of pubbing, gigging, quizzing, exploring, swimming and footballing. For D&D, F&F and BBQs. For Pictionary, Articulate and boardgame nights, pizza parties, tea breaks, book club and Quarantine Taskmaster.

Thank you, Friedrich, for sharing two offices (long live Office 68 Vol 1 and Vol 2!) for the duration of our respective PhDs and the subsequent weirdness following discussions of politics, history and silliness. Dean and Poppy, I have learnt and laughed so much with the two of you and I was very lucky to have been trapped in a house with you this year. Thank you to Harriet for introducing me to the 4pm MBA tea breaks and Thursday films, and always offering guidance and reassurance. Thank you Tamasine for keeping me grounded with lifestyle chats and talk of future adventures and brightening up my evenings with quarantine Zoom chats. And finally, my journey through academia and Plymouth has paralleled with my friend, teammate, real-life and sporting Captain Troy. Why thank ye Troy(!), for immeasurable friendship and support, and pushing me to think outside the box, be it football, video editing or discussions.

Finally, thank you to the staff and students at the MBA. I've been based here for 5 years and I wouldn't have wanted it any other way. The MBA fostered an amazing environment for my PhD and that stems from the people who work there, throughout the organisation. The friendly atmosphere and being able to chat to anyone from essential staff to IT department to senior management at tea breaks and elsewhere made me feel a part of a special community. I know that the MBA will maintain its unique approach and continues to thrive in delivering excellent marine science.

Definitions and Abbreviations

μ: .....organism growth rate

•OH: .....hydroxyl radical

$^1O_2$: .....singlet oxygen

AEP: .....alternate energetic pathways

AOX: .....alternate oxidase

APX: .....ascorbate peroxidase

ASW: .....artificial seawater

ATP: .....adenosine triphosphate

CAT: .....catalase

CEF: .....cyclic electron flow

ChlOrp1: .....chloroplast-localised roGFP2-Orp1

DCMU: .....3-(3,4-dichlorophenyl)-1,1-dimethylurea

DMSO: .....dimethyl sulfoxide

DPI: .....diphenyleneiodonium chloride

DTT: .....dithiothreitol

DUOX: .....dual oxidase

EDM: .....energetic dissipation mechanisms

eGFP: .....enhanced green fluorescent protein

eROS: .....extracellular ROS

EST:..... expressed sequence tag

ETC: .....electron transport chain

F_0: .....dark adapted minimum fluorescence

F_0': ..... light adapted minimum fluorescence

FCR: .....Ferricyanide reduction activity

F_M: .....dark adapted maximum fluorescence

F_M': .....light adapted maximum fluorescence

Definitions and Abbreviations

Fm': ..... the steady state maximum fluorescence following saturating peaks during actinic light exposure.

FRE: ..... ferric reductase

FSW: ..... filtered seawater

Ft': ..... the steady state minimum fluorescence following actinic light stabilisation

Fv/Fm: ..... maximum quantum efficiency of PSII photochemistry

Fv'/Fm': ..... operating efficiency of PSII in light

GFP: ..... green fluorescent protein

GR: ..... glutathione reductase

GSH: ..... glutathione

GSSG: ..... glutathione disulphide

H_2O_2: ..... hydrogen peroxide

HAB: ..... harmful algal bloom

HL: ..... high light

iROS: ..... intracellular ROS

Mal-OAA: ..... Malate–oxaloacetate shuttle

Min: ..... minutes

ML: ..... medium light

$NADP^+$: ..... icotinamide adenine dinucleotide phosphate

NADPH: ..... reduced nicotinamide adenine dinucleotide phosphate

NOX: ..... NADPH oxidase

NPQ: ..... non-photochemical quenching

O_2^-: ..... superoxide anion

OPP: ..... oxidative pentose phosphate pathway

OR: ..... oxidoreductase protein

Orp1: ..... roGFP2-Orp1 protein

PBS: ..... phosphate buffered saline

PCD: .....programmed cell death

PSI: .....photosystem 1

PSII: .....photosystem 2

PtNOX: .....*Phaeodactylum tricornutum* NADPH oxidase

qP: .....the coefficient of photochemical quenching, an estimate of open PSII reaction centres

Rboh: .....respiratory burst oxidase homologue

ROS: .....reactive oxygen species

s: .....second

SHAM: .....salicylhydroxamic acid

SoD: .....superoxide dismutase

STEAP: .....six-transmembrane epithelial antigen of the prostate

TMD: .....transmembrane domain

TMET: .....transmembrane electron transport

YFP: .....yellow fluorescent protein

Chapter 1 Introduction

1.1 An introduction to diatoms

1.1.1 Diatom biology, ecology, and evolution

Diatoms are a key group of photosynthetic organisms. These unicellular microalgae are found in many aquatic environments including freshwater, brackish, marine, and polar ice. Diatoms first appeared 180 million years ago (Sims *et al.*, 2006) and are taxonomically split into pennate (bilateral symmetry) and centric (radial symmetry) diatoms (Round *et al.*, 1990; Medlin & Kaczmarska, 2004). There is great morphological diversity within diatoms. Cell size ranges from a few µm to several mm (Leblanc *et al.*, 2012) and species number estimates range from 12,000-200,000 (Mann & Droop, 1996; Guiry, 2012; Malviya *et al.*, 2016). Through this diversity, models estimate diatoms contribute 20-40% of ocean primary productivity (Nelson *et al.*, 1995; Field *et al.*, 1998; Mann, 1999) and strongly affect biogeochemical cycling, particularly silica (Tréguer *et al.*, 1995).

Though the diatom cell structure shares core features with other unicellular eukaryotic algae (Fig 1.1), specific features help identify diatoms. For example, diatom chloroplast pigments differ from several algal groups. Diatoms utilise chlorophyll a, c and fucoxanthin for light harvesting and β carotene, diatoxanthin and diadinoxanthin as photoprotective carotenoids (Kuczynska *et al.*, 2015). The number of chloroplasts can vary greatly between diatom species, from one in a small pennate like *Phaeodactylum tricornutum* to hundreds in a large centric like *Odontella sinesis* (Round *et al.*, 1990; Schober *et al.*, 2019). However, the unique feature of diatoms is the cell wall composed of silica, known as a frustule. The frustule is composed of the larger epitheca section which encompasses the smaller hypotheca, like a Petri dish (Fig 1.1). The frustule is physically strong, likely acting as a defence against predation (Hamm *et al.*, 2003) but some structural evidence suggests it also promotes light absorbance for photosynthesis (Romann *et al.*, 2015). Production of the frustule is a highly intricate process that occurs during mitosis. After cell division, one daughter cell retains the epitheca and the other the hypotheca. The previous hypotheca becomes the epitheca for the new daughter cell. This results in a gradual decline in cell size in the population, requiring sexual reproduction for the cell to enlarge again. Silicic acid is uptaken from the surrounding medium and transported to the internal silica deposition vesicle where it is deposited in a controlled manner to generate each new hypotheca (Hildebrand *et al.*, 2018; Yee *et al.*, 2020). Upon completion, the new hypotheca is exocytosed and merges with the epitheca to form the complete frustule.

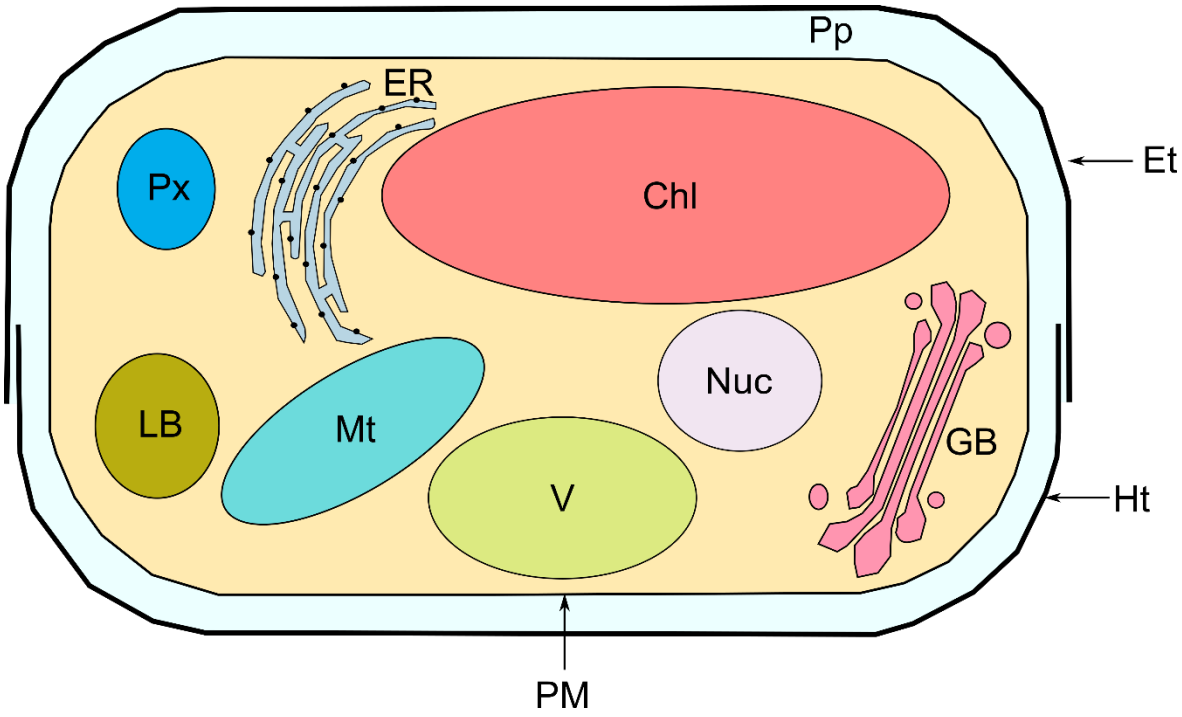

Figure 1.1 The typical diatom cell structure.

The figure indicates the presence but not the quantity, shape or size of cell organelles. Structure based on descriptions in Medlin & Kaczmarska (2004) and Falciatore *et al.* (2019). Chl = chloroplast. Et = epitheca. ER = endoplasmic reticulum. GB = Golgi body. Ht = hypotheca. LB = lipid body. Mt = mitochondria. Nuc = nucleus. PM = plasma membrane. Pp = periplasm. Px = peroxisome.

Diatoms have had a complex evolutionary history. They acquired their plastid by secondary endosymbiosis, whereby a red alga was engulfed by an ancestral non-photosynthetic host cell, resulting in the plastid possessing four membranes (Cavalier-Smith, 2002; Bhattacharya *et al.*, 2004). Genomic analysis has indicated that green and red algal-derived genes are present in diatom genomes (Bowler *et al.*, 2008). A cryptic endosymbiosis is proposed where an initial green algal symbiont was later replaced by the red algal symbiont (Dorrell & Smith, 2011; Dorrell *et al.*, 2017), though this is controversial (Deschamps & Moreira, 2012). Diatoms also contain significant quantities of bacterial genes, implying extensive horizontal gene transfer (Fan *et al.*, 2020) which can occur through bacterial conjugation (Karas *et al.*, 2015). Alongside this unusual evolution, diatoms possess surprising metabolic pathways, such as a functioning urea cycle typical of animal cells (Armbrust *et al.*, 2004). Consequently, diatom genomes are described as mix and matched genomes (Armbrust, 2009).

This genetic diversity could help explain the ecological success and flexibility of diatoms. Diatoms have many remarkable adaptations to thrive in changing and challenging

environments. For example, polar diatoms can tolerate four months of darkness without compromising their photosynthetic activity (Kennedy *et al.*, 2019) while pelagic oceanic diatoms in iron-depleted waters have modified their photosynthetic apparatus to reduce iron requirements (Strzepek & Harrison, 2004). Alongside this, diatoms use carbon-concentrating mechanisms, such as efficient carbonic anhydrase enzymes or bicarbonate transporters, to mitigate low oceanic CO_2 concentrations (Hopkinson *et al.*, 2011; Young *et al.*, 2016; Chrachri *et al.*, 2018). Following exposure to more favourable conditions, such as nutrient resupply, diatoms respond rapidly to outcompete other phytoplankton, forming blooms. Diatom blooms are seasonal occurrences, with a winter-spring bloom and less regular upwelling blooms (Smayda & Trainer, 2010). Abiotic factors such as temperature, light and concentration of nutrients such as iron and silicic acid strongly affect the dynamics of diatom blooms (Egge & Aksnes, 1992; Sommer & Lengfellner, 2008; Krause *et al.*, 2019). Thus, in high nutrient low chlorophyll regions such as the Southern Ocean, iron fertilisation experiments can initiate diatom blooms (Boyd *et al.*, 2000; Tsuda *et al.*, 2003; Quéguiner, 2013), which has been proposed as a potential geoengineering strategy to help combat climate change (Vaughan & Lenton, 2011).

1.1.2 Diatom signalling pathways

There is increased interest in understanding the cellular mechanics for how diatoms respond to constantly changing abiotic (light, temperature, salinity, O_2 etc) and biotic factors. Analyses of diatom genomes and the advent of genetic approaches are revealing specific signalling pathways and responses to stimuli of high complexity (Armbrust *et al.*, 2004; Kroth, 2007). In areas such as membrane excitability and associated signalling pathways, there are intriguing similarities to metazoans. Diatom cells have similar resting potentials to animal cells and are capable of generating rapid action potentials through Na^+ or Ca^{2+} influx (Taylor, 2009; Verret *et al.*, 2010; Taylor *et al.*, 2012). Both metazoans and diatoms exist in an environment with a high external Na^+ concentration and diatoms can use the Na^+ gradient to assist transport into the cell (Bhattacharyya & Volcani, 1980; Taylor *et al.*, 2012). Furthermore, influx of Ca^{2+} through a novel class of membrane channels known as EuKCaTAs underpins a rapid signalling response to hypoosmotic shock (Helliwell *et al.*, 2019). There is also genomic evidence for other diatom membrane proteins involved with membrane excitability such Hv1 proton channels (Taylor *et al.*, 2011). Regarding P-type ATPases, little experimental or genomic characterisation has occurred in marine diatoms. A putative P-type ATPase in *Nitzschia alba* has been suggested to drive a Na^+ gradient to promote silicate uptake (Sullivan & Volcani, 1974; Bhattacharyya & Volcani, 1980) but a gene sequence has not been identified. In contrast, 17 P-type ATPases are

reported in the *T. pseudonana* genome, though a deeper description is not mentioned (Lopez *et al.*, 2005). A protein that groups closely to a *Symbiodinium* P-type H^+-ATPase has also been reported in the *P. tricornutum* genome, with no experimental characterisation as to its function (Bertucci *et al.*, 2010). Though research in diatoms is limited, P-type ATPases such as H^+-ATPase, Na^+-ATPase and Na^+/K^+-ATPase have been described in other marine algae and stramenopiles including red algae, green algae, raphidophytes and oomycetes (Shono *et al.*, 2001; Barrero-Gil *et al.*, 2005; Chan *et al.*, 2012; Raven & Beardall, 2020; Kumari & Rathore, 2020), which could aid future attempts to identify P-type ATPases in diatoms.

Recently, it has been shown that reactive oxygen species (ROS) signalling is likely important in regulating diatom physiology (Rosenwasser *et al.*, 2014; Mizrachi *et al.*, 2019). Transcriptomic and proteomic approaches have demonstrated that diatoms can rapidly and intricately change their cellular physiology in response to different stimuli. Abiotic stimuli include nutrient depletion and resupply (Allen *et al.*, 2008; Bidle & Bender, 2008; Rosenwasser *et al.*, 2014), high light stress (Nymark *et al.*, 2009; Mizrachi *et al.*, 2019), osmotic shock (Falciatore *et al.*, 2000; Helliwell *et al.*, 2019) and daily diurnal rhythm (Ashworth *et al.*, 2013; Annunziata *et al.*, 2019). Biotic interactions can occur with neighbouring cells, both in supportive and antagonistic manners. Some diatom species produce sex pheromones to attract and initiate diatoms together for sexual reproduction (Chepurnov *et al.*, 2004; Moeys *et al.*, 2016; Bilcke *et al.*, 2020). Bacteria can detoxify toxic compounds for diatoms (Hunken *et al.*, 2008) or trigger diatom cell death (Amin *et al.*, 2015; van Tol *et al.*, 2017). In contrast, diatom-derived cyanogen bromide can affect bacterial biofilm formation (Vanelslander *et al.*, 2012) while diatom polyunsaturated aldehydes such as decadienal can reduce fertility and egg hatching success in predatory copepods (Miralto *et al.*, 1999; Ianora *et al.*, 2004). Furthermore, decadienal can trigger a signalling cascade resulting in programmed cell death (PCD) in diatoms, leading to greater aldehyde production (Casotti *et al.*, 2005; Vardi *et al.*, 2006, 2008).

1.2 Reactive oxygen species (ROS)

ROS are chemically reactive molecules formed through the one step electron reduction of molecular oxygen. The best-studied ROS are superoxide anions ($^{\bullet}O_2^-$), hydrogen peroxide (H_2O_2) and hydroxyl radicals ($^{\bullet}OH$) (Fig 1.2.). Typically, a free electron will reduce oxygen to the superoxide anion. Superoxide can be converted to hydrogen peroxide through natural dismutation (simultaneous reduction and oxidation of a substrate) or catalysed by the enzyme superoxide dismutase (SoD). The hydroxyl radical is formed when H_2O_2 is partially reduced, such as through the Fenton reaction where transition state metals such as Fe^{2+} or Cu^{2+} are oxidised by H_2O_2 (Sutton & Winterbourn, 1989).

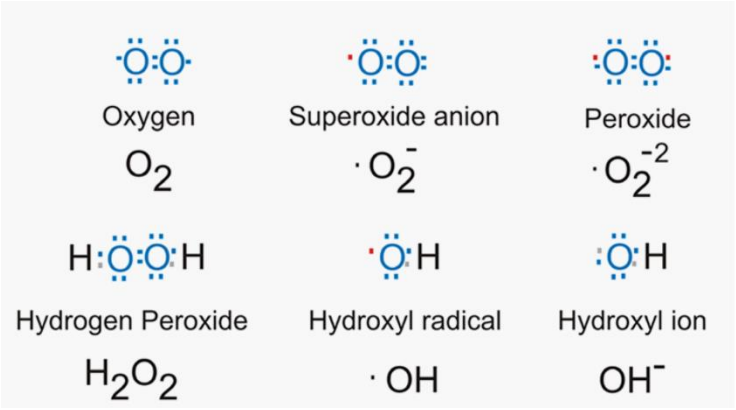

Figure 1.2 Structure of the most common ROS and equations for creation of superoxide, hydrogen peroxide and hydroxyl radicals.

Red dots represent unpaired electrons. Figure adapted from Biotek, 2014.

ROS can be formed abiotically through photolysis or radiolysis (Micinski *et al.*, 1993; Garg *et al.*, 2007b; Houée-Levin & Bobrowski, 2013). Substantial quantities are also generated during cellular metabolism when electrons leak out of photosynthetic or respiratory electron transport chains (ETC) (Pfannschmidt, 2003; Murphy, 2009). In photosynthetic organisms, H_2O_2 generation in the chloroplast can be 30-100x greater than the mitochondria (Hossain *et al.*, 2015). The photosynthetic ETC is vulnerable to stressors such as high light. As light intensity increases photosystem electron flow, if carbon fixation or the availability of electron acceptors such as $NADP^+$ does not correspondingly increase, the photosystem becomes over-reduced, enhancing the generation of damaging ROS (Ledford & Niyogi, 2005; Edreva, 2005). Thus, stressors that reduce photosynthetic efficiency can also result in ROS generation. Other intracellular ROS sources include within peroxisomes (Schrader & Fahimi, 2006) and enzymatic sources such as lipoxygenase (Catalano *et al.*, 2005) and xanthine oxidase (Shin *et al.*, 2008). In addition, NADPH oxidase generates extracellular ROS (eROS) which can affect neighbouring cells (Bedard & Krause, 2007; Miller *et al.*, 2009). Thus, cells are constantly being exposed to ROS.

Due to their high reactivity, ROS can damage cells. ROS can oxidise many biomolecules, causing DNA strand breaks, lipid and protein chain breaks and enzymatic inactivation (Beckman & Ames, 1997; Berlett & Stadtman, 1997; Das & Roychoudhury, 2014). Cells have developed enzymes and low weight antioxidant molecules to detoxify ROS. These include superoxide dismutase (SoD), ascorbate peroxidase (APX), catalase (CAT), peroxiredoxins, glutathione reductase (GR) and glutathione (GSH) (Noctor & Foyer, 1998; Das & Roychoudhury, 2014). Typically, each antioxidant has a specific ROS target. For example, SoD converts superoxide to H_2O_2. SoD is highly conserved, found in all three kingdoms of life (Miller, 2012) and a recent estimate suggested SoD, peroxiredoxins and CAT may have evolved 4.1-3.6 billion years ago,

prior to the great oxygenation event (Inupakutika *et al.*, 2016). When ROS production exceeds antioxidant capacity, the resulting damage and cellular impairment is called oxidative stress. This continuous cellular damage from ROS has famously been proposed to be the cause of cellular aging (Harman, 1956) but is contentious (Hekimi *et al.*, 2011).

Uncontrolled production of ROS leads to oxidative stress. However, low levels of ROS or localised production can participate in cell signalling. Environmental stresses (light, salt, heat shock) can increase ROS production by damaging metabolic pathways (Das & Roychoudhury, 2014; Hossain *et al.*, 2015). The subsequent intracellular ROS production can act as a stress signal, stimulating cell recovery. ROS production and scavenging can affect cellular redox biology and signalling as ROS can oxidise thiol groups on cysteine residues in proteins (Mittler *et al.*, 2011). By accepting electrons from thiol groups, ROS oxidation creates a disulphide bond between two cysteine residues (Dickinson & Chang, 2011; Poole, 2015). This alters the protein structure and can lead to signalling cascades. Thus, ROS acts as a secondary messenger. H_2O_2 is an effective signalling molecule. It can oxidise protein cysteine residues, has a comparatively high cellular half-life (>1 ms) and is cell membrane permeable, passing directly through membranes or through membrane aquaporin channels (Bienert & Chaumont, 2014; Mittler, 2017). In contrast, superoxide, as a charged molecule, cannot directly pass through the cell membrane but can infrequently pass through membranes using chloride channels (Hawkins *et al.*, 2007; Mumbengegwi *et al.*, 2008). Superoxide can also oxidise protein cysteine residues but dismutates more rapidly than hydrogen peroxide (cellular half-life 1-4 µs), allowing more localised signalling. Hydroxyl radicals are less effective signalling molecules, as they are short-lived (cellular half-life 1 ns) and react indiscriminately with biomolecules. The different ROS properties allows specific, controlled alteration of the cellular redox state.

1.3 Intracellular ROS signalling in diatoms

ROS signalling in mammals is vital for cell physiology. For example, mitochondrial-derived ROS are implicated in regulation of PCD in mammalian cells (Fleury *et al.*, 2002; Murphy, 2009). Diatoms also use ROS signalling, which has been demonstrated most extensively in the model diatom *P. tricornutum*. *P. tricornutum* has had a 'redoxeome' characterised: proteins hypothesised to be vulnerable to ROS oxidation and thus candidates for ROS signalling. These redoxeome proteins are components of many metabolic pathways including photosynthesis, glycolysis, antioxidant production and nitrogen metabolism amongst others (Rosenwasser *et al.*, 2014). *P. tricornutum* has been successfully transformed to express the redox state biosensor protein (roGFP2) localised to different cellular compartments. Through this, exogenous H_2O_2 addition was shown to activate PCD by targeted oxidation of mitochondria or

chloroplast (Graff van Creveld *et al.*, 2015; Mizrachi *et al.*, 2019). These studies used relatively high concentrations of H_2O_2 (100-150 µM), though it was argued that these concentrations may be achieved during oxidative stress in response to stresses such as high light or iron limitation (Graff van Creveld *et al.*, 2016; Mizrachi *et al.*, 2019). External chemical signals such as cyanogen bromide or decadienal can also alter the redox state of cellular compartments (Vardi *et al.*, 2006; Graff van Creveld *et al.*, 2015). Decadienal can potentially underlie complex intercellular signalling through the production of nitric oxide in *P. tricornutum*. Nitric oxide migrates to neighbouring cells, enters and triggers PCD (Vardi *et al.*, 2006, 2008). In other marine diatoms, nitric oxide and polyunsaturated aldehydes trigger intracellular ROS production, affecting photosynthesis and activating PCD (Gallina *et al.*, 2014, 2015, 2016). Controlled intracellular ROS production is an important component of diatom redox signalling.

1.4 NADPH oxidase (NOX)

In addition to intracellular ROS production, many eukaryotes (including diatoms) produce extracellular ROS (eROS) (Bedard *et al.*, 2007; Schneider *et al.*, 2016; Zinser, 2018). Despite the risk of ROS accumulation and oxidative stress, this biotic eROS production is used for many functions including defence and intercellular signalling (Marino *et al.*, 2012; Sirokmany *et al.*, 2016). Biotic eROS can originate from passive diffusion of intracellular H_2O_2 but the most widespread and best studied mechanism is through the enzyme NADPH oxidase (NOX).

1.4.1 NOX structure

NOX is a family of membrane-bound enzymes that transport electrons across cell membranes, typically to the cell exterior, where they react with oxygen resulting in ROS (Bedard & Krause, 2007; Sumimoto, 2008), predominantly superoxide. NOX proteins have a conserved structure composed of cytosolic and transmembrane regions (Fig 1.3A). Flavin adenine dinucleotide (FAD) and nicotinamide adenine dinucleotide phosphate (NADPH) binding sites occur at the C-terminus. Cellular NADPH binds and donates electrons which are shuttled through the FAD region to the membrane. Within the membrane are six transmembrane domains (TMDs). Of the six, TMD3 and TMD5 are strongly conserved, possessing two histidine residues in each TMD. They provide ligand sites for the binding of Fe from two haem groups (Fig 1.3B). Electrons are transferred through the membrane via the haem groups (Sumimoto, 2008). The outer haem group has a small cavity above it. Recently, it was proposed that oxygen is reduced to superoxide here, possibly electrostatically catalysed by a positively charged arginine residue (Magnani *et al.*, 2017). By generating eROS and oxidising NADPH, NOX can affect redox states on both sides of the plasma membrane. Humans have seven NOX proteins: NOX1-5 and Dual

oxidase (DUOX) 1-2. NOX1-4 are similar in structure but NOX5 differs, possessing an EF-hand domain that can bind Ca^{2+}. DUOX proteins also have EF hands, and a peroxidase region, though DUOX proteins produce H_2O_2 rather than superoxide.

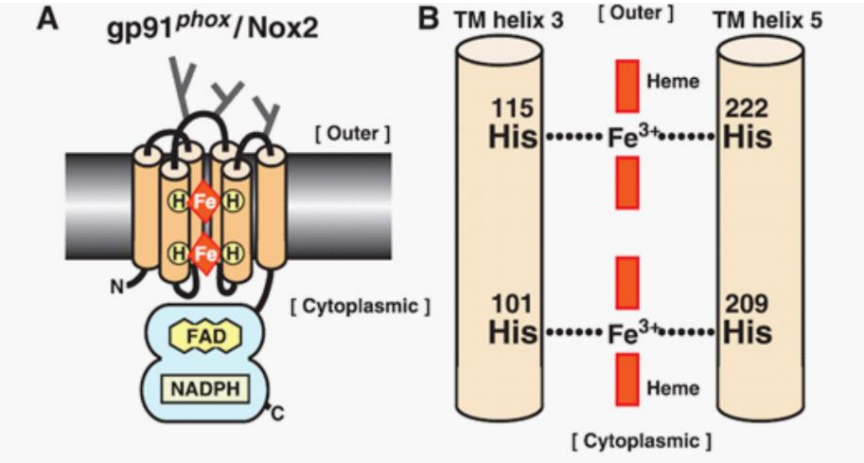

Figure 1.3 . The detailed structural components of NOX2.

Figure taken from Sumimoto, 2008. A) The structure of NOX2, the representative NOX protein. Conserved structures are the C-terminus FAD and NADPH binding sites and the six TMDs, represented by cylinders. B) The conserved ferric reductase domain. Within the 3rd and 5th TMD are four histidine residues that interact with two haem groups in the membrane.

1.4.2 NOX identification

NOX proteins are part of the Ferric-Reductase Domain (FRD) superfamily that includes ferric reductase (FRE), six-transmembrane epithelial antigen of the prostate (STEAP) and MsrQ/YedZ proteins (Zhang *et al.*, 2013; Juillan-Binard *et al.*, 2016). The ferric reductase domain contains the transmembrane haems (Fig 1.3B) that facilitate transmembrane electron transport to reduce a substrate (Zhang *et al.*, 2013). While NOX proteins reduce molecular oxygen to superoxide, FRE reduces Fe^{3+} to Fe^{2+} assisting iron uptake (Zhang *et al.*, 2013). STEAP and MsrQ/YedZ reduce extracellular metals (Knutson, 2008) or methionine sulfoxide (Juillan-Binard *et al.*, 2016). FRE and NOX exhibit considerable sequence similarity. They both have the ferric reductase domain, FAD and NADPH binding sites and six TMDs. *In silico* identification of NOX can be unreliable, leading to NOX being misidentified as FRE (Rossi *et al.*, 2017).

Methods for identifying NOX including measuring gene expression under iron limiting conditions as FRE is upregulated whereas NOX shows no change (Waters *et al.*, 2002; Herve *et al.*, 2006; Jain *et al.*, 2014). Alternatively, detecting compromised eROS production in putative *NOX* knockout mutants (Foreman *et al.*, 2003; Lardy *et al.*, 2005; Takemoto *et al.*, 2007; Rossi *et*

al., 2017) or following application of chemical inhibitors like diphenyleneiodonium chloride (DPI) or SoD, are frequently used methods (Kupper *et al.*, 2002; Ross *et al.*, 2005; Mydlarz & Jacobs, 2006; Kim *et al.*, 2007).

1.4.3 NOX activity in humans

The best characterised role of NOX in animals relates to defence against pathogens. In humans, the first NOX protein (NOX2) was identified in phagocytic cells and is an important part of human immune response. When NOX is activated, a rapid increase in ROS occurs, in most cases extracellularly. This is called the respiratory or oxidative burst, as oxygen levels decrease near the activated cells (Doke, 1983; Bolwell *et al.*, 1995). NOX2 is unusual as its oxidative burst occurs intracellularly in a phagosome (Fig 1.4). NOX2 (also known as $gp91^{phox}$) requires several subunits to bind together to activate. NOX2 is plasma membrane bound along with subunit $p22^{phox}$. When a pathogen is ingested, the plasma membrane internalises to create a phagosome. $gp91^{phox}$ combines with $p22^{phox}$ in the membrane, forming flavocytochrome b_{558} (Bedard & Krause, 2007; Panday *et al.*, 2015). Cytosolic regulatory components $p40^{phox}$, $p47^{phox}$ and $p67^{phox}$ combine when $p47^{phox}$ is phosphorylated and the complex moves to the membrane, combining with flavocytochrome b_{558}. Two small nucleotide binding proteins Rac2 and Rap1A bind to the complex and create the active oxidase. NOX1-4 also require similar components for activation whereas NOX5 and DUOX do not require subunits. The activated NOX2 uses NADPH-derived electrons to reduce oxygen in the phagosome to superoxide to target the pathogen or combine with other chemicals to enhance the reactivity (Panday *et al.*, 2015). NOX2 activity is crucial for human health. Mutations to any of the NOX2 components leads to chronic granulomatous disease (CGD), resulting in greater susceptibility to pathogens (Roos, 2019). The other human NOX proteins are spatially distributed in the human body, but their respective regulation and function are less clear. While NOX2 localises primarily to phagocytic cells, other NOX proteins are found in the colon (NOX1, NOX3, DUOX1), spleen (NOX5), testis (NOX5), thyroid (NOX4, DUOX1-2), kidney (NOX4) and the inner ear (NOX3) (Panday *et al.*, 2015; Sirokmany *et al.*, 2016). NOX3 is involved in the formation of ear otoconia (Paffenholz *et al.*, 2004), while DUOX is key for thyroid hormone synthesis (Donkó *et al.*, 2005).

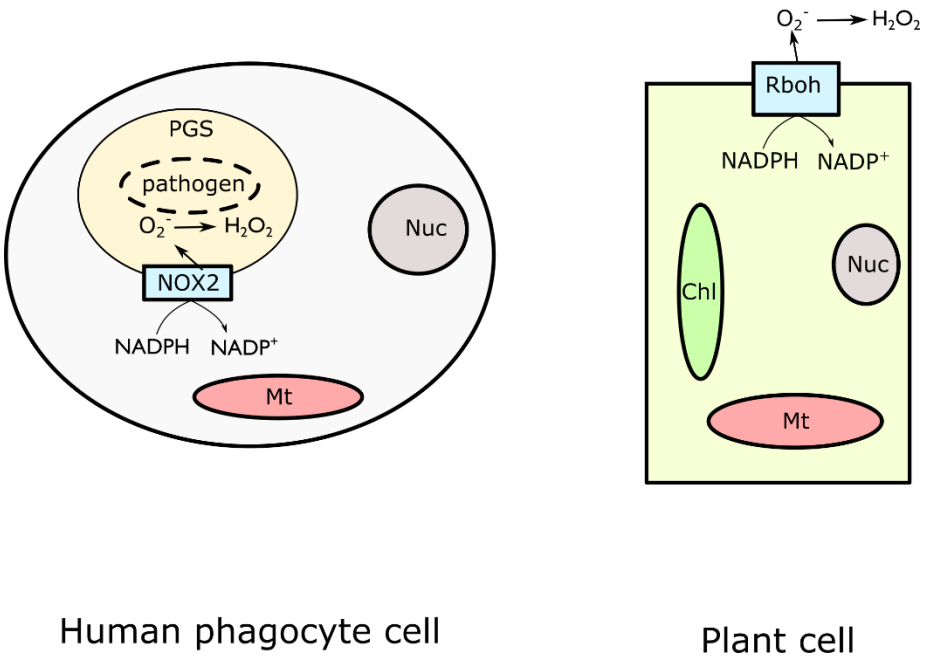

Figure 1.4 A simple comparison of ROS production between human NOX2 and plant NOX (Rboh).

NOX2 creates ROS in an internal phagosome whereas plant NOX proteins create ROS outside the plasma membrane such as in the apoplast. Both mechanisms reduce oxygen using electrons from the opposite side of the membrane. PGS= phagosome. Nuc= nucleus. Mt=mitochondria. Chl=chloroplast.

1.5 NOX and eROS functions in different lineages

NOX proteins are widespread across eukaryotes (Fig 1.5), including diatoms (Anderson *et al.*, 2011). Increasing research has focused on unicellular algal eROS production (Hansel *et al.*, 2016; Schneider *et al.*, 2016; Diaz & Plummer, 2018; Diaz *et al.*, 2019). To understand diatom NOX proteins and their function(s), it is important to review NOX and eROS production in well studied systems such as animals and plants, alongside lesser studied but more evolutionary or environmentally relevant lineages.

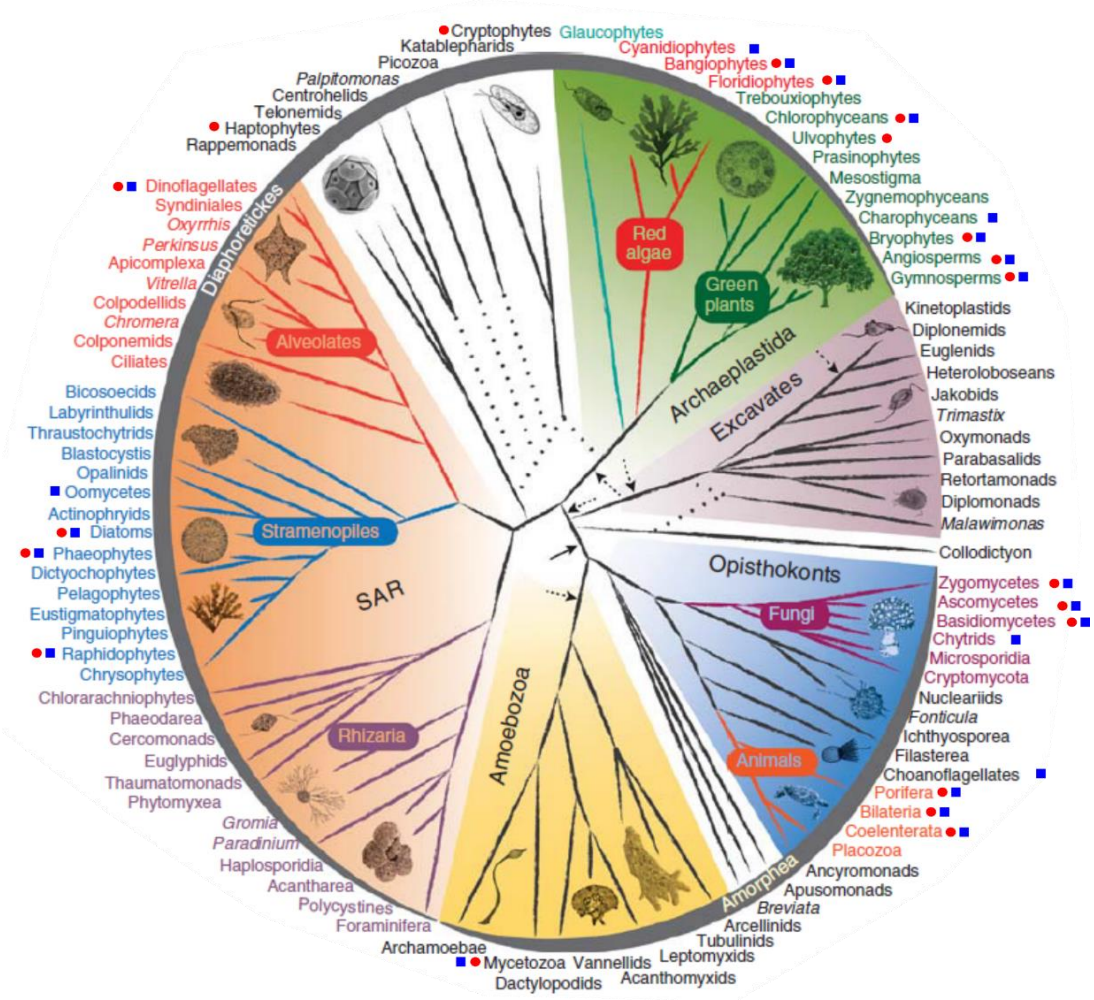

Figure 1.5 eROS production is widespread in eukaryotes.

Red circles indicate previous studies have reported eROS production in this lineage. Blue squares indicate evidence of NOX protein involved, relying on a characterised or a putative sequence, or DPI addition resulting in reduced eROS. Phylogenetic image adapted from Burki, 2014.

1.5.1 eROS production and NOX proteins in animals

NOX proteins are widely distributed in animals. Two genomic screens have found NOX proteins in 103 animal species (Kawahara *et al.*, 2007; Gandara *et al.*, 2017), representing vertebrates, cnidarians, sponges, echinoderms, nematodes, molluscs and annelids. Defence is a common function for animal NOX proteins, with reduced immune function in *NOX* knocked-down/out mice, zebrafish, *Drosophila* or *Caenorhabditis elegans* (Ha *et al.*, 2005; Fujita *et al.*, 2010; Flores *et al.*, 2010; Van Der Hoeven *et al.*, 2015). Animal NOX and eROS production has other functions. This includes promoting protein crosslinks to stabilise cuticle formation in *C. elegans* (Edens *et al.*, 2001) or as a signalling mechanism following wounding in zebrafish (Niethammer *et al.*, 2009), heat exposure in corals (Mydlarz & Jacobs, 2006) and urchin egg fertilisation,

(Wong *et al.*, 2004). Finally, the sponge *Sycon* sp. displays high constitutive superoxide production without stimuli (Peskin *et al.*, 1998), suggesting an as yet unknown function.

1.5.2 eROS production and NOX proteins in plants (Embryophytes)

Plant NOX homologues are known as respiratory burst oxidase homologues (Rboh). Over 30 screened species from bryophytes, angiosperms and gymnosperms possess Rboh proteins (Wang *et al.*, 2013; Kaur *et al.*, 2018; Maksimov *et al.*, 2018). Notably, all plant Rboh proteins possess EF hands, as is the case for NOX5 from humans. Consequently, ROS: Ca^{2+} signalling crosstalk is a frequent component of plant NOX activity. *Arabidopsis thaliana* possesses 10 Rboh homologues (RbohA-J) (Marino *et al.*, 2012). Rboh functions are surprisingly diverse, particularly for ROS signalling roles.

Several Rboh proteins are well characterised with roles in plant cell growth. For example, RbohC eROS production is crucial for root hair growth (Foreman *et al.*, 2003) as *rbohc* knockout mutants showed stunted root hair growth. ROS production was essential to activate Ca^{2+} channels and create an intracellular tip high Ca^{2+} gradient associated with polarised growth. ROS also functions to promote crosslinking of the newly expanding cell wall. ROS production oscillates with reductions in extracellular pH, weakening the cell wall, allowing expansion (Monshausen *et al.*, 2007, 2009). Oxidative bursts similarly are required for pollen tube expansion, with intracellular Ca^{2+} and protein phosphorylation required to activate RbohH and RbohJ (Potocky *et al.*, 2007; Kaya *et al.*, 2014; Maksimov *et al.*, 2018). Like humans, Rboh derived eROS occurs as a defence response (Doke, 1983; Levine *et al.*, 1994), with RbohD and RbohF the source of the ROS burst in *A. thaliana* (Torres *et al.*, 2002). This eROS has multiple roles in cell defence including direct antimicrobial activity, cell signalling or promoting cell wall cross linkages (Levine *et al.*, 1994; Liu *et al.*, 2010).

Rboh-mediated eROS production is also used for signalling during abiotic stress responses, involving intercellular signalling with a ROS wave (Miller *et al.*, 2009). Oxidative bursts from NOX proteins are normally localised to the area of stimuli. However, wounding *A. thaliana* triggered RbohD-dependent eROS production that rapidly spread throughout the whole plant, travelling at 8.4 cm min^{-1} (Miller *et al.*, 2009). The authors propose Rboh-derived superoxide in the apoplast dismutates to H_2O_2. H_2O_2 enters neighbouring cells and activates Ca^{2+} channels, causing an increase in cytosolic Ca^{2+}. This in turn activates RbohD to produce more ROS allowing a self-propagating ROS wave. ROS waves could be triggered following high light, heat and aphid exposure (Miller *et al.*, 2009). Other researchers have reported similar oxidative

bursts following stresses such as salt stress (Xie *et al.*, 2011; Evans *et al.*, 2016), cold stress (Zhang *et al.*, 2018) and hypoxia (Wang *et al.*, 2016).

Rboh proteins interact with other signalling molecules and regulatory mechanisms in addition to Ca^{2+}. Plant hormones are common effectors as Rboh-derived ROS can activate or interact with signalling pathways involving abscisic acid (Kwak *et al.*, 2003; Pengtao & Chun-Peng, 2008; Suzuki *et al.*, 2013), hydrogen sulphide (Scuffi *et al.*, 2018), nitric oxide (Desikan *et al.*, 2004), jasmonic acid (Maruta *et al.*, 2011) and salicylic acid (Herrera-Vásquez *et al.*, 2015). Finally, ROS waves may interact with electrical signalling in plants. Heat shock or light stress can trigger concurrent elevations in extracellular potential and ROS. This is suppressed in *rbohd* mutants, suggesting electrical-ROS signalling may be a part of the plant stress response (Suzuki *et al.*, 2013; Choi *et al.*, 2017).

1.5.3 eROS production and NOX proteins in fungi

NOX genes have been identified in 30 species of fungi, including both unicellular and multicellular fungi (Grissa *et al.*, 2010; Rossi *et al.*, 2017). Fungal NOX proteins are represented by three sub families: A, B & C (Aguirre *et al.*, 2005). NOX-A and NOX-B protein structure resembles human NOX2 whereas NOX-C contains calcium-binding EF hands, like plant NOX proteins and human NOX5. Most research suggests fungal oxidative bursts are involved in signalling to activate cellular differentiation during the formation of specialised structures. Using Δ*Nox* mutants or DPI treatment to inhibit ROS production results in non-development of specialised structures (such as sexual fruiting bodies) in unicellular and multicellular ascomycete fungi (Lara-Ortiz *et al.*, 2003; Malagnac *et al.*, 2004; Egan *et al.*, 2007; Rossi *et al.*, 2017). Other consequences of Δ*Nox* mutants are reduced virulence in *Magnaporthe grisae* (Egan *et al.*, 2007; Segmuller *et al.*, 2008; Giesbert *et al.*, 2008) and the symbiotic fungus *Epichloë festucae* switches its relationship with its host from mutualistic to antagonistic (Tanaka *et al.*, 2006). Over- or under-expression of *S. cerevisae* NOX affects regulation of PCD and actin cytoskeleton (Rinnerthaler *et al.*, 2012). In some fungi, polarity and subunit proteins are required to form a functioning NOX complex to trigger eROS production (Takemoto *et al.*, 2011; Siegmund *et al.*, 2013; Lacaze *et al.*, 2015), again regulating virulence (Marschall & Tudzynski, 2016). Finally, several fungal NOX proteins localise to the endoplasmic reticulum rather than the plasma membrane, suggesting NOX activity creates an intracellular oxidative burst as opposed to an extracellular burst (Rinnerthaler *et al.*, 2012; Siegmund *et al.*, 2013; Lacaze *et al.*, 2015).

1.5.4 eROS production and NOX proteins in brown algae (Phaeophyceae)

NOX proteins have not been characterised in brown algae as no clear NOX homologues are present in the *Ectocarpus* genome (Cock *et al.*, 2010). However, eROS production is widespread. In a screen of 45 brown algal species, only four did not demonstrate either oxidative bursts or constitutive production of eROS (Kupper *et al.*, 2002). Alginate oligosaccharides, components of brown algal cell walls, frequently induce oxidative bursts following their addition to Laminariale sporophytes (Kupper *et al.*, 2001, 2002). The oxidative bursts from *Laminaria digitata* were inhibited by DPI, implicating a NOX protein source. Similarly, lipopolysaccharides (LPS) from five different Gram-negative bacteria also caused an oxidative burst (Kupper *et al.*, 2006). Inhibition of the oxidative burst enhanced sporophyte susceptibility to bacterial infection (Kupper *et al.*, 2002). Thus, the oxidative burst may represent a defence response against a pathogen causing damage or death in neighbouring algal cells. However, lipopolysaccharide-stimulated bursts were absent in species tested from six Phaeophyceae orders, so it is not a uniform brown algal response (Kupper *et al.*, 2002).

Fucoid thalli from 10 species display high constitutive H_2O_2 production (Kupper *et al.*, 2002). However, intracellular oxidative bursts are also observed at the rhizoid cell apex in *Fucus serratus* embryos following hyperosmotic shock. (Coelho *et al.*, 2002). Inhibition of the oxidative burst by DPI led to increased cellular bursting, while pre-treatment with H_2O_2 enhanced tolerance to hyperosmotic shock. In addition, ROS production caused an elevation of cytosolic Ca^{2+}, again eliminated through DPI addition. This activity resembles cell wall strengthening and ROS signalling seen in plant root hairs (Foreman *et al.*, 2003). Localised ROS production is also associated with polarised cell development in *F. serratus*. *F. serratus* zygotes displayed a tip-high ROS gradient at the geminating rhizoid pole, alongside an associated apical gradient of cytosolic Ca^{2+} levels (Coelho *et al.*, 2008), again highlighting Ca^{2+}-ROS interactions.

1.5.5 eROS production and NOX proteins in red algae (Rhodophyceae)

NOX proteins have been described in five red algal species (*Chondrus crispus, Cyanidioschyzon merolae, Galdieria sulphuraria, Pyropia haitanensis, Pyropia yezoensis*) and have a unique NOX structure (Herve *et al.*, 2006; Luo *et al.*, 2015). Alongside conserved components such as the NADPH and FAD binding regions, these NOX proteins have 10 transmembrane domains (TMD) compared to six in plants, animals and fungi (Herve *et al.*, 2006; Luo *et al.*, 2015). EF hands are absent in red algal NOX proteins. Red algae *NOX* genes are upregulated following different environmental stimuli. Heat shock, mechanical damage, oligoagar (the red algal equivalent of oligosaccharides (Weinberger *et al.*, 1999)) or the bacterial flagellin Flg22 addition and high

salinity increase NOX mRNA expression in three different red algal species (Luo *et al.*, 2015; de Oliveira *et al.*, 2017; Wang *et al.*, 2018). Furthermore, NOX is involved in sexual reproduction of *Pyropia yezoensis*, with mRNA expression and eROS increasing during transition to the sexually reproducing phase (Uji *et al.*, 2020).

Red algal extracellular oxidative bursts occur following various stimuli including mechanical wounding in *Eucheuma platycaladum* (Collen & Pedersen, 1994), exposure of *Gracilaria conferta* to oligoagars, and addition of the epiphytic green alga *Acrochaete operculata* to *Chondrus crispus* gametophytes (Bouarab *et al.*, 1999). However, in *C. crispus*, the burst did not increase pathogen death but enhanced resistance to infection, suggesting a signalling role.

1.5.6 eROS production and NOX proteins in green algae (Chlorophyceae)

NOX and eROS production research has been limited to two green algal species. The unicellular microalga *Chlamydomonas reinhardtii* possesses two NOX homologues (Anderson *et al.*, 2011) responsible for constitutive extracellular superoxide production (Anderson *et al.*, 2016). These NOX proteins are structurally unusual, possessing only four TMDs in contrast to six in animal, plant, and fungal NOX. *C. reinharditii* superoxide production is enhanced with light intensity, potentially implicating involvement with photosynthesis. In addition, chemical inhibition of *C. reinharditii* NOX with DPI partially inhibits PCD activation suggesting a possible signalling role (Pérez-Pérez *et al.*, 2012). The macroalga *Dasycladus vermicularis* uses a likely NOX-derived oxidative burst as a part of the wound response (Ross *et al.*, 2005, 2006), though a NOX gene has not been identified.

1.5.7 eROS production and NOX proteins in marine phytoplankton

eROS production in unicellular algae has been recorded since the late 1980s (Palenik *et al.*, 1987; Palenik & Morel, 1988). Recent research efforts have focused on accurate quantification of per-cell ROS production and sampling more diverse species (Diaz & Plummer, 2018). Marine phytoplankton eROS production is widespread with dominant or bloom-forming microalgal species such as *Prochlorococcus*, *Synechococcus*, *Phaeocystis*, *Emiliania huxleyi*, *Karenia brevis* and *Chattonella marina* producing significant amounts of eROS (Diaz *et al.*, 2018; Sutherland *et al.*, 2019; Plummer *et al.*, 2019). Biologically-derived superoxide has been estimated to be a sink for 5-19% of the marine oxygen budget, with phytoplankton considered the most prominent source (Sutherland *et al.*, 2020). While eROS measurements are increasing, little is known of the distribution of NOX proteins in many of these lineages. However, the sensitivity of phytoplankton

eROS production to DPI may support NOX proteins as a source (Kim *et al.*, 2000; Kustka *et al.*, 2005; Saragosti *et al.*, 2010; Anderson *et al.*, 2016).

Harmful algal bloom (HAB) species produce higher amounts of eROS than non-harmful species (Diaz & Plummer, 2018). The HAB raphidophyte *C. marina* is the best studied species. *C. marina* has an exceptionally high eROS production rate (>10 pmol cell^{-1} hour^{-1} superoxide and H_2O_2) (Marshall *et al.*, 2005b; Diaz *et al.*, 2018), comprising both constitutive production and oxidative bursts (Oda *et al.*, 1994; Nakamura *et al.*, 1998). As a stramenopile alga, it may use a similar mechanism to diatoms. NOX proteins are implicated as the source of eROS in *C. marina* as DPI reduces eROS production and a NOX2 homologue was reported using Southern blot analysis (Kim *et al.*, 2000). Recent RNA-seq suggests the genetically similar *Chattonella antiqua* has six NOX proteins, with two possessing six TMDs and four possessing 11 TMDS (Shikata *et al.*, 2019). eROS in *C. marina* is implicated for many functions. Application of bacterial or fish metabolites increases eROS production and the eROS is thought to contribute to the toxicity of *C. marina* (Oda *et al.*, 1992, 1998; Nakamura *et al.*, 1998; Kim *et al.*, 2007). Other proposed functions include enhancing iron uptake (Garg *et al.*, 2007a; Liu *et al.*, 2007) and a link with light, as increasing light intensity enhances eROS production (Li *et al.*, 2015). However, photosynthesis inhibitors do not immediately affect production (Marshall *et al.*, 2002; Liu *et al.*, 2007) and production in darkness remains comparatively high (Diaz *et al.*, 2018). There is also support for eROS acting as a growth stimulant. Per-cell production decreases as cell density increases (Marshall *et al.*, 2005a; Diaz *et al.*, 2018) and production is higher in exponential phase cells than stationary phase cells (Oda *et al.*, 1995; Garg *et al.*, 2007b). Furthermore, addition of CAT and SoD disrupts *C. marina* morphology and growth rate (Oda *et al.*, 1995). This suggests eROS production is vital and may have a signalling role for regulating bloom dynamics (Marshall *et al.*, 2005a; Diaz & Plummer, 2018).

Dinoflagellate HAB species have high eROS production (>100 fmol cell^{-1} hour^{-1}) comparable to raphidophytes (Yamasaki *et al.*, 2004; Marshall *et al.*, 2005b; Mardones *et al.*, 2015; Diaz *et al.*, 2018). Like *C. marina*, this high production is proposed to contribute to their toxicity (Kim *et al.*, 1999) and per-cell production of HAB dinoflagellates reduces during stationary phase growth (Kim *et al.*, 1999). However, nontoxic *Symbiodinium* species also have high eROS production rates, possibly originating from a NOX protein (Mydlarz & Jacobs, 2004; Saragosti *et al.*, 2010). *Symbiodinium* eROS production is constitutive and increases in light (Saragosti *et al.*, 2010) but oxidative bursts also occur following sonic wounding (Mydlarz & Jacobs, 2004).

Finally, there have been isolated studies on other unicellular algal groups. *Emiliania huxleyi* produces constitutive levels of eROS, enhanced further by light intensity (Plummer *et al.*, 2019)

and viral infection (Evans *et al.*, 2006). The widespread cryptophyte *Geminigera* has high per-cell production (2-15 fmol cell^{-1} hour $^{-1}$) that decreases with cell density, again suggesting a signalling role (Sutherland *et al.*, 2019).

1.5.8 eROS production and NOX proteins in prokaryotes

eROS production and putative NOX proteins are widespread in terrestrial and marine bacteria (Diaz *et al.*, 2013; Hajjar *et al.*, 2017), with three of the most globally abundant marine bacteria (*Synechococcus*, *Prochlorococcus*, *Pelagibacter*) producing ROS constitutively (Sutherland *et al.*, 2019), likely contributing significantly to total biological eROS production in the oceans (Sutherland *et al.*, 2020). A NOX protein from cyanobacteria was recently used to determine the first crystal structure of NOX (Magnani *et al.*, 2017). Bacterial eROS production is linked with several functions. Several bacteria use extracellular superoxide to reduce Fe^{3+} to the more bioavailable Fe^{2+}, assisting iron uptake (Rose *et al.*, 2005; Rose, 2012; Roe & Barbeau, 2014; Hajjar *et al.*, 2017). However, this is not a universal function in marine bacteria (Wirtz *et al.*, 2010). In addition, *Trichodesmium* eROS production increases in light compared to darkness, while per-colony eROS production decreases as cell density increases (Hansel *et al.*, 2016).

1.5.9 eROS production and NOX proteins in marine diatoms

Diatom eROS production has been recorded in eight species (Table 1.1). Most research has focused on Thalassiosirales diatoms such as *Thalassiosira weissflogii*. Whilst cellular eROS production by *T. weissflogii* (0.25-1.4 fmol cell^{-1} hour^{-1}) is less than HAB species, including *Pseudo-nitzschia* sp. (Diaz *et al.*, 2018), it is relatively high compared to other non-harmful unicellular algae (Rose *et al.*, 2008; Schneider *et al.*, 2016). *NOX* gene sequences have been identified in three diatom species: *Phaeodactylum tricornutum*, *Thalassiosira pseudonana* and *Seminavis robusta*. Interestingly, *P. tricornutum* and *T. pseudonana* NOX proteins resemble red algae NOX proteins with 10 TMDs (Herve *et al.*, 2006; Anderson *et al.*, 2011). In *S. robusta,* a NOX protein was recently described with EF hands, resembling plant Rboh proteins (Bilcke *et al.*, 2020). The availability of diatom transcriptomes and genome resources has increased substantially in the last decade (Lommer *et al.*, 2012; Keeling *et al.*, 2014; Mock *et al.*, 2017; Osuna-cruz *et al.*, 2020) so there is an opportunity for wider NOX screening.

íá

Table 1.1 Literature reporting extracellular ROS production in diatoms.

Nt = not tested.

Species	Type of diatom	Increased eROS with light intensity?	Cited papers
Amphiprora kufferathii	Pennate	Y	(Hunken et al., 2008)
Coscinodiscus sp.	Centric	N	(Hansel et al., 2016)
Nitzschia epithemioides	Pennate	Y	(Waring et al., 2010)
Phaeodactylum tricornutum	Pennate	Y	(Laohavisit et al., 2015; Schneider et al., 2016)
Pseudo-nitzschia sp.	Pennate	Nt	(Diaz et al., 2018)
Thalassiosira oceanica	Centric	Y	(Schneider et al., 2016; Diaz et al., 2019)
Thalassiosira pseudonana	Centric	Y	(Kustka et al., 2005; Rose et al., 2008; Waring et al., 2010; Laohavisit et al., 2015; Schneider et al., 2016)
Thalassiosira weissflogii	Centric	Y	(Kustka et al., 2005; Rose et al., 2008; Milne et al., 2009; Schneider et al., 2016)

The function of diatom NOX-derived eROS is debated. A role for eROS promoting iron reduction and uptake, like some cyanobacteria, has been investigated in *T. pseudonana* and *T. weissflogii*. However, iron limitation has no effect on superoxide production (Kustka *et al.*, 2005; Rose *et al.*, 2008) and addition of SoD to remove superoxide does not affect Fe uptake rates (Kustka *et*

al., 2005). While diatom-derived superoxide can reduce Fe^{3+} to Fe^{2+}, the authors suggested Fe^{2+} quickly reoxidises to Fe^{3+} before cellular uptake (Kustka *et al.*, 2005). *S. robusta* NOX proteins were recently shown to be upregulated in one mating type during sexual reproduction (Bilcke *et al.*, 2020). Though eROS was not measured in the study, this implies a role for NOX-derived ROS signalling between different cells. Similarly, *Pseudo-nitzschia* per-cell eROS production decreases as cell density increases, suggesting a possible signalling role for ROS (Diaz *et al.*, 2018)

The most common parameter affecting eROS production in diatoms is light intensity. In six diatoms, increased light intensity leads to increased eROS (Table 1.1). In two species (*Amphiprora kufferathii, Nitzschia epithemioides*), the eROS is suggested to originate from increased photosynthetic ROS production, such as increased superoxide being formed through the Mehler reaction (Hunken *et al.*, 2008; Waring *et al.*, 2010). The superoxide dismutates to H_2O_2, which passes through cell membranes and exits the cell. However, there is evidence for NOX activity being responsible in other species. *NOX* gene homologues are present in *P. tricornutum* and *T. pseudonana* genomes (Herve *et al.*, 2006) and the NOX inhibitor DPI greatly reduces light-dependent eROS production in *P. tricornutum* and *T. weissflogii* (Kustka *et al.*, 2005; Laohavisit *et al.*, 2015). A more detailed characterisation of *P. tricornutum* NOX (Laohavisit *et al.*, 2015) showed that of its two NOX proteins, PtNOX1 is affected by the light regime. Continuous light increased *PtNOX1* gene expression after four days whereas *PtNOX2* expression was not significantly affected. Alongside this, *P. tricornutum* extracellular superoxide production increases in light and superoxide production correlates to the size of its chloroplast (Laohavisit *et al.*, 2015). This implies that diatom NOX proteins are involved with photosynthesis.

An alternative mechanism of eROS production was recently revealed in *Thalassiosira oceanica* (Diaz *et al.*, 2019). *T. oceanica* eROS production increases in light and is inhibited by DPI, resembling NOX activity. However, a glutathione reductase (GR) protein was shown to be responsible. Screening extracellular protein extracts of *T. oceanica*, a GR homologue was found to produce superoxide that could be inhibited by DPI. Furthermore, the homologue possessed TMD regions suggesting the protein is membrane bound. Adding glutathione disulphide (GSSG, the normal GR substrate) to the protein extract or live cells resulted in reduced superoxide, suggesting oxygen and GSSG can compete for substrate reduction. This raises important questions regarding the relative roles of GR and NOX proteins in the generation of eROS in marine phytoplankton.

1.6 The link between eROS production and light intensity

1.6.1 The diatom chloroplast and photosynthetic electron transport chain structure

A proposed explanation for the correlation of eROS production and light in unicellular algae is that it represents a protective photophysiology strategy by removing excess electrons in the photosynthetic ETC, thereby helping to balance the ATP: NADPH ratio (Davey *et al.*, 2003; Hansel *et al.*, 2016). A brief description of the ETC structure and function in the diatom chloroplast follows to assist understanding. The diatom chloroplast structure differs from higher plants. In diatoms, there are four envelope membranes as opposed to two in higher plants, stemming from a secondary endosymbiosis event. Within the chloroplast, thylakoid membranes are loosely stacked, normally in groups of three to form grana (Bedoshvili *et al.*, 2009; Flori *et al.*, 2017), contrasting the denser stacks of thylakoid membranes observed in higher plants (Grouneva *et al.*, 2013). As with other photosynthetic eukaryotes, the chloroplast functions to use light energy to fix CO_2 to organic compounds, using light-dependent and light-independent phases (Scarsini *et al.*, 2019). The light-dependent phase of photosynthesis takes place in the thylakoid membranes where the major photosynthetic protein complexes (photosystem II (PSII), cytochrome b_6f, photosystem I (PSI), ATP synthase) are localised. At PSII, the oxygen evolution complex splits water, providing electrons and protons. Light harvesting complexes in PSII and PSI absorb photons and transfer the associated energy to their respective reaction centres to excite electrons. Intermediary electron carriers such as plastoquinone's shuttle the excited electrons along the ETC stepwise from PSII to cytochrome b_6f to PSI. The electron flux is used to acidify the lumen, creating a ΔpH across the thylakoid membrane. ATP synthase uses this proton gradient to generate ATP. At the end of the ETC, ferredoxin-$NADP^+$ reductase uses the electron to reduce the terminal electron acceptor $NADP^+$ to NADPH. The generated ATP and NADPH can then be used in the chloroplast stroma for the light-independent phase. The Calvin-Benson-Bassham cycle consumes ATP and NADPH in a 3:2 ratio for CO_2 fixation. However, stoichiometry calculations suggest that linear electron flow creates typically lower ratios (2.5:2), creating a discrepancy in the required production of ATP for carbon fixation and other cellular processes. In addition, reduced availability of $NADP^+$ as an electron acceptor results in over-reduction of the photosystem. This can occur during high electron flow, enhancing electron leakage, ROS generation and oxidative stress (Yoshida *et al.*, 2007). It is therefore important for photosynthetic organisms to increase the ATP: NADPH ratio but not to use up electron acceptors.

1.6.2 Strategies to prevent photosystem over-reduction

Several mechanisms in plants and algae have been proposed to increase the ATP:NADPH ratio and prevent photosystem over-reduction (Forti *et al.*, 2003; Kramer & Evans, 2011; Cardol *et al.*, 2011). Cyclic electron flow (CEF) recycles electrons around PSI, creating the ∆pH across the thylakoid membrane required for ATP production without producing NADPH. Several pathways provide alternate electron sinks prior to acceptance by $NADP^+$ as this ensures $NADP^+$ availability but maintains the ∆pH for ATP production. This includes the Water-Water cycle where ferredoxin transfer electrons to oxygen instead of $NADP^+$, creating superoxide (Mehler reaction). The resulting superoxide is detoxified by SoD and CAT, creating water. Again, thylakoid ∆pH is maintained without producing NADPH. In plants, the malate–oxaloacetate (Mal–OAA) shuttle uses photosynthetically produced NADPH to reduce oxaloacetate to malate. Malate is consumed in the mitochondria, resulting in increased ATP. In plants this is not considered a significant contributor to balancing the ATP: NADPH ratio (Niyogi, 2000). However, diatoms use a similar strategy called metabolic coupling (Bailleul *et al.*, 2015). Here, chloroplast electrons are dissipated by shuttling excess reductant into the mitochondria to be consumed and ATP from the mitochondria can also be shuttled to the chloroplast. Compared to plants, diatom metabolic coupling is more frequently used to dissipate excess photosynthetic electrons during high light exposure (Broddrick *et al.*, 2019) but also improve the efficiency of mitochondrial and chloroplast electron flow under normal conditions (Bailleul *et al.*, 2015). The correlation of eROS production and light intensity could also support photoprotection. NOX may use excess NADPH to dissipate photosynthetic electrons by creating eROS. As diatoms are unicellular marine organisms, it may be assumed that the accumulation of ROS around their cells is less likely to occur than in multicellular organisms such as plants. Typically, oceanic steady state ROS concentrations reach pico-nanomolar concentrations (Zinser, 2018), which is tolerable for most diatoms (Drábková *et al.*, 2007; Hunken *et al.*, 2008; Graff van Creveld *et al.*, 2015). Therefore the risk of severe oxidative stress resulting from a build-up of biologically derived eROS is low and thus enzymatic eROS production could be a useful strategy to help balance the ATP: NADPH ratio.

Table 1.2 Summary of the range of functions of NOX-derived eROS.

NOX function	**Observed in**
Defence response	Animals, plants, brown algae, red algae, raphidophyte,
Cell wounding response	Animals, plants, green algae, dinoflagellates
Nutrient uptake	Raphidophytes, bacteria
Abiotic stress signalling	Animals, plants, brown algae, red algae

Redox signalling (sexual reproduction, PCD)	Animals, fungi, red algae, diatoms, green algae
Cellular differentiation	Fungi, slime moulds
Increased light intensity	Raphidophytes, dinoflagellates, coccolithophores, cyanobacteria, diatoms
Cell wall cross link promotion/ chemical synthesis	Animals, plants, brown algae, green algae
Growth stimulant	Raphidophyte, dinoflagellates, crytophytes, cyanobacteria, diatoms

1.7 General conclusions and aims of the thesis

From examining the literature, there are several trends apparent. Though best characterised in animals, plants and fungi, NOX proteins are widespread amongst eukaryotes and have a diverse range of functions (Table 1.2). Organism defence is a well-studied, common function but NOX and its derived eROS are frequently used in signalling pathways. Large genomic databases and genetic transformations allow reliable phenotype identification such as greater pathogen susceptibility or compromised cellular growth. Algal eROS production rates and its derived functions are diverse between species. Similarly, algal NOX proteins are structurally diverse but have received limited characterisation, particularly in unicellular algae. Identification of NOX protein functions has often relied on DPI inhibition but molecular tools such as gene expression analysis can add new insights. Interestingly, diatoms have alternate mechanisms for generating eROS, through GR proteins (Diaz *et al.*, 2019) so diatom eROS production may not originate necessarily from NOX proteins. Finally, oxidative bursts in microalgae are rare, with constitutive production of eROS more common. Additionally, the correlation of light intensity to eROS production has only been reported in marine phytoplankton. This relationship may relate to electron dissipation but has not been investigated fully. This thesis used these identified trends and knowledge gaps to guide the investigations in the following chapters.

Chapter 2: What is the wider distribution of NOX proteins in marine diatoms?

This Chapter exploited the recent increase in diatom genomic and transcriptomic datasets to screen diatoms for the presence of NOX or GR proteins. NOX proteins were hypothesised to be more abundant than GR proteins amongst diatoms. In addition, attempts were made to identify any sequence motifs or residues that could assist future identification of NOX proteins.

Chapter 3: How does light affect eROS production and plasma membrane electron transport in different diatom species?

This Chapter used OxyBURST Green and potassium ferricyanide assays to explore the differences in eROS production and plasma membrane electron transport between three diatom species. It was expected that there would be significant differences between species, and differences in eROS production would be reflected in changes to plasma membrane electron transport. Furthermore, the effect of light was investigated on the respective assays, with increased light intensity expected to correlate with increased eROS production in the three species.

Chapter 4: How does *Phaeodactylum tricornutum* respond to different levels of exogenous addition of H_2O_2?

This Chapter attempted to genetically transform *P. tricornutum* with different redox biosensors to allow monitoring of changes in redox state dynamics. Following successful transformation, the tolerance of *P. tricornutum* to differing concentrations of H_2O_2 was tested by measuring changes to cellular parameters, including growth and photophysiology.

Chapter 5: What is the role of NOX in the model diatom Phaeodactylum tricornutum?

Phytoplankton eROS production is significantly affected by light levels, implicating a functional involvement with photosynthesis. This Chapter investigated the function of NOX proteins in *P. tricornutum* by measuring changes in cellular parameters following application of a chemical inhibiter of NOX. It was hypothesised that photosynthetic parameters would be highly susceptible to NOX inhibition, reflecting NOX involvement in photosynthesis. The effects of metabolic inhibitors of respiration and photosynthesis were also measured, focussing on resultant changes to cell redox state.

Chapter 2 The unusual phylogeny and structure of diatom NOX proteins

2.1 Introduction

NADPH oxidase (NOX) proteins are a group of enzymes characterised by their unusual function of producing extracellular reactive oxygen species (ROS) such as superoxide (O_2^-) or hydrogen peroxide (H_2O_2). NOX proteins are highly studied in humans, with seven distinct proteins described: NOX1-5 and Dual oxidase (DUOX) 1-2 (Bedard & Krause, 2007). The human NOX2 protein structure is well characterised due to the importance of NOX2 in the human immune response. The core protein components are the six N-terminus transmembrane regions, with haem groups present in the third and fifth transmembrane domains (TMDs), and FAD and NADPH binding sites at the C-terminus (Sumimoto, 2008). When activated, NADPH binds to the protein and donates an electron. The electron is shuttled through the enzyme to the FAD domain and across the membrane via the haem groups, where it reduces extracellular molecular oxygen to superoxide (Sumimoto, 2008). Different human NOX proteins have structural variations. NOX5 possesses an EF hand domain, allowing interaction with intracellular calcium (Ca^{2+}) for signalling pathways (Guzik *et al.*, 2008), while DUOX proteins have EF hands and peroxidase regions, and produce extracellular H_2O_2 (Donkó *et al.*, 2005).

Despite initial suggestions (Lalucque & Silar, 2003), NOX proteins are widespread, occurring in plants (Kaur *et al.*, 2018), fungi (Grissa *et al.*, 2010), red algae (Herve *et al.*, 2006), green algae (Anderson *et al.*, 2011), diatoms (Anderson *et al.*, 2011; Laohavisit *et al.*, 2015), cyanobacteria, (Magnani *et al.*, 2017) and bacteria (Hajjar *et al.*, 2017). Nonetheless, NOX proteins are not ubiquitous, as they can be absent in lineages such as Rhizaria or individual species within lineages (Sumimoto, 2008; Zhang *et al.*, 2013; Gandara *et al.*, 2017). NOX proteins within different lineages can have structural differences to the classic human NOX2 structure. Plant NOX proteins, also called respiratory burst oxidase homologues (Rboh), have EF hands like NOX5 (Marino *et al.*, 2012). Depending upon the species, fungal NOX proteins may also possess EF hands (Takemoto *et al.*, 2007). Algal NOX proteins have received limited research but display significant structural differences in the number of TMDs. In contrast to the traditional six TMDs, red algae NOX proteins possess 10 TMDs (Herve *et al.*, 2006), whereas the green alga *Chlamydomonas reinharditii* NOX only has four TMDs (Anderson *et al.*, 2011). Structurally different NOX proteins (e.g. Rboh, red algae, NOX1-4, DUOX1-2) have separate phylogenetic clustering (Kawahara *et al.*, 2007; Gandara *et al.*, 2017; Kaur *et al.*, 2018) which suggests a diversification of NOX protein structure and function between different lineages.

Ferric reductase (FRE) proteins are closely related to NOX proteins. They also have six TMDs, the TMD3 and TMD5 haem groups, and FAD and NADPH binding sites (Sumimoto, 2008; Zhang *et al.*, 2013). However, the target substrate differs as FRE proteins use donated electrons to reduce Fe^{3+}

to Fe^{2+}, assisting iron uptake (Zhang *et al.*, 2013). Though there can be structural differences between NOX and FRE, such as some NOX proteins possessing EF hands, the large structural similarity creates difficulties in distinguishing whether a sequence codes a putative NOX or FRE protein. For example, a NOX identification algorithm unintentionally included FRE proteins (Hajjar *et al.*, 2017) while experimental testing of presumed FRE proteins in unicellular fungi demonstrated derived superoxide generation, supporting a NOX identity (Rinnerthaler *et al.*, 2012; Rossi *et al.*, 2017). Thus, experimental validation has typically been required to confirm a putative NOX or FRE protein (Waters *et al.*, 2002; Jain *et al.*, 2014; Rossi *et al.*, 2017). Recently, the first atomic crystal structure of a NOX protein was published (Magnani *et al.*, 2017) and highlighted three amino acid residues (Arg256, His313 and His317) that are predicted to combine to form a cavity for oxygen reduction. This cavity may determine the respective targets of NOX and FRE proteins. Examining how conserved these amino acid residues are could improve accuracy for identifying putative NOX or FRE proteins from sequences.

Putative diatom NOX proteins have been identified in three species: *Phaeodactylum tricornutum*, *Seminavis robusta* and *Thalassiosira pseudonana.* The proteins in *P. tricornutum* and *T. pseudonana* resemble red algal NOX proteins, possessing 10 TMDs (Anderson *et al.*, 2011) and eROS production has been recorded in several diatoms, including *P. tricornutum* and *T. pseudonana* (Laohavisit *et al.*, 2015; Hansel *et al.*, 2016; Schneider *et al.*, 2016; Diaz & Plummer, 2018). Whilst NOX function in diatoms has not been well characterised, some evidence suggests increased light duration can alter *NOX* gene expression in *P. tricornutum* (Laohavisit *et al.*, 2015).

NOX proteins are well characterised and therefore the most likely enzymatic candidate for diatom eROS production. However, a recent proteomics approach showed extracellular superoxide in *Thalassiosira oceanica* originates from glutathione reductase (GR) proteins located in the plasma membrane (Diaz *et al.*, 2019). This suggests other proteins contribute to extracellular superoxide production in diatoms. Large differences exist in per-cell eROS production between different diatoms (Schneider *et al.*, 2016). Different diatoms may have different enzymes responsible for eROS production or use eROS production to different extents. The phylogenetic distribution of diatom NOX has not been studied. Whilst the availability of fully sequenced diatom genomes remains limited (Armbrust *et al.*, 2004; Bowler *et al.*, 2008; Lommer *et al.*, 2012), a large-scale transcriptome project (Marine Microbial Eukaryote Transcriptome Sequencing Project, MMETSP) has created gene expression data for >60 diatom species (Keeling *et al.*, 2014).

The increased availability of diatom genetic data allows focused research into the diversity of different eROS producing enzymes. Here, the presence and diversity of diatom NOX and GR proteins was investigated by characterising their structure and phylogeny. Comparing diatom NOX

diversity to existing NOX proteins revealed a large diversity and abundance in diatom NOX proteins with intriguing evolutionary implications. Alongside this, conserved motifs between NOX proteins were explored to assist future attempts to identify NOX proteins.

2.2 Methods

2.2.1 Confirmation of P. tricornutum NOX

Candidate *P. tricornutum* and *T. pseudonana NOX* gene sequences have been described previously (Herve *et al.*, 2006; Anderson *et al.*, 2011; Laohavisit *et al.*, 2015). Using red algal sequences as a query, the *P. tricornutum* genome available in the Joint Genome Institute (JGI, https://jgi.doe.gov/) was searched for the two *NOX* genes reported in Laohavisit et al. (2015) and are described henceforth as PtNOX1 and PtNOX2. Expression levels of the *NOX* genes, alongside *P. tricornutum FRE* genes, were then investigated in several available transcriptome databases (Allen *et al.*, 2008; Sapriel *et al.*, 2009; Ovide *et al.*, 2018) and the diatom EST database (http://www.diatomics.biologie.ens.fr/EST3/index.php).

2.2.2 Screening of diatom NOX and glutathione reductase (GR) sequences

A sequence similarity search was used to investigate the distribution of diatom NOX and GR proteins. The amino acid sequence derived from PtNOX1 (accession number XP_002179812.1) was used as the protein query sequence for NOX screening and ToGR1 (accession number EJK45974), identified by Diaz et al. (2019), was the query for GR. The genomes of *T. pseudonana*, *T. oceanica*, *Fragilariopsis cylindrus*, *Pseudo-nitzshia multistrata* and *Fistulifera solaris* were searched using NCBI BLASTP. The draft genome of *Pseudo-nitzshia multiseries* was searched using JGI while Gust Bilcke (Ghent University, Belgium) kindly supplied access to the *Semiavis robusta* genome from the *Semiavis robusta* genome sequencing project (Osuna-cruz *et al.*, 2020). From the MMETSP database, 55 diatom species transcriptomes were retrieved and searched. Diatoms were taxonomically classified as araphid pennate, raphid pennate, polar centric or radial centric. For sequence mining, an initial cut off value of 1E-10 was established to filter out radically different sequences. Databases were also searched using *Arabidopsis thaliana* Rboh-F (accession number NP_564821.1) and *A. thaliana* Ferric Chelate-Reductase 2 (accession number NP_001322968.1) as a query to improve confidence in putative NOX sequence hits. Hits demonstrating greater similarity to Ferric Chelate Reductase 2 than PtNOX1 were disregarded. The selected sequences were then manually inspected using multiple sequence alignments in Bioedit 7.2.6, and for protein sequence functional domain analysis using Interpro (http://www.ebi.ac.uk/interpro/, (Mitchell *et al.*, 2018)).

For GR analysis, NCBI and MMETSP databases were searched for sequence homologues within diatoms, plants, humans and algae. Diatom species searched included species with and without confirmed NOX proteins to allow comparison to GR distribution. As with Diaz et al., (2019)

transmembrane predictions were made using Phobius (http://phobius.sbc.su.se/). If graphical display of posterior label probability for transmembrane domain exceeded 0.5 (scale of 0-1) and matched with computer prediction for transmembrane domains, the protein was considered to have a transmembrane region.

2.2.3 Phylogenetic analysis

To understand the evolution of diatom NOX proteins, diatom protein sequences were aligned against other major groups of NOX proteins. Previously established NOX sequences utilised by Kawahara et al. (2007) were included alongside more recently identified oomycete and other algal sequences. All sequences were acquired from NCBI or JGI. FRE proteins were also used in this tree, using sequences from Zhang et al. (2013). GR proteins were obtained from a range of species in NCBI. For NOX and GR phylogenetic analysis, sequences were aligned using the T-Coffee Expresso algorithm (Tommaso *et al.*, 2011). The alignment was then manually edited in Bioedit to remove gaps. Phylogenetic trees were made using the Maximum Likelihood method in MEGA7.

2.3 Results

2.3.1 Identification of NOX proteins in P. tricornutum

It was important to confirm whether previously proposed *P. tricornutum* sequences encode for NOX proteins rather than FRE proteins. Two proteins were found in the JGI *P. tricornutum* genome with significant similarity to established red algal NOX proteins. These two proteins matched sequences described by Laohavisit et al (2016). However, in the JGI database, these proteins are annotated as FRE4 and FRE5. Expression levels of hypothetical *PtNOX1-2* and *PtFRE1-3* were compared in several published datasets. *PtFRE1-3* transcripts are highly expressed in iron limiting conditions (Allen *et al.*, 2008), resembling the typical expression patterns of *FRE* gene expression in plants and fungi (Jain *et al.*, 2014; Saikia *et al.*, 2014). *PtNOX1-2* genes are not upregulated in iron limiting conditions (Table 2.1). The same result occurred in the *P. tricornutum* EST dataset, where *PtFRE1-3* ESTs were identified more frequently in iron limiting conditions (Fig 2.1.) This experimental evidence, alongside similarity to red algal NOX protein sequences, indicates that FRE4-5 were mis-annotated and should be renamed PtNOX1-2 respectively. Gene expression levels in other datasets show other differences between FRE and NOX proteins in *P. tricornutum*. Notably, *PtNOX1* is upregulated when the cells are in the oval morphotype, compared to fusiform or triradiate form (Ovide *et al.*, 2018). In the EST dataset, *PtNOX1* is highly expressed in the tropical strain Pt9, while *PtNOX2* is most highly expressed following decadienal treatment.

Table 2.1 Comparison of transcript expression levels of *PtFRE1-3* and *PtNOX1-2* in *P. tricornutum*.

Numerical values indicate fold level increase of gene expression from real time-qPCR. - indicates no reported change in gene expression.

Gene	JGI Protein ID	Iron Limitation (Allen et al. 2008)	Morphotype (Ovide et al. 2018)	Silicon Limitation (Sapriel et al., 2009)
FRE1	54486	100	-	2.75
FRE2	46928	100	-	7.10
FRE3	54940	10-100	-	
FRE4 (*PtNOX1*)	54409	-	2.8	-
FRE5 (*PtNOX2*)	55631	-	-	-

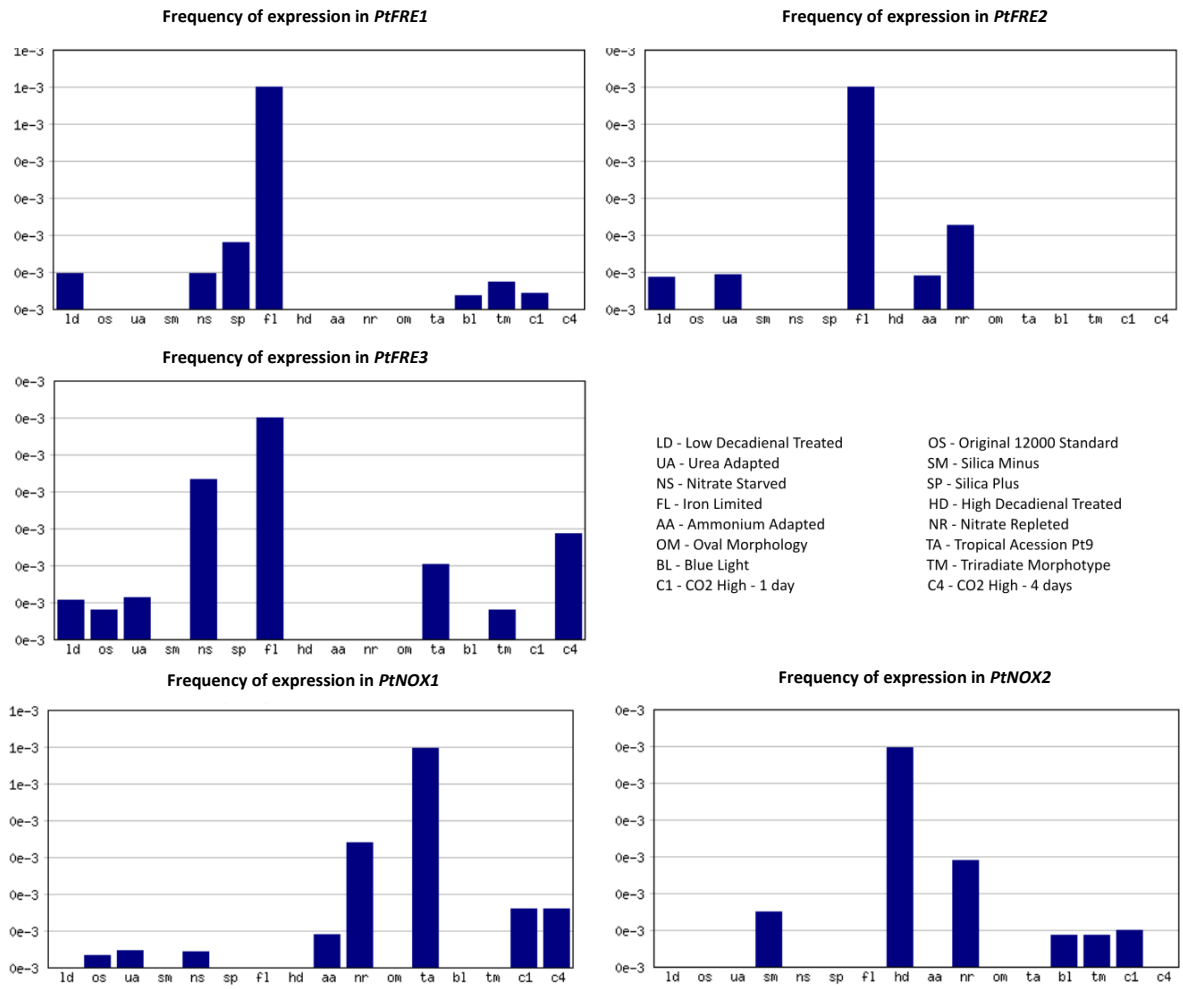

Figure 2.1 Frequency of *P. tricornutum FRE* and *NOX* genes under different environmental conditions in EST libraries.

Graphs are taken directly from EST database (http://www.diatomics.biologie.ens.fr/EST3/index.php) and combined for this figure. *PtNOX1* and *PtNOX2* are annotated as FRE4 and FRE5 in JGI database.

2.3.2 Distribution of NOX proteins

Using PtNOX1 as a protein search query, seven diatom genomes and 55 transcriptomes were screened for NOX homologues. 155 sequences had hits to PtNOX1. Manual inspection of aligned sequences and analysis of protein domain organisation filtered these sequences down to 52 putative NOX proteins from 31 diatom species (Table 2.2., list of all species searched in Appendix A1). NOX proteins were distributed between all four taxonomic subgroups of diatoms. NOX proteins were found in all seven fully sequenced diatom genomes. Diatom NOX proteins were most frequently found in pennate diatoms (Table 2.2). Most pennate diatoms possessed a single NOX protein but several raphid pennates possessed two or more. *S. robusta* had the highest number of NOX proteins in a single species with five (Appendix A1).

2.3.3 Types of NOX protein

Phylogenetic and structural analysis of NOX proteins revealed a divergence in the types of NOX proteins (Table 2.3, Fig 2.2). Therefore, the NOX proteins were classified into four groups: Class 1, Class 2, Class 3, and NOX-like. Diatom proteins were present in all four groups, unlike any other examined lineage (Table 2.3, Fig 2.2). Two diatoms (*Asterionellopsis glacialis*, *Amphipora* sp.) and one green alga (*Klebsormidium nitens*) had NOX proteins from multiple Classes (one Class 1 and one Class 3 NOX protein).

Table 2.2 The abundance of NOX proteins differs between the four taxonomic groups.

Each diatom species screened was categorised by its taxonomic classification (araphid pennate, raphid pennate, polar centric and radial centric). NOX protein abundance was recorded within each taxonomic group.

Taxonomic group	**Species searched**	**Total NOX proteins obtained**	**Species with NOX proteins**	**Species without NOX proteins**	**% of species searched possessing a NOX protein**
Araphid pennate	9	10	7	2	77%
Raphid pennate	19	26	14	5	73%
Polar centric	26	14	10	16	38%
Radial centric	9	2	2	7	22%

Table 2.3 The distribution of each Class of diatom NOX protein differs between the four diatom taxonomic groups.

From the NOX protein screen, the abundance of each Class of NOX protein is reported within each diatom taxonomic group.

Type of NOX Class	**Diatom Taxonomic Group**				**Total number of NOX proteins per Class**
	Araphid pennate proteins	**Raphid pennate proteins**	**Polar centric proteins**	**Radial centric proteins**	
Class 1	4	5	2	1	12
Class 2	0	19	1	0	20
Class 3	6	2	7	1	16
NOX-like	0	0	4	0	4

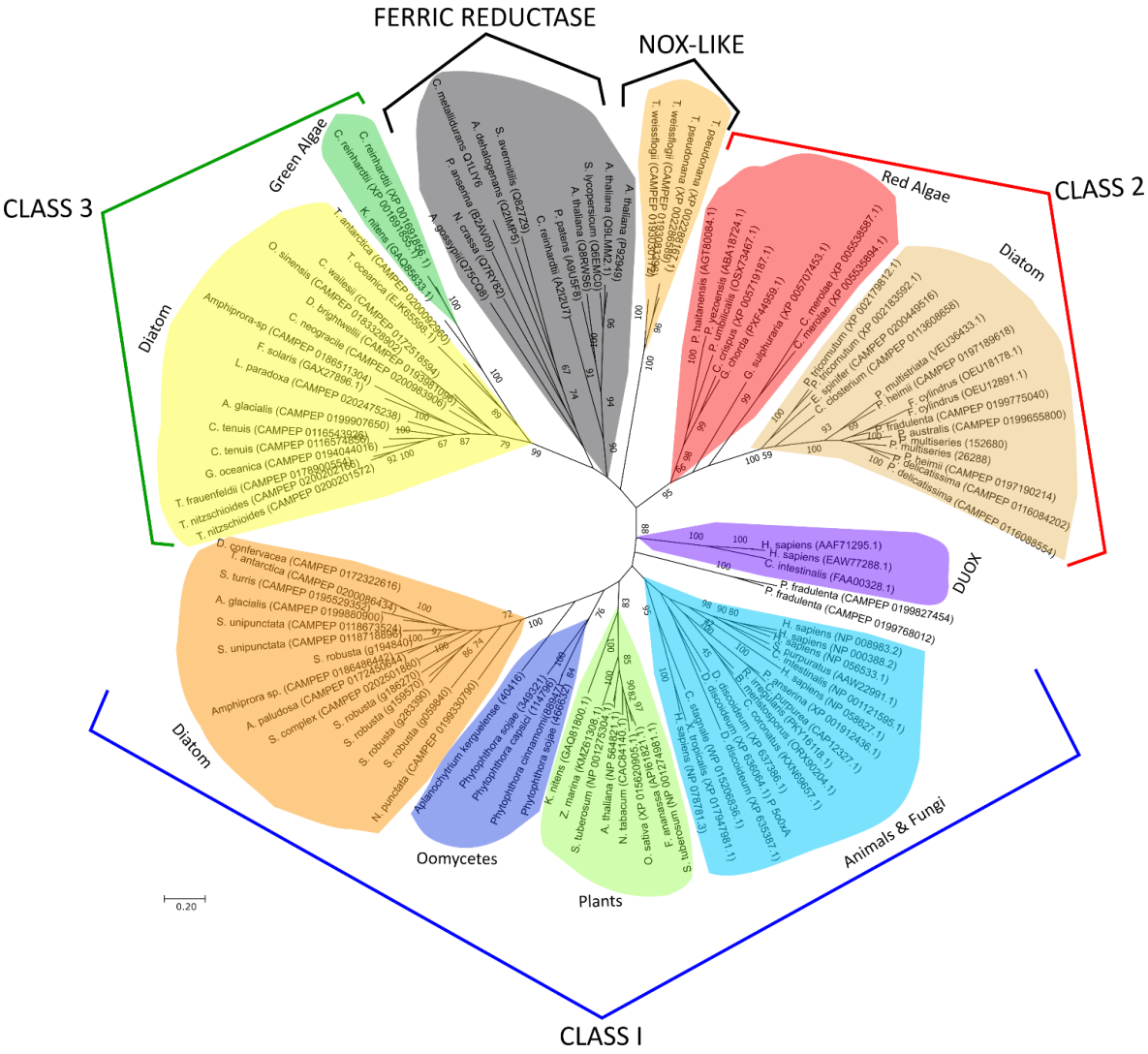

Figure 2.2 Phylogenetic tree of NOX proteins in eukaryotes.

Protein sequences were aligned using T-Coffee Espresso (Tommaso *et al.*, 2011) prior to creation of the phylogenetic tree in MEGA7 . The phylogenetic analysis was performed using the Maximum Likelihood method based on the Poisson correction (Zuckerkandl & Pauling, 1965). The tree with the highest log likelihood (-49926.71) is shown. Initial tree(s) for the heuristic search were obtained automatically by applying Neighbor-Joining and BioNJ algorithms to a matrix of pairwise distances estimated using a JTT model, and then selecting the topology with superior log likelihood value. The tree is drawn to scale, with branch lengths measured in the number of substitutions per site. The analysis involved 109 protein sequences. All positions with less than 95% site coverage were eliminated. That is, fewer than 5% alignment gaps, missing data, and ambiguous bases were allowed at any position. Each sequence contained 297 positions in the final dataset. Evolutionary analyses were conducted in MEGA7 (Kumar *et al.*, 2016). Bootstrap values below 65 are not shown for clarity.

2.3.3.1 Class 1 NOX proteins composition and structure

Class 1 sequences contained well-characterised human, plant and fungal NOX proteins alongside diatoms, oomycetes (stramenopile water moulds) and one green alga sequence (Fig 2.2). Class 1 diatom proteins grouped close to oomycetes and plants. The proteins resembled the classical structure of NOX proteins: six transmembrane regions and core central regions including FAD binding site, riboflavin-synthase beta barrel and the ferric reductase transmembrane component-like domain (Fig 2.3.). Class 1 diatom proteins possessed 1-3 EF hands, also seen in plant Rboh, oomycete NOX, human NOX5 and DUOX, and several fungal NOX proteins. Two proteins from *P. fradulenta* were exceptions as these proteins did not group with other Class 1 diatom NOX proteins, grouping closer to DUOX proteins. Interpro structure analysis revealed these proteins possess six TMDs and the core NOX structure, but no EF hands or peroxidase region as seen in DUOX proteins. However, the sequences originate from a transcriptome database, so the additional domains could be missing due to incomplete transcripts. Diatom Class 1 proteins were present in all taxonomic groups, though more proteins originated from pennate diatoms (Table 2.3).

2.3.3.2 Class 2 NOX proteins composition and structure

Class 2 NOX proteins were restricted to diatom and red algal NOX proteins, and included PtNOX1-2 from *P. tricornutum*. Class 2 proteins possess 10 TMD regions alongside the core conserved regions (FRT, FR-FAD, FAD-8, RBS, FNR, NAD, Fig 2.3). Class 2 diatom proteins were slightly different to red algal NOX, possessing no ferric reductase transmembrane component-like domain (Fig 2.3). Interestingly, NOX from unicellular red algae *Galdieria sulphuraria* and *Cyanidioschyzon merolae* also had no FRT region, yet this domain was present in NOX from multicellular red algae. Apart from one exception (the polar centric *Extubocellulus spinifer*), Class 2 diatoms were predominately from raphid pennate diatoms (Table 2.3).

2.3.3.3 Class 3 NOX proteins composition and structure

Class 3 NOX proteins were restricted to diatom and green algal lineages. This group is phylogenetically distinct from Class 1 and Class 2 NOX proteins and represents a poorly characterised group of NOX proteins. There were structural similarities to Class 1 NOX proteins, as all possessed the conserved core components (Fig 2.3). Diatoms also had six TMDS, though the green alga *C. reinharditii* only had four, in line with previous work (Anderson *et al.*, 2011). Class 3 NOX proteins were evenly sourced between centric and pennate diatoms, contrasting Class 1 and 2 proteins that were predominantly originating from pennate diatoms (Table 2.3).

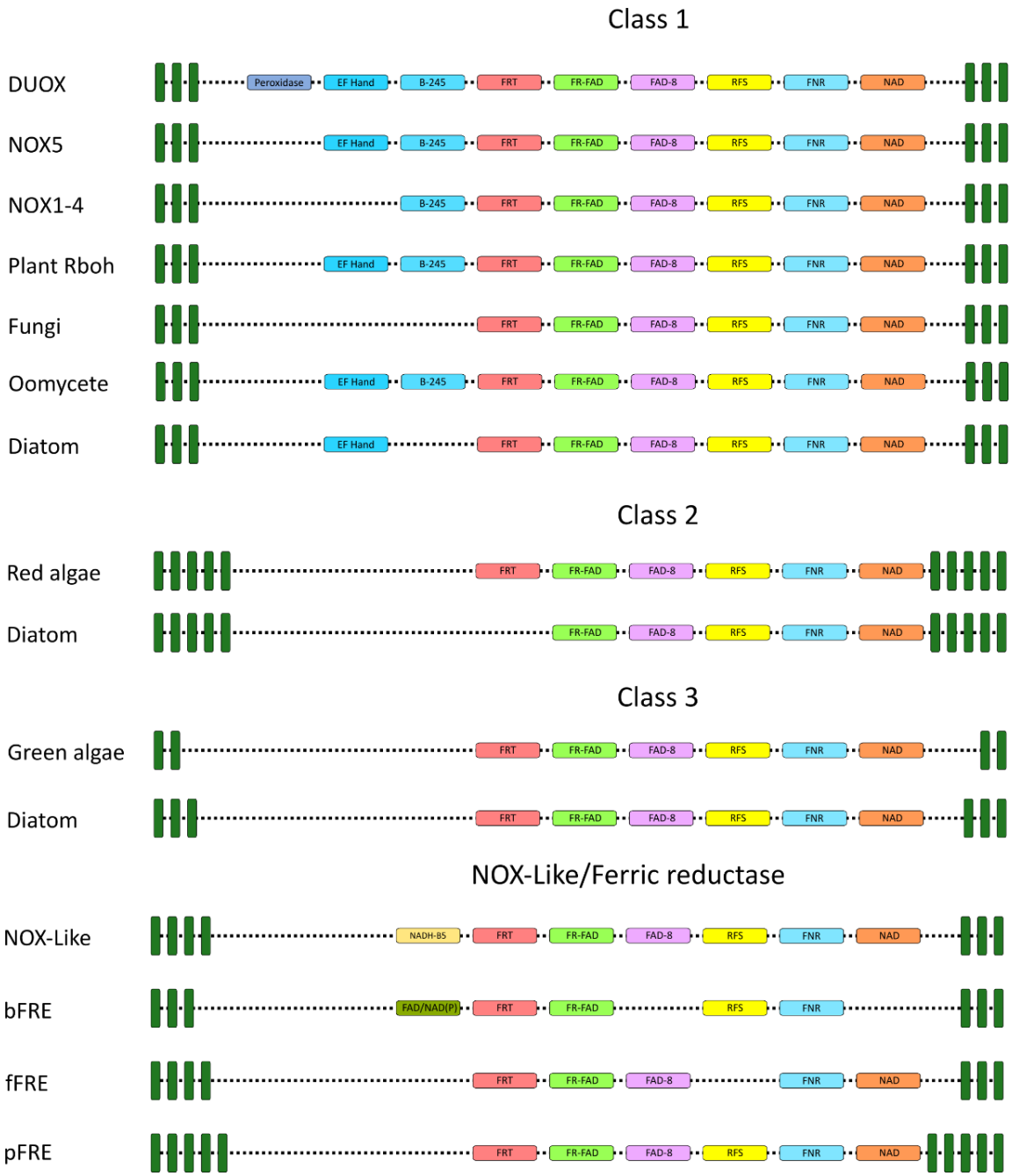

Figure 2.3 Comparison of conserved structural domains between NOX Classes and FRE proteins.

The protein domains are taken from Interpro sequence analysis. Diagram does not indicate precise order of domains within each protein but represents a comparison between conserved domains. bFRE = bacterial ferric reductase, fFRE= fungi ferric reductase and pFRE = plant ferric reductase. Peroxidase= Haem peroxidase. EF Hand= EF Hand domain. B-245 =Cytochrome b245, heavy chain. FRT= Ferric reductase transmembrane component-like domain. FR-FAD= FAD-binding domain, ferredoxin reductase-type. FAD-8= FAD Binding 8. RBS= Riboflavin-synthase beta barrel. FNR=

Ferredoxin-NADP reductase (FNR), nucleotide-binding domain. NAD= Ferric reductase, NAD Binding domain. NADH-B5= NADH: cytochrome b5 reductase-like. FAD/NAD(P)= Oxidoreductase FAD/NAD(P)-binding. Green cylinders represent transmembrane domains (TMD).

2.3.3.4 NOX-like and FRE proteins composition and structure

Four diatom proteins from *T. pseudonana* and *T. weissflogii* were classified as NOX-like due to their unusual structure and phylogeny. These proteins resemble NOX proteins with conserved core components and seven TMDs. However, NOX-like proteins possess an additional NADH: cytochrome b5 reductase-like domain. Searching the genome of *T. pseudonana* resulted in no other NOX proteins. This contrasts with previous work suggesting this species has two NOX proteins, each containing 10 TMDs, in the genome (Herve *et al.*, 2006; Anderson *et al.*, 2011). The gene encoding a NOX-like protein in *T. weissflogii* was found in its transcriptome database. This group was closely aligned to plant, bacterial and fungal FRE proteins (Fig 2.2). There were structural differences between FRE and NOX-like proteins. Bacterial and fungal FRE proteins had 6-7 TMDs alongside reduced core conserved regions, lacking FAD Binding 8, Riboflavin-synthase beta barrel or the Ferric reductase, NAD Binding domain (Fig 2.3). Plant FRE possessed the conserved domains with 10 TMDs. No known existing NOX or FRE protein contains the NADH: cytochrome b5 reductase-like domain. However, *T. pseudonana* and *T. weissflogii* produce eROS, inhibited with DPI (Davey *et al.*, 2003; Laohavisit *et al.*, 2015). Without experimental evidence, it is difficult to confirm whether these proteins function as a NOX, FRE or have an alternate function. Though they group closely with FRE proteins, these proteins are described as NOX-like, rather than FRE or NOX.

2.3.4 NOX protein conserved motifs and residues

The different NOX proteins were examined for the presence of key protein motifs and conserved amino acid residues to assist future identification of NOX proteins. Eight possible identification motifs were examined (Fig 2.4, Table 2.4). These were Arg256, His313 and His317, referring to position in NOX5 in *C. stagnale* (Magnani *et al.*, 2017), Thr178 and Gly179, referring to position in human NOX2 (Zhang *et al.*, 2013), the TMD3 and 5 amino acid gap (13 amino acids separate the two histidine residues at TMD3, 12 separate the histidine residues in TMD5, (Sumimoto, 2008)) and a new motif identified here as the double histidine associated with TMD5 (Fig 2.4). Of the eight described motifs, two (His313, Gly179) were present in every investigated sequence, including FRE sequences. One motif (Thr178) was absent from FRE proteins but present in almost all proposed NOX or NOX-like sequences. In *C. stagnale* and Class 3 NOX-containing diatoms, it

was replaced by a structurally similar serine amino acid. Of the remaining motifs, there were small patterns but there was no universal distribution, summarised in Fig 2.4 and Table 2.4. Notably, Arg256 was absent in Class 3 NOX containing diatoms, NOX-like proteins and the bacterial and plant FRE. It was present in all other NOX proteins and fungal FRE. Arg256 was also occasionally replaced by the structurally similar lysine amino acid while His317 was only present in Class 1 proteins and multicellular red algae. Thus, Arg256 and His317 cannot be considered reliable motifs to identify NOX proteins as previously proposed (Magnani *et al.*, 2017).

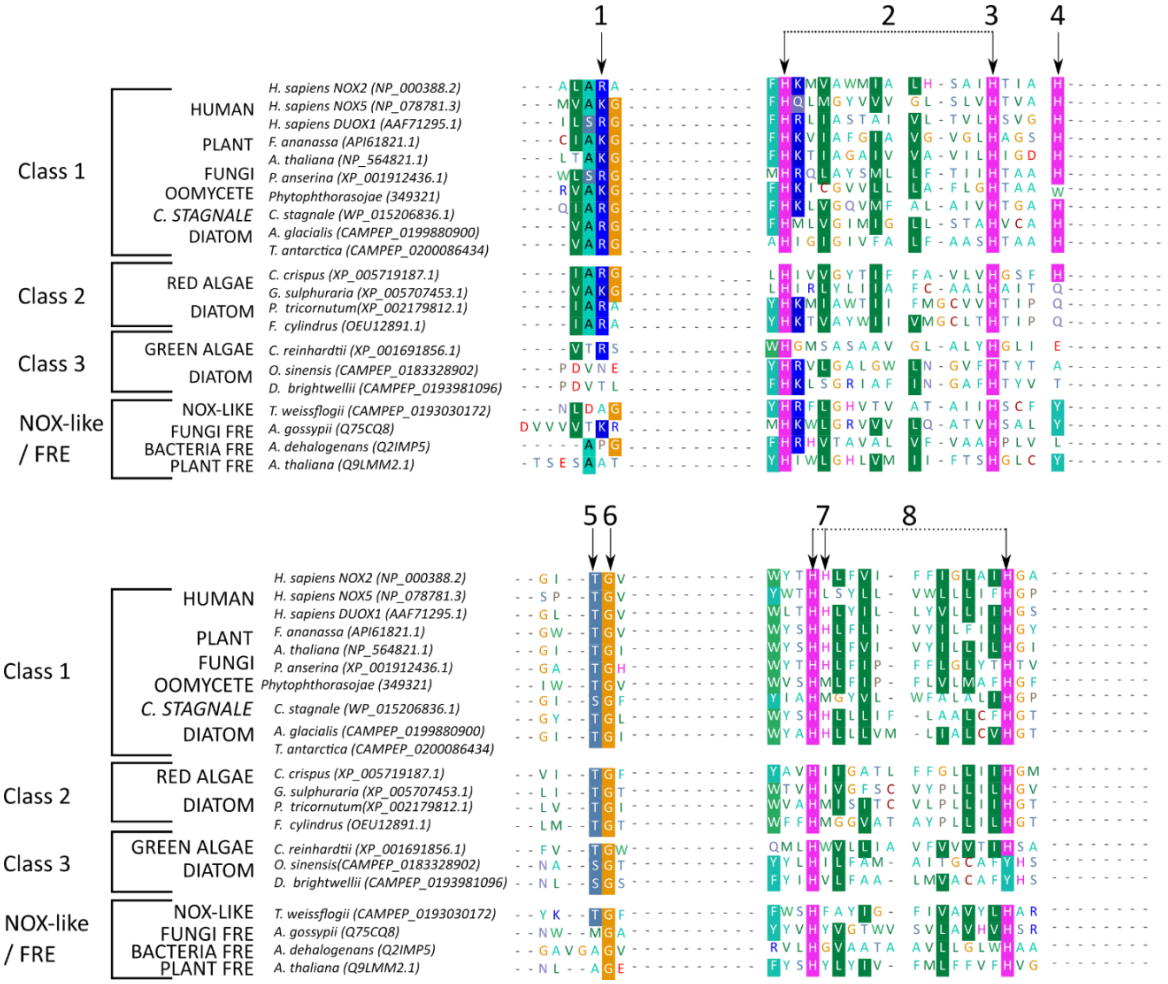

Figure 2.4 Comparison of the conserved motifs between different NOX and FRE proteins.

Figure shows Arg256 (1), the amino acid gap of TMD3 (2), His313 (3), His317 (4), Thr178 (5), Gly179 (6), the double histidine of TMD5 (7) and the amino acid gap of TMD5 (8). The sequences presented here have been manually trimmed to assist the display of conserved motifs.

Table 2.4 Comparison of conserved motifs between NOX and FRE sequences.

Transmembrane gap refers to the number of amino acids between the two histidine residues in 3rd and 5th transmembrane regions respectively. For example 13:12 indicates a 13 amino acid gap in TMD3 and 12 in TMD5. Yellow boxes in Arg256 and Thr178 indicate replacement with chemically similar amino acids. Lys= lysine. Ser= serine.

	Arginine 256	**Histidine 313**	**Histidine 317**	**Threonine 178**	**Glycine 179**	**Transmembrane 3:5 amino acid gap**	**Transmembrane 5 double histidine**
Human NOX2	Y	Y	Y	Y	Y	13:12	Y
Human NOX5	N-Lys	Y	Y	Y	Y	13:12	N
Human DUOX	Y	Y	Y	Y	Y	13:12	Y
Plants	N-Lys	Y	Y	Y	Y	13:12	Y
Fungi	Y	Y	Y	Y	Y	13:12	Y
C. stagnale	Y	Y	Y	N-Ser	Y	13:12	N
Oomycete	N-Lys	Y	Y	Y	Y	13:12	N
Diatom Class 1	Y	Y	Y	Y	Y	13:12	Y
Red algae	Y	Y	Y	Y	Y	13:13	N

Diatom Class 2	Y	Y	N	Y	Y	14:13	N
Green Algae (*Chlamydomonas*)	Y	Y	N	Y	Y	13:13	N
Diatom Class 3	N	Y	N	N-Ser	Y	13:13	N
NOX-like	N	Y	N	Y	Y	13:12	N
Fungi FRE	Y	Y	N	N	Y	13:13	N
Bacteria FRE	N	Y	N	N	Y	13:13	N
Plant FRE	N	Y	N	N	Y	13:13	N

2.3.5 GR phylogeny

Recently, GR proteins in *T. oceanica* were demonstrated to produce eROS (Diaz *et al.*, 2019). The present study investigated whether there was a link between the presence of GR proteins and NOX distribution. Broadly, GR proteins split into two separate groups, which are referred to as Group 1 and Group 2 (Fig 2.5). Group 1 is composed of GR proteins from plants, red algae, and diatoms while Group 2 comprises animal, brown algae, coccolithophore and diatom sequences. Most diatoms screened possessed GR proteins from both groups (Table 2.5). However, there were exceptions. *F. solaris*, *Nitzschia punctata*, *P. tricornutum* and *Rhizosolenia setigera* had proteins from Group 1 while *T. oceanica*, *Thalassiosira antartica* and *Entomoneis* sp. only had Group 2 GR proteins (Table 2.5). Additionally, when the proteins were analysed for predicted TMDs, only three species had proteins with transmembrane regions: *T. oceanica (*accession number *EJK71311.1,* accession number EJK45974), *Cylindrotheca clostridium* (CAMPEP_0113620486, CAMPEP_0113607194) and *F. cylindrus (*accession number *OEU20380.1)*. Finally, when comparing GR distribution to NOX distribution, there appeared to be little pattern between the two proteins (Table 2.6).

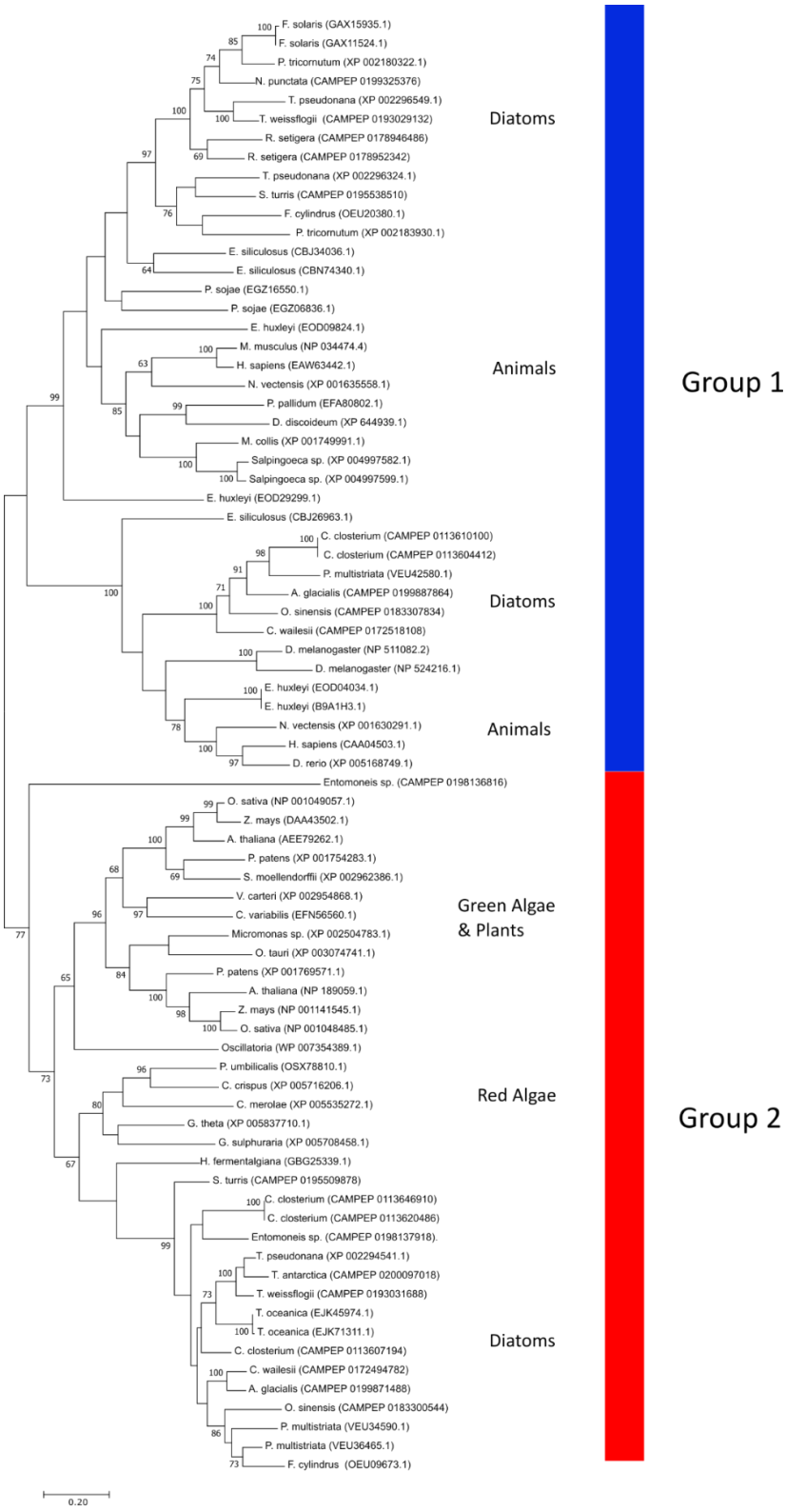

Figure 2.5 Phylogeny of GR proteins across different lineages.

The evolutionary history of different glutathione reductase proteins was inferred by using the Maximum Likelihood method based on the Poisson correction model. The tree with the highest log likelihood (-40068.46) is shown. The percentage of trees in which the associated taxa clustered together is shown next to the branches. Initial tree(s) for the heuristic search were obtained automatically by applying Neighbor-

Join and BioNJ algorithms to a matrix of pairwise distances estimated using a JTT model, and then selecting the topology with superior log likelihood value. The tree is drawn to scale, with branch lengths measured in the number of substitutions per site. The analysis involved 77 protein sequences. All positions with less than 95% site coverage were eliminated. That is, fewer than 5% alignment gaps, missing data, and ambiguous bases were allowed at any position. Each sequence contained 431 positions in the final dataset. Evolutionary analyses were conducted in MEGA7.

Table 2.5 Comparison of presence and absence of NOX and GR proteins within selected diatom species.

Green box indicates presence of protein in species while red indicates absence. Diatoms were selected as representatives of different lineages and included species with no identified NOX or NOX-like proteins.

Species	Diatom Type	Class 1 NOX	Class 2 NOX	Class 3 NOX	NOX-Like	No NOX	Group 1 GR	Group 2 GR	Total number of GR proteins	GR proteins with TMDs
Odontella sinensis	Polar Centric								2	
Thalassiosira oceanica	Polar Centric								2	2 (GR2)
Thalassiosira pseudonana	Polar Centric								3	
Thalassiosira antarctica	Polar Centric								1	
Thalassiosira weissflogii	Polar Centric								2	

Coscinodiscus wailesii	Radial Centric								2	
Rhizosolenia setigera	Radial Centric								2	
Stephanopyxis turris	Radial Centric								2	
Asterionellopsis glacialis	Araphid Pennate								2	
Cylindrotheca closterium	Raphid Pennate								5	2 (GR2)
Entomoneis sp	Raphid Pennate								2	
Fistulifera solaris	Raphid Pennate								2	
Fragilariopsis cylindrus	Raphid Pennate								2	1 (GR1)

Nitzschia punctata	Raphid Pennate								1	
Phaeodactylum tricornutum	Raphid Pennate								2	
Pseudo-nitzschia multistriata	Raphid Pennate								3	

2.4 Discussion

2.4.1 Diatom NOX diversity is unusually high

Previous studies of NOX diversity focused largely on NOX proteins in plants or animals (Kawahara *et al.*, 2007; Gandara *et al.*, 2017; Kaur *et al.*, 2018). The present study has used NOX proteins from lesser-studied lineages to examine the structural and phylogenetic differences between different types of NOX proteins. Diatom NOX proteins are widespread, present in 50% of species screened. Notably, diatom NOX proteins possess greater structural and phylogenetic diversity than other lineages studied thus far. This unexpected diversity in diatoms has allowed the creation of a new classification of NOX proteins with different Classes, defined by their structural and phylogenetic differences. Animal NOX have three structurally different types of NOX (NOX1-4, NOX5, DUOX1-2) (Kawahara *et al.*, 2007) but all belong to the Class 1 group. In contrast, diatoms have three structurally different types of NOX, and a NOX-like protein, all belonging to different Classes. Class 3 and NOX-like proteins are previously undescribed while the Class 2 diversity is expanded. This represents a vast increase to the two diatoms previously predicted to possess NOX proteins similar to red algae (Herve *et al.*, 2006). Raphid pennates appear highly likely to possess Class 2 proteins. As many algal species are known to produce eROS (Kupper *et al.*, 2002; Marshall *et al.*, 2005b; Diaz & Plummer, 2018), greater screening of algae may reveal further patterns in the type of NOX Class used.

It is unclear why diatoms have more diverse NOX proteins than other lineages. Possibly the structural diversity relates to specific NOX Class functions. Diatom Class 1 proteins possess calcium binding EF hands, which suggests changes in cytosolic Ca^{2+} concentration could regulate the protein. In plants, Ca^{2+} and Rboh-derived ROS regulate cellular signalling pathways including polarised cellular growth and abiotic stress responses (Foreman *et al.*, 2003; Kaya *et al.*, 2014; Kurusu *et al.*, 2015). Similar ROS: Ca^{2+} interactions are reported in brown algae during osmotic shock (Coelho *et al.*, 2002, 2008). While diatoms also use Ca^{2+} to regulate hypo-osmotic shock (Falciatore *et al.*, 2000; Helliwell *et al.*, 2019), a similar ROS: Ca^{2+} interaction is yet to be shown in diatoms. However Ca^{2+} and reactive nitrogen species interact to activate diatom PCD (Vardi *et al.*, 2006). Recent work has demonstrated upregulation of a Class 1 NOX during *S. robusta* sexual reproduction (Bilcke *et al.*, 2020). This pathway in *S. robusta* would be a suitable area to investigate diatom ROS: Ca^{2+} interactions.

Class 2 and 3 proteins have had comparatively little functional characterisation. Red algal Class 2 proteins are implicated in pathogen defence (Luo *et al.*, 2015; de Oliveira *et al.*, 2017) similar to

plants (Levine *et al.*, 1994; Liu *et al.*, 2010). Class 3 proteins in *C. reinharditii* may be involved in autophagy (Pérez-Pérez *et al.*, 2012) and dissipation of excess photosynthetically-derived reductant (Anderson *et al.*, 2016). Intriguingly, Class 2 diatom NOX proteins predominantly occur in raphid pennates and the Class 2 protein PtNOX1 was upregulated in the oval morphotype of *P. tricornutum*. This is the only *P. tricornutum* morphotype that possesses a raphe (Lewin *et al.*, 1958; Ovide *et al.*, 2018). As the raphe allows cell movement on surfaces, this may suggest a link between cell movement and Class 2 NOX activity. In humans, ROS derived from NOX5 is proposed to enhance spermatozoa mobility (Musset *et al.*, 2012) while NOX1, 2 and 4 are involved in cell-cell adhesion (Hurd *et al.*, 2012; Schröder, 2013). Furthermore, there also appears to be a relationship between light level and NOX expression in *P. tricornutum* (Laohavisit *et al.*, 2015).

This study also found unusual NOX-like proteins in *T. weissflogii* and *T. pseudonana*. These species were predicted to have NOX proteins, as they produce eROS that can be inhibited through the NOX inhibitor DPI (Kustka *et al.*, 2005; Laohavisit *et al.*, 2015). Furthermore, a putative protein resembling a Class 2 NOX has been described in *T. pseudonana* (Anderson *et al.*, 2011). However, the present study groups *T. pseudonana* and *T. weissflogii* NOX proteins with the NOX-like proteins (Fig 2.2). NOX-like proteins notably possess a NADH: cytochrome b5 reductase-like region alongside core NOX structure. NADH: cytochrome b5 reductase proteins are diverse one-electron reduction enzymes (Percy & Lappin, 2008). One of the enzymes' known function is the reduction of oxygen to superoxide (Samhan-Arias & Gutierrez-Merino, 2014). Since the genome of *T. pseudonana* was screened, it is unlikely the lack of Class 1-3 NOX proteins is due to transcriptome sequencing limitations. Therefore, the NOX-like proteins may represent an alternate mechanism for eROS production, but further validation is required.

2.4.2 T. oceanica-like GR proteins are uncommon in marine diatoms

A recent paper highlighted that eROS production by *T. oceanica* is due to the activity of GR proteins (Diaz *et al.*, 2019). GR normally reduces GSSG to glutathione using electrons from intracellular NADPH as part of the antioxidant response (Noctor & Foyer, 1998). However, a membrane-bound GR in *T. oceanica* uses intracellular NADPH to reduce extracellular oxygen to superoxide (Diaz *et al.*, 2019). Moreover, this finding questioned whether the GR or NOX proteins are the source of eROS in other marine diatoms. The present study suggests the *T. oceanica* type of transmembrane GR is uncommon within marine diatoms (Table 2.5). In contrast to *T. oceanica*, the majority of diatom GR proteins tested lack a TMD region (Diaz *et al.*, 2019). Like *T. oceanica, Cylindrotheca closterium* also possesses two Group 2 GR proteins with TM domains, potentially allowing further investigation of the role of diatom GR proteins in generating eROS. However, *C. closterium* also possesses a Class 2 NOX protein while *T. oceanica* has a Class 3 NOX protein. Care

should be taken if using DPI to reduce eROS production in these species as DPI inhibits both GR and NOX proteins. Using GSSG as a competitive inhibitor should reveal if the eROS production originates from a GR protein (Diaz *et al.*, 2019). It also appears unlikely that the GRs in *P. tricornutum*, *F. solaris* or *N. punctate* are responsible for eROS production, as the GR proteins belong exclusively to Group 1 and lack TMDs (Fig 2.5, Table 2.5). Until another enzymatic source is implicated, eROS from these species most likely originates from their respective NOX proteins. This hypothesis is further tested in Chapter 5.

2.4.3 An evolutionary explanation for diatom NOX diversity

The lack of NOX phylogeny data has limited evolutionary interpretations of NOX proteins but using diatoms and diverse algal lineages offers new insights. Based on the structural differences of red algal NOX proteins, it was previously suggested that Class 2 NOX proteins may have diverged prior to an ancestral NOX protein that evolved into fungal, plant and animal NOX (Zhang *et al.*, 2013; Kaur *et al.*, 2018), though this is unresolved (Kawahara *et al.*, 2007). The occurrence of Class 1 NOX proteins in diatoms and oomycetes highlights Class 1 NOX proteins are present in many diverse lineages. Thus, the ancestral NOX proteins evolved very early in eukaryotic evolution and likely resembled Class 1 NOX proteins (Inupakutika *et al.*, 2016). It follows that Class 2 and 3 NOX proteins, which have a more limited distribution, evolved after Class 1 proteins. Two possible evolutionary scenarios may explain why diatoms retained all three NOX Classes (Fig 2.6). In scenario 1, Class 2 and 3 proteins evolved shortly after the Class 1 NOX protein and the ancestral species possessed all three NOX Classes. There followed extensive gene loss, predominantly of Class 2 and 3 as lineages developed, resulting in only red algae, green algae and diatoms retaining Class 2 and/or Class 3 NOX proteins (Fig 2.6). Class 1 NOX gene loss is common between different species of the same phyla (Gandara *et al.*, 2017). This scenario suggests Class 1 was preferentially retained over Class 2 and 3 in most lineages, resulting in wider diversity. In scenario 2, Class 2 and 3 proteins emerged independently in red and green algal lineages and the respective genes were transferred to diatoms through secondary or tertiary endosymbiosis events. One algal endosymbiosis theory states the stramenopile ancestor acquired a green algal symbiont that was subsequently replaced with a red algal symbiont (Dorrell & Smith, 2011; Dorrell *et al.*, 2017). Scenario 2 suggests the two symbionts transferred their independently acquired NOX proteins to the host (Fig 2.6). In this scenario, only secondary or tertiary endosymbiotic algae (Bhattacharya *et al.*, 2004) should have Class 2 or Class 3 NOX proteins outside of the ancestral green and red algae. A recent study suggested the raphidophyte *Chattonella marina* and the dinoflagellate *Karenia mikimotoi* possess NOX proteins with 10-11 TMDs (Shikata *et al.*, 2019). These species are also from multiple-endosymbiosis lineages and the number of TMDs suggests a Class 2 NOX

protein. As scenario 2 requires fewer gene loss events, and Class 2 or 3 proteins are absent in non-photosynthetic organisms, scenario 2 is the more likely explanation. The endosymbiotic history of many algae is still unresolved. More studies of NOX protein distribution in relation to the proposed evolutionary history of different algal classes could shed light on the evolutionary processes that have given rise to the observed extant distributions.

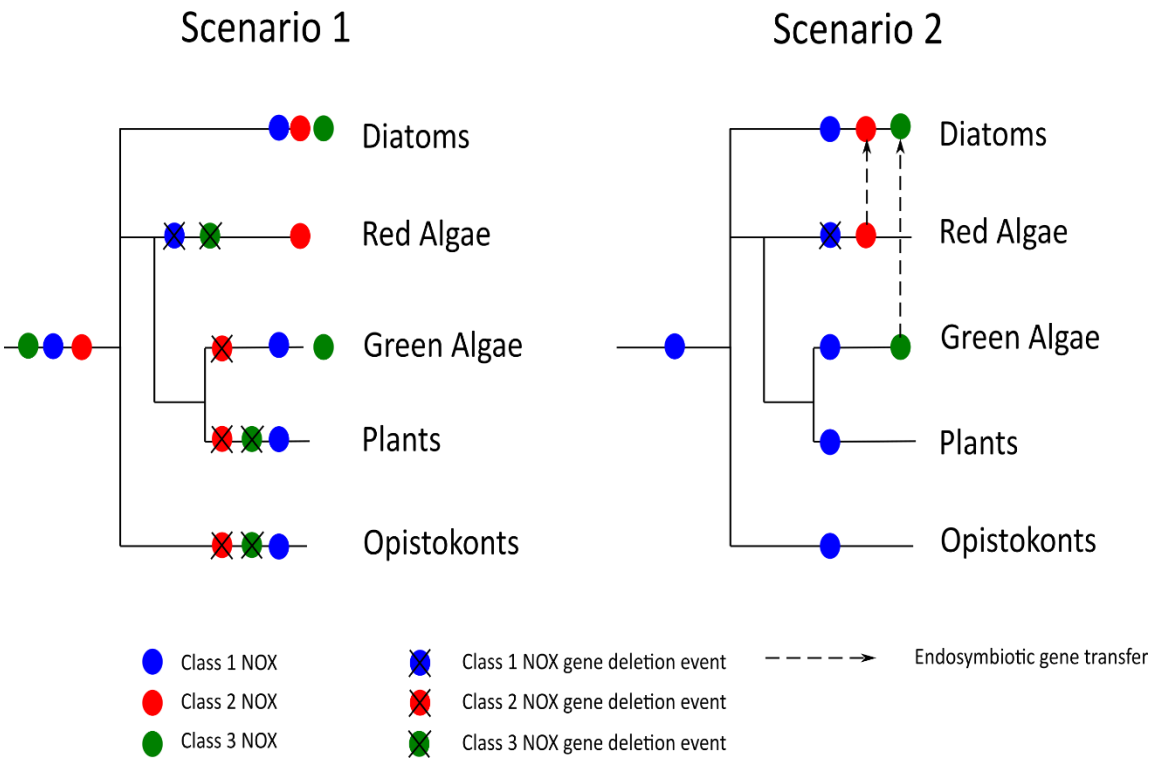

Figure 2.6 Possible scenarios explaining the unusual diversity of NOX proteins in diatoms.

Scenario 1 suggests the three Classes evolved simultaneously shortly after the initial development of the ancestral NOX. As lineages split away, gene loss occurred in each lineage. Only diatoms retained all three Classes. Scenario 2 suggests Class 1 type proteins resembled the ancestral NOX protein and spread between lineages. Independent evolution of Class 2 and Class 3 occurred within red and green algae lineages. These proteins transferred to other lineages through endosymbiotic events and subsequent gene transfer.

2.4.4 Strategies for identifying future NOX proteins

The functions of putative NOX and FRE proteins are difficult to determine without extensive experimental analysis. Unfortunately, a conclusive NOX identification motif/residue for discriminating between the sequences could not be identified, opposing previous suggestions (Sumimoto, 2008; Zhang *et al.*, 2013; Magnani *et al.*, 2017). Thr178 was the best candidate and though it occasionally was substituted with a chemically similar serine, it was still absent from FRE

proteins. Future attempts to identify NOX and FRE would have to be aware of this to avoid confusion. Class 1 and 2 proteins are easier to identify. Screening for Thr178 alongside distinguishing structural features such as EF hands in Class 1 and 10 TMDs for Class 2 could identify NOX from these Classes. In contrast, Class 3 proteins are more difficult, due to greater structural similarity to FRE proteins and lacking some of the conserved motifs seen in Class 2 and 3 such as Arg256. However, their close phylogenetic relationship to characterised green algal NOX (Anderson *et al.*, 2016) supports their identity as NOX. Further characterisation and studies using Class 3 proteins will help. However, as NOX-like and GR (Diaz *et al.*, 2019) proteins have been shown to potentially contribute to eROS production in other systems, care is required to match biochemical activity to a specific protein. NOX proteins may be the best characterised eROS source but are not the sole enzymatic source.

2.4.5 Conclusions

This work has demonstrated the benefit of utilising diverse algal species for understanding the evolution of the NOX protein family. Diatom NOX proteins are unusually diverse in phylogeny and structure. The reason for this diversity is unclear but may imply diverse functions for diatom NOX proteins. Moreover, the diatom diversity has implications for how the NOX protein evolved. Experimental evidence is important for confirming NOX as the eROS source, especially as there may be alternative non-NOX sources of eROS in diatoms. While identification of NOX proteins from sequences is complicated, similar screens of other algal groups can only improve the understanding of the different NOX Classes and may help identify a universally conserved NOX motif or residue

Chapter 3 Extracellular ROS production and plasma membrane electron transport in three marine diatoms

3.1 Introduction

It is increasingly clear that extracellular reactive oxygen species (eROS) production by marine phytoplankton is widespread (Diaz & Plummer, 2018). The most common ROS are superoxide and hydrogen peroxide (H_2O_2), which possess longer lifespans than other ROS (Mittler, 2017). ROS can be formed abiotically through photolysis (Micinski *et al.*, 1993) and interactions with redox-active compounds (Rose, 2012), whereby electrons reduce molecular oxygen and create ROS variants. Oceanic steady state levels of superoxide are higher than if solely derived from abiotic means (Rose *et al.*, 2010; Zinser, 2018; Sutherland *et al.*, 2020) and correlate with chlorophyll *a* concentration (Rusak *et al.*, 2011). Furthermore, high steady state levels of ROS are apparent at depths where photolysis would be reduced (Palenik & Morel, 1988; Rose *et al.*, 2008). Thus, biologically derived ROS contributes significantly to oceanic steady state concentrations of ROS (Rose *et al.*, 2008; Diaz *et al.*, 2013; Sutherland *et al.*, 2020).

Biologically derived eROS can be generated through various mechanisms. H_2O_2 is membrane permeable. Thus respiration- or photosynthesis-derived H_2O_2 can cross membranes and exit the cell (Palenik *et al.*, 1987; Suggett *et al.*, 2008). External superoxide may also dismutate to H_2O_2. Due to the charged nature of superoxide, it has low membrane permeability (Hawkins *et al.*, 2007; Milne *et al.*, 2009) and so external superoxide must be generated by phytoplankton plasma membrane oxidoreductase proteins, enzymes that catalyse electron transfer between different molecules (Diaz & Plummer, 2018). The most widely studied transmembrane oxidoreductase protein is NADPH oxidase (NOX) (Sumimoto, 2008), which transfers electrons from intracellular NADPH to extracellular oxygen. The NOX enzyme family is widespread, being found in eukaryotes and prokaryotes (Herve *et al.*, 2006; Kawahara *et al.*, 2007; Anderson *et al.*, 2011; Hajjar *et al.*, 2017). NOX is also used for diverse functions including defence, intercellular signalling, promoting cell wall cross linkages, as a growth stimulant and a possible role in electron dissipation for photosynthesis (Foreman *et al.*, 2003; Monshausen *et al.*, 2007; Miller *et al.*, 2009; Cachat *et al.*, 2015; Hansel *et al.*, 2016; Diaz *et al.*, 2018).

Some studies have demonstrated that increasing light intensity correlates with greater microalgal eROS production (Anderson *et al.*, 2016; Schneider *et al.*, 2016). Similarly, phytoplankton trans-plasma membrane electron transport (TMET), the movement of intracellular electrons through the plasma membrane to the cell surface, can increase in high light intensities (Lomas *et al.*, 2000; Li *et al.*, 2015). It is proposed that this is a cellular response to remove excess electrons derived from increased photosynthetic activity during high light conditions (Davey *et al.*, 2003). Thus, it acts as safety valve relieving the cell of excess reductant (Niyogi, 2000), alleviating potential internal electron leakage and subsequent oxidative stress. The rate of TMET in phytoplankton

varies between species and there is significant interest in exploiting it for electricity production through biophotovoltaic devices (Bombelli *et al.*, 2011; McCormick *et al.*, 2015; Anderson *et al.*, 2016). NOX may be a significant contributor to TMET as the NOX inhibitor diphenyleneiodonium chloride (DPI) significantly reduces TMET in the diatom *Thalassiosira weissflogii* (Davey *et al.*, 2003). However, in other algae, such as iron deficient *Chlamydomonas reinharditii*, DPI has only a small effect on TMET (Eckhardt & Buckhout, 1998), suggesting that other oxidoreductase enzymes may be primarily responsible for TMET (Jones & Morel, 1988; Lynnes *et al.*, 1998).

Amongst phytoplankton, diatoms display constitutive production of eROS in contrast to oxidative bursts seen in other algae (Bouarab *et al.*, 1999; Kupper *et al.*, 2002). There is also great variability in per-cell production of superoxide and H_2O_2 between species, with the centric diatom *Thalassiosira weissflogii* and the toxic pennate species *Pseudo-nitzschia* sp. having high production rates (Schneider *et al.*, 2016; Diaz *et al.*, 2018). Most studies have shown that diatom eROS production is greater in light than darkness (Milne *et al.*, 2009; Schneider *et al.*, 2016; Diaz *et al.*, 2019). However, dark diatom eROS production rates can still be substantial (Diaz *et al.*, 2018). Regarding diatom TMET, the limited work has focused on electrons reducing external Fe^{3+} to Fe^{2+} (Nimer *et al.*, 1998, 1999). Species differences are apparent with *T. weissflogii* having particularly high TMET activity (Nimer *et al.*, 1999; Davey *et al.*, 2003). In contrast to diatom eROS production, increasing light intensities (>180 µmol photons m^{-2} s^{-1}) have been shown to decrease TMET in four diatoms tested (Davey *et al.*, 2003). This discrepancy between TMET and eROS production hasn't been explored further. However, *T. weissflogii* TMET and eROS production are both reduced in the presence of DPI (Davey *et al.*, 2003; Kustka *et al.*, 2005), implicating the involvement of NOX proteins in both activities.

In this chapter, eROS production and TMET activity were investigated in three marine diatoms: one centric (*T. weissflogii*), one raphid pennate (*Phaeodactylum tricornutum*), and one araphid pennate (*Asterionellopsis glacialis*). These represent three different NOX classes reported in the previous chapter. *T. weissflogii* has an atypical NOX-like protein (see Chapter 2) but has been the diatom species most frequently used for measuring eROS production. *P. tricornutum* has a Class 2 NOX protein. TMET and eROS production are uncharacterised in *A. glacialis*, though it is predicted to have Class 1 and Class 3 NOX proteins (see Chapter 2). Comparing TMET and eROS production in these three different species allowed better understanding of the dynamics of diatom TMET and eROS production. It is shown that there are clear species differences in TMET and eROS production. Furthermore, light intensity caused complex effects depending on the species or assay examined.

3.2 Methods

3.2.1 Cell culture and physiology measurements

A. glacialis (PLY 607) and *T. weissflogii* (PLY 541) were acquired from the Plymouth Culture Collection. *P. tricornutum* (CCAP1055/1) was acquired from Culture Collection of Algae and Protozoa (SAMS limited, Scottish Marine Institute (Oban, UK)). Diatoms were grown in F/2 +Si medium (Guillard & Ryther, 1962) derived from twice filtered seawater (FSW, 0.2 µm prefilter (Sartorius, England) followed by 30 kilodalton filter (GE Healthcare, UK)) collected at site L4 (50° 15.00' N, 4° 13.02' W) in the English Channel. All species were cultured on a 16:8 hour light: dark cycle, at 40-45 µmol m^{-2} s^{-1} photon flux density, measured using a LI-250A light meter (LI COR, USA). Cell culture flasks (green plug tissue culture, SARSTEDT, Germany) were manually shaken once per day. *P. tricornutum* was maintained at 18°C and *T. weissflogii* and *A. glacialis* were maintained at 15°C. Cell counts were undertaken using a Beckman Coulter counter for *P. tricornutum*, a haemocytometer for *A. glacialis* and a Sedgewick Rafter counting chamber for *T. weissflogii*. Cells used for experiments were taken from early to mid-exponential growth. *P. tricornutum* density was 3-4.5x10^6 mL^{-1}, *T. weissflogii* was 1-1.5x10^5 mL^{-1} and *A. glacialis* was 2.5-4x10^5 mL^{-1}. Maximum quantum efficiency of photosystem II (Fv/Fm) was measured using an AquaPen 110-C fluorimeter (Photon Systems Instruments, Czech Republic) after dark adapting cells for 20 min.

3.2.2 Chemical preparation

100 mM potassium ferricyanide ($K_3[Fe(CN)_6]$, Sigma-Aldrich) and 100 mM potassium ferrocyanide ($K_4[Fe(CN)_6]$, Sigma-Aldrich) working stocks were prepared in FSW the day prior to experiments and were kept in the dark until use. Working stocks (1 mg mL^{-1}) of OxyBURST™ Green H_2HFF-BSA (Thermo Fisher Scientific) were made by dissolving powder in 1 mL of phosphate buffered saline (PBS) solution as per manufacturer's instruction. These working stocks were maintained at 4°C wrapped in foil. Diphenyleneiodonium chloride (DPI, Sigma-Aldrich) was dissolved in DMSO (1 mM working stock) while 3-(3,4-dichlorophenyl)-1,1-dimethylurea (DCMU, Sigma-Aldrich) was dissolved in ethanol (10 mM working stock). During potassium ferricyanide or OxyBURST assays, inhibitors were added 1 min prior to OxyBURST or ferricyanide addition at a concentration of 1 µM for DPI (0.1% v/v DMSO) and 10 µM for DCMU (0.1% v/v ethanol).

3.2.3 Potassium ferricyanide reduction assay for TMET

The methodology from Davey *et al.*, (2003) using 420 nm absorbance of potassium ferricyanide was adapted to measure ferricyanide reduction activity (FCR) as a proxy for TMET. Potassium ferricyanide has a maximum absorbance at 420 nm, whereas potassium ferrocyanide has minimal absorbance. Therefore, electron reduction of ferricyanide to ferrocyanide results in a decrease in 420 nm absorbance. For each FCR measurement, 4 mL of cells were removed from culture flasks into clear plastic tubes (Thermo Fisher Scientific). Filtered seawater (FSW) was used as a blank control. Potassium ferricyanide (250 µM) was added to cells and blank control, and 1 mL of medium was immediately removed for baseline absorbance. The sample was centrifuged (13,000 g, 2 min) with the supernatant (3x 200 µL) added to a clear 96 well plate (SARSTEDT, Germany). Absorbance was measured in a plate reader (CLARIOstar Plus, BMG Lab Tech, Germany) at 420 nm. The remaining medium in tubes were returned to their respective temperature-controlled rooms. After two hours, the process was repeated as above for an end time measurement. The difference in 420 nm absorbance at 0 and 2 hours for each sample was calculated and adjusted for background ferricyanide reduction by removing the change in the blank sample. A standard curve of 420 nm absorbance vs potassium ferricyanide concentration was generated (Fig 3.1) and used to calculate the moles of ferricyanide reduced per cell and unit time, creating the ferricyanide reduction activity (FCR) value. Each measurement was taken in triplicate.

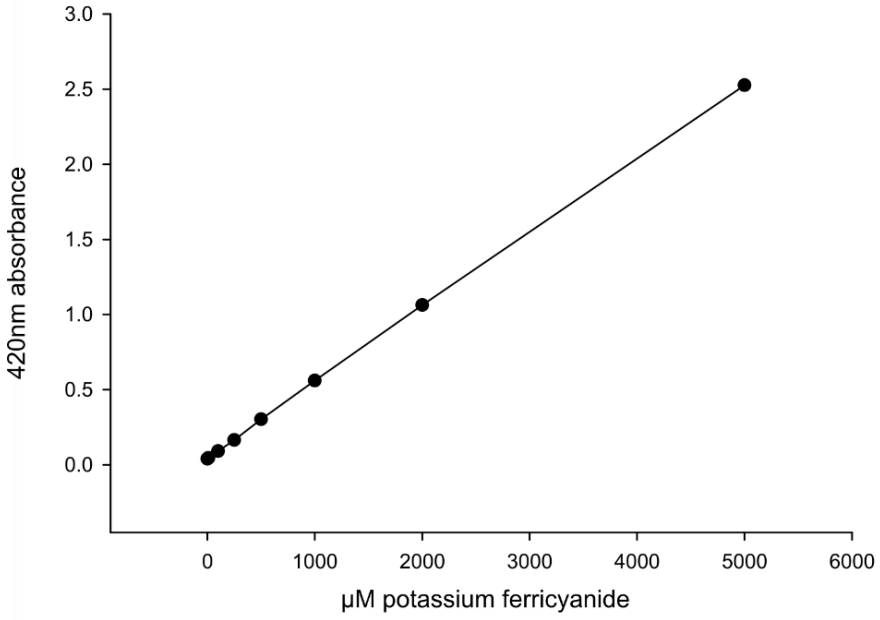

Figure 3.1 A standard curve of 420 nm absorbance vs potassium ferricyanide concentration.

Equation for line of best-fit (linear regression) Y=0.0005x. This equation was used to calculate the amount of ferricyanide reduced per sample in each experiment. R^2 =0.9998.

3.2.4 OxyBURST Green assay for eROS production

OxyBURST™ Green H_2HFF-BSA (Thermo Fisher Scientific) was used to measure eROS production. OxyBURST consists of a reduced dye H_2HFF conjugated to bovine serum albumin, ensuring the dye-protein conjugate is too large to enter cells. Thus, only eROS can oxidise the dye, causing an increase in dye fluorescence (Fc OxyBURST Assay Reagents, https://www.thermofisher.com/order/catalog/product/O13291#/O13291). Experiments were designed to resemble the FCR assay. 4 mL cells or FSW (as a blank control), were extracted in triplicate and added to clear plastic tubes. OxyBURST was added to cells and FSW control (final concentration 2 µg mL^{-1}). 1 mL of sample was removed and centrifuged (13,000 g, 2 min) before supernatant (3 x 200 µL) was transferred into a flat black, 96 well plate (Greiner). Fluorescence was measured in a plate reader (CLARIOstar Plus, BMG Lab Tech) (excitation: emission at 475:515 nm) at time point zero. The remaining medium in tubes were returned to their respective temperature-controlled rooms and another sample was processed 2 hours later. Each light intensity FSW control values were subtracted from cell data. Values were then expressed as the relative change in fluorescence compared to each experiment listed control.

3.2.5 Light intensity

Following T0 measurement, three light levels were tested in both assays. For darkness samples, tubes were wrapped in aluminium foil (representing 0 µmol photons m^{-2} s^{-1} photon flux density) until measurement 2 hours later. Light treatments were generated by placing tubes at different distances to LED solid-state strips within the respective temperature controlled culture room. Medium light (ML) conditions were kept at 40-45 µmol photons m^{-2} s^{-1}. This is the light intensity cells were cultured at. LED solid-state strips were used for high light treatments (HL) of 200 µmol photons m^{-2} s^{-1}. For each light intensity, a respective blank control was used to ensure normalisation of values in case light intensity affected the assay baseline absorbance or fluorescence.

3.2.6 Statistical analysis

All statistics were calculated using Sigma Plot 14 statistical software. Data were tested for normality and equality of variance using Shapiro-Wilk and Brown-Forsythe tests. If data passed

both tests, datasets were analysed using a one-way ANOVA and Tukey post hoc tests. If datasets failed precursor tests, datasets were analysed using a Kruskal-Wallis one-way analysis of variance on ranks and a Tukey post hoc test. Statistical significance of data was indicated if $P<0.05$.

3.3 Results

3.3.1 Validation of FCR assay

To validate the FCR assay, several preliminary experiments were carried out. *T. weissflogii* has high constitutive FCR activity (Davey *et al.*, 2003) so was used to test the assay validity by measuring 420 nm absorbance under different conditions (Fig 3.2). Samples containing potassium ferrocyanide or *T. weissflogii* ± potassium ferrocyanide had low absorbance and no significant change in absorbance was seen after two hours. In comparison, potassium ferricyanide absorbance was much higher but also did not change in two hours. As anticipated, the only significant change seen was in *T. weissflogii* + 250 µM potassium ferricyanide (one-way ANOVA, P=0.013).

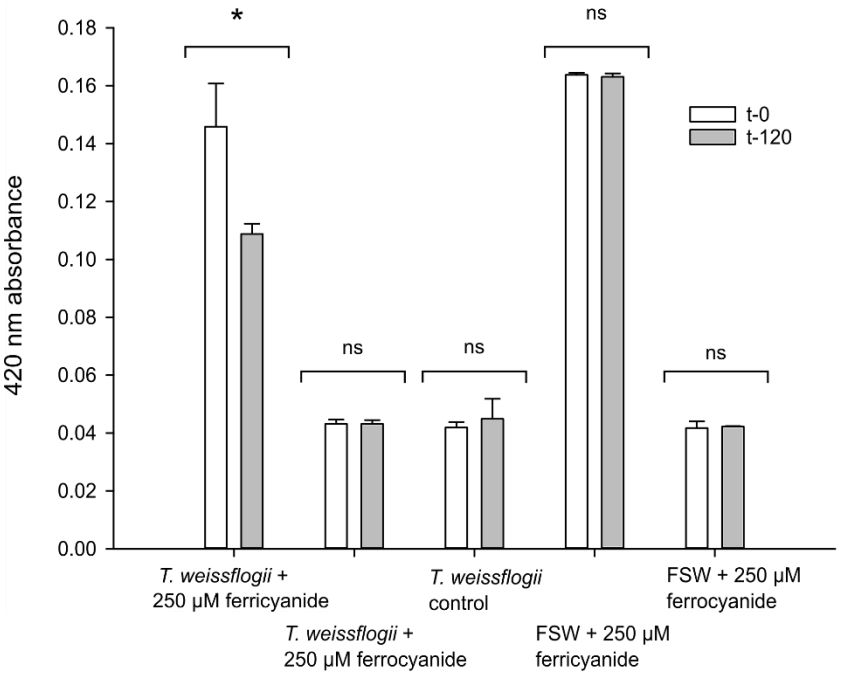

Figure 3.2 Comparison of 420 nm absorbance in the presence of potassium ferricyanide or potassium ferrocyanide.

Change in 420 nm absorbance was measured with different combinations of potassium ferricyanide or ferrocyanide with different media. Absorbance was measured at the start of the experiment (t-0) and after 120 min (t-120). Differences were tested using one-way ANOVA. * P=<0.05. ns = no significant difference. Error bars represent standard deviations based on three biological replicates with three technical replicates.

3.3.2 Comparison of baseline FCR activity and eROS production

An initial comparison of the relative FCR activity of the three species was investigated at 45 µmol photons m^{-2} s^{-1} light intensity (Fig 3.3A). *T. weissflogii* FCR activity of 12 femtomole $cell^{-1}$ min^{-1} was significantly higher than *A. glacialis* (one-way ANOVA, P=<0.001) and two orders higher than *P. tricornutum* (one-way ANOVA, P=<0.001). A similar pattern was observed in the OxyBURST assay. *T. weissflogii* had the highest per-cell eROS production, followed by *A. glacialis* and *P. tricornutum* (Fig 3.3B). However, after the dataset failed a test of normality, only *T. weissflogii* and *P. tricornutum* were significantly different (Kruskal-Wallis, P=<0.05).

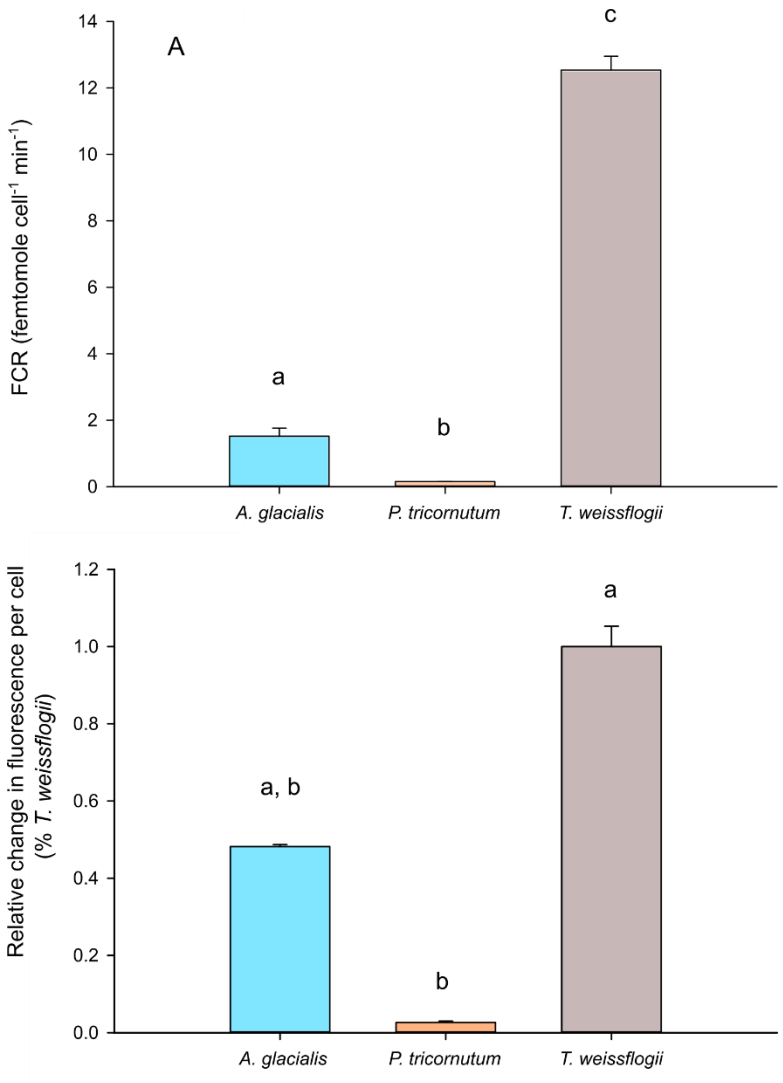

Figure 3.3 Baseline comparison of (A) FCR activity and (B) eROS production between three test species.

Data are representative of the three species sampled at mid exponential phase of growth, but data were obtained in separate independent experiments. OxyBURST values are normalised to change in fluorescence in *T. weissflogii* (ΔF $cell^{-1}$ min^{-1}). Statistical comparison used a one-way ANOVA with Tukey post hoc test for FCR and a

Kruskal-Wallis test on ranks with Manns Pairwise Multiple Comparison test for eROS production. Different letters indicate statistical significance (P=<0.05). Error bars indicate standard deviation of three-four biological replicates with three technical replicates.

3.3.3 Effect of NOX inhibition on FCR activity and eROS production

DPI irreversibly inhibits the FAD domain of NOX, preventing electron transport so it was predicted that DPI would reduce both FCR and eROS production. 1 µM DPI caused a reduction but not complete inhibition in FCR and eROS assays in *T. weissflogii* and *P. tricornutum* (Fig 3.4). In *T. weissflogii*, DPI decreased FCR activity by 23% (one-way ANOVA, P=<0.001) and eROS by 79% (P=<0.001) whereas in *P. tricornutum*, DPI decreased FCR activity by 24% (P=<0.05) and eROS production by 68%. DPI had no effect on FCR in *A. glacialis* (Fig 3.4) (P=0.102) but significantly decreased eROS production by 30% (Fig 3.5) (P=<0.05).

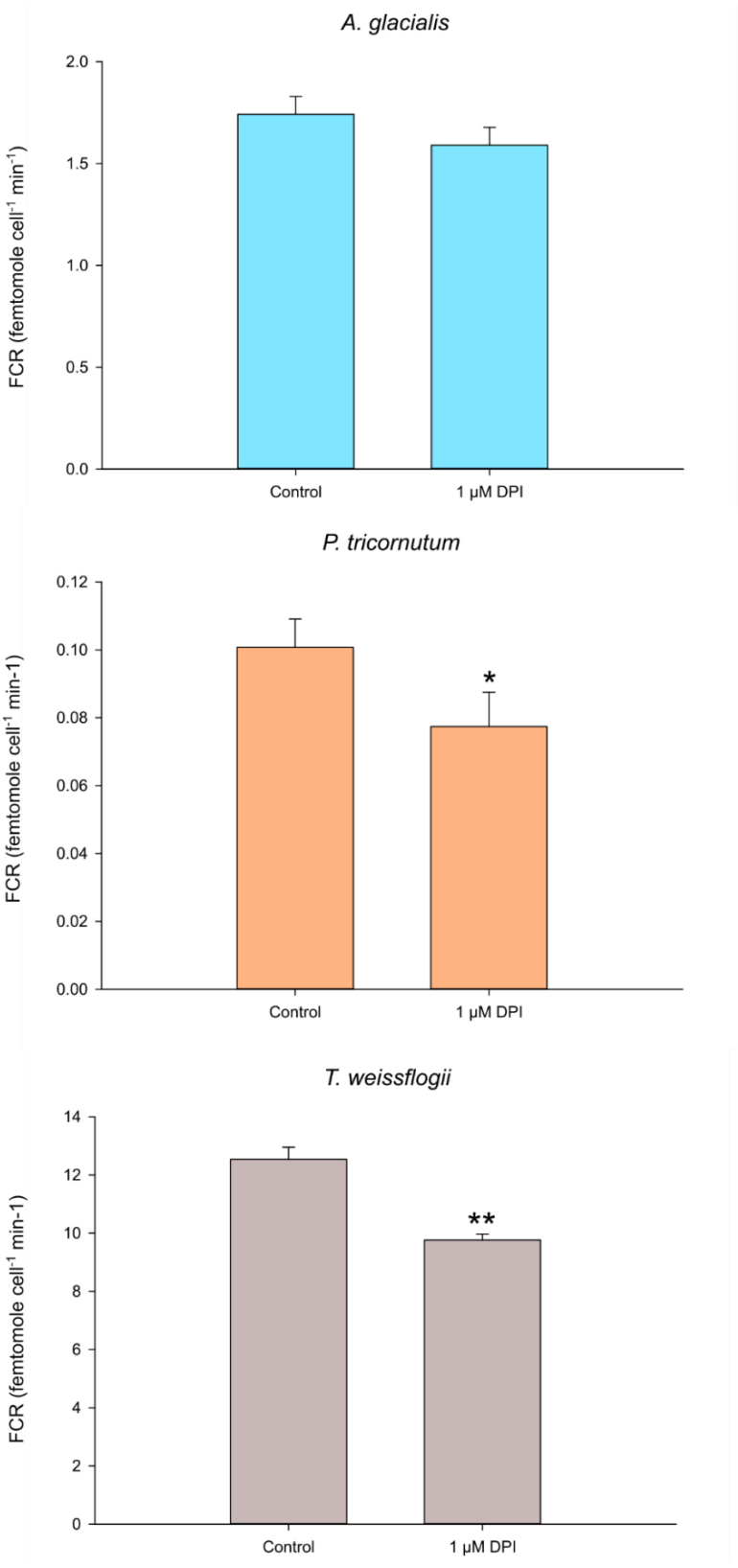

Figure 3.4 The effect of DPI on FCR activity.

Following 1 µM DPI addition, a reduction in FCR activity was seen after two hours. A one-way ANOVA showed significant differences in *T. weissflogii* and *P. tricornutum*. * P=<0.05. ** P<0.001. Error bars show standard deviations based on three biological replicates with three technical replicates.

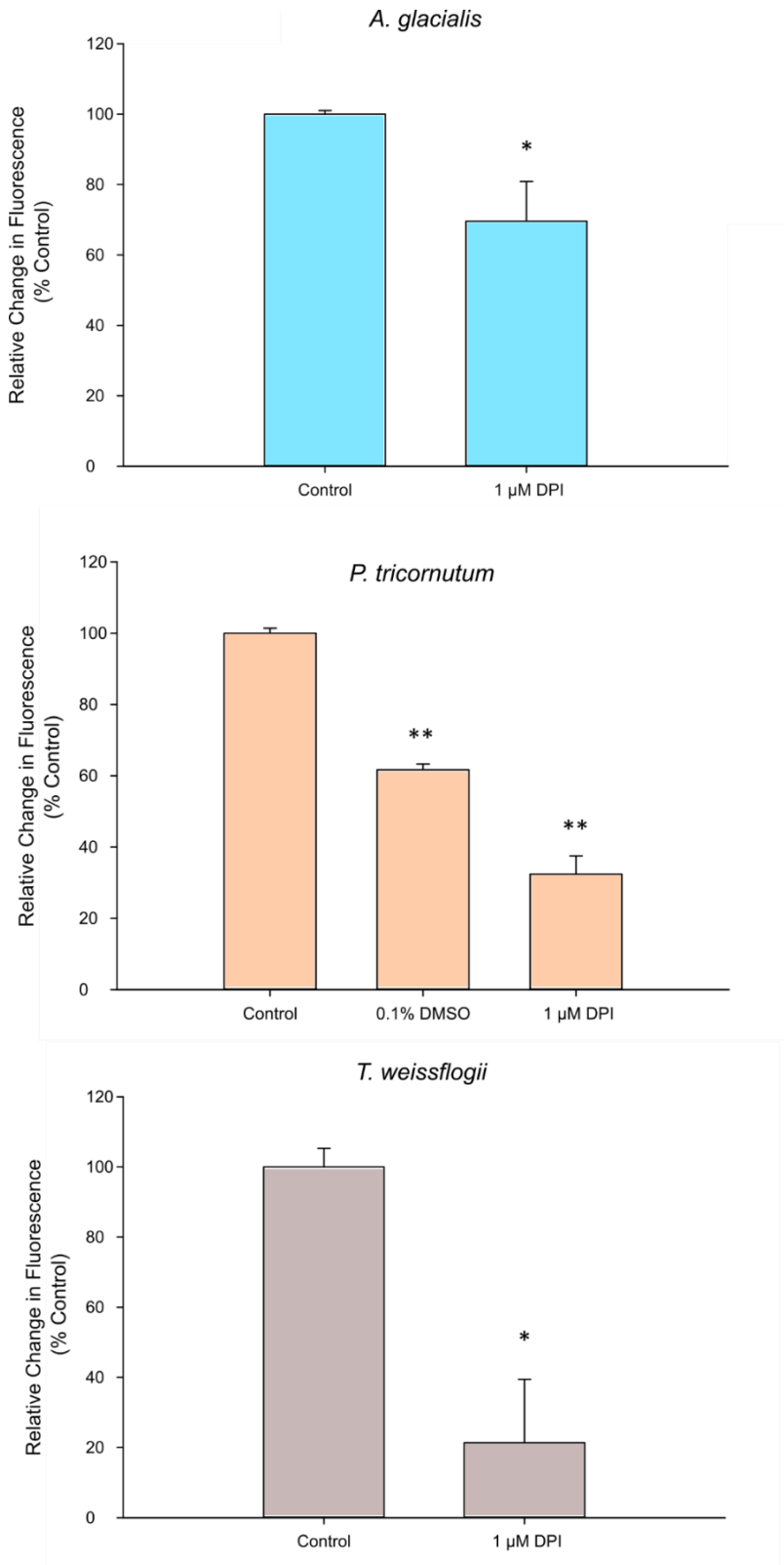

Figure 3.5 The effect of DPI on eROS production.

Following pretreatment with 1 µM DPI, OxyBURST fluorescence was reduced in species after two hours compared to control treatment. Only *P. tricornutum* was tested with a DMSO blank control. A one-way ANOVA tested for significant differences between treatments and control. * P=<0.05. ** P<0.001. Error bars show

standard deviations based on three biological replicates with two-three technical replicates.

The OxyBURST assay with *P. tricornutum* was the only test that used a DMSO control. Surprisingly, 0.1% v/v DMSO significantly reduced eROS production by 38% (Fig 3.5). The difference in reduction between DMSO and DPI was still significant (P=<0.05). The effects of DMSO and ethanol on both the FCR and OxyBURST assays were tested further with *P. tricornutum*. Both solvents had no significant effect on FCR activity (one-way ANOVA, P=0.683), though there was unusually large variability within the data (Fig 3.6A.) Surprisingly, solvents had strong effects in the OxyBURST assay (Fig 3.6B). Though 0.1% v/v ethanol reduced eROS production, this reduction was not statistically significant (Kruskal-Wallis one-way analysis of variance on ranks, P=0.372). 0.1% v/v DMSO significantly reduced eROS production (Kruskal-Wallis one-way analysis of variance on Ranks, P=0.020). To account for this, *A. glacialis* and *T. weissflogii* DPI values were normalised to account for DMSO reduction. DMSO was assumed to account for a 38% reduction of DPI values. In *T. weissflogii*, DMSO adjusted DPI was 41% lower than control treatment and still significantly different to the control (one-way ANOVA, P=0.020). In *A. glacialis*, DMSO adjusted DPI values were not significantly reduced compared to control *A. glacialis* (one-way ANOVA, P=0.308).

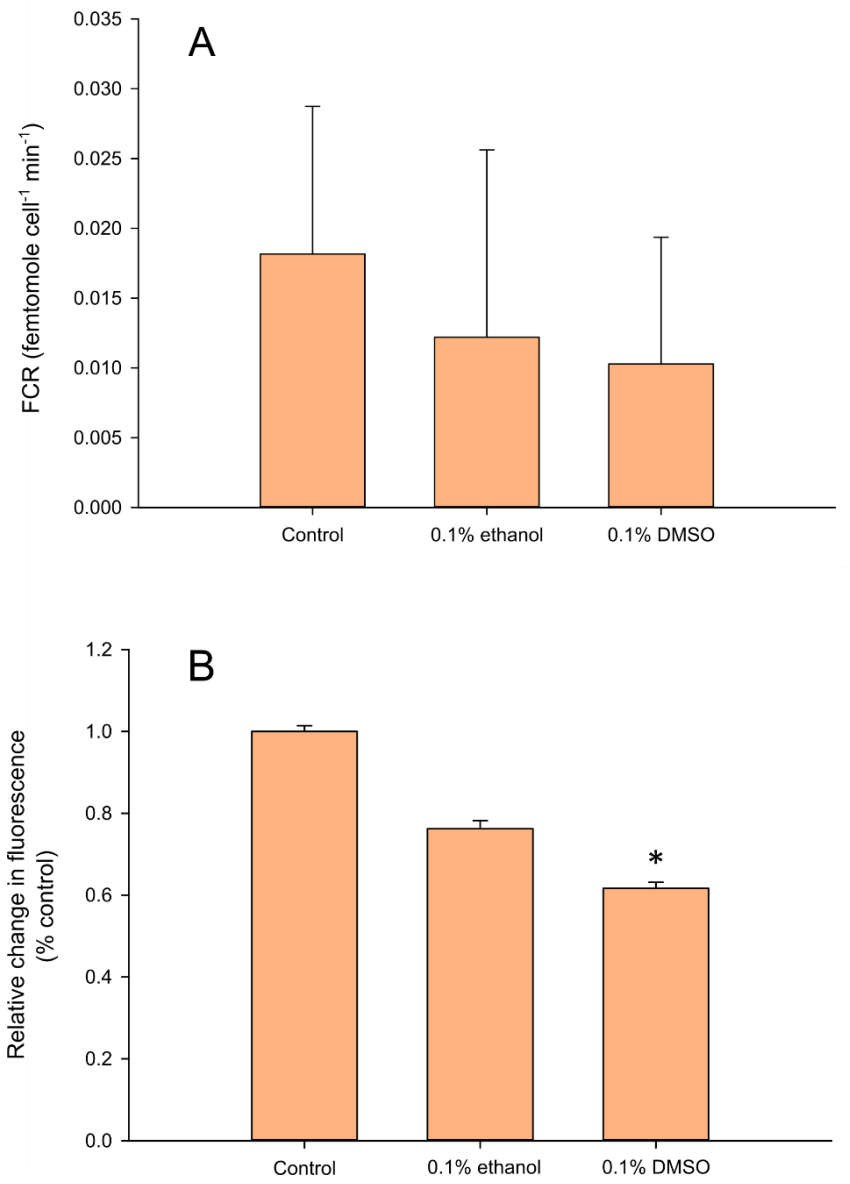

Figure 3.6 The effect of solvents on FCR activity and eROS production in *P. tricornutum*.

P. tricornutum was incubated with either 0.1% v/v ethanol, or 0.1% v/v DMSO with either 250 µM potassium ferricyanide or 2 µg mL^{-1} OxyBURST for two hours. The OxyBURST values are shown relative to the total change in fluorescence in the untreated *P. tricornutum* control. FCR values were tested for statistical differences using a one-way ANOVA. OxyBURST values failed a Shapiro-Wilk test of normality so a Kruskal-Wallis one-way analysis of variance on ranks assessed statistical difference comparing differences to the control. *= $P<0.05$. Error bars show standard deviation based on three biological replicates with three technical replicates.

3.3.4 Effect of light intensity on FCR

FCR activity was investigated under darkness, medium light (ML, 45 µmol photons m^{-2} s^{-1}), high light (HL, 200 µmol photons m^{-2} s^{-1}) and with the photosynthesis inhibitor DCMU added in ML (Fig 3.7.). Compared to darkness control, ML significantly reduced FCR only in *T. weissflogii* (P=0.019). However, HL completely inhibited FCR activity in all species (one-way ANOVA, P<0.001). 10 µM DCMU had no effect on *P. tricornutum* but significantly reduced FCR compared to darkness and ML in *A. glacialis* and *T. weissflogii* (P=<0.001).

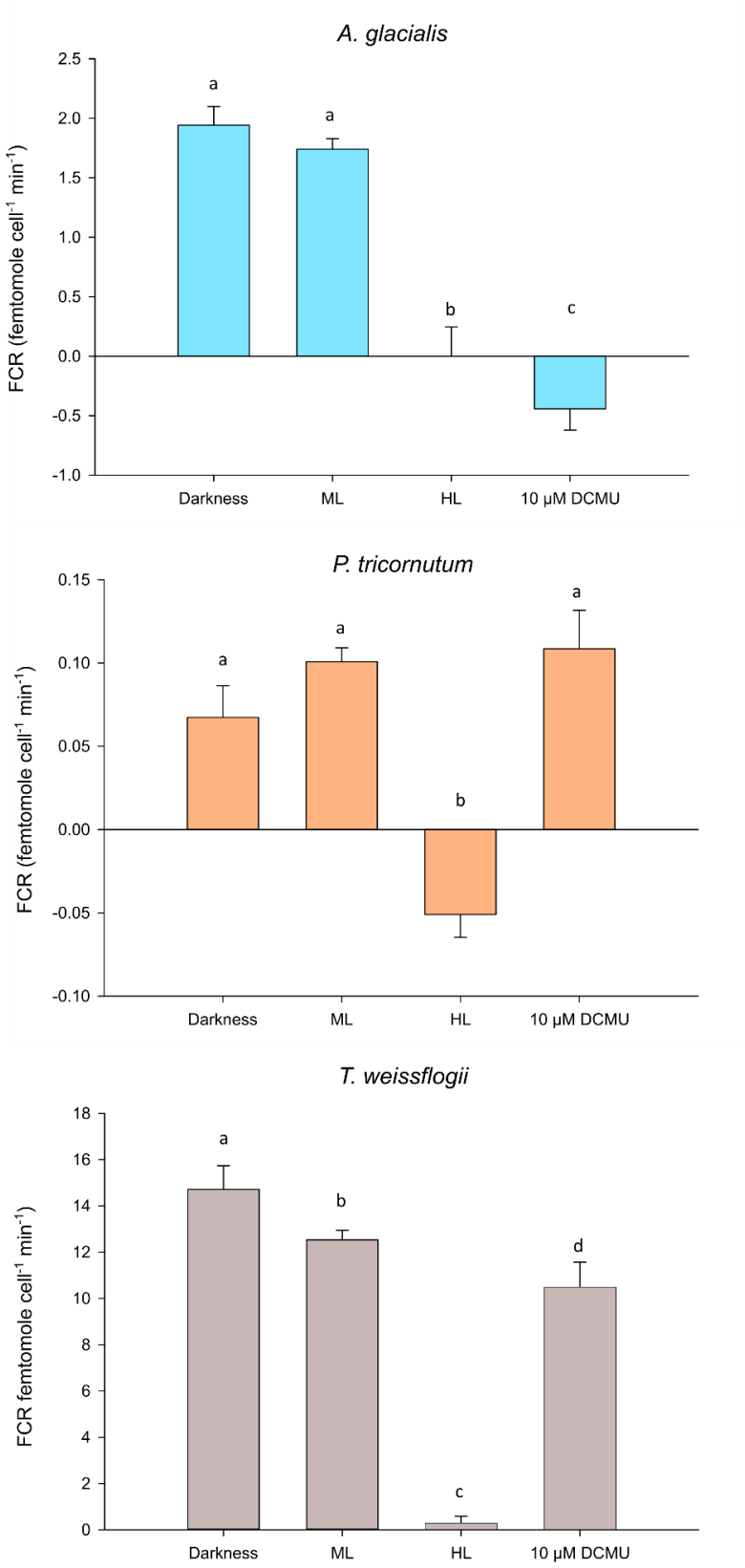

Figure 3.7 Effect of light intensity and the photosynthesis inhibitor DCMU on FCR activity.

FCR activity was compared in darkness, medium light (ML, 40 µmol photons m^{-2} s^{-1}) and high light (HL, 200 µmol photons m^{-2} s^{-1}). Inhibition of photosynthesis with 10 µM DCMU, dissolved in ethanol, was tested at ML conditions. Statistical comparison used

a one-way ANOVA with Tukey post hoc test. Different letters indicate statistical significance (P=<0.05). Error bars show standard deviation based on three replicates with three technical replicates.

3.3.5 Effect of light intensity on eROS production

Light intensity effects were then tested on diatom eROS production. Light intensity significantly affected eROS production (Fig 3.8). ML and HL treatments significantly enhanced *A. glacialis* and *P. tricornutum* eROS production (one-way ANOVA, P=<0.05) compared to the darkness control. However, ML or HL had no significant effect on eROS in *T. weissflogii.* 10 µM DCMU significantly enhanced eROS production in all species. No ethanol control was used for the OxyBURST assays for DCMU addition. However, as 0.1% v/v ethanol reduced control fluorescence, and eROS production increased in all DCMU assays, the actual DCMU increase may be higher than seen in the graphs.

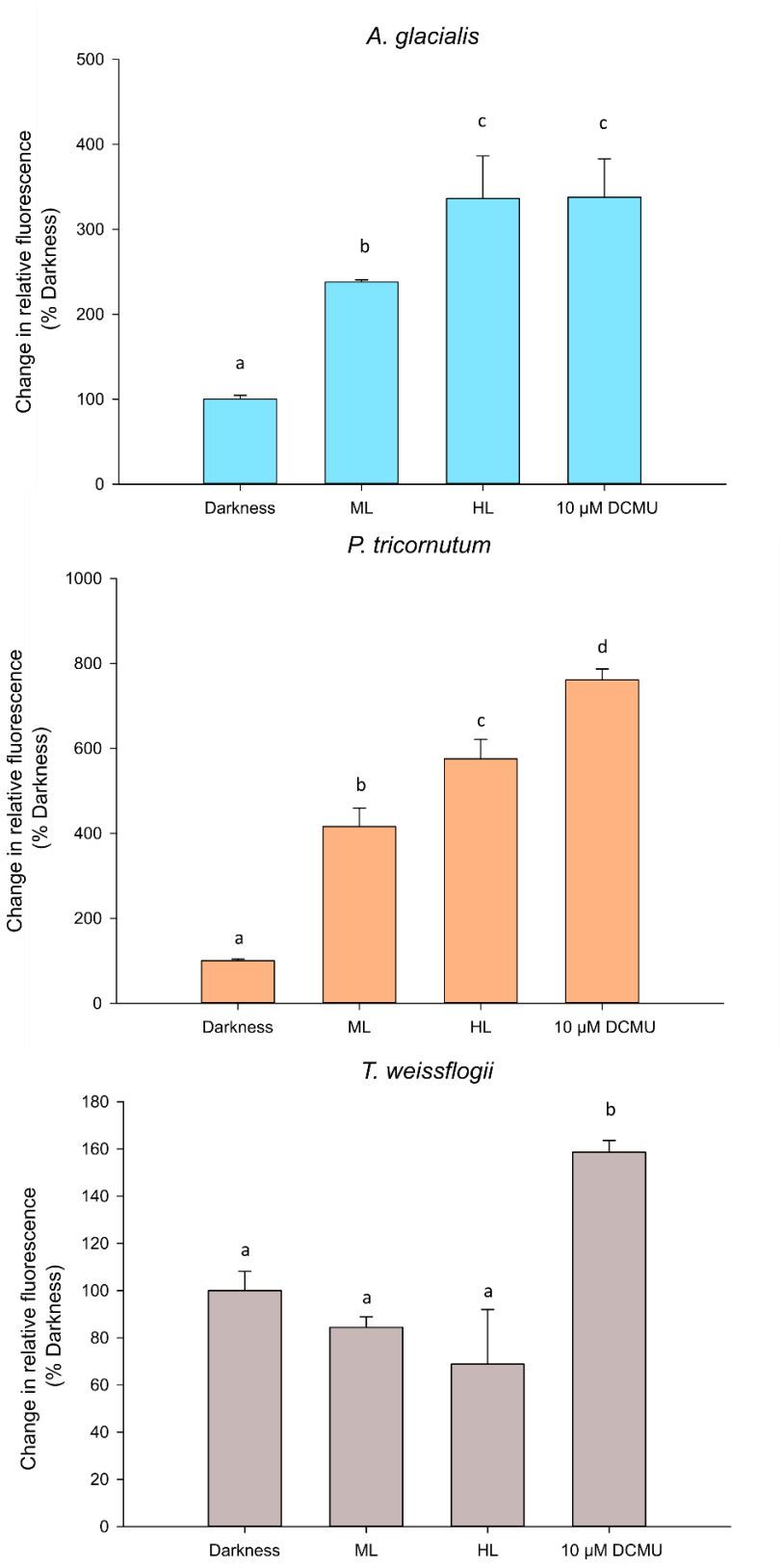

Figure 3.8 Effect of light intensity and the photosynthesis inhibitor DCMU on eROS production.

eROS production by each species, monitored through OxyBURST fluorescence. Changes in fluorescence are normalised to the darkness control. Medium light intensity is 45 µmol photons m^{-2} s^{-1} and high light (HL) is 200 µmol photons m^{-2} s^{-1}. 10 µM DCMU, dissolved in ethanol, was added under ML conditions. Statistical

comparison used a one-way ANOVA with Tukey post-hoc test. Different letters indicate statistical significance. Error bars show standard deviation based on three replicates and three technical replicates.

3.4 Discussion

3.4.1 Diatom species differences in TMET and eROS production

In this chapter, eROS production and FCR activity as a proxy for TMET were measured in three marine diatoms under different conditions. Clear distinctions were seen between the three species. *T. weissflogii* had a substantially higher constitutive rate of FCR than *A. glacialis* and *P. tricornutum* and a higher eROS production rate than *P. tricornutum*. Phytoplankton eROS production rates are diverse, even between species of the same genus (Marshall *et al.*, 2005b; Schneider *et al.*, 2016). This diversity is emphasised here by the first measurements of FCR in *P. tricornutum*, and relative eROS production and FCR in *A. glacialis*, further highlighting species differences in baseline production. The calculated FCR values of *T. weissflogii* (12-15 fmole cell^{-1} min^{-1} vs 0.1-10 amol FCR cell^{-1} µm^{-2} min^{-1}) are comparable to a previous study (Davey *et al.*, 2003). *T. weissflogii* has one of the highest measured rates of diatom FCR and eROS production (Davey *et al.*, 2003; Milne *et al.*, 2009; Schneider *et al.*, 2016), along with *T. eccentrica* (Davey *et al.*, 2003) or *Pseudo-nitzschia* sp. (Diaz & Plummer, 2018; Diaz *et al.*, 2018). Typically, the highest per cell levels of superoxide stem from toxic raphidophytes or dinoflagellates (Marshall *et al.*, 2005b; Diaz *et al.*, 2018), where the high eROS production is suggested to contribute significantly to the species toxicity (Oda *et al.*, 1998; Kim *et al.*, 1999; Yamasaki *et al.*, 2004). *T. weissflogii* is not a toxic alga, so an alternate function for its high eROS production must exist.

3.4.2 NOX involvement in TMET and eROS production

There is likely underlying mechanistic diversity between diatom FCR activity and eROS production based on the effects of DPI. DPI has been widely used to inhibit NOX activity (Kupper *et al.*, 2001; Foreman *et al.*, 2003; Lara-Ortiz *et al.*, 2003; Wong *et al.*, 2004; Lardy *et al.*, 2005) and the significant reduction of FCR and eROS production in *P. tricornutum* and *T. weissflogii* in the presence of DPI supports NOX involvement in these species. As FCR activity in these species was less severely affected by the presence of DPI than eROS production (20-30% reduced FCR activity vs 70-80% reduced eROS production), a significant proportion of FCR activity likely originates from DPI-insensitive TMET enzymes. DPI has previously been shown to have limited effect on *C. reinharditii* TMET for iron reduction (Eckhardt & Buckhout, 1998). Other phytoplankton TMET enzymes include nitrate reductase and ferric reductase but their respective activities have not been tested in the presence of DPI (Jones & Morel, 1988; Lomas *et al.*, 2000; Lomas & Glibert, 2000; Maldonado & Price, 2001). The greater sensitivity of eROS production to DPI suggests eROS production is a better indicator of NOX activity. However, there is also species diversity as eROS production in *A. glacialis* was less sensitive to DPI than *P. tricornutum* and *T. weissflogii*. As

recently demonstrated with glutathione reductase (GR) in *T. oceanica* (Diaz *et al.*, 2019), there may be greater enzymatic diversity in diatoms for eROS production.

The low concentration of DPI used could also explain the incomplete reduction of eROS and FCR. There is no consensus for what concentration of DPI is suitable for complete eROS inhibition within phytoplankton (Eckhardt & Buckhout, 1998; Rose *et al.*, 2005; Anderson *et al.*, 2016). Marine diatoms have been treated with DPI concentrations ranging from 2-60 µM DPI (Davey *et al.*, 2003; Kustka *et al.*, 2005; Diaz *et al.*, 2019), with 10 µM DPI reducing *T. weissflogii* FCR by 75% (Davey *et al.*, 2003) and 20 µM DPI completely inhibiting *P. tricornutum* eROS production (Laohavisit *et al.*, 2015). This implies using >1 µM DPI would result in greater eROS or FCR inhibition. However, in *C. marina* increasing DPI concentration from 1 µM to 50 µM did not result in complete inhibition of extracellular superoxide production (25% inhibition to 50% inhibition) (Kim *et al.*, 2000).

Furthermore, caution is needed when using DPI. DPI is a flavoprotein inhibitor, binding irreversibly to the FAD domain that is present in NOX proteins and the NOX-like protein of *T. weissflogii*. Flavoproteins are widespread and versatile proteins (Massey & Hemmerich, 1980; Hefti *et al.*, 2003). Therefore, using high DPI concentrations risks inhibiting other flavoproteins and negatively affecting cellular function. The reduction in eROS production or FCR activity may be due to DPI toxicity and not NOX inhibition. However, while 1 µM DPI may not completely inhibit extracellular activity, there is less likelihood of non-specific toxicity (Riganti *et al.*, 2004) as plasma membrane NOX proteins are more likely targeted over intracellular flavoproteins.

3.4.3 Light intensity effects on TMET and eROS production

Light intensity had complex effects on eROS production and FCR activity, with each species showing different responses (Fig 3.9, Table 3.1). However, there were broad patterns. Medium light increased eROS production (*A. glacialis*, *P. tricornutum*) and decreased FCR activity (all species). DCMU addition increased eROS production (all species) and decreased FCR activity (*A. glacialis*, *T. weissflogii*). The contrasting effects of high light, which decreased diatom FCR but increased eROS matches previous observations (Davey *et al.*, 2003; Laohavisit *et al.*, 2015; Schneider *et al.*, 2016; Diaz *et al.*, 2019), though this is the first study to directly compare the two assays. Furthermore, lower light intensities were required in the present study for FCR inhibition (complete inhibition at 200 µmol photons m^{-2} s^{-1} vs 50% inhibition at 380-880 µmol photons m^{-2} s^{-1}) (Davey *et al.*, 2003). High light inhibition of FCR has been proposed to result from reduced generation of non-photosynthetic sources of reductant such as the oxidative pentose phosphate pathway (OPP) (Davey *et al.*, 2003). However, the lack of inhibition of eROS production in high

light in *A. glacialis* and *P. tricornutum* (Fig 3.8) suggests the source of reductant is not a limiting factor. Several studies have shown high light can trigger increased photosynthetically-derived ROS in plants and algae (Suggett *et al.*, 2008; Waring *et al.*, 2010; Exposito-Rodriguez *et al.*, 2017; Mizrachi *et al.*, 2019). The increased eROS production in high light could originate from increased cellular H_2O_2 diffusing out of the cell and oxidising the dye. However, previous work with OxyBURST has suggested the dye is more specific to superoxide than H_2O_2 (Monshausen *et al.*, 2007), implicating a membrane oxidoreductase source. Thus, a clear explanation for the findings is not immediately obvious. Increasing TMET and eROS production during high light have both been suggested as phytoplankton strategies to dissipate excess reductant (Lomas *et al.*, 2000; Davey *et al.*, 2003; Hansel *et al.*, 2016; Diaz *et al.*, 2019). As the present work has demonstrated significant mechanistic differences between TMET and eROS production in marine diatoms (Fig 3.7, 3.8), perhaps eROS production is prioritised for high light derived electron dissipation over other TMET mechanisms. As extracellular O_2 is an abundant electron acceptor compared to other acceptors such as Fe^{3+} (Kustka *et al.*, 2005), eROS production may represent a more viable electron dissipation mechanism. In high light, eROS producing enzymes may be upregulated while other TMET enzymes such as ferric reductase may be downregulated. Hence, increased eROS production but overall reduced TMET activity. However, further work comparing gene expression or enzyme activity of different TMET enzymes under high light would be required to test this and explain the discrepancy between eROS and TMET.

Table 3.1 Comparison of the responses of each species to different treatments in each assay.

The effects shown indicate significant differences to the darkness control.

	A. glacialis	***P. tricornutum***	***T. weissflogii***
FCR activity			
Medium light	-	-	↓
High light	↓	↓	↓
10 µM DCMU	↓	-	↓
eROS production			
Medium light	↑	↑	-
High light	↑	↑	-
10 µM DCMU	↑	↑	↑

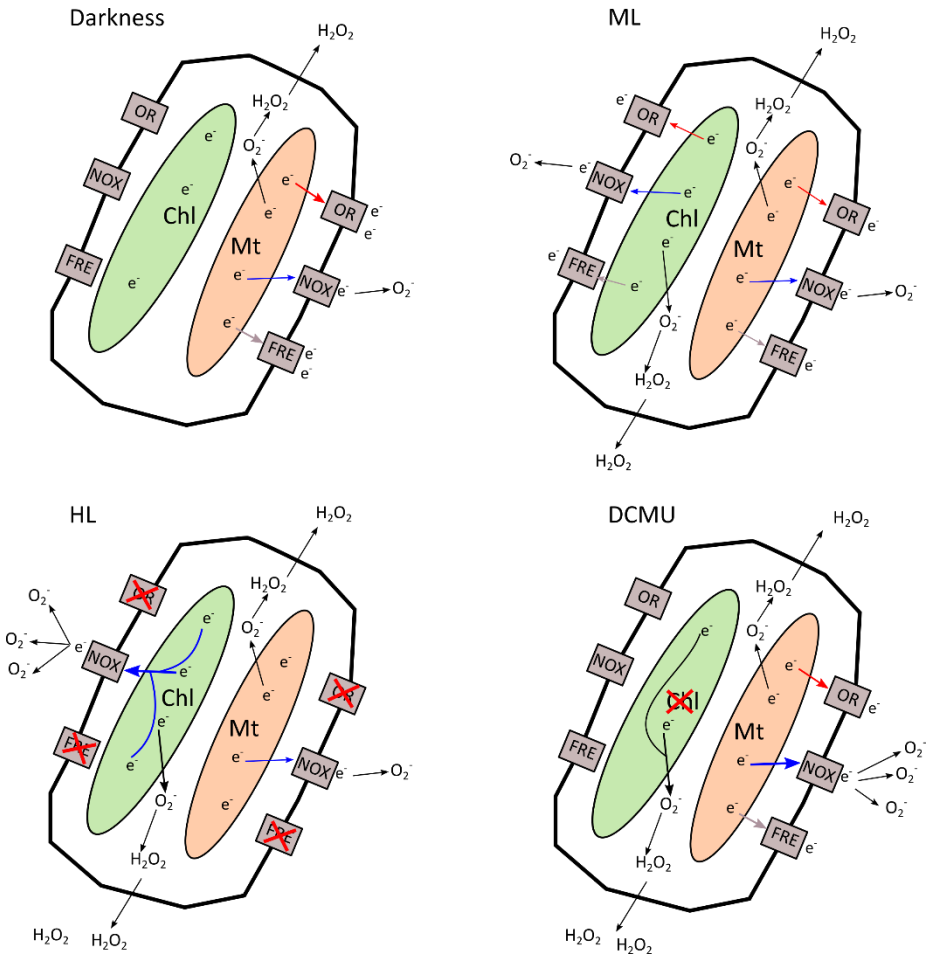

Figure 3.9 . A generalised model for how light intensity may affect marine diatom TMET and eROS production.

Under different conditions, electrons are directed to oxidoreductase enzymes (red arrows), NOX enzymes (blue arrows), ferric reductase enzymes (brown arrows) or to intracellular oxygen (black arrows). Electrons are supplied from the mitochondria or chloroplast. Chl= chloroplast, Mt= mitochondria, NOX= NADPH oxidase, FRE= ferric reductase, OR= other general oxidoreductase proteins.

The results following DCMU addition highlights another interesting research area: the source of intracellular electrons. DCMU inhibits electron flow through PSII, preventing O_2 evolution and the formation of NADPH (Miura *et al.*, 1981) which is the electron source for several oxidoreductase enzymes. Previous work has shown DCMU reduces TMET in several microalgae and cyanobacteria (Lynnes *et al.*, 1998; Weger & Espie, 2000; Davey *et al.*, 2003; Bombelli *et al.*, 2011), which has also been shown here in *A. glacialis* and *T. weissflogii* (Fig 3.7). This supports photosynthetically derived NADPH as the primary supplier of electrons for TMET in several algal species. In other microalgae (*C. marina, Heterosigma akashiwo*), DCMU has no immediate effect on eROS production (Oda *et al.*, 1998; Marshall *et al.*, 2002; Liu *et al.*, 2007). However, DCMU increased eROS production in all three diatoms. Though DCMU can generate chloroplast superoxide in plants (Ozgur *et al.*, 2015), the low membrane permeability of superoxide and the previously

mentioned specificity of OxyBURST to superoxide over H_2O_2 suggests an enzymatic source over cellular diffusion. It is unclear why inhibiting PSII would increase enzymatic eROS production. However, it does suggest other non-photosynthetic electron sources are available to diatoms. One option is increased OPP activity, which can generate cytoplasmic NADPH (Gruber *et al.*, 2009; Osada *et al.*, 2017). *C. reinharditii* can increase production of OPP components in darkness, to maintain high dark TMET activity (Xue *et al.*, 1998). Alternatively, a NADPH pool may exist. DCMU only reduced *C. marina* superoxide production after five hours exposure (Marshall *et al.*, 2002), which could support the presence of a reductant pool. If there is a comparable NADPH pool within diatoms, a two-hour experiment may not deplete the pool enough for a reduction in TMET or eROS. Future investigations into diatom TMET or eROS production should consider monitoring how assay activity changes over an extended time period.

T. weissflogii unusually maintained high eROS and FCR activity in darkness. While contrasting previous work reporting *T. weissflogii* eROS production increases with light (Milne *et al.*, 2009; Schneider *et al.*, 2016), the high FCR activity and eROS production regardless of light intensity suggests photosynthesis is not the primary electron source for maintaining high TMET in *T. weissflogii* (Davey *et al.*, 2003). Only *Pseudo-nitzschia* sp. has displayed comparably high dark production of eROS amongst diatoms (Diaz *et al.*, 2018), which also may have a similar electron supply. This constitutive production in all conditions reaffirms the species difference in diatom reductant generation. Whether the uniqueness of *T. weissflogii* relates to its NOX-like protein (Chapter 2), rather than a traditional NOX, could be worth investigating further.

3.4.4 Conclusions

This study characterised the dynamics of eROS production and TMET in three diatom species. While there are species specific differences, there are broad consistencies with previous literature. *T. weissflogii* has high rates of eROS production and TMET compared to *P. tricornutum* and *A. glacialis*. DPI strongly inhibited eROS production in *T. weissflogii* and *P. tricornutum*, supporting NOX involvement. The reduced effect of DPI on FCR suggests NOX has a relatively small involvement in TMET. Therefore, FCR is a less viable method for measuring NOX activity. Finally, light intensity has diverse effects depending on the species monitored. *A. glacialis* and *P. tricornutum* demonstrate similar patterns, suggesting photosynthesis and light play important roles in supplying electrons for TMET and eROS. *T. weissflogii* is affected to a lesser degree, with only HL and DCMU reducing its capacity for TMET, hinting at specialised cellular mechanics to facilitate this. The differences seen between these species demonstrate complex mechanics involved in plasma membrane electron transport and ROS generation.

Chapter 4 Using the fluorescent biosensor roGFP2-Orp1 to explore H_2O_2 dynamics in *Phaeodactylum tricornutum*

4.1 Introduction

Reactive oxygen species (ROS) are an unavoidable metabolic by-product within cells and have important consequences for cellular physiology. They form through incomplete reduction of oxygen, which commonly occurs in metabolic pathways (photosynthesis, respiration) that incur electron leakage from electron transport chains. There are different types of ROS (superoxide, hydrogen peroxide, hydroxyl radicals) with different chemical properties and sources (Mittler, 2017). ROS are strong oxidants and in high concentrations cause extensive damage to cellular machinery, leading to oxidative stress. Cells have developed an array of antioxidants to detoxify ROS, using small molecular weight molecules such as glutathione in conjunction with specific enzymes such as glutathione reductase, superoxide dismutase or ascorbate peroxidase (Noctor & Foyer, 1998; Miller, 2012).

Despite the risk of oxidative stress, ROS are important for healthy cell metabolism (Mittler *et al.*, 2011). ROS can oxidise protein thiol groups on cysteine residues, altering the protein structure and function. Thus, the 'redox state' of the cell, and the tendency of protein cysteine residues to be oxidised, changes with the production and scavenging of cellular ROS, resulting in altered signalling pathways (Mittler *et al.*, 2011). A common pathway that incorporates ROS signalling is programmed cell death (PCD), where exceeding a threshold level of ROS triggers a signalling pathway resulting in a controlled death. ROS-associated PCD occurs in many species including unicellular organisms (Murik & Kaplan, 2009; Farrugia & Balzan, 2012; Gallina *et al.*, 2015; Petrov *et al.*, 2015) and ROS can also act as a stress signal (Rijstenbil *et al.*, 1994; Morelli & Scarano, 2004). Furthermore, the type of ROS produced potentially allows specificity with respect to the target (D'Autréaux & Toledano, 2007). In particular, hydrogen peroxide (H_2O_2) may act as a highly suitable signalling molecule as it is relatively stable, membrane permeable and strongly targets cysteine residues, allowing greater spatial and temporal influence (Miller *et al.*, 2009; Mittler, 2017; Smirnoff & Arnaud, 2019).

Certain environmental conditions can affect cellular ROS production in microalgae, triggering cellular responses. Nutrient stress (Allen *et al.*, 2008; Rosenwasser *et al.*, 2014), salinity (Rijstenbil, 2003; Hernando *et al.*, 2015), high light exposure (Waring *et al.*, 2010), viral infection (Evans *et al.*, 2006) and CO_2 limitation (Vardi *et al.*, 1999) can generate intracellular ROS, altering cellular response. Extracellular sources of ROS, originating from biotic sources such as enzymatic activity (Kustka *et al.*, 2005; Marshall *et al.*, 2005a) or abiotic sources such as light-stimulated splitting of oxygen (Micinski *et al.*, 1993), can also affect cells. Oceanic steady-state ROS levels typically range from pico- to nanomolar concentrations (Rose, 2012; Zinser, 2018), often varying with depth, type of ROS and time of day (correlating with sunlight) (Rose *et al.*, 2008; Shaked *et al.*, 2010; Diaz *et*

al., 2016). Changing concentrations of ROS and alterations to the cellular redox state are likely frequent occurrences for photosynthetic microalgae. Unsurprisingly, ROS can have complex impacts on cells. Pre-exposure of H_2O_2 in plants, microalgae and macroalgae promotes expression of stress genes and enhances survival to subsequent stress (Dring, 2005; Hossain *et al.*, 2015). For example, H_2O_2 triggers protective encystment in the dinoflagellate *Lingulodinium polyedrumand* (Ganini *et al.*, 2013). In contrast, pre-treatment of H_2O_2 to *Chlamydomonas reinharditii* results in sensitisation to future stresses (Murik & Kaplan, 2009; Murik *et al.*, 2014). Complex bimodal threshold responses to increasing concentrations of H_2O_2 also occur in some mammalian cells (Kaneko *et al.*, 1994; Nakamura *et al.*, 2003).

Various methods exist for the detection and quantitation of ROS. These include fluorescent dyes such as 2',7'-dichlorodihydrofluorescein diacetate (H_2DCF-DA) or dihydrorhodamine 123 (DHR) (Coelho *et al.*, 2002; Gallina *et al.*, 2014), chemiluminescent dyes such as methyl Cypridina luciferin analog (MCLA) (Kustka *et al.*, 2005) or conversion of tetrazolium compounds such as nitroblue tetrazolium chloride (NBT) or 2,3-bis-(2-methoxy-4-nitro-5-sulfophenyl)-2H-tetrazolium-5-carboxanilide (XTT) (Waring *et al.*, 2010; Laohavisit *et al.*, 2015). However, several problems are associated with these methods. They are often non-reversible and lack specificity (particularly in fluorescent dyes), resulting in reduced reliability and artefact generation. Furthermore, some dyes generate intermediate radicals that cause artificial inflation of fluorescence values (Dikalov & Harrison, 2012; Kalyanaraman *et al.*, 2012). To avoid these issues, there has been a shift towards the introduction of genetically encoded fluorescent redox biosensor proteins in amenable species. Here, the fluorescence of the expressed protein changes depending on the concentration of the ROS substrate. Biosensors use reversible target binding, allowing live cell imaging of dynamic responses. Moreover, using ratiometric biosensors (whereby the protein fluorescence spectrum changes with ROS concentration) allows reliable measurements regardless of reporter concentration. A number of redox biosensors exist using redox-sensitive green (roGFP2) or yellow (rxYFP) fluorescent proteins to detect cellular redox state changes (Ren & Ai, 2013; Schwarzlander *et al.*, 2016). These biosensors have two engineered cysteine residues susceptible to ROS oxidation. ROS oxidation creates a disulphide bond that alters the biosensor structure, affecting fluorescence properties.

Specialised ROS biosensors include the H_2O_2 specific biosensors HyPer (Belousov *et al.*, 2006) and roGFP2-Orp1 (Gutscher *et al.*, 2009) and a probe for glutathione redox potential, roGFP2-Grx1 (Gutscher *et al.*, 2008). roGFP2-Orp1 and HyPer have different mechanisms for targeting H_2O_2 (Fig 4.1.). roGFP2-Orp1 functions by a redox relay system utilising a yeast peroxidase, Orp1. Only H_2O_2 can oxidise Orp1, generating a disulphide bond in the Orp1 domain. The oxidation transfers to roGFP2, altering its fluorescence (Gutscher *et al.*, 2009). The HyPer biosensor consists of circularly

permuted YFP coding sequence conjugated to the regulatory domain of the H_2O_2 sensing protein OxyR from *Escherichia coli*. H_2O_2 binds to the OxyR domain and the consequent disulphide bond alters the conformation of HyPer, altering its fluorescent properties (Belousov *et al.*, 2006). These biosensors can reveal intimate dynamics of H_2O_2 signalling. Recently, plants expressing HyPer or roGFP2-Orp1 were used to investigate high light derived H_2O_2 chloroplast signalling and H_2O_2 crosstalk with hydrogen sulphide (Exposito-Rodriguez *et al.*, 2017; Scuffi *et al.*, 2018; Nietzel *et al.*, 2019). Of the two H_2O_2 biosensors, HyPer has a greater dynamic range compared to roGFP2-Orp1. However, HyPer is pH sensitive and so is unsuitable in certain situations (Schwarzlander *et al.*, 2016).

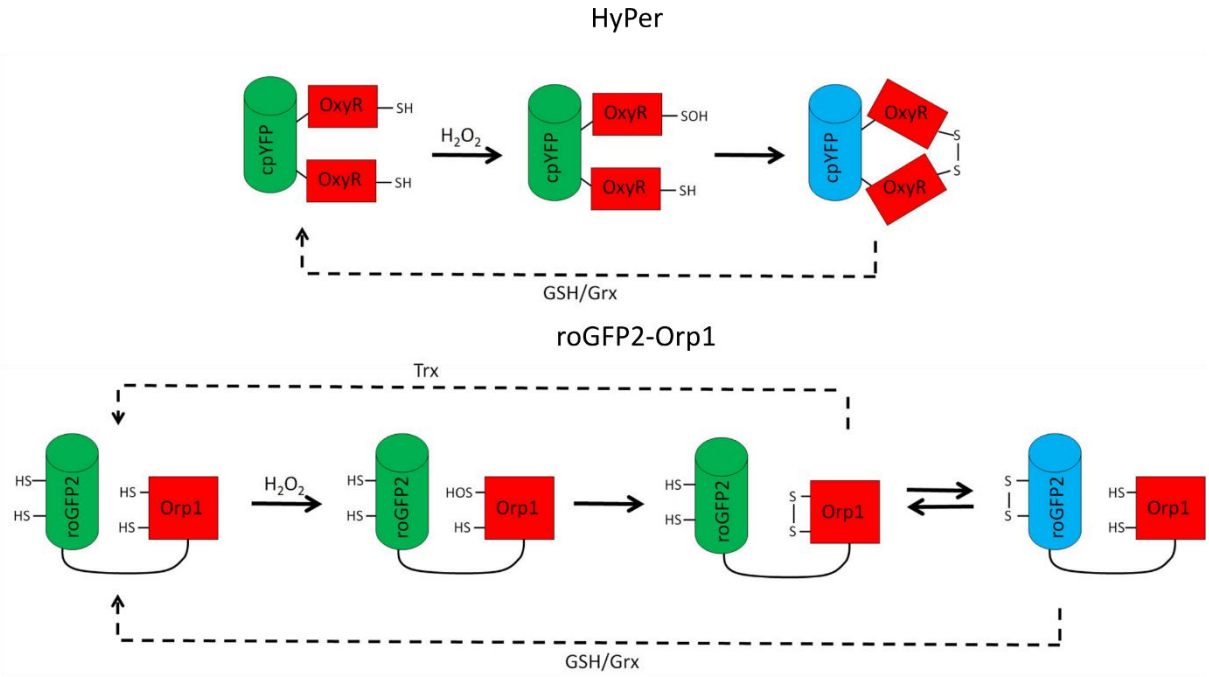

Figure 4.1 Comparison of the differing methods of action for H_2O_2 sensing in HyPer and roGFP2-Orp1.

Figure taken from Van Laer & Dick, (2016). Green regions indicate reduced fluorescent domains. Blue regions indicate oxidised fluorescent domains. Red regions indicate H_2O_2 specific binding domains. Glutathione/glutaredoxin (GSH/Grx) and/or thioredoxin (Trx) binding reduces biosensors.

Recently, roGFP2 expressed in *Phaeodactylum tricornutum* and *Thalassiosira pseudonana* has highlighted localised redox state signalling in response to environmental conditions (Rosenwasser *et al.*, 2014; Volpert *et al.*, 2018). For example, nitrate starvation or high light stress trigger chloroplast oxidation (Rosenwasser *et al.*, 2014; Mizrachi *et al.*, 2019) while infochemicals (decadienal, cyanogen bromide) oxidise the mitochondria in *P. tricornutum* (Graff van Creveld *et al.*, 2015). Compartment oxidisation and population PCD in *P. tricornutum* are strongly correlated (Graff van Creveld *et al.*, 2015, 2016; Mizrachi *et al.*, 2019). There has been a strong focus on PCD

activation in *P. tricornutum* by exogenous H_2O_2 addition, but complex interactions determine the effect. For example, 80 µM H_2O_2 or high light intensities (>1000 µmol photons m^{-2} s^{-1}) result in a split population response of redox-tolerant or redox-sensitive cells in *P. tricornutum*. Redox-sensitive cells undergo chloroplast oxidation and PCD within 24 hours whereas redox-tolerant cells survive (Mizrachi *et al.*, 2019). Adding higher concentrations of H_2O_2 (100-150 µM) oxidises the mitochondria as well as the chloroplast (Graff van Creveld *et al.*, 2015), suggesting H_2O_2 concentration is an important component of the signalling response.

This chapter describes the successful introduction and characterisation of the H_2O_2 specific biosensor roGFP2-Orp1 into *P. tricornutum*. Using roGFP2-Orp1 to monitor cytosolic H_2O_2 concentrations, dose dependent effects of exogenous H_2O_2 (50-200 µM) on cellular physiology were reported. Diverse concentration and temporal dependent effects of H_2O_2 on photophysiology parameters are reported.

4.2 Methods

4.2.1 Cell culture

Apart from the R-GECO strain (Helliwell *et al.*, 2019), all other *P. tricornutum* strains were grown in F/2 + Si medium (Guillard & Ryther, 1962) derived from twice filtered seawater (FSW) acquired at site L4 in the English Channel, as described in Chapter 3. R-GECO cells were maintained in artificial seawater (ASW, 450 mM NaCl, 30 mM $MgCl_2$, 16 mM $MgSO_4$, 8 mM KCl, 10 mM $CaCl_2$, 2 mM $NaHCO_3$, and 97 µM H_3BO_3) supplemented with F/2 nutrients. Cells were cultured in green plug culture flasks (SARSTEDT) on a 16:8 hour light: dark cycle, at 40-45 µmol s^{-1} m^{-2} photon flux density, measured using a LI-250A light meter (LI COR, USA) at 18°C. Cells were subcultured weekly and experiments used early-mid exponential phase cells. Cells were counted with a Beckman Coulter Counter.

4.2.2 Biolistic transformation of biosensor proteins into P. tricornutum

Different redox biosensors were designed for transformation into *P. tricornutum* (sequences listed in Appendix B1.). roGFP2 and roGFP2-Grx detect cellular redox state and glutathione redox potential respectively. roGFP2-Orp1, roGFP2-Tsa and roGFP2-ChlOrp1 detect H_2O_2. All gene sequences apart from roGFP2-ChlOrp1 were initially acquired from Addgene database (https://www.addgene.org) by Dr Glen Wheeler. roGFP2-ChlOrp1 was designed by adding chloroplast transit peptide OEE1 (Gruber *et al.*, 2007) to previously designed roGFP2-Orp1 sequence. All gene sequences were then codon optimised, synthesised and cloned into the shuttle vector pPha-T1 (Appendix B2) at restriction sites EcoRI and BamHI by Genscript (https://www.genscript.com/). pPha-T1 encodes antibiotic resistance for ampicillin in *E. coli* and Zeocin (InvivoGen) in *P. tricornutum*. Redox biosensor plasmids were introduced into *P. tricornutum* using the biolistic method previously described (Kroth, 2007; Helliwell *et al.*, 2019). *P. tricornutum* cells were harvested at a density of $5x10^6$ mL^{-1} and spread on 50% FSW, 1.5% w/v agar plates supplemented with F/2 + Si nutrients. 1.5 µg plasmids were adhered to 3 mg tungsten particles (0.6 µm diameter, BioRad) with 0.1 M spermidine and 2.5 M calcium chloride and then dried upon macrocarriers. Plasmids were introduced into cells by microparticle bombardment using a PDS-1000 He Particle Delivery System (Bio-Rad, USA) with 1350 psi rupture disks. Thereafter cells were left for 24 hours at 18°C before being streaked onto 50% FSW, 1.5% w/v agar plates supplemented with Zeocin (75 µg mL^{-1}) and F/2 + Si. Cells grew for four weeks at 18°C and resistant colonies were re-plated onto new Zeocin plates for two weeks. Colonies were inoculated into F/2 + Si medium for six days to trigger a return to fusiform morphotype for fluorescence analysis with confocal microscopy (Zeiss LSM 510). Cells were initially examined for

biosensor fluorescence and localisation using excitation: emission at 488:500-530 nm. Chlorophyll fluorescence was detected at 488: >580 nm.

4.2.3 Detection and characterisation of intracellular H_2O_2 using a plate reader assay

H_2O_2 changes in *roGFP2-Orp1* cells were measured by tracking fluorescence changes using a CLARIOstar Plus plate reader (BMG Labtech, Germany). 200 µL of early exponential phase *roGFP2-Orp1* cells (2-3x10^6 mL^{-1}) were taken from culture flasks and added to individual wells in a flat bottom, black, 96 well plate (Greiner) alongside six wells of FSW as a background control. roGFP2-Orp1 fluorescence was measured through excitation: emission detection of 400±20 nm: 520±10 nm and 475±15 nm: 520±10 nm. Average background FSW fluorescence was subtracted from values. Dividing the two emission fluorescence values creates a ratiometric 400:475 nm value, or Orp1 value, as a measure of cytosolic H_2O_2 (see Fig 4.2.) that represents the relative amount of cytosolic H_2O_2. The 400:475 nm value allows intercellular comparison regardless of difference in protein expression between cells. For time course experiments, time point values were divided by the starting 400:475 nm value (F_1/F_0). Starting values typically showed small variation between treatments. Normalisation to the starting value allowed clearer reporting of the relative increase in 400:475 nm value between treatments. 100 mM dithiothreitol (DTT) (Sigma-Aldrich), 1 mM menadione (Sigma-Aldrich) and 10 mM H_2O_2 (30% w/w solution, Sigma-Aldrich) master stocks were prepared using FSW as a solvent. Chemicals were added to *P. tricornutum* culture flasks, which were sampled at each time point. Flasks were maintained at 18°C at 40-45 µmol photons m^{-2} s^{-1}.

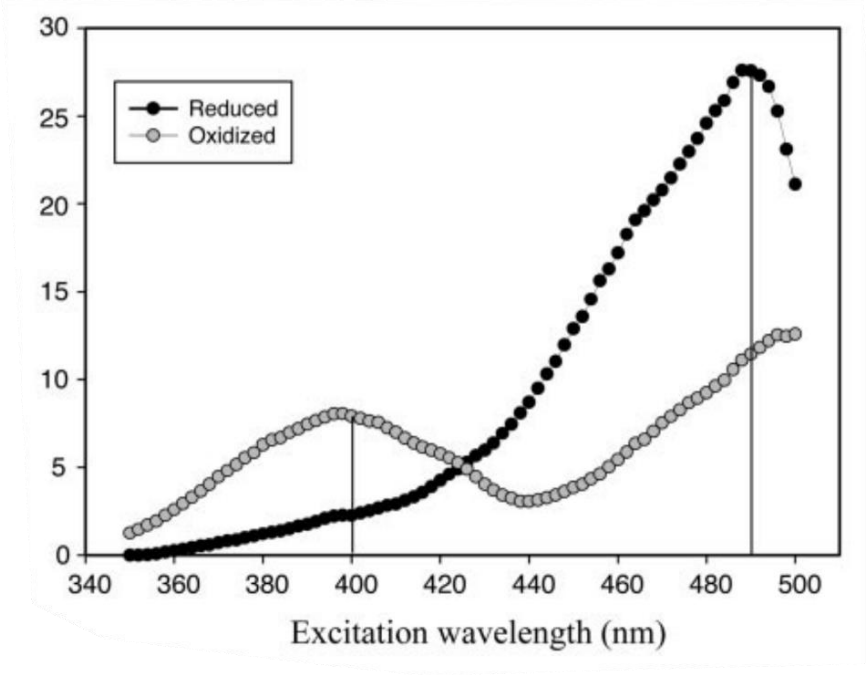

Figure 4.2 Excitation spectra of roGFP2.

Y axis displays relative fluorescence levels. Depending upon the level of oxidation, the fluorescence emission at 520 nm will increase or decrease at different excitation wavelengths (400 nm and 475 nm). Dividing the fluorescence from 400 nm excitation by fluorescence at 475 nm excitation gives a ratiometric value indicating redox state. roGFP2-Orp1 is structurally similar and has the same spectra. Thus, the 400:475 nm value indicates H_2O_2 concentration. Adapted from Dooley *et al.*, (2004).

4.2.4 Screening and measurement of chloroplast-targeted roGFP2-Orp1

Following chloroplast-targeted roGFP2-Orp1 (referred to below as roGFP2-ChlOrp1) transformation, colonies were grown in liquid medium (F/2 + Si + 75 µg mL^{-1} Zeocin). 2x198 µL of each colony were added to a black multiwell plate. Controls of 2x198 µL of FSW, wild type *P. tricornutum* and *roGFP2-Orp1* cells were also added. Biosensor fluorescence was monitored at excitation: emission wavelengths of 400:520 nm and 475:520 nm using a CLARIOstar Plus plate reader. Cells that responded to addition of 100 µM H_2O_2 within 10 min were selected for subsequent confocal and fluorescence imaging. When a suitable colony was found, wild-type *P. tricornutum* and *roGFP2-ChlOrp1* cells were grown to $2x10^6$ mL^{-1}. Changes in ChlOrp1 protein fluorescence following addition of 100 µM H_2O_2 was tracked for two hours using a plate reader. Wild-type *P. tricornutum* 400 nm and 475 nm fluorescence was subtracted from ChlOrp1 values, to remove chlorophyll autofluorescence.

4.2.5 Detection of intracellular H_2O_2 using epifluorescence microscopy

roGFP2-Orp1 cells were examined using an epifluorescence microscope (Leica DMi8). A glass bottom Petri dish was treated with 0.01% v/v Poly-L-Lysine (Sigma-Aldrich) and early exponential phase cells were left to settle for 15 min prior to washing twice with FSW. roGFP2-Orp1 fluorescence was measured through excitation: emission of 400:520 nm and 475:520 nm. Imaging was optimised with low intensity excitation and infrequent imaging to prevent photobleaching and subsequent effect on 400:475 nm value. Cells remained in darkness between images. For light stress experiments, transmission light was switched on to illuminate cells between image acquisition. A LI-250A light meter was used to convert arbitrary transmission light intensity to photon flux density (µmol photons m^{-2} s^{-1}). Images were analysed with Leica LAS X software. Regions of interest corresponding to individual cell shapes were drawn and 400 nm and 475 nm excitation fluorescence values were obtained. Three random background areas of the image were chosen to assess mean background fluorescence. Mean background fluorescence was removed from each excitation value prior to 400:475 nm calculation. 400:475 nm ratio values were normalised to starting values consisting of the average 400:475 nm value of the first four time points.

4.2.6 Monitoring intracellular Ca^{2+} and H_2O_2 through perfusion experiments

Transformed *P. tricornutum* cells expressing the Ca^{2+} biosensor R-GECO were kindly provided by Dr Katherine Helliwell (Helliwell *et al.*, 2019). For perfusion experiments, *roGFP2-Orp1* and *R-GECO* cells were grown to equivalent cell density ($2x10^6$ mL^{-1}). A glass bottom Petri dish was treated with 0.01% v/v poly-L-lysine. Cells were settled in the Petri dish for 30 min at 18°C. R-GECO detects calcium elevations through changes in fluorescence (excitation: emission 575:630 nm). The relative increase in Ca^{2+} (F_1/F_o) was measured after subtraction of background fluorescence, where F_o is starting value and F_1 is specific time point. *R-GECO* cells were imaged every 500 ms. 400 nm excitation settings developed high noise-signal problems so roGFP2-Orp1 was used in a non-ratiometric manner, using only excitation: emission at 475:520 nm. The relative change in intracellular H_2O_2 levels was calculated as $1-(F_1/F_0)$ using 475 nm fluorescence values, since 475 nm fluorescence is inversely related to H_2O_2 concentration. *roGFP2-Orp1* cells were imaged every 15 s. For time course measurements, *roGFP2-Orp1* and *R-GECO* cells rested for 10 s for pre-perfusion values. Cells were then were perfused with ASW for 75 s, followed by ASW containing 50 µM, 100 µM or 150 µM H_2O_2 for 75 s and then the original ASW for 75 s.

4.2.7 Long term changes in cellular parameters following H_2O_2 addition

roGFP2-Orp1 cells were grown to 2.5x10^6 cells mL^{-1}. Flasks of 30 mL cells were used with three replicates for each treatment. Cytosolic H_2O_2 was monitored using the plate reader assay as described above. Chlorophyll fluorescence parameters were recorded using AquaPen fluorimeters (Photon Systems Instruments, Czech Republic). F_0 indicates photosystem II (PSII) minimum dark-adapted fluorescence, F_m indicates PSII maximum dark-adapted fluorescence, Fv/Fm indicates maximum quantum efficiency of PSII and non-photochemical quenching (NPQ) indicates the level of absorbed energy dissipated as heat. AquaPen AP 110/C measured Fv/Fm and AquaPen-C AP 110-C measured the other parameters. Due to the time duration required for NPQ values, it was not possible to measure all treatments at the same time without a significant time delay resulting in both morning and afternoon measurements. To minimise diurnal variations in photosynthetic parameters, the 50 µM and 150 µM H_2O_2 treatments took place one day after the control and 100 µM H_2O_2 treatments. Cell density was adjusted to 2.5x10^6 cells mL^{-1} by dilution with FSW prior to measurements. 2 mL of cells were removed from each culture flask and dark adapted for 20 min at 18^oC. NPQ was monitored with instrument settings as described in Serif *et al.* (2017) (700 µmol photons m^{-2} s^{-1} red actinic light, 3000 µmol photons m^{-2} s^{-1} saturating pulse and 20% measuring light pulses. NPQ induction curves were used to acquire F_0 and F_M values. H_2O_2 was added from 10 mM stock to each flask to create concentrations of 0 (FSW blank), 50 µM, 100 µM and 150 µM H_2O_2. Each parameter was measured before H_2O_2 addition and 30, 60, and 180 min post-addition. For longer term monitoring (>1 day), wild-type *P. tricornutum* cells were diluted to a starting concentration of 3x10^5 cells mL^{-1} prior to H_2O_2 addition. Cell density was tracked using a Beckman Coulter Counter. Growth rate was calculated using the formula $\mu = (\text{Ln } D_1\text{-}D_0)/ (T_1\text{-}T_0)$. µ is growth rate, D_1 and D_0 represent the log transformed cell density and T_1 and T_0 represent the days of growth.

4.2.8 Statistical analysis

All statistics were calculated using SigmaPlot 14 statistical software. Data were tested for normality (Shapiro-Wilk) and equality of variance (Brown-Forsythe). Data were tested for normality and equality of variance using Shapiro-Wilk and Brown-Forsythe tests. If data passed both tests, datasets were analysed using a one-way ANOVA and Tukey post hoc tests. If datasets failed precursor tests, a Kruskal-Wallis test on ranks in conjunction with a Tukey post hoc or Dunns Method test was used. Statistical significance of data was indicated if $P<0.05$.

4.3 Results

4.3.1 Screening and transformation with roGFP2-Orp1

Transformation of *P. tricornutum* resulted in over 30 Zeocin resistant colonies from roGFP2 and roGFP2-Orp1 plasmids. No colonies grew following transformation with roGFP2-Grx or roGFP2-Tsa plasmids. Following confocal screening, no roGFP2 colonies contained fluorescent cells but two roGFP2-Orp1 colonies were fluorescent with roGFP2-Orp1 expressed in the cytosol (Fig 4.3A). Further screening using epifluorescence microscopy confirmed fluorescence following excitation at 400 nm and 475 nm (Fig 4.3E,F). The colony exhibiting the greatest fluorescence was picked and subcultured into new medium, to allow growth for subsequent analysis.

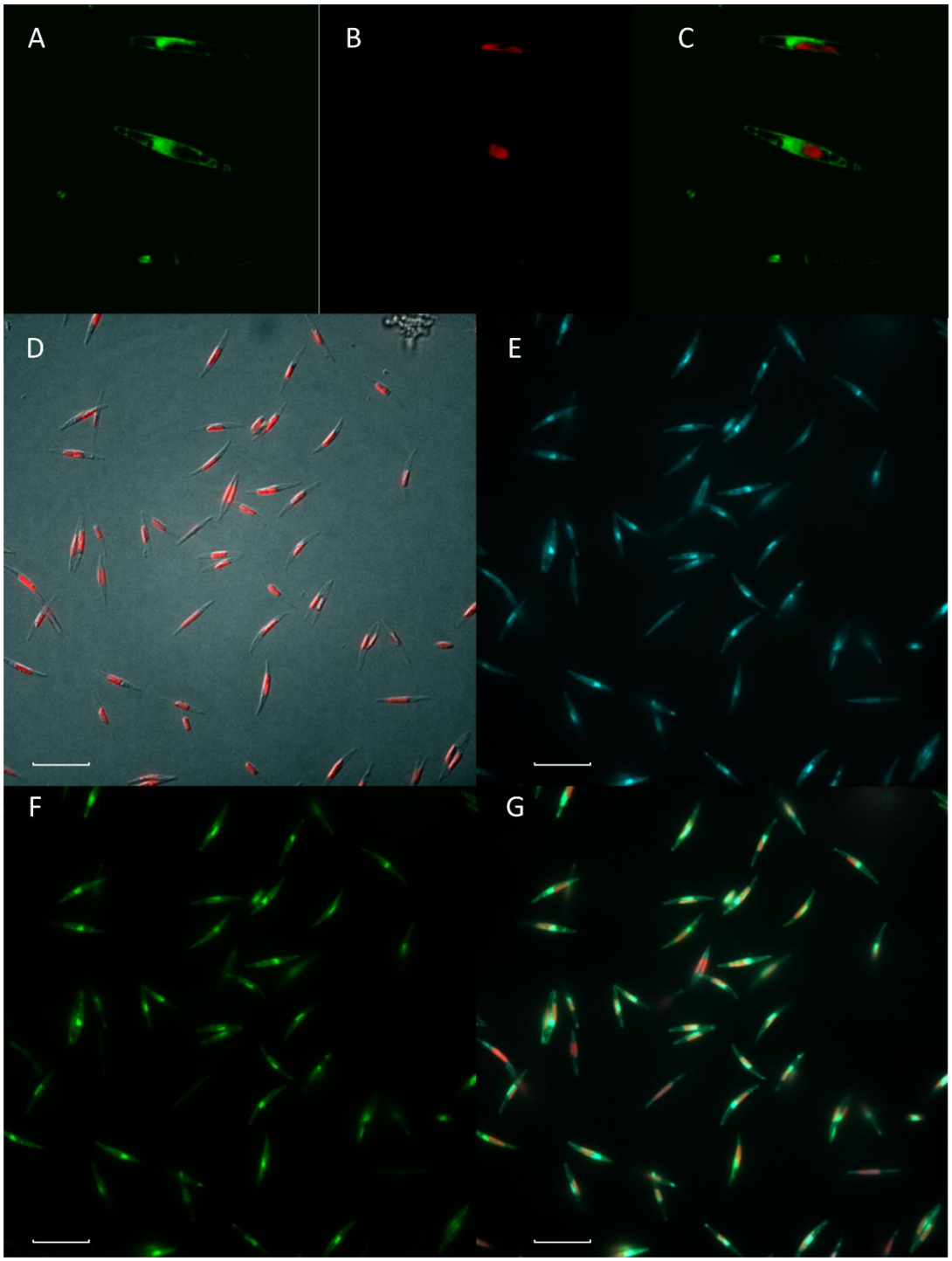

Figure 4.3 roGFP2-Orp1 is expressed in the cytosol of *Phaeodactylum tricornutum*. A-C) Confocal microscopy of *roGFP2-Orp1* cells. A) Cytosolic roGFP2-Orp1 fluorescence at 488 nm excitation. B) Chlorophyll fluorescence. C) Merged roGFP2-Orp1 and chlorophyll fluorescence. (D-G) Epifluorescence microscopy of roGFP2-Orp1 cells. D) Chlorophyll and DIC. E) 400 nm excitation, F) 475 nm excitation and G) merged 400 nm, 475 nm, and chlorophyll images. Scale bar = 25 µm. Scale bar unavailable for images A, B and C.

4.3.2 Characterisation of roGFP2-Orp1

To validate the response of roGFP2-Orp1 to H_2O_2, transformed cells were monitored following H_2O_2 addition using a plate reader assay. Control *roGFP2-Orp1* cells showed stable 400:475 nm values over 180 min of measurements (Fig 4.4). Addition of 100 µM H_2O_2 led to a significant rapid increase in 400:475 nm value, peaking at 5 min post addition (two-way ANOVA, $P<0.001$). The 400:475 nm value remained constant for 30 min before a large decrease, reaching control values after 120 min. DTT is a strong reducing agent. It was used to fully reduce roGFP2-Orp1 cysteine residues and therefore reduce the 400:475 nm value to its minimum value, as used previously with roGFP2 (Rosenwasser *et al.*, 2014; Mizrachi *et al.*, 2019). 1 mM DTT had no significant effect in the first 60 min (two-way ANOVA, $P>0.05$), suggesting that baseline cytosolic H_2O_2 levels are maintained at low concentrations. 60 min post DTT addition, cytosolic H_2O_2 increased slightly significantly (two-way ANOVA, $P<0.001$) compared to control values. 1% v/v ethanol and 1% v/v DMSO had no effect on intracellular H_2O_2 levels throughout the time course (two-way ANOVA, $P>0.05$). Menadione is a quinone that rapidly induces superoxide radicals (Sirisha *et al.*, 2014) and so was used to distinguish between H_2O_2 and superoxide effects. Menadione induced an significant increase in 400:475 nm value (two-way ANOVA, $P<0.001$), peaking after 60 min with no substantual reduction to control values. This peak was lower than the peak value following 100 µM H_2O_2 addition. The increase is likely due to conversion of superoxide to H_2O_2 through antioxidants such as superoxide dismutatase, as roGFP2-Orp1 is insensitive to superoxide.

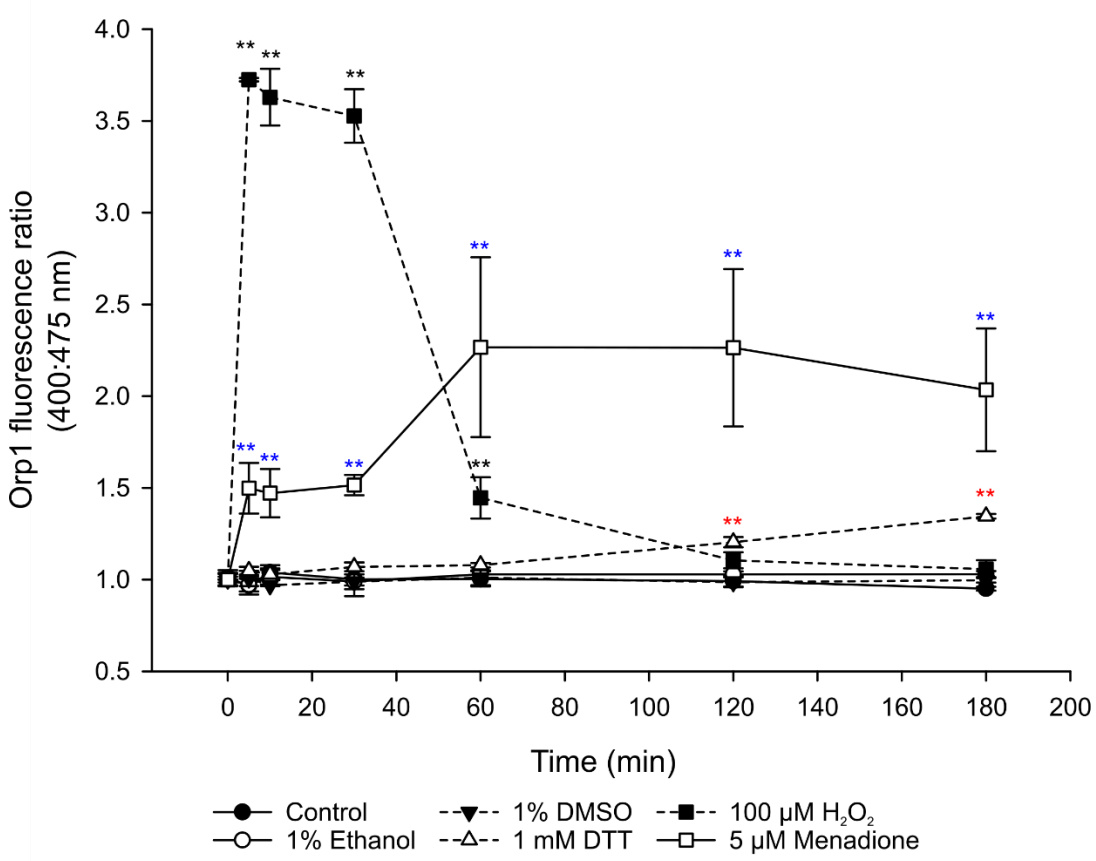

Figure 4.4 Responses of roGFP2-Orp1 in *P. tricornutum*.

Following chemical addition after t=0, 400:475 nm values were tracked over 180 min. Error bars for each data point represent standard deviations based on three biological replicates with two-three technical replicates. A two-way ANOVA tested statistical significance between control values and added chemicals at each time point. ** P=<0.001. Black asterisk indicates test between control and 100 µM H_2O_2, blue indicates test between control and 5 µM menadione and red indicates test between control and 1 mM DTT.

4.3.3 Transformation and screening of roGFP2-ChlOrp1

Transformation of *P. tricornutum* with roGFP2-ChlOrp1 resulted in 49 colonies growing in Zeocin media. Changes in 400:475 nm ratio for each colony were monitored following addition of 100 µM H_2O_2 using the plate reader. 10 colonies had increased 400:475 nm values and were screened using confocal microscopy. Of the 10, eight displayed GFP fluorescence, though fluorescence intensity varied between colonies. Fluorescence predominantly localised to the chloroplast (Fig 4.5) but several transformants had weak additional punctate fluorescence (Fig 4.5A). The brightest colony was subcultured into new medium and maintained for further characterisation.

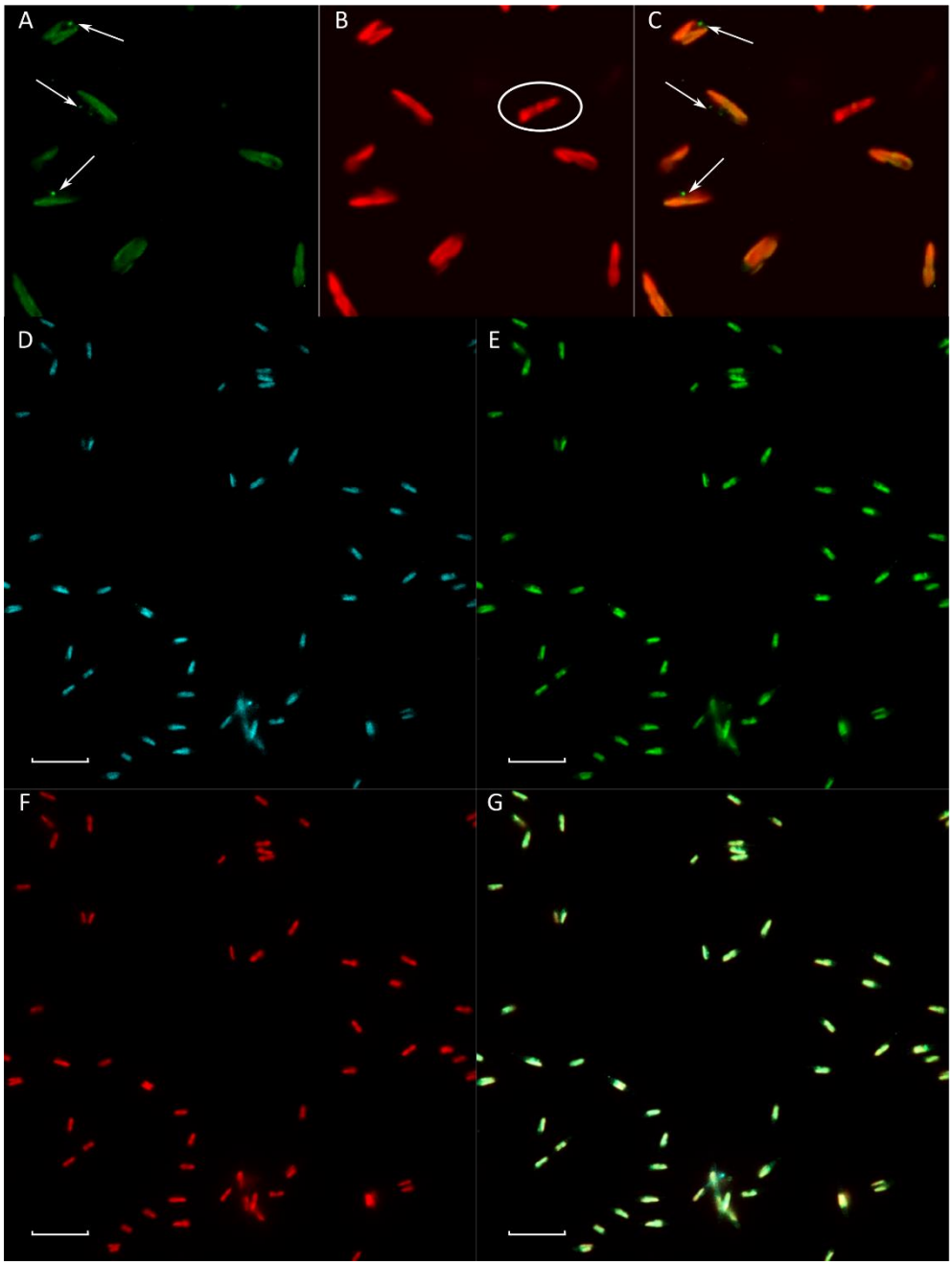

Figure 4.5 Expression of roGFP2-ChlOrp1 in *P. tricornutum*.

Confocal microscopy (A, B, C) confirmed roGFP2-ChlOrp1 is expressed in the chloroplast, though there was minor localisation outside of the chloroplast (white arrows). A) GFP, B) chlorophyll, C) overlaid image. Note the absence of expression in the white circled cell in B) representing a control for chlorophyll autofluorescence and confirming successful localisation. Cell fluorescence was also detected through epifluorescence microscopy (D-G). D) 400 nm, E) 475 nm, F) chlorophyll fluorescence and G) overlaid 400 nm, 475 nm, and chlorophyll fluorescence. Scale bar = 25 µm. Bar not available for images A, B and C.

4.3.4 Effects of H_2O_2 on roGFP2-ChlOrp1

roGFP2-ChlOrp1 400:475 nm values obtained with the plate reader were highly variable throughout the time course, even in the control (Fig 4.6A). 100 µM H_2O_2 increased the 400:475 nm value within 10 min before declining. By 60 min, the H_2O_2 treated cells showed a 400:475 nm value lower than the control. The high degree of variation in 400:475 nm value originated primarily from the 400 nm fluorescence values. Under reduced conditions, the 400 nm fluorescence is only slightly higher than background 400 nm fluorescence observed in wild-type cells. Therefore, slight variations in roGFP2-ChlOrp1 400 nm fluorescence can result in negative 400 nm values when subtracting the wild-type fluorescence. To counteract this, the reporter was used non-ratiometrically, tracking changes in 475 nm fluorescence in the plate reader (Fig 4.6B). Comparable to cytosolic H_2O_2 results, there was an immediate increase in chloroplast H_2O_2 before declining 10 min post addition. By 60 min, 100 µM H_2O_2 treated cells had returned close to pretreatment values. Though further work is required to optimise the protocol, there is the potential for monitoring chloroplast localised H_2O_2 in *P. tricornutum*.

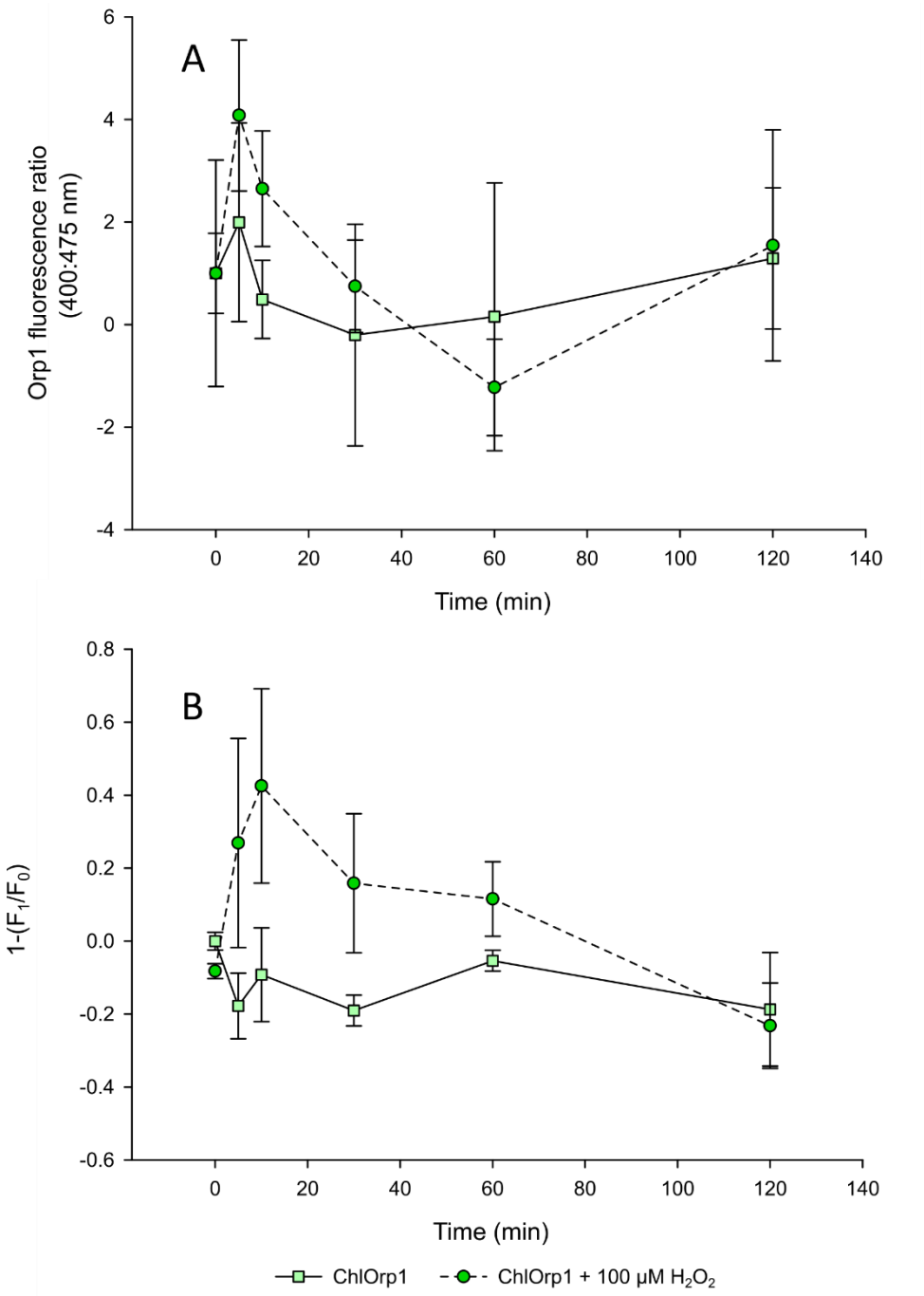

Figure 4.6 Characterising the response of roGFP2-ChlOrp1 to addition of 100 µM H_2O_2.

Chloroplast H_2O_2 was monitored using a plate reader to detect changes in roGFP2-ChlOrp1 fluorescence. A) 400:475 nm values. B) Relative change in inverted 475 nm fluorescence ($1-(F_1/F_0)$). Increase in value indicates increase in chloroplast H_2O_2. Error bars for each data point represent standard deviation based on three biological replicates with two technical replicates.

4.3.5 Effects of H_2O_2 on P. tricornutum cell physiology

Previous work has indicated that exogenous H_2O_2 can have significant effects on diatom physiology (Graff van Creveld *et al.*, 2015; Mizrachi *et al.*, 2019; Murik *et al.*, 2019), including oxidation of cellular compartments within one min of addition. Differing quantities of H_2O_2 result in compartment-specific signalling and PCD 24 hours post addition in *P. tricornutum*. Here, changes to physiological parameters at different temporal scales were examined in relation to cytosolic H_2O_2 concentration using roGFP2-Orp1.

4.3.5.1 Long term effect (days) of exogenous H_2O_2 addition to P. tricornutum

Exogenous H_2O_2 had a clear dose-dependent effect on cell growth (Fig 4.7A. Table 4.1). 50 µM H_2O_2 had no effect on growth or Fv/Fm. However, decreased growth occurred at higher H_2O_2 concentrations. 200 µM H_2O_2 inhibited cell growth for five days and Fv/Fm decreased within one hour, reaching 0.27 after 24 hours (Fig 4.7B). However, Fv/Fm returned to control values by day five. Cell growth resumed, albeit at a slower growth rate than the control, after day five. 100-150 µM H_2O_2 treatments caused small transient declines in Fv/Fm within the first day of addition. After day three, minimal differences in Fv/Fm were seen between the control and 50-150 µM H_2O_2 treatments.

Table 4.1 Comparison of growth rate between the different H_2O_2 treatments. Data are the mean of three replicates. Growth rate was calculated using population density at day zero and day three. 200 µM H_2O_2 growth rate using days five and eight is also presented in brackets, corresponding to resumption of growth.

Treatment	Growth rate
Control	0.87 ± 0.04
50 µM H_2O_2	0.87 ± 0.04
100 µM H_2O_2	0.77 ± 0.03
150 µM H_2O_2	0.67 ± 0.06
200 µM H_2O_2	0.20 ± 0.04 (0.78 ± 0.05)

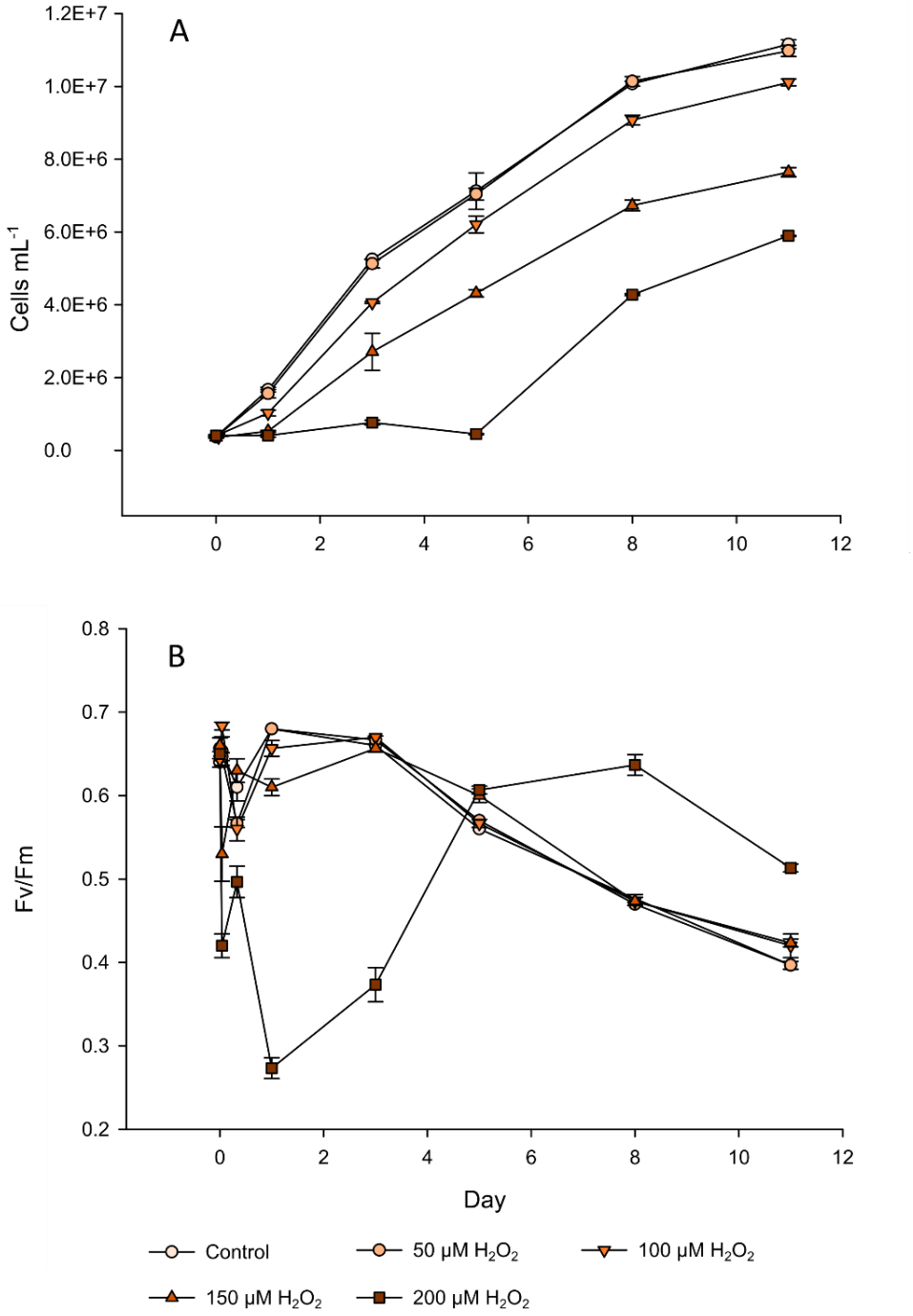

Figure 4.7 H_2O_2 concentration affects growth and photosynthetic efficiency of *P. tricornutum.*

A) Cell density and B) Fv/Fm were monitored after addition of H_2O_2. Fv/Fm measurements occurred at 0, 1, and 4 hours after addition on the first day. Error bars indicate standard deviation for three replicates.

4.3.5.2 Medium term (min to hour) effects of exogenous H_2O_2 addition to P. tricornutum

All H_2O_2 treated *roGFP2-Orp1* cells showed an increase in cytosolic H_2O_2 within 30 min of addition, with 100 µM and 150 µM H_2O_2 treatments showing a four-fold increase (Fig 4.8A). Within 60 min, 50 µM and 100 µM H_2O_2 treatment 400:475 nm values returned close to pre-treatment levels. 150 µM H_2O_2 treatment returned to pretreatment levels after 180 min.

The concentration of H_2O_2 added correlated with changes in Fv/Fm, F_o and F_m values. These parameters remained constant in the control and 50 µM treatments over 180 min (Fig 4.8B, Table 4.2). 100 µM H_2O_2 reduced F_0, F_M and Fv/Fm for 30 min post addition. 150 µM H_2O_2 reduced Fo and Fm parameters for 60 min, though Fv/Fm values at 60 min were not significantly different to starting values (Kruskal-Wallis test, P=0.071). Complete recovery of photophysiology parameters to pretreatment values occurred in both H_2O_2 treatments by the next respective time point. Thus, photophysiology recovery correlated with the return of cytosolic H_2O_2 to pre-treatment levels. NPQ values were more variable following H_2O_2 addition (Fig 4.8C). 100 µM H_2O_2 caused a continual increase in NPQ at every time point following addition, peaking after 180 min. In comparison, 150 µM H_2O_2 suppressed NPQ for 60 min before a significant increase occurred after 180 min.

Table 4.2 Comparison of F_0 and F_M values acquired from NPQ graphs at different time points and concentrations of H_2O_2. Error bars represent standard deviation of three replicates.

F_0					**F_M**			
	0 min	**30 min**	**60 min**	**180 min**	**0 min**	**30 min**	**60 min**	**180 min**
Control	2470.3 ± 32.5	2644 ± 135.4	2611.3 ± 18.7	2730.6 ± 117.4	14304.6 ± 172.1	14695 ± 112.5	14402.3 ± 113.1	14402.3 ± 181.2
50 µM H_2O_2	2275.6 ± 32.5	2340.6 ± 86.1	2503 ± 85.6	2590 ± 99.8	13513.3 ± 195.8	13860.3 ± 504.2	13600.3 ± 685.9	14174.3 ± 116.9
100 µM H_2O_2	2470.6 ± 65.5	1300.6 ± 56	2633.3 ± 56	2622 ± 19	14434.6 ± 394	4400 ± 221	15150 ± 325	14196.3 ± 359.9
150 µM H_2O_2	2275.3 ± 32.5	913.6 ± 61.1	980.6 ± 249.6	2503 ± 65	13308 ± 49.4	2621.6 ± 170.1	3338.3 ± 1698	13286.3 ± 248

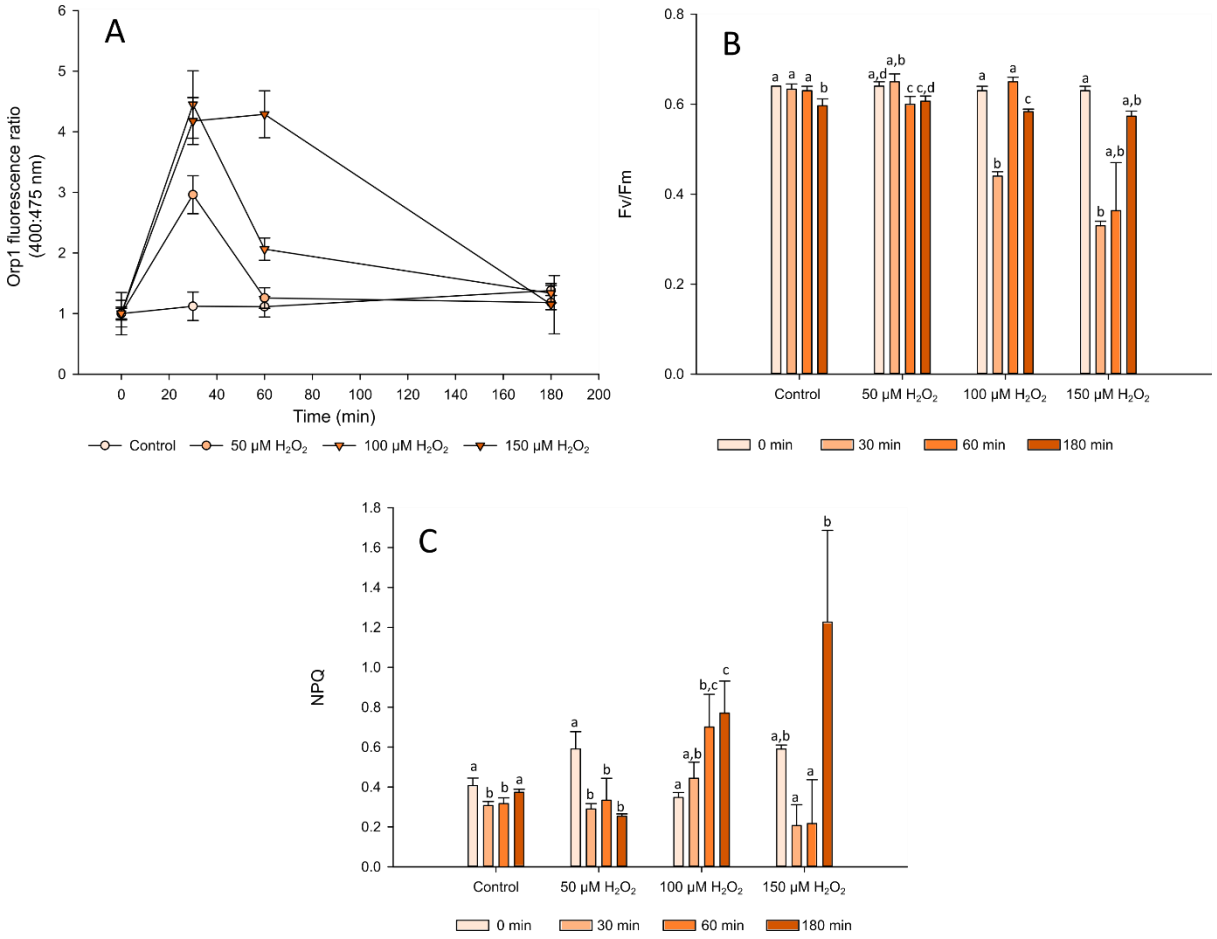

Figure 4.8 H_2O_2 concentration affects physiological parameters in roGFP2-Orp1 cells.

Following addition of H_2O_2 to flasks of *roGFP2-Orp1* cells, A) intracellular H_2O_2 level, B) Fv/Fm and C) NPQ were monitored over 180 min. Due to the treatments occurring on two separate days (control and 100 µM H_2O_2 on day 1, 50 µM and 150 µM H_2O_2 on day 2), statistical analysis compared the effect of time within each H_2O_2 treatment for Fv/Fm and NPQ graphs, rather than between H_2O_2 treatments. All data were tested using a one-way ANOVA, except for 150 µM H_2O_2 Fv/Fm dataset which failed a normality test and so was tested using a Kruskal-Wallis one-way analysis of variance on ranks. Different letters indicate significant differences within H_2O_2 treatments ($P<0.05$). Fv/Fm and NPQ data represents triplicate values. roGFP2-Orp1 data represents triplicate data (two technical replicates). Error bars show standard deviation.

4.3.5.3 Short term effects of H_2O_2 on P. tricornutum

The rate at which H_2O_2 enters the cells was investigated by monitoring changes in cytosolic H_2O_2 in response to H_2O_2 perfusion. Within 30 s, all concentrations of H_2O_2 triggered a rapid increase in cytosolic H_2O_2 (Fig 4.9). This increase continued for the H_2O_2 perfusion duration (75 s). 100 µM

and 150 µM H_2O_2 caused greater increases in cytosolic H_2O_2 than 50 µM H_2O_2, though all three treatments had overlapping error bars. Subsequent ASW perfusion reduced cytosolic H_2O_2 slightly after 30 s in the 50 µM H_2O_2 treatment but not in the 100-150 µM treatments.

Exogenous H_2O_2 addition can cause cytosolic Ca^{2+} elevations in plants (Wu *et al.*, 2020). To see if similar elevations occur in diatoms, Ca^{2+} elevations were monitored in *P. tricornutum* expressing the cytosolic Ca^{2+} biosensor R-GECO following H_2O_2 perfusion. The initial ASW perfusion triggered a transient elevation of cytosolic Ca^{2+} in most cells. However, few calcium elevations were seen following the switch to perfusion of new media of ASW (control) or H_2O_2 (Fig 4.10). No subsequent elevations were seen in ASW and 50 µM H_2O_2 treatment. 100 µM and 150 µM H_2O_2 treatments infrequently induced cytosolic Ca^{2+} elevations, representing less than 10% of cells measured. Thus, while H_2O_2 perfusion can trigger cytosolic Ca^{2+} elevations, it only occurs in a small proportion of cells.

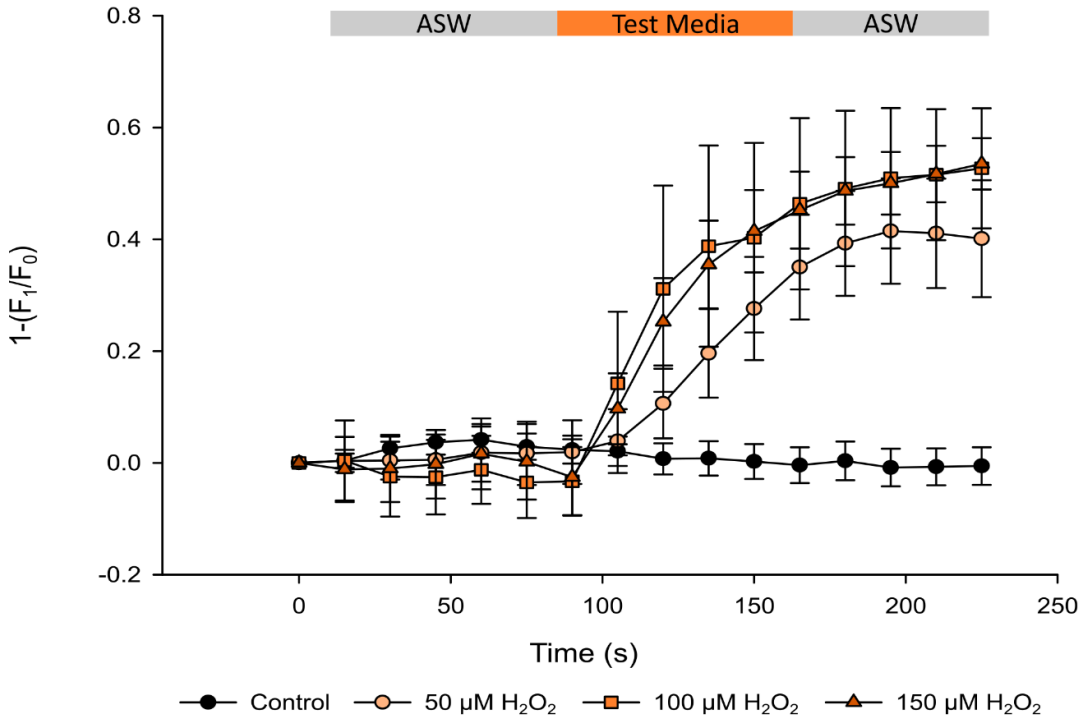

Figure 4.9 Rapid changes in roGFP2-Orp1 fluorescence following perfusions of different concentrations of H_2O_2.

Using epifluorescence microscopy, relative decrease in 475 nm fluorescence, representing cytosolic H_2O_2, was monitored following perfusion with ASW containing 50 µM, 100 µM or 150 µM H_2O_2. 1-(F_1/F_0) conversion represents increasing H_2O_2. Error bars show standard deviation of cells from one experiment (n=21-27 cells).

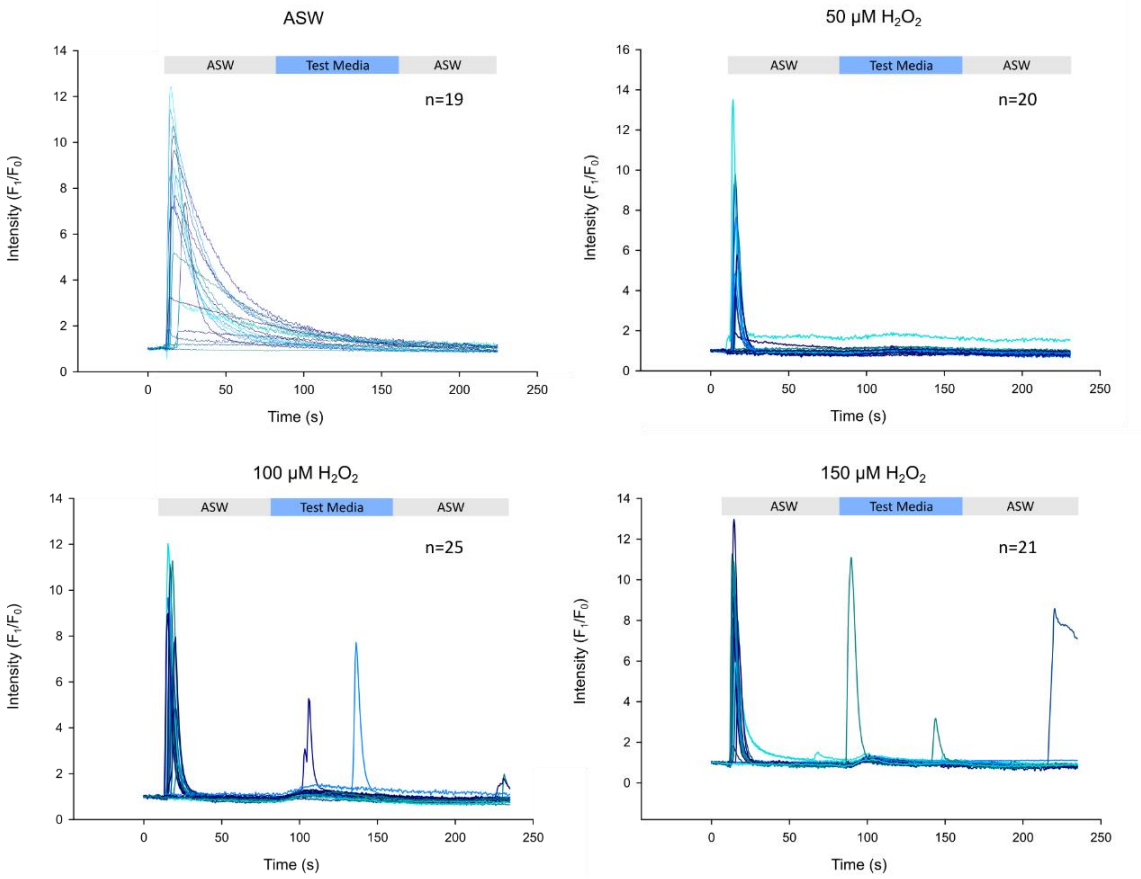

Figure 4.10 Elevations of cytosolic Ca^{2+} detected with R-GECO following different treatments of hydrogen peroxide.

Epifluorescence microscopy tracked *R-GECO* cells following perfusion of ASW or different H_2O_2 concentrations. Plots represent individual cell changes in R-GECO fluorescence, indicating cytosolic Ca^{2+} from a single experiment.

4.3.6 High light triggers a reversible increase in cytosolic H_2O_2

Previous work has demonstrated that high light can generate chloroplast-localised ROS in diatoms (Mizrachi *et al.*, 2019), with a noticeable population split of treated cells into tolerant or sensitive to light stress. This study therefore examined whether high light intensities could also increase cytosolic H_2O_2 using epifluorescence microscopy. Exposure to 60 (LL) and 200 (ML) µmol photons m^{-2} s^{-1} for 10 min had minimal effect on 400:475 nm ratio in *roGFP2-Orp1* cells (Fig 4.11). However, by 520 s, 1000 µmol photons m^{-2} s^{-1} (HL) resulted in a significant increase of 400:475 nm ratio compared to 60 µmol photons m^{-2} s^{-1} (Kruskal-Wallis, Dunns method P=<0.007) and 200 µmol photons m^{-2} s^{-1} (Kruskal-Wallis, Dunns method P=<0.009). The HL ratio increase peaked at 1020 s (Fig 4.11C), just after the end of the light period. Following return to darkness, the HL 400:475 nm ratio started to decline. After almost 10 min of darkness, the 400:475 nm ratio remained significantly higher than LL and ML values (one-way ANOVA, Tukey post hoc P<0.001).

Cells in high light had greater variation regarding the level of increase in the 400:475 nm ratio (Fig 4.12) compared to the treatments of 60 µmol photons m^{-2} s^{-1} and 200 µmol photons m^{-2} s^{-1} treatments. In high light, 86% of cells increased their cytosolic H_2O_2 level by at least 25% and 26% of cells increased their cytosolic H_2O_2 levels by at least 50% (Fig 4.12). Comparable to Mizrachi et al. (2019), there is single cell heterogeneity in tolerating high light and preventing increases in cytosolic H_2O_2.

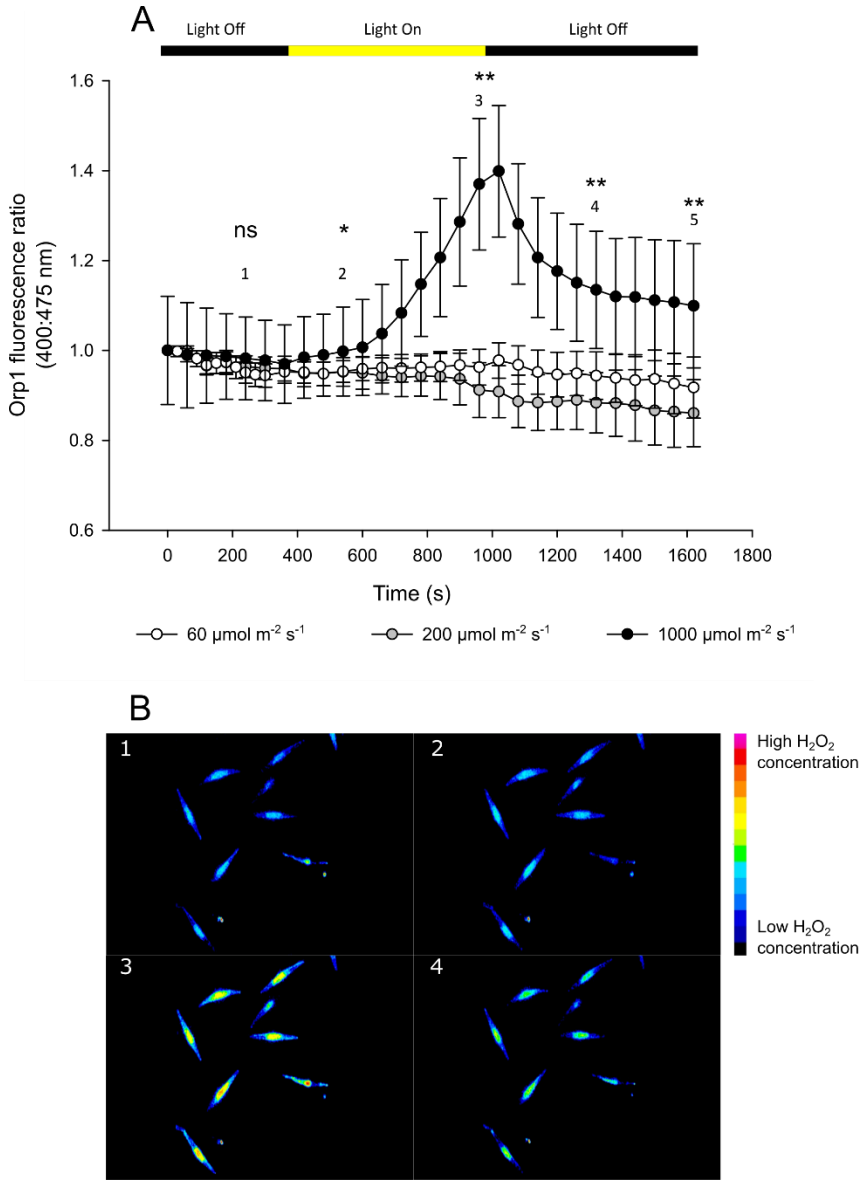

Figure 4.11 High light intensities trigger cytosolic H_2O_2 production.

Using epifluorescence microscopy, high light intensities cause *roGFP2-Orp1* cells to produce cytosolic H_2O_2. A) Data points are from one experiment for an average of 17 cells for 60 µmol photons m^{-2} s^{-1}, 19 for 200 µmol photons m^{-2} s^{-1} and 15 for 1000 µmol photons m^{-2} s^{-1}. The effect of light on 400:475 nm ratio at timepoints 1-5 was tested for significant differences between light regimes. The datasets at time points 1, 2 & 3 on graph failed normality or equal variances precursor tests so were tested

for statistical significance with a Kruskal-Wallis one-way analysis of variance on ranks. Datasets 4-5 were tested with a one-way ANOVA. ns = non-significant. * P= <0.05. ** P= <0.001. B) Pseudo coloured images of 400:475 nm ratio in cells during high light treatment. 1 = 240 s. 2 = 540 s. 3 = 960 s. 4 = 1320 s. Blue colours indicate low 400:475 nm ratio, bright colours indicate higher ratios. Scale bar not available. Error bars show standard deviation.

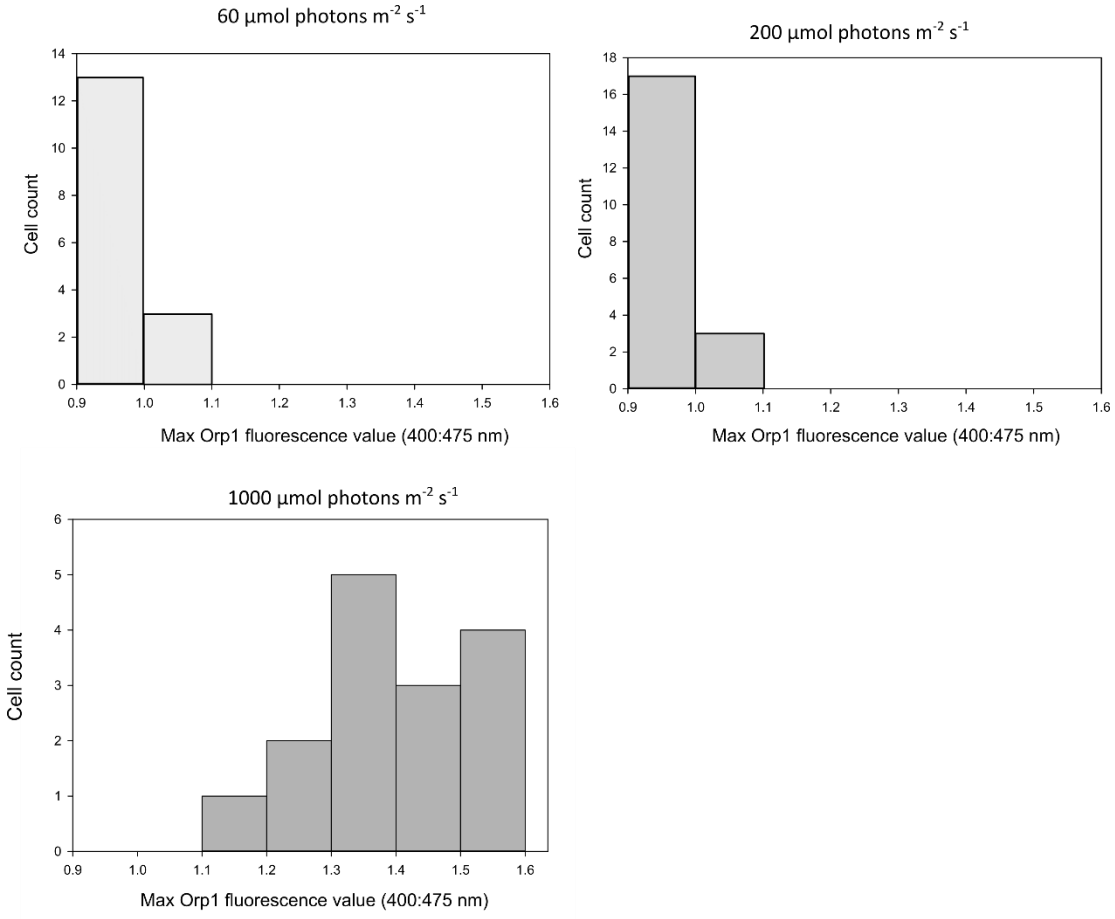

Figure 4.12 Breakdown of individual cell maximum 400:475 nm values under the different light regimes.

roGFP2-Orp1 cells were assessed for relative cytosolic H_2O_2 increase during the three different light intensities. Frequency histograms represent one experiment with 17 cells from 60 µmol photons m^{-2} s^{-1}, 19 from 200 µmol photons m^{-2} s^{-1} and 15 cells from 1000 µmol photons m^{-2} s^{-1} from the experiment shown above.

4.4 Discussion

4.4.1 Successful expression of roGFP2-Orp1 in P. tricornutum

In this study, dose dependent effects of exogenous H_2O_2 were recorded in *P. tricornutum* following successful transformation with roGFP2-Orp1 and roGFP2-ChlOrp1. roGFP2-Orp1 allows specific monitoring of H_2O_2 dynamics and its subsequent effects, rather than compartment redox state as used previously (Rosenwasser *et al.*, 2014; Graff van Creveld *et al.*, 2015). As H_2O_2 is considered an important signalling molecule (Smirnoff & Arnaud, 2019), this allows a more focused investigation into diatom ROS signalling dynamics. Exogenous H_2O_2 addition has significant effects on growth and photophysiology in *P. tricornutum*. Previous studies have reported significant impacts from different concentrations of H_2O_2 in diatoms but have monitored these effects for 24 hours or less (Graff van Creveld *et al.*, 2015, 2016; Mizrachi *et al.*, 2019; Murik *et al.*, 2019). This is the first study to report long-term reductions in cell growth following addition of H_2O_2 concentrations above 50 µM. In line with previous studies, there are also changes to cellular physiology over the first 180 minutes post-addition (Graff van Creveld *et al.*, 2015; Mizrachi *et al.*, 2019), again implicating concentration-specific thresholds.

4.4.2 How tolerant is P. tricornutum to H_2O_2?

P. tricornutum has an efficient system for dealing with increased cytosolic H_2O_2. H_2O_2 is highly membrane permeable, increasing cytosolic H_2O_2 levels within 30 s of perfusion (Fig 4.9). However, during continued exposure, *P. tricornutum* can restore cytosolic H_2O_2 to baseline levels within 180 minutes (Fig 4.8). It is likely that increased production of antioxidants, such as CAT, detoxify cellular H_2O_2 and reduce cytosolic concentrations (Murik *et al.*, 2019), though external detoxification of H_2O_2 by antioxidant secretion may also contribute. Thus, large concentrations of H_2O_2 (>150 µM) are required to overwhelm cellular defences and cause cell death (Fig 4.7). This correlates to previous studies suggesting 150-200 µM H_2O_2 is the maximum tolerance of *P. tricornutum* (Graff van Creveld *et al.*, 2015; Murik *et al.*, 2019), which is also comparable to other marine diatoms (Drábková *et al.*, 2007a; Thamatrakoln *et al.*, 2012). However, rapid H_2O_2 removal in the cytoplasm and chloroplast intriguingly contrasts with previous redox state monitoring using roGFP2 in *P. tricornutum* (Graff van Creveld *et al.*, 2015; Mizrachi *et al.*, 2019). It was reported that addition of 100 µM H_2O_2 results in sustained cytosol and chloroplast oxidation for at least 240 and 300 minutes respectively (Graff van Creveld *et al.*, 2015; Mizrachi *et al.*, 2019). This suggests that though H_2O_2 can be detoxified rapidly, the subsequent shift in redox state may have long lasting implications for the cell (Graff van Creveld *et al.*, 2015; Volpert *et al.*, 2018). Thus, roGFP2-Orp1 can provide alternative insights to redox state results from using roGFP2.

4.4.3 H_2O_2 addition affects P. tricornutum photophysiology

ROS can affect photosynthesis in plants by causing photoinhibition or activating signalling pathways (Gechev *et al.*, 2002; Murata *et al.*, 2007; Exposito-Rodriguez *et al.*, 2017). Unsurprisingly, H_2O_2 strongly affected *P. tricornutum* photophysiology parameters (Fig 4.8, Table 4.2). Concentrations of H_2O_2 at 100 µM or greater gave rise to transient declines in F_0, F_M and Fv/Fm. This effect has been observed in both macro and microalgae (Dummermuth *et al.*, 2003; Drábková *et al.*, 2007b,a; Hunken *et al.*, 2008; Thamatrakoln *et al.*, 2012). Fv/Fm, F_o and F_m all recovered as cytosolic H_2O_2 levels reduced, suggesting the concentration of cellular H_2O_2 correlates to inhibition of photosynthetic parameters. In plants, exogenous application of H_2O_2 to chloroplasts can inhibit the Calvin cycle (Kaiser, 1976, 1979) and reduce O_2 evolution via damage to the O_2 evolution complex (Song *et al.*, 2006). As a number of *P. tricornutum* chloroplast proteins are redox sensitive (Rosenwasser *et al.*, 2014), H_2O_2 may disrupt photosynthesis and PSII efficiency in *P. tricornutum* by directly inhibiting enzymes. Alternatively, H_2O_2 may result in increased generation of hydroxyl radicals through the Fenton reaction, damaging photosystem components (Pospíšil *et al.*, 2004). In cyanobacteria, H_2O_2 addition increases F_o, implicating thylakoid damage (Drábková *et al.*, 2007b,a). The decline in F_o in *P. tricornutum* suggests a different effect of H_2O_2. In plant chloroplasts, H_2O_2 addition during light can quench chlorophyll fluorescence. This is suggested to indicate greater photochemical quenching, and increased H_2O_2 detoxification by increased activity of the Water-Water cycle (Neubauer & Schreiber, 1989; Miyake *et al.*, 1991; Miyake & Asada, 1992). A similar scenario may occur in *P. tricornutum*, with H_2O_2 above a certain threshold reducing PSII efficiency, leading diatoms to increase photochemical quenching to help remove excess H_2O_2.

H_2O_2 had distinct effects on NPQ activity depending on the concentration used. NPQ dissipates excess light energy as heat, reducing the risk of chloroplast ROS generation during photosynthesis. The different threshold responses of 50, 100 and 150 µM H_2O_2 resembles heat shock regulation of NPQ in tobacco plants (Hideg *et al.*, 2008). 42°C had no effect on NPQ, 44°C caused upregulation of NPQ and 46°C caused suppression of NPQ. 46°C was also associated with excess ROS production. In contrast, inhibition of NOX proteins and reducing ROS production in *Arabidopsis thaliana* resulted in suppressed NPQ activation during heat shock (Białasek *et al.*, 2017). Thus, ROS can have a complex role in regulating NPQ. Diatom NPQ is significantly higher than in plants, and is a crucial component of the diatom light stress response (Ruban *et al.*, 2004; Lepetit *et al.*, 2013; Goss & Lepetit, 2015). H_2O_2 may act as a stress signal in *P. tricornutum* whereby excessive production of chloroplast H_2O_2 activates NPQ.

4.4.4 Heterogenous responses to H_2O_2 in P. tricornutum

Recent research has shown that single cell signalling responses occur within a *P. tricornutum* population during redox stress (Mizrachi *et al.*, 2019). In that study, 80 µM H_2O_2 or high light exposure oxidised the chloroplast in a small subset of the population and resulted in PCD in affected cells. Cells survived if their chloroplast redox status remained reduced. Broadly similar single-cell heterogeneity in response to H_2O_2 occurred in the present study. Like Mizrachi et al. (2019), *P. tricornutum* cells displayed high variability in the extent of cytosolic H_2O_2 increase following high light stress. Cells exhibiting elevated cytosolic H_2O_2 may correlate to the cells exhibiting the chloroplast oxidation described previously (Mizrachi *et al.*, 2019), though far fewer cells were examined in the present study (Fig 4.12). In addition, a small subset of cells displayed a Ca^{2+} elevation following H_2O_2 perfusion. ROS:Ca^{2+} interactions are commonly reported in plants (Foreman *et al.*, 2003; Kimura *et al.*, 2012; Kaya *et al.*, 2014; Wu *et al.*, 2020) and some macroalgae (Coelho *et al.*, 2002, 2008) as both Ca^{2+} and ROS can trigger increased levels of the other for signalling pathways. Notably in *P. tricornutum*, exogenous H_2O_2 caused a universal increase in cytosolic H_2O_2. Thus, the limited number Ca^{2+} elevations reflect differing sensitivity and responses to H_2O_2 in individual cells. In contrast, hypo-osmotic shock generates a population-wide increase in cytosolic Ca^{2+} in *P. tricornutum* (Helliwell *et al.*, 2019). The isolated Ca^{2+} elevations may reflect the health of individual cells or relate to the susceptibility of individual *P. tricornutum* cells to undergo chloroplast oxidation and subsequent PCD.

4.4.5 Through what action does H_2O_2 addition reduce cell growth?

Following addition of 100-150 µM H_2O_2, *P. tricornutum* reduced cytosolic H_2O_2 to pre-treatment levels within three hours post-treatment (Fig 4.8A). Despite this removal, concentrations of H_2O_2 greater than 100 µM negatively affected longer term cell growth. Previous studies have suggested exogenous H_2O_2 activates diatom PCD within 24 hours of addition if a threshold concentration is met (Thamatrakoln *et al.*, 2012; Graff van Creveld *et al.*, 2015, 2016; Mizrachi *et al.*, 2019; Murik *et al.*, 2019). Thus, in the present study, increasing H_2O_2 concentration may have increased the percentage of the population engaging in PCD and therefore reduced the number of viable cells (Fig 4.7). Cell mortality rates were not monitored here so it is unknown how many of the counted cells post day 1 were viable. There is some evidence suggesting H_2O_2 addition and *P. tricornutum* PCD correlates to organelle oxidation. For example, 80 µM H_2O_2 only triggered PCD in cells whose chloroplasts were oxidised by H_2O_2 addition (Mizrachi *et al.*, 2019) whereas 150 µM H_2O_2 triggers complete mitochondria and chloroplast oxidation leading to PCD in >90% of the population (Graff van Creveld *et al.*, 2015). Increasing H_2O_2 concentrations may have increased the proportion of cells undergoing PCD, reducing overall growth rates. However, cells treated with 100-150 µM

H_2O_2 maintained high Fv/Fm and continued growth (Fig 4.7), which suggests a healthy population. In *T. pseudonana* and the cyanobacterium *Microcystis aeruginosa*, high Fv/Fm following H_2O_2 addition correlates with reduced levels of PCD (Bouchard & Purdie, 2011; Thamatrakoln *et al.*, 2012). Thus, other interactions may reduce cell growth. Cells may have a reduced energy balance due to increased repair of photophysiology damage or increased antioxidant expression to remove H_2O_2 (Murik *et al.*, 2019), both of which could compromise growth. Cellular growth following treatment with 200 µM H_2O_2 only resumed when Fv/Fm returned to healthy values (Fig 4.7, Table 4.1), perhaps after complete H_2O_2 removal or cellular component repair. Alternatively, as many proteins in *P. tricornutum* are redox sensitive (Rosenwasser *et al.*, 2014), increasing concentrations may trigger different signalling pathways resulting in growth suppression as opposed to cell death.

4.4.6 Are the quantities of exogenous H_2O_2 environmentally relevant?

Maximum reported steady state concentrations of oceanic H_2O_2 are in the nanomolar range (Zinser, 2018), which is far lower than the micromolar concentrations used here. H_2O_2 concentrations could exceed nanomolar concentrations under certain conditions. Rainfall, proximity to ocean surface and exposure time to sunlight correlate to increased H_2O_2 concentrations (Rose *et al.*, 2008; Roach *et al.*, 2015; Zinser, 2018) while steady state H_2O_2 concentrations during blooms of microalgal species with high eROS production rates, such as raphidophytes (Marshall *et al.*, 2005b), have not been reported. However, the results reported in the present study more likely represent responses to increases in intracellular ROS following stress. These increases can be highly localised (e.g. chloroplast) and therefore may have stronger effects by affecting localised redox sensitive proteins (Rosenwasser *et al.*, 2014). For example, 10 µM H_2O_2 inhibits Calvin Cycle activity by 50% in isolated spinach chloroplasts (Kaiser, 1976). Localised levels are also more likely to reach higher concentrations than average bulk concentrations. Though H_2O_2 is membrane-permeable, antioxidant defences may reduce the concentration reaching other cellular compartments, unless facilitated by the cell with compartment contact points (Exposito-Rodriguez *et al.*, 2017; Flori *et al.*, 2017). Thus, stressors that generate specific localised increases such as high light are more likely to affect signalling responses. Previous work has shown exposing *P. tricornutum*, *Nitzschia epithemioides* and *T. pseudonana* to >1000 µmol photons m^{-2} s^{-1} generates chloroplast ROS within 30 minutes (Waring *et al.*, 2010; Mizrachi *et al.*, 2019). As the full intensity of sunlight reaches 2000 µmol photons m^{-2} s^{-1} (Long *et al.*, 1994), extended exposures to high light intensities may generate concentrations of cellular ROS to levels that trigger the threshold responses seen in this present study. Interestingly, high light exposure induced cytoplasmic H_2O_2 after six minutes, a faster response than in previous

studies (Fig 4.11). However, temperature was not controlled for this set up, which may have contributed to H_2O_2 generation, as seen in plants (Vacca *et al.*, 2004; Hideg *et al.*, 2008). Thus, further work would require validation of the role heat stress plays.

4.4.7 Conclusions

Exogenous H_2O_2 rapidly increases cytosolic H_2O_2, which is removed within a few hours. However, H_2O_2 concentrations above a threshold level leads to photophysiology disruption and inhibition of growth. roGFP2-Orp1 is a specific and versatile tool that allows analysis of single cells or populations of cells and has shown that cellular H_2O_2 concentrations differ from cellular redox state. While the induction of H_2O_2 stress in this study is artificial, the diversity of responses suggests that there are specific threshold responses, which can result in long-lasting changes to cellular physiology. The quantities of H_2O_2 used are unlikely to be experienced in nature but the threshold responses hint at specific H_2O_2 signalling. High light stress is a likely source of ROS. Future work using roGFP2-ChlOrp1 and roGFP2-Orp1 can further reveal the importance of H_2O_2 in altering cellular physiology.

Chapter 5 Characterisation of the function of NOX proteins in *Phaeodactylum tricornutum*

5.1 Introduction

NADPH oxidase (NOX) is a widely distributed enzyme utilised for extracellular ROS (eROS) production. In plants, animals and fungi, NOX derived ROS functions are well characterised and include: defence (Liu *et al.*, 2010; Cachat *et al.*, 2015); regulation of cellular development (Malagnac *et al.*, 2004; Wong *et al.*, 2004; Lardy *et al.*, 2005); wound response and promotion of cell wall growth (Sagi *et al.*, 2004; Monshausen *et al.*, 2007); and stress response signalling (Miller *et al.*, 2009; Marino *et al.*, 2012; Evans *et al.*, 2016). NOX proteins are therefore highly important for growth, development and survival. For example, human NOX2 absence contributes to chronic granulomatous disease (Roos, 2019) while *Rboh-C* mutants in *Arabidopsis thaliana* have compromised root hair growth (Foreman *et al.*, 2003; Monshausen *et al.*, 2007).

NOX research in algae is more limited but merits further attention as algal NOX proteins are structurally different to opisthokont and plant NOX proteins (Chapter 2, Herve *et al.*, 2006; Anderson *et al.*, 2011). NOX proteins have been described or are predicted in red algae (Herve *et al.*, 2006; Luo *et al.*, 2015), brown algae (Kupper et al., 2001), green algae (Ross *et al.*, 2006; Anderson *et al.*, 2016), diatoms (Herve *et al.*, 2006; Laohavisit *et al.*, 2015), dinoflagellates (Saragosti *et al.*, 2010) and raphidophytes (Kim *et al.*, 2000; Shikata *et al.*, 2019). Multicellular brown and red algae use NOX in a manner similar to plants for defence and stress signalling (de Oliveira et al., 2017; Kupper et al., 2001, 2002; Luo et al., 2015, Wang et al., 2018). The multicellular green alga *Dasycladus vermicularis* uses NOX during wound responses, similar to plants (Ross et al., 2005, 2006). Unicellular algal NOX proteins have diverse functions. Harmful algal species such as *Chattonella marina* may use NOX-derived eROS as a defence response (Oda *et al.*, 1995; Nakamura *et al.*, 1998; Kim *et al.*, 2000). However, in *C. marina*, eROS also acts as a growth factor, with per-cell production decreasing as cell density increases (Oda *et al.*, 1995; Garg *et al.*, 2007a; Diaz & Plummer, 2018). Cyanobacteria such as *Lyngbya majuscula* use eROS production to enhance iron uptake (Rose *et al.*, 2005), though this function is not supported in marine diatoms. While diatom superoxide can reduce Fe^{3+} to the more bioavailable Fe^{2+}, superoxide production had no significant effect on cellular iron uptake (Kustka *et al.*, 2005).

In diatoms and other unicellular algae, eROS production correlates with light intensity. In four diatoms (*Phaeodactylum tricornutum*, *Thalassiosira weissflogii*, *Thalassiosira oceanica*, *Thalassiosira pseudonana*), increasing light intensity correlates to increasing eROS production, predominantly in the form of superoxide (Milne *et al.*, 2009; Laohavisit *et al.*, 2015; Schneider *et al.*, 2016; Diaz *et al.*, 2019). This increase is inhibited using a chemical inhibitor (diphenyleneiodonium chloride, DPI), suggesting NOX or another flavoprotein involvement. Similar light associated eROS increases occur

in other unicellular algae such as *Chlamydomonas reinhardtii* (Anderson *et al.*, 2016), *Emiliania huxleyi* (Plummer *et al.*, 2019), *Symbiodinium* (Saragosti *et al.*, 2010) and *Trichodesmium* (Hansel *et al.*, 2016). Light regime (diurnal vs continuous exposure) can also affect NOX gene expression in *P. tricornutum* (Laohavisit et al., 2015). *PtNOX1* shows greater gene expression in continuous light after 4 days than diurnal exposed cells. However, this expression shifts after 8 days, with diurnal expression of *PtNOX1* surpassing expression in continuous light cells. Comparatively, *PtNOX2* gene expression, while being lower than *PtNOX1*, shows minimal changes between light regimes. Additionally, the same study reported *P. tricornutum* chlorophyll content correlates with extracellular superoxide production (Laohavisit et al., 2015). Together, this implies a relationship between light level/photosynthesis and eROS production in *P. tricornutum* and other unicellular algae. A proposed explanation is that eROS production represents an electron dissipation mechanism (Davey *et al.*, 2003) where under high light regimes, excess electrons are exported out of the cell to reduce extracellular oxygen.

High light intensities poses a risk to cells by overexcitation and excessive reduction of the photosynthetic electron transport chain (Edreva, 2005). By saturating the capacity of $NADP^+$ to accept excess photosystem-derived electrons, it promotes electron leakage and generates ROS, causing photoinhibition through photosystem damage and inhibition of repair mechanisms (Murata *et al.*, 2007; Takahashi & Murata, 2008). Thus, photosynthetic organisms have many mechanisms for dealing with excess light stress (Fig 5.1). Some of these strategies can also balance the ATP:NADPH ratio by dissipating excess NADPH or increasing ATP generation (Kramer & Evans, 2011). These strategies can be broadly classified as alternative electron pathways (AEP, Bailleul *et al.*, 2015) or energetic dissipation mechanisms (EDM). Non-photochemical quenching (NPQ) is a mechanism whereby absorbed energy is dissipated as heat rather than photochemistry. Diatoms are efficient at upregulating NPQ compared to plants (Ruban *et al.*, 2004). Cyclic electron flow (CEF) is an AEP where electrons are cycled around PSI to generate ATP instead of NADPH. This is common in plants and green algae (Forti *et al.*, 2003; Bailleul *et al.*, 2015). Additionally, chloroplast oxygen rather than $NADP^+$ may accept excess electrons, generating superoxide (the Mehler reaction). The chloroplast superoxide is rapidly detoxified to water through the actions of superoxide dismutase and ascorbate peroxidase. As photosynthetic electrons are initially generated by the water splitting complex of PSII, this electron pathway is also called the Water-Water cycle (Waring *et al.*, 2010; Cardol *et al.*, 2011). Recently, metabolic coupling was described in diatoms (Bailleul *et al.*, 2015). This strategy shuttles reductant and ATP between the mitochondria and chloroplast depending on the organelle's energetic requirements. As plastid product requirements rapidly change depending on the light intensity, shuttling products when required can dissipate excess reductant or increase the efficiency

of energetic use in diatoms (Broddrick *et al.*, 2019). Plants have a similar strategy called the malate–oxaloacetate (Mal–OAA) shuttle (Noguchi & Yoshida, 2008). However, it is predominantly used for dissipating excess reductant whereas metabolic coupling can balance the ATP:NADPH ratio under low light as well as dissipate excess reductant (Bailleul *et al.*, 2015; Broddrick *et al.*, 2019). In diatoms, mitochondrial alternative oxidase (AOX) is part of metabolic coupling. This enzyme represents an alternative pathway to Complex III in the mitochondrial electron transport chain (ETC). Instead of being used to generate ATP, electrons are dissipated harmlessly into heat. However, this helps prevent ETC over-reduction. Chloroplast- or mitochondrial-derived reductant can be dissipated through AOX (Bailleul *et al.*, 2015; Murik *et al.*, 2019), thus regenerating $NADP^+$. Plants also use AOX to dissipate excess mitochondrial-derived reductant (Yoshida *et al.*, 2007; Cvetkovska & Vanlerberghe, 2012). NOX activity may act as an additional EDM and AEP for excess reductant whereby excess chloroplast NADPH would be transported to NOX. Extracellular oxygen accepts excess electrons, allowing $NADP^+$ regeneration. Recently, a similar mechanism was proposed to occur in *T. oceanica*, using a membrane-bound glutathione reductase (GR) protein, rather than NOX, as the enzymatic mechanism (Diaz *et al.*, 2019). However, the use of eROS to dissipate excess electrons has not explicitly been tested in *P. tricornutum,* nor has NOX involvement been confirmed.

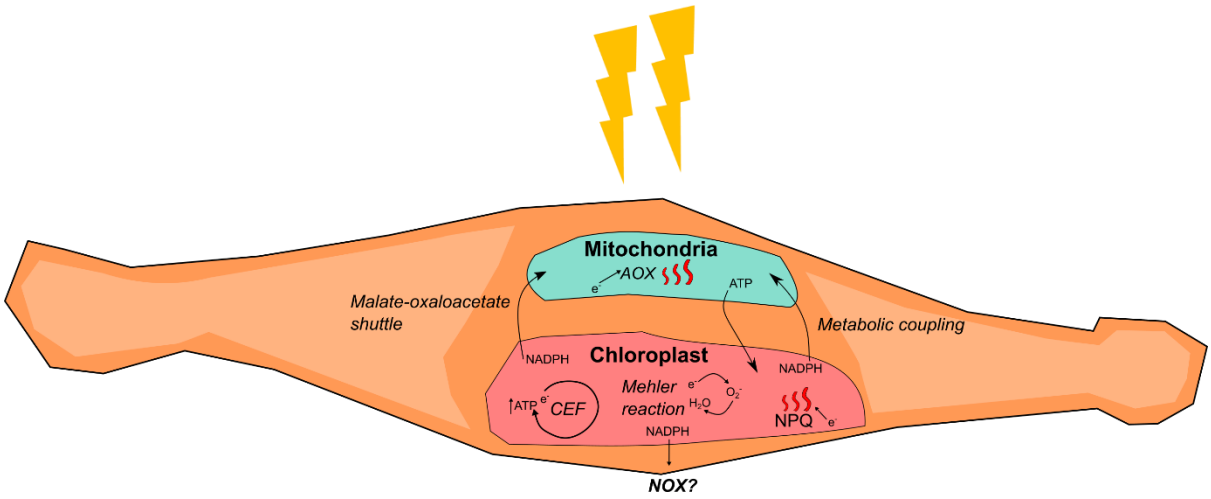

Figure 5.1 A simplified model of some of the main mechanisms for diatoms to dissipate excess electrons, or for balancing the ATP:NADPH ratio.

If NOX is a mechanism for coping with excess light, NOX inhibition should result in dramatic effects on photosynthetic parameters. NOX localisation was determined in *P. tricornutum* and the effects of inhibiting NOX proteins and other metabolic components was monitored to assess if NOX function relates to electron dissipation. Photosynthetic parameters, intracellular ROS (iROS) and eROS production were monitored in response to different inhibitors. In addition, two other diatoms were screened for similar responses to assess if this strategy is widespread.

5.2 Methods

5.2.1 Cell culture

P. tricornutum (CCAP1055/1) was acquired from Culture Collection of Algae and Protozoa (SAMS limited, Scottish Marine Institute (Oban, UK)). *A. glacialis* (PLY 607) and *T. weissflogii* (PLY 541) were acquired from the Plymouth Culture Collection. Diatoms were grown in F/2 + Si medium (Guillard & Ryther, 1962) derived from twice filtered seawater (FSW) collected at site L4 in the English Channel as described in Chapter 3. All species were cultured in green plug culture flasks (SARSTEDT) on a 16:8 hour light: dark cycle, at 40-45 µmol m^{-2} s^{-1} photon flux density, measured using a LI-250A light meter (LI COR, USA). *P. tricornutum* strains were maintained at 18°C, and *T. weissflogii* and *A. glacialis* at 15°C, in respective controlled temperature rooms. For growth experiments, cells were grown in triplicate green plug culture flasks (30-40 mL). Cells were counted using a Beckman Coulter counter for *P. tricornutum*, a haemocytometer for *A. glacialis* and a Sedgewick Rafter counting chamber for *T. weissflogii*. For experiments, cells were sampled at early to mid-exponential growth. Fv/Fm values of ≥0.60 for *P. tricornutum* and *T. weissflogii*, ≥0.55 for *A. glacialis* were considered to reflect cells with optimal photosynthetic efficiency.

5.2.2 Chemical preparation

1 mM diphenyleneiodonium chloride (DPI, Sigma-Aldrich) master stock was dissolved in DMSO. 100 mM salicylhydroxamic acid (SHAM, Sigma-Aldrich) and 10 mM 3-(3,4-dichlorophenyl)-1,1-dimethylurea (DCMU, Sigma-Aldrich) master stocks were dissolved in ethanol. 10 mM glutathione disulphide (GSSG, Sigma-Aldrich) master stocks were prepared using FSW as a solvent. 1 mg mL^{-1} master stock of OxyBURST™ Green H_2HFF-BSA (Thermo Fisher Scientific) was prepared by dissolving powder in 1 mL of phosphate buffered saline solution as per manufacturer's instruction. All master stocks were maintained at 4°C in darkness.

5.2.3 Measurements of eROS production, photosynthetic parameters and cytosolic H_2O_2

eROS production was measured using OxyBURST Green using methods described in Chapter 3. Photosynthetic parameters (Fv/Fm, Fo, Fm, Fm', Ft, Fv'/Fm', qP, NPQ) were measured using AquaPen handheld fluorometers as described in Chapter 4. Apart from Fv/Fm, all parameters were calculated using NPQ induction curves from AquaPen-C AP 110-C (AquaPen Manual, 2018). Fv'/Fm' represents the working quantum efficiency of PSII in light and was calculated using the formula:

Fv'/Fm'= (Fm'-Ft')/Fm' (Maxwell & Johnson, 2000). Ft' equals the steady state minimum fluorescence following actinic light stabilisation and Fm' equals the steady state maximum fluorescence following saturating peaks during actinic light exposure. qP represents the coefficient of photochemical quenching, an estimate of open PSII reaction centres (Maxwell & Johnson, 2000). Cytosolic H_2O_2 levels were assessed using a plate reader with *roGFP2-Orp1* cells as described in Chapter 4.

5.2.4 Effect of DPI on photosynthetic parameters

The effect of DPI in darkness, medium light (ML, 40-45 µmol photons m^{-2} s^{-1}) and high light (HL, 200 µmol photons m^{-2} s^{-1}) was investigated in *roGFP2-Orp1* cell cultures by monitoring cytosolic H_2O_2 and photosynthetic parameters. Cells were grown in bulk to $2.6x10^6$ cells mL^{-1} under ML conditions. Due to the time delay required for triplicate NPQ measurements, the different light treatments were taken on different days. Cells were divided between treatment flasks. Darkness treatments were measured on day one, ML on day two and HL on day three. Cell densities for ML and HL treatments were adjusted to $1x10^6$ and $5x10^5$ cells mL^{-1} respectively on day one with F/2 + Si medium so that cells would be at a similar density and growth phase for experiments. However, there were small differences in cell density between light treatments. Dark-adapted cells were 2.6 $x10^6$ cells mL^{-1}, ML cells were $2.2x10^6$ cells mL^{-1} and HL cells were 1.8 $x10^6$ cells mL^{-1}. Cell health was monitored prior to treatments via Fv/Fm measurement (healthy cells= ≥0.60). All experiments began at 10 am each morning. Cells were darkened by wrapping tubes in aluminium foil. High light was provided with a GroBeam solid state light source (Tropical Marine Centre, UK). 1 µM DPI was added after initial starting values were measured. Photosynthetic and cytosolic H_2O_2 values were recorded at 30, 60 and 180 min. When not being sampled, cell flasks were maintained at 18°C. A two-way repeated measures ANOVA compared the effect of DPI within its respective light treatment but not between different light treatments.

5.2.5 Oxygen evolution measurements

Oxygen measurements were determined using a PyroScience OXVIAL4 respiration vial with integrated optical oxygen sensor, and Firesting O_2 and temperature sensor. 50 mL of early exponential phase cells were centrifuged (1000 rpm (Heraeus Megafuge 40R, Thermo Fisher Scientific), 20 min, 18°C) to a pellet. Fresh FSW medium was added to cells to suspend them in new low O_2 medium. Cells were left to recover for one hour before counting to confirm cell density ($2.5x10^6$ cells mL^{-1}). 4 mL of medium were placed into an OXVIAL vial, with 0.1% v/v DMSO control, 1

µM DPI or 10 µM DCMU. The vial was placed into a water jacket maintained at 18°C with magnetic stirring. Cells were left for 25 min at low light (<10 µmol photons m^{-2} s^{-1}) to stabilise baseline oxygen levels. Cells were then exposed to differing light levels and changes in media O_2 concentration were monitored. The regime was as follows: medium light (60 µmol photons m^{-2} s^{-1}) for 180 s, darkness for 180 s, high light (250 µmol photons m^{-2} s^{-1}) for 180 s. Light levels were adjusted through use of two GroBeam solid state lighting strips and a LI-250A light meter. The change in O_2 levels was calculated using the formula: $(D_1-D_0) / (t_1-t_0)$, where t_0 is starting measurement time, t_1 end measurement time, and D indicates O_2 level at respective time points. The units for the change were adjusted to µmol L^{-1} O_2 evolution $cell^{-1}$ s^{-1}. The change in O_2 medium concentration in darkness represented cellular respiration rate. Respiration rate was assumed to be constant regardless of light intensity. This was added to net O_2 evolution values to give total O_2 production rates.

5.2.6 Statistical analysis

All statistics were calculated using Sigma Plot 14 statistical software with statistical tests listed where appropriate. Data were tested for normality (Shapiro-Wilk) and equality of variance (Brown-Forsythe) prior to analysis. Statistical significance of data was indicated if $P<0.05$.

5.2.7 Cloning of PtNOX1 & PtNOX2

Specific *P. tricornutum* NOX primers were designed (Table 5.1, Primer3, http://bioinfo.ut.ee/primer3/) to flank the entire open reading frame of PtNOX1 and PtNOX2. Genes were amplified from *P. tricornutum* genomic DNA using iProof DNA polymerase (Bio-Rad). PCR conditions were 98°C for 3 min, followed by 30 cycles of 98°C for 10 s, 62°C for 30 s, and 72°C s for 80 s. Gel electrophoresis confirmed primer product with bands of 2.2kb, corresponding to PtNOX1 & 2 gene size (both genes are 2248 base pairs long). PCR products were blunt end cloned into the *StuI* site of vector pPha-T1-Venus (Appendix C1). pPha-T1-Venus creation is described fully by Helliwell *et al.* (2019) but briefly represents the original pPha-T1 vector (Zaslavskaia *et al.*, 2000) containing a codon-optimised Venus eGFP, and encodes for ampicillin and Zeocin/bleomycin antibiotic resistance. Cloning PtNOX1 and PtNOX2 into pPha-T1-Venus creates C-terminal Venus tagged fusion proteins for both PtNOX1 and PtNOX2. Competent *E. coli* (One SHOT Top 10, Thermo Fisher Scientific) were heat shock transformed (ice for 12 min, 42°C for 2 min, ice for 2 min) with PtNOX1-2 plasmids. *E. coli* media were then plated onto LB medium + 100 µg ampicillin plates and left at 37°C overnight. *E. coli* colonies were screened by colony PCR (Figs. 5.2, 5.3, Table 5.1) and sequencing (Biosource, Cambridge) to confirm successful ligation in the correct direction of each gene. *E. coli* colonies

expressing successfully ligated PtNOX1-2 plasmids were grown in LB + 100 µg ampicillin media overnight at 37°C. Cells pellets were extracted (3500 x *g*, 5 min) and PtNOX1-2 plasmids were purified using a QIAprep spin miniprep kit (Qiagen).

5.2.8 Genetic transformation of P. tricornutum

P. tricornutum was transformed using biolistic transformation (Kroth, 2007). 400 mL of cells were grown to $3x10^6$ mL^{-1} and concentrated through centrifugation (4000 rpm (Heraeus Megafuge 40R, Thermo Fisher Scientific), 10 min). Cells were then plated onto 50% FSW 1.5% w/v agar plates supplemented with F/2 + Si nutrients and allowed to recover overnight. 1.5-5 µg of PtNOX1-2 plasmids were adhered to 3 mg tungsten particles (0.6 µm diameter) with 0.1 M spermidine and 2.5 M calcium chloride, and then dried on macrocarriers. Biolistic bombardment was carried out with a gene gun (PDS-1000 He Particle Delivery System, Bio-Rad, USA) with 1350 psi rupture disks and, cells were left overnight. Cells were replated the next morning onto 50% FSW 1.5% w/v agar plates supplemented with Zeocin (75 µg mL^{-1}) and F/2 + Si nutrients. Cells grew for four weeks at 18°C and resistant colonies were re-plated to liquid medium containing 75 µg mL^{-1} zeocin to grow for confocal screening.

5.2.9 Screening of P. tricornutum colonies for NOX localisation

Zeocin resistant colonies were screened using confocal microscopy (Zeiss LSM 510) for Venus fluorescence using excitation: excitation at 488:500-530 nm for GFP and 488:>650 nm for chlorophyll. Transformed cells expressing NOX-Venus proteins were compared to wild type cells at same microscope settings.

Table 5.1 Primers used for extraction of *NOX* genes and screening of Venus tagged *NOX* sequences.

Primer	Sequence
PtNOX1 gene cloning forward	ATGGTAACGGTAAAAGCTTCCTC
PtNOX1 gene cloning backward	AAAATTCTCCTTGTGGACCAGC
PtNOX2 gene cloning forward	ATGGAGCACATATGTTTCGCACG
PtNOX2 gene cloning backward	AAAATTCTCCTTGTGGACTGCAA

pPha-T1 *fcpB* promoter colony screening (fcpB-P)	TCACGGTCTTCTTCGAGTCC
Venus post-sequence colony screening (Ven-P)	CTTGTGACCGTTGACGTCTC
PtNOX1 colony screening A (P1-A)	GAACTCGTACGTACCCCACA
PtNOX1 colony screening B (P1-B)	TTCTCGTTGCGTCTCTTTGC
PtNOX2 colony screening A (P2-A)	GCCCCAGACCATCATGAGTA
PtNOX2 colony screening B (P2-B)	GAAGCTCTAGACAAGGCCCA

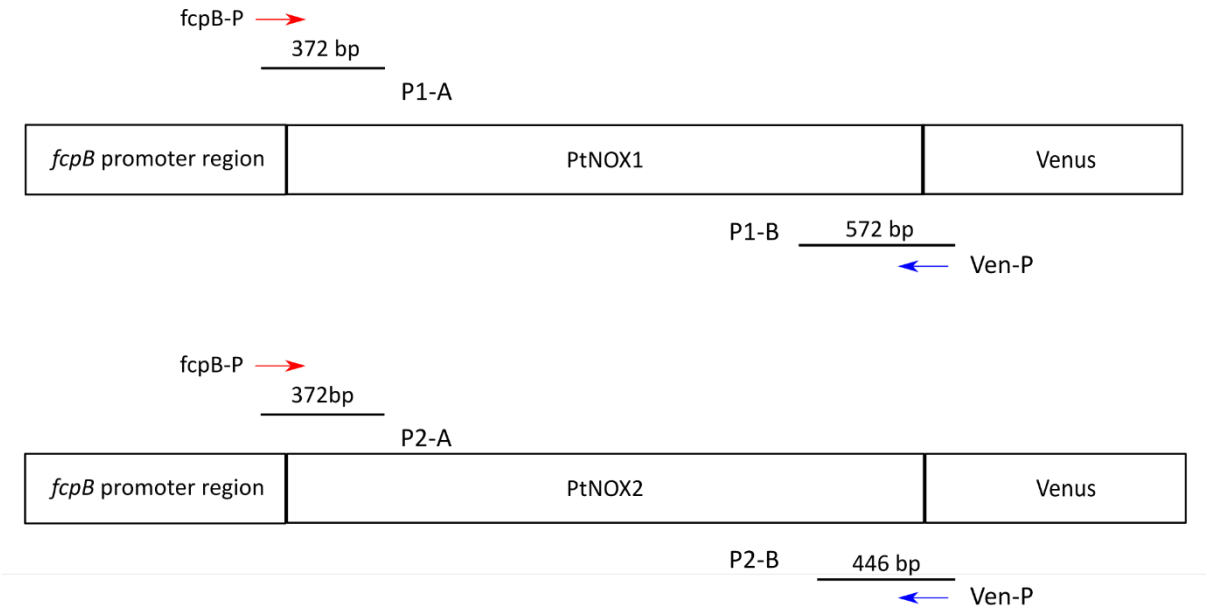

Figure 5.2 Primer positions used for colony PCR screening of potential NOX-Venus constructs.

The scheme shows the position of colony screening primers, to test for correct direction of the ligated PCR product. Arrows indicate direction of primer product. Ligation of the original PCR product in the correct direction will create a specific product size shown above the line.

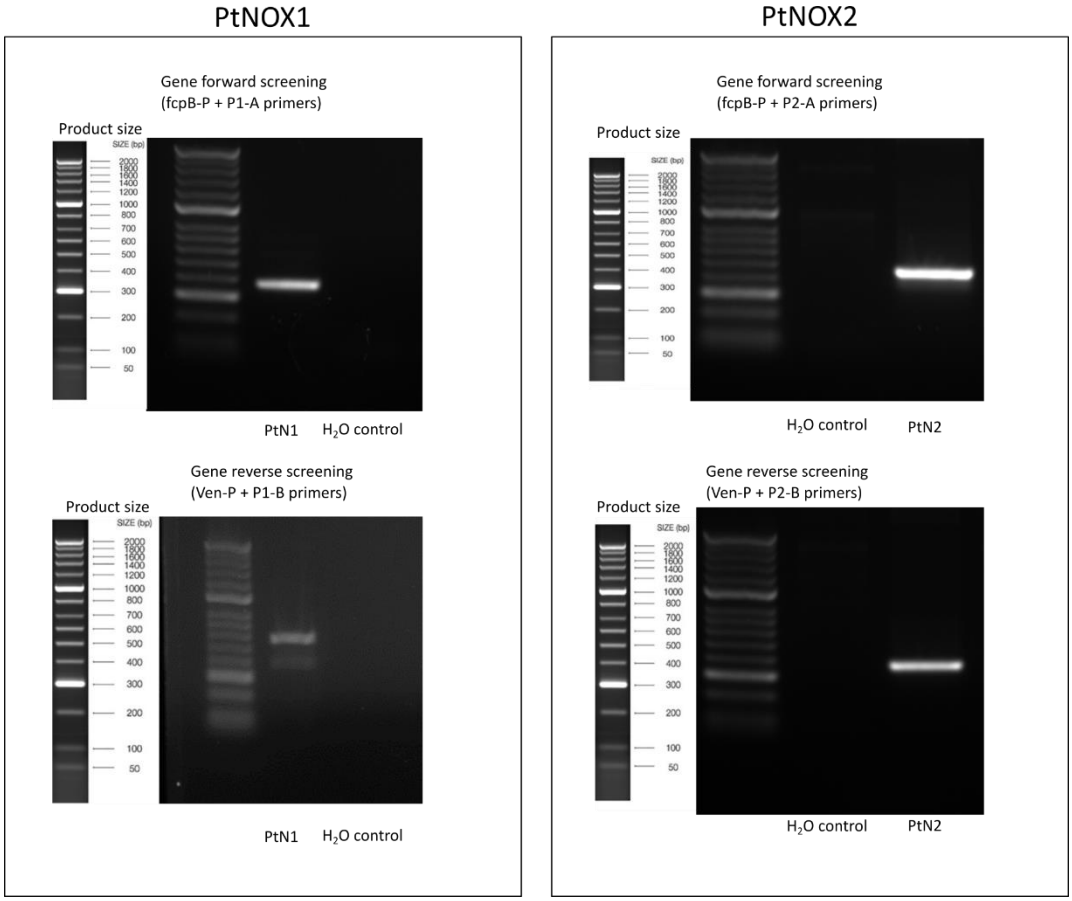

Figure 5.3 Gel screening of successfully transformed *E. coli* colonies with Venus tagged PtNOX1 and PtNOX2.

Screening primers from Table 5.1 and Fig 5.2 successfully show correct direction ligation of PtNOX1-2. Expected product size for primer pairs fcpB-P and P1-A, and fcpB-P and P2-A was 372 bp. Expected product size for primer pairs Ven-P and P1-B was 572 bp while expected size for Ven-P and P2-B was 446 bp.

5.3 Results

5.3.1 Localisation of PtNOX1

Biolistic transformation of PtNOX1 resulted in eight Zeocin resistant *P. tricornutum* colonies after four weeks on Zeocin plates. Confocal screening revealed successful PtNOX1 localisation in one colony (Fig 5.4). PtNOX1 localises predominantly to the plasma membrane. While some fluorescence co-occurs in the green channel localised to the chloroplast, it is likely due to chlorophyll autofluorescence as a similar signal is seen in wild type cells. Transformation of PtNOX2 resulted in 16 Zeocin resistant colonies. No GFP fluorescence was detected with confocal microscopy.

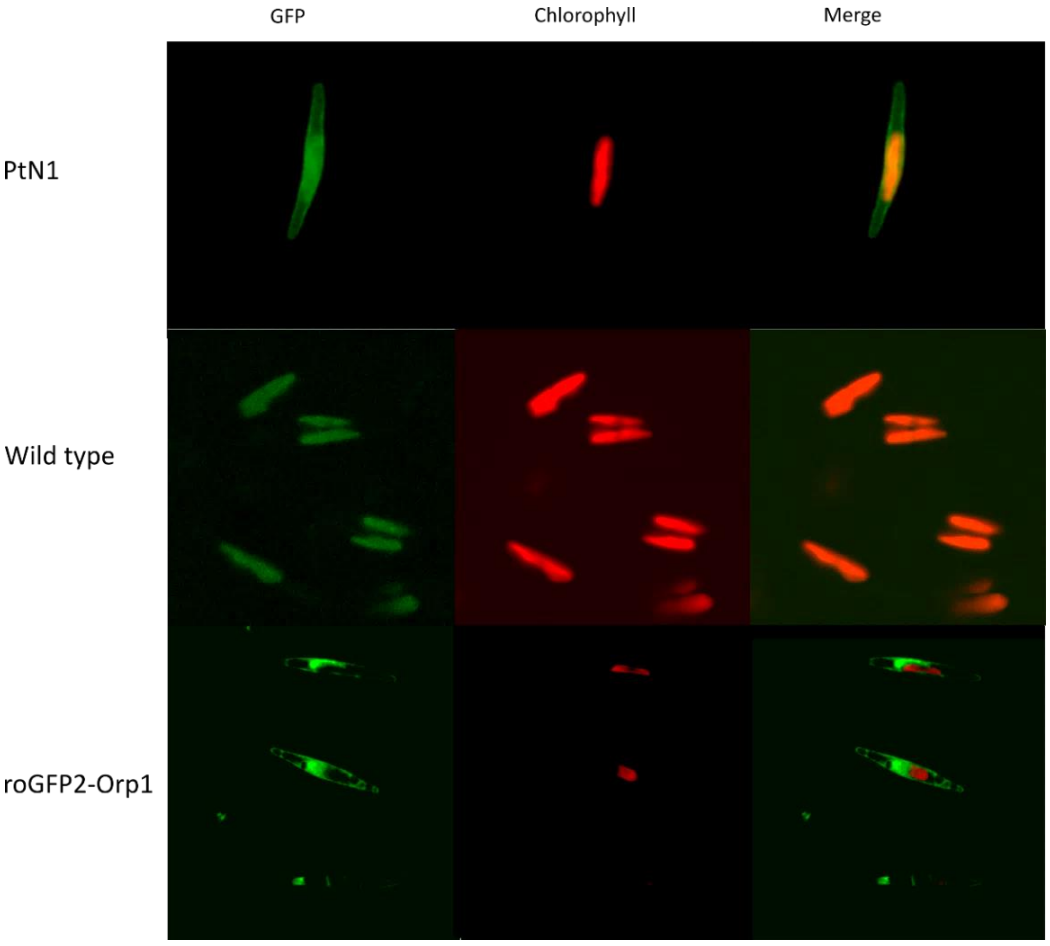

Figure 5.4 PtNOX1 localises to *P. tricornutum* plasma membrane.
PtNOX1 tagged with Venus and wild type *P. tricornutum* cells were examined for GFP (excitation: emission 488:500-530 nm) and chlorophyll (excitation: emission488:>650 nm) fluorescence using confocal microscopy (63x oil objective, scale bar not available). *roGFP2-Orp1* cells were imaged separately to wild-type and *PtNOX1* cells but are displayed to demonstrate cytoplasmic GFP localisation for comparison.

5.3.2 Chemical inhibition of NOX triggers dose-dependent effects on cellular physiology

A pilot study demonstrated DPI causes a dose dependent increase in cytosolic H_2O_2 in *roGFP-Orp1* cells (Fig 5.5). 5-10 µM DPI increased cytosolic H_2O_2 after 120 min to a level comparable to those obtained following 50 µM H_2O_2 addition (Fig 5.5). A follow-up experiment further tested the concentration effect of DPI on Fv/Fm and cytosolic H_2O_2. This more rigorous experiment confirmed the dose-dependent increase in cytosolic H_2O_2 with DPI (Fig 5.6A, B). 0.5 µM DPI had no effect on cytosolic H_2O_2 after 180 min whereas 2 µM and 5 µM DPI caused 2-fold and 4-fold increases in cytosolic H_2O_2. Increased DPI concentration led to faster decline of Fv/Fm (Fig 5.6C). Significant Fv/Fm decline occurred within 60 min of 0.5-1 µM DPI treatments (one-way ANOVA, $P<0.05$) and within 30 min for 2-5 µM DPI (one-way ANOVA, $P<0.05$).

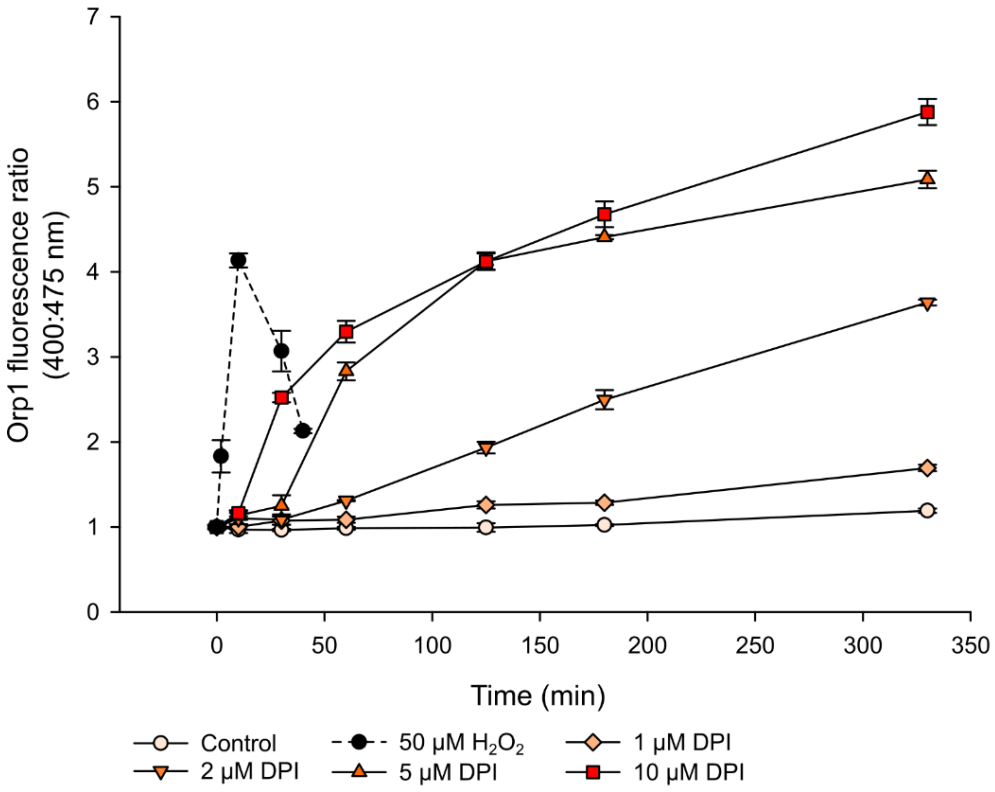

Figure 5.5 Pilot study demonstrating a dose dependent increase in cytosolic H_2O_2 with DPI.

roGFP2-Orp1 cells are $6x10^6$ cells mL^{-1}. Error bars show standard deviation for one biological replicate with three technical replicates. No DMSO control was used as Fig 4.4 demonstrated no effect of DMSO on 400:475 nm value up at least 1% v/v DMSO. All DPI additions used less than this amount of DMSO.

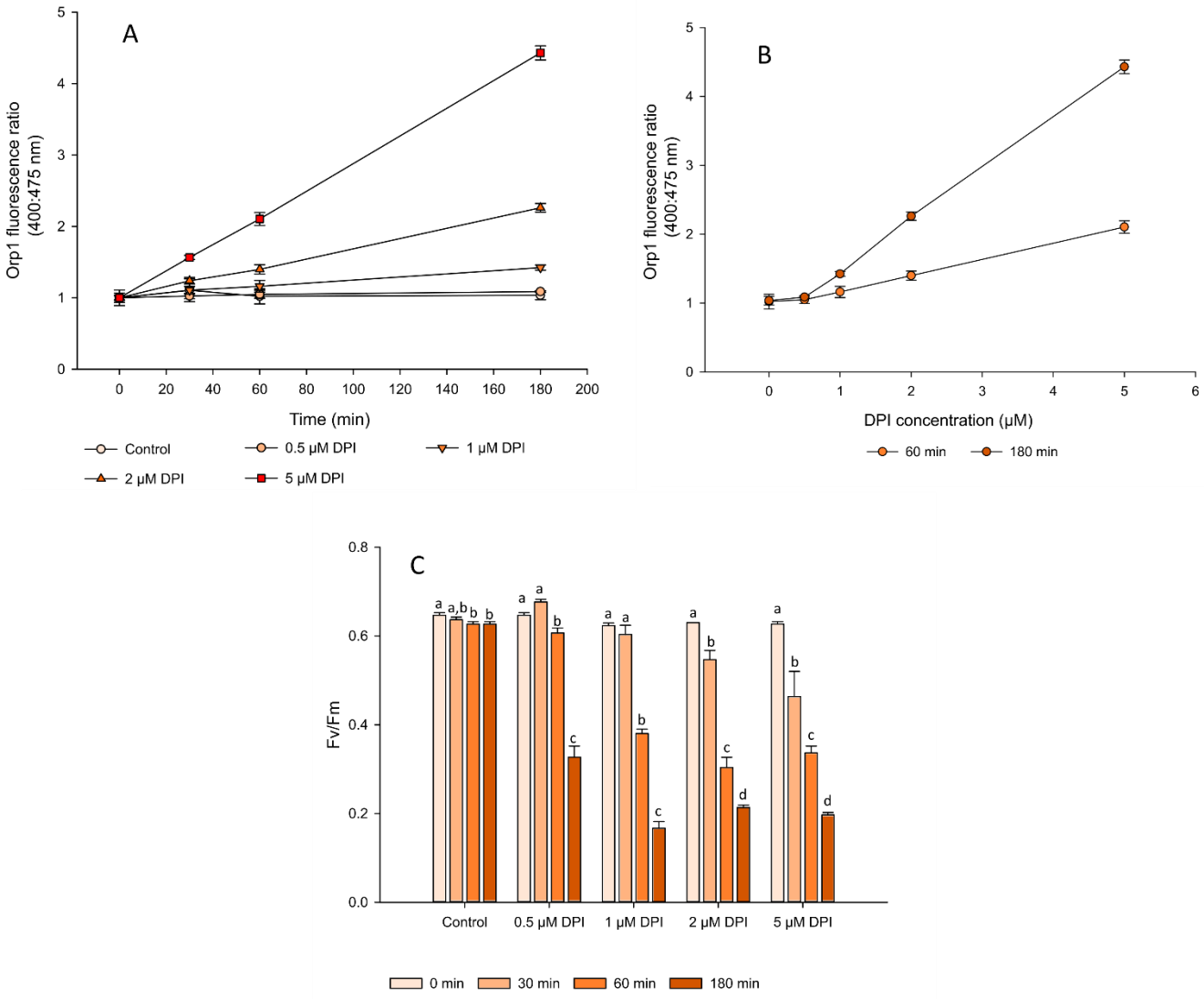

Figure 5.6 DPI concentration affects cytosolic H_2O_2 and photosynthetic efficiency. A) Cytosolic H_2O_2 increased with DPI concentration in *roGFP2-Orp1* cells ($3x10^6$ cells mL^{-1}). B) A dose-response curve for DPI and cytosolic H_2O_2 concentration at different time points. C) Increasing concentrations of DPI reduce Fv/Fm in *roGFP2-Orp1* cells. No DMSO solvent was added to control. Different letters indicate significant effects of time within each DPI treatment (one-way ANOVA, Tukey post hoc test, $P<0.05$). Fv/Fm data use triplicate values. Orp1 values represent triplicate values with three technical replicates. Error bars indicate standard deviation.

1 µM and 10 µM DPI inhibited wild-type *P. tricornutum* growth, with 10 µM DPI resulting in a large reduction in cell density (Fig 5.7A). Fv/Fm was also affected with 1 µM DPI reducing Fv/Fm by 65% one day post addition. A small recovery occurred two days post addition (Fig 5.7B). 10 µM DPI caused an immediate decline in Fv/Fm, reaching 0 after one day. The complete loss of Fv/Fm alongside reduction of cell density suggests 10 µM DPI causes population death to *P. tricornutum*. Based on the concentration dependent effects of DPI on cell physiology and the previously reported reduction on *P. tricornutum* eROS production (Chapter 3), 1 µM DPI was chosen as a suitable concentration for further experiments.

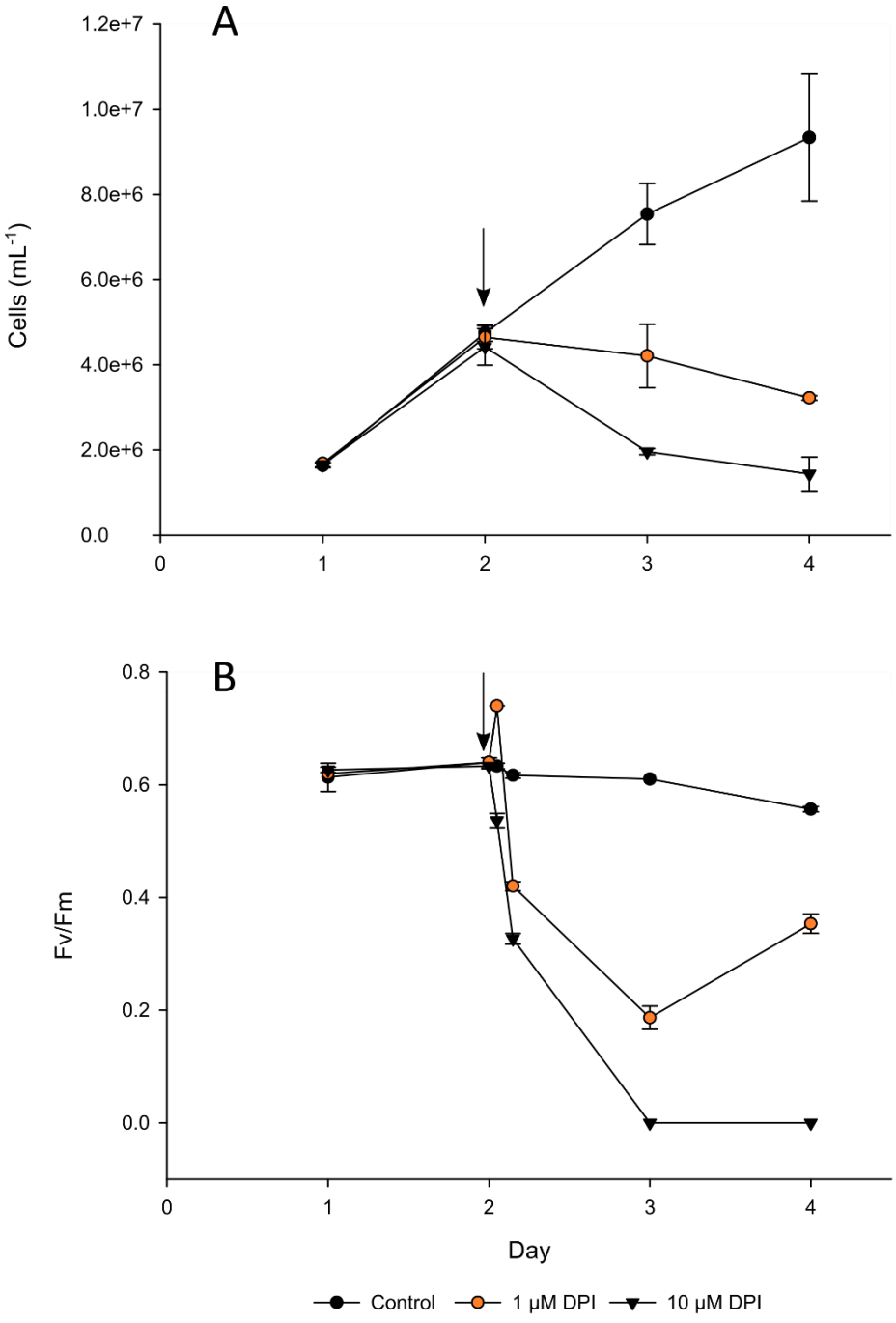

Figure 5.7 DPI reduces long-term cell viability in wild-type *P. tricornutum*.
A) Cell growth declined following addition of 1 µM or 10 µM DPI. B) DPI concentration affected decline of Fv/Fm. Fv/Fm was monitored at 30 min and 120 min post DPI addition. DPI was added on day two, indicated by arrow. Fv/Fm measurements occurred concurrent with cellular growth measurements on day three and four. No DMSO solvent was added to control. Error bars show standard deviation for three replicates.

5.3.3 Interactions of light intensity and NOX inhibition on cellular physiology

Increasing light intensity should result in greater photosynthetic electron flow. Experiments were carried out to test whether NOX inhibition would diminish the cell's capacity for coping with excess photosynthetic electrons. Cytosolic H_2O_2 values were stable in ML (40 µmol photons m^{-2} s^{-1}) and Darkness controls over 180 min but declined slightly in HL (200 µmol photons m^{-2} s^{-1}). DPI addition increased cytosolic H_2O_2 in all light treatments (Fig 5.8A). Surprisingly, Darkness + DPI produced the greatest increase in cytosolic H_2O_2 after 180 min. ML + DPI and HL + DPI produced similar increases in cytosolic H_2O_2 after 180 min.

In all light treatments, DPI significantly reduced Fv/Fm (Fig 5.8B, two-way repeated measures ANOVA, $P<0.001$), NPQ (Fig 8C, two-way repeated measures ANOVA, $P<0.05$) and qP (Fig 5.8D, two-way repeated measures ANOVA, $P<0.001$) compared to their respective controls. Increased light intensity triggered greater and faster reductions of Fv/Fm. Darkness + DPI showed a significant 33% reduction ($P<0.001$) in Fv/Fm after 180 min. In contrast, HL + DPI significantly reduced Fv/Fm after only 30 min ($P=0.004$) and Fv/Fm was reduced to 10% of its starting value after 180 min.

Control NPQ values increased with time in Darkness and HL conditions but progressively declined in ML (Fig 5.8C, Table 5.2). In all treatments, DPI reduced NPQ ($P<0.05$). Following an initial drop after 30 min, Darkness + DPI NPQ was stable for the remainder of the experiment. NPQ in ML + DPI and HL + DPI declined with time, with greater declines occurring in HL + DPI. However, the HL and HL + DPI dataset failed a Shapiro-Wilk normality test ($P<0.050$) and caution should be taken for this dataset.

DPI reduced qP (the proportion of open PSII reaction centres) values to 0-0.1 within 30 min in all treatments, with the greatest decline occuring in Darkness + DPI (Fig 5.8D, Table 5.2). Though some recovery was apparent at subsequent timepoints, all qP values in DPI treatments remained significantly lower than controls ($P<0.001$). HL + DPI exihibited the strongest recovery, reaching 0.25 compared to 0.11 in Darkness + DPI after 180 min. However, the ML and ML + DPI dataset failed Brown-Forsythe equal variance test ($P<0.050$), and so also requires some caution.

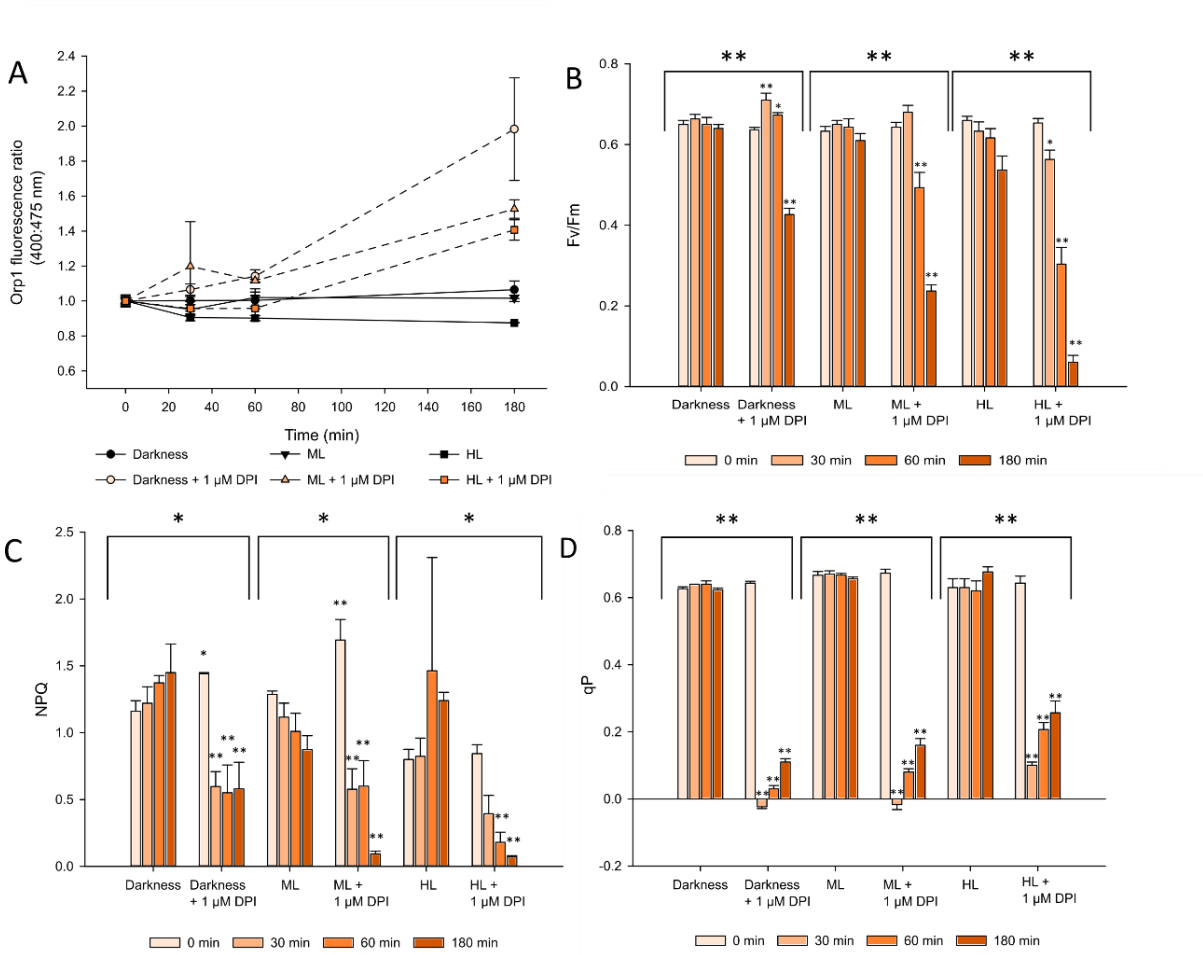

Figure 5.8 Light intensity in conjunction with DPI addition affects cellular parameters. 1 µM DPI was added to *roGFP2-Orp1* cells in darkness, ML (40 µmol photons m^{-2} s^{-1}) and HL (200 µmol photons m^{-2} s^{-1}). A) Changes in cytosolic H_2O_2, B) Fv/Fm, C) NPQ and D) qP were monitored. No DMSO solvent was added to controls. A two-way repeated measures ANOVA assessed the effect of DPI treament with time and within each light intensity for Fv/Fm and NPQ. Asterisks indicate significant differences to control treatment at each time point. * P<0.05. ** P<0.001. Orp1 data use triplicates with three technical replicates. NPQ and Fv/Fm data use triplicate values. Error bars show standard deviation.

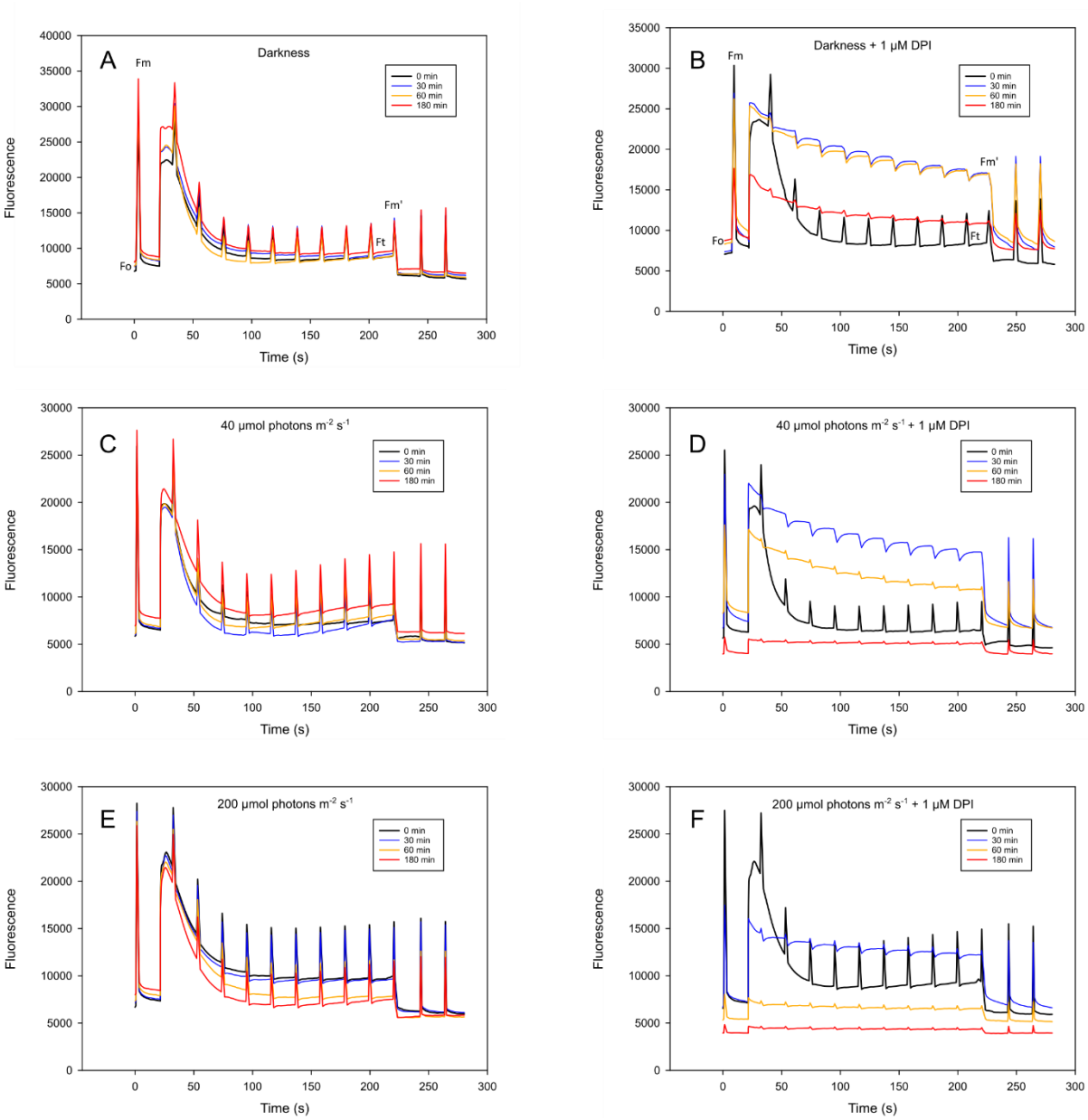

Figure 5.9 DPI in conjunction with light affects chlorophyll fluorescence during NPQ induction curves.

Following treatment of darkness (A, B), ML (C, D) or HL (E, F), dark-adapted cells were exposed to 3000 µmol photons m^{-2} s^{-1} saturating light pulse and 700 µmol photons m^{-2} s^{-1} actinic light to induce NPQ. Letters (Fo, Fm, Fm', Ft) on graphs (A, B) indicate where chlorophyll fluorescence parameters were extracted from the NPQ induction curve and highlight the differences between the control (A, C, E) and DPI (B, D, F) treatments. Data represent the average of three replicates. Error bars are not shown for clarity.

NPQ induction curves were significantly affected by DPI and increasing light intensity amplified the effects of DPI on chlorophyll fluorescence (Fig 5.9). After 30 min, DPI treatment drastically slowed fluorescence quenching during actinic light, resulting in increased Ft compared to controls (Table 5.2, Fig 8B, D, F). The lack of quenching may explain why saturating light induced fluorescence peaks (Fm') were suppressed or inverted (Fig 5.9B, D, F, Table 5.2) compared to control. Consequently, DPI completely suppressed Fv'/Fm' in all light intensities within 30 min with no recovery (Table 5.2). As time progressed, DPI treated cells showed reduced total chlorophyll fluorescence. After 180 min in ML and HL treatments, the chlorophyll fluorescence showed little change throughout the induction, suggesting extensive damage to PSII machinery.

Table 5.2 Summary of the effects of 1 µM DPI on photosynthetic parameters under different light intensities.

Fv/Fm was calculated using AquaPen parameters. All other parameters calculated from NPQ induction curve.

Parameter	**Darkness**				**Darkness + DPI**				**ML**				**ML + DPI**				**HL**				**HL + DPI**			
Time (min)	*0*	*30*	*60*	*180*	*0*	*30*	*60*	*180*	*0*	*30*	*60*	*180*	*0*	*30*	*60*	*180*	*0*	*30*	*60*	*180*	*0*	*30*	*60*	*180*
Fv/Fm	0.65 ± 0.01	0.66 ± 0.01	0.65 ± 0.01	0.64 ± 0.01	0.63 ± 0.01	0.71 ± 0.01	0.67 ± 0.01	0.42 ± 0.01	0.63 ± 0.01	0.65 ± 0.01	0.64 ± 0.02	0.61 ± 0.01	0.64 ± 0.01	0.68 ± 0.01	0.49 ± 0.03	0.23 ± 0.01	0.66 ± 0.01	0.63 ± 0.02	0.61 ± 0.02	0.53 ± 0.03	0.65 ± 0.01	0.56 ± 0.02	0.30 ± 0.04	0.06 ± 0.01
Fo	6762 ± 33	7434 ± 291	7531 ± 131	8073 ± 554	7065 ± 104	7368 ± 448	8312 ± 612	8734 ± 2003	5862 ± 134	5971 ± 163	6101 ± 146	6957 ± 491	5657 ± 32	6718 ± 954	8268 ± 706	3966 ± 234	6697 ± 130	7152 ± 479	7347 ± 455	8008 ± 689	6577 ± 187	6697 ± 766	5332 ± 171	3955 ± 104
Fm	29173 ± 82	31643 ± 294	31719 ± 130	33919 ± 1070	30343 ± 312	26908 ± 179	26225 ± 817	17631 ± 4247	25954 ± 671	26192 ± 393	26279 ± 357	27634 ± 854	25531 ± 98	22985 ± 663	17632 ± 1180	5754 ± 254	28262 ± 248	27385 ± 1276	26355 ± 2863	25878 ± 1661	27493 ± 455	17501 ± 2092	8041 ± 221	4843 ± 56
Ft’	8810 ± 281	9157 ± 411	8810 ± 149	9569 ± 799	8355 ± 65	17122 ± 1028	16905 ± 1967	10901 ± 2721	7477 ± 289	7499 ± 293	8052 ± 505	9168 ± 541	6469 ± 197	14760 ± 1331	10804 ± 684	5103 ± 148	9796 ± 309	9601 ± 1572	7824 ± 2127	7499 ± 518	9319 ± 538	12191 ± 2272	6545 ± 432	4367 ± 18
Fm’	13513 ± 509	14272 ± 676	13373 ± 315	13904 ± 1347	12430 ± 123	16927 ± 1051	17090 ± 1965	11205 ± 2769	11346 ± 422	12408 ± 742	13145 ± 1076	14781 ± 903	9504 ± 497	14684 ± 1398	11075 ± 733	5255 ± 184	15735 ± 717	15117 ± 1854	11693 ± 4335	11541 ± 587	14922 ± 808	12689 ± 2448	6838 ± 460	4519 ± 32

NPQ	1.16 ± 0.07	1.22 ± 0.12	1.37 ± 0.05	1.45 ± 0.21	1.44 ± 0.01	0.59 ± 0.11	0.55 ± 0.20	0.58 ± 0.19	1.28 ± 0.02	1.11 ± 0.10	1.01 ± 0.13	0.87 ± 0.10	1.69 ± 0.15	0.57 ± 0.15	0.6 ± 0.19	0.09 ± 0.02	0.8 ± 0.07	0.82 ± 0.13	1.46 ± 0.84	1.24 ± 0.06	0.84 ± 0.06	0.39 ± 0.13	0.18 ± 0.07	0.07 ± 0.01
Fv'/Fm'	0.347 ± 0.01	0.358 ± 0.01	0.341 ± 0.01	0.311 ± 0.01	0.327 ± 0.00	-0.011 ± 0.01	0.0108 ± 0.01	0.0274 ± 0.00	0.340 ± 0.01	0.395 ± 0.02	0.386 ± 0.01	0.379 ± 0.01	0.318 ± 0.02	-0.0054 ± 0.01	0.0243 ± 0.00	0.0287 ± 0.01	0.377 ± 0.01	0.366 ± 0.03	0.306 ± 0.10	0.350 ± 0.01	0.375 ± 0.00	0.0384 ± 0.01	0.0427 ± 0.00	0.0335 ± 0.00
qP	0.62 ± 0.01	0.64 ± 0	0.64 ± 0.01	0.62 ± 0.01	0.64 ± 0.01	-0.02 ± 0.01	0.03 ± 0.01	0.11 ± 0.01	0.66 ± 0.01	0.67 ± 0.01	0.66 ± 0.01	0.65 ± 0.01	0.67 ± 0.01	-0.016 ± 0.02	0.08 ± 0.01	0.16 ± 0.02	0.63 ± 0.03	0.63 ± 0.03	0.62 ± 0.03	0.67 ± 0.02	0.64 ± 0.02	0.1 ± 0.01	0.21 ± 0.02	0.25 ± 0.04

1 µM DPI significantly reduced *P. tricornutum* O_2 evolution (Fig 5.10A) by 63% at 60 µmol photons m^{-2} s^{-1} (one-way ANOVA, P<0.001) and by 55% at 250 µmol photons m^{-2} s^{-1} (one-way ANOVA, P<0.001) light treatments. For comparison, 10 µM DCMU, which inhibits PSII electron transport in the chloroplast, completely inhibited O_2 evolution at 60 µmol photons m^{-2} s^{-1} (one-way ANOVA, P<0.001) and reduced evolution by 84% at 250 µmol photons m^{-2} s^{-1} (one-way ANOVA, P<0.001). 1 µM DPI significantly reduced *P. tricornutum* dark O_2 consumption by 47% (Fig 5.10, one-way ANOVA, P=0.004) while DCMU had no significant effect (one-way ANOVA, P=0.420).

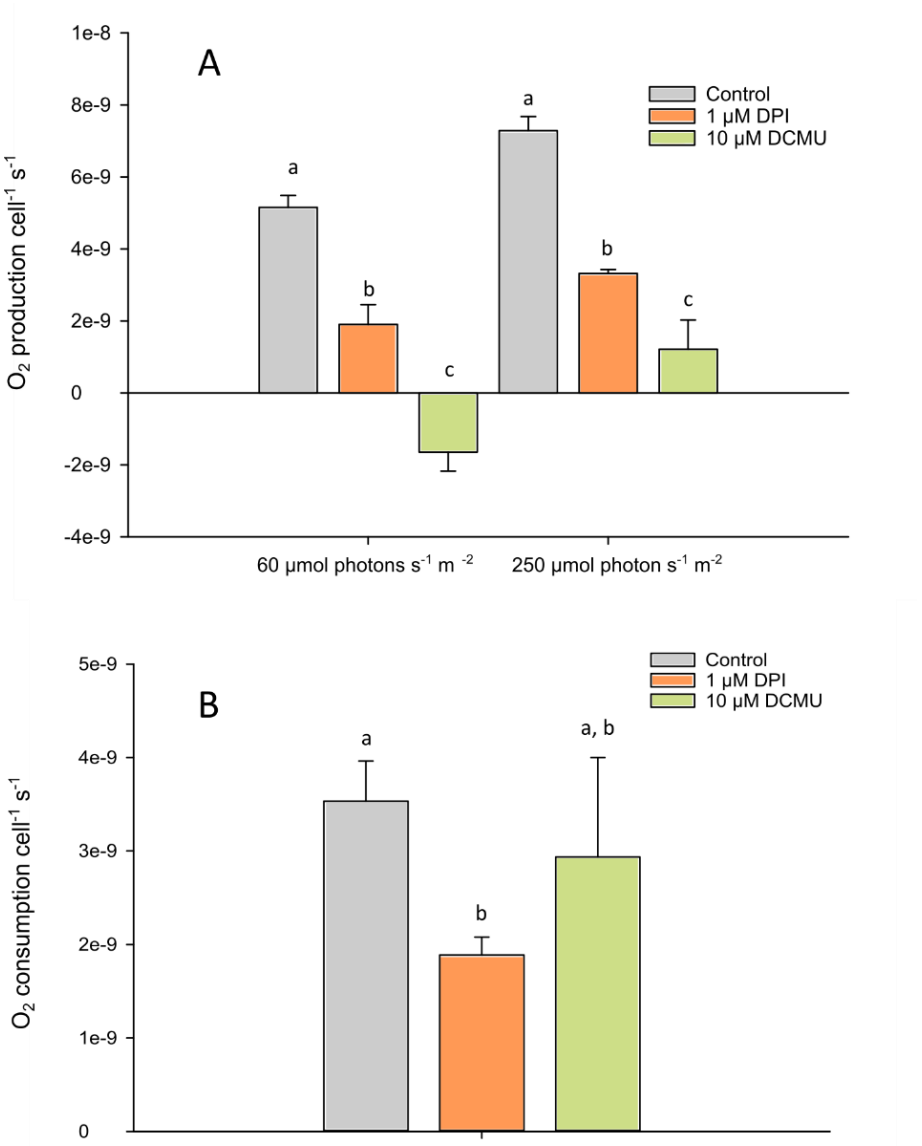

Figure 5.10 DPI and DCMU affect O_2 evolution and consumption in *P. tricornutum*. Measurements began following 30 min incubation with chemical inhibitors. A) Effects of inhibitors on O_2 evolution at different light intensities. B) O_2 consumption in darkness with different inhibitors. Different letters indicate significant difference within each light intensity (one-way ANOVA, Tukey post hoc test, P<0.05). Control

contained 0.1% v/v DMSO. Error bars indicate standard deviation for three biological replicates.

5.3.4 Differing effects of NOX inhibition in A. glacialis and T. weissflogii.

DPI can have non-specific effects on cellular parameters alongside inhibiting NOX proteins (Riganti *et al.*, 2004). Thus, it was important to test whether the DPI effects on *P. tricornutum* photosynthetic physiology are due to inhibiting its Class 2 NOX protein (Chapter 2) or non-specific effects. The effect of DPI on Fv/Fm was tested in two marine diatoms with different Classes of NOX protein (Fig 5.11). *T. weissflogii* has a NOX-like protein (Chapter 2). DPI caused a significant increase in Fv/Fm 60 min post addition (two-way repeated measures ANOVA, P=0.002) before a significant reduction after 180 min (P<0.001). *A. glacialis* has Class 1 and 3 NOX proteins (Chapter 2). 1 µM DPI had no effect on Fv/Fm in *A. glacialis* over 180 min, though there was a significant decline (ca 25%) 24 hours post-addition to 0.44 (two-way repeated measures ANOVA P<0.001).

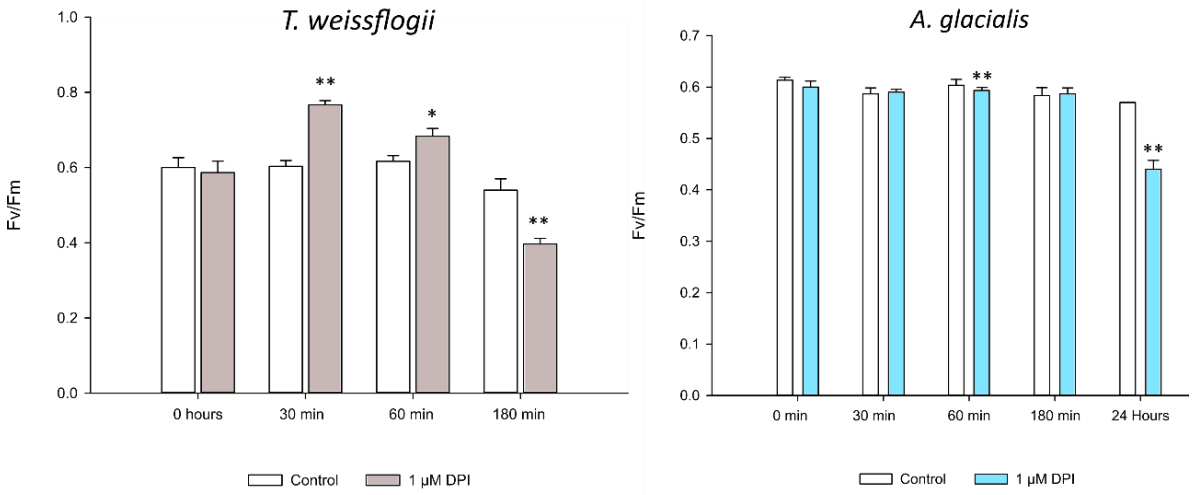

Figure 5.11 DPI has contrasting effects on Fv/Fm in *T. weissflogii* and *A. glacialis*. Cells were exposed to 1 µM DPI at medium light intensity (45-50 µmol photons m^{-2} s^{-1}). *T. weissflogii* density = 1.1x10^5 mL^{-1}. *A. glacialis* density = 6.7x10^5 cells mL^{-1}. Two-way repeated measures ANOVA compared DPI addition to control at each time point. Asterisks indicate significant differences between control and DPI at each time point. *P<0.05 ** P<0.001. No DMSO solvent was added to control. Error bars indicate standard deviation for three replicates.

5.3.5 GSSG has no effect on P. tricornutum eROS production.

Recent work has demonstrated that eROS production in *T. oceanica* originates from a plasma membrane glutathione reductase (GR) rather than a NOX protein (Diaz *et al.*, 2019). In *T.*

oceanica, glutathione disulphide (GSSG) competes with extracellular O_2 for reduction by GR and thus competitively inhibits *T. oceanica* eROS production. Using OxyBURST Green to measure eROS production, 10 µM and 200 µM GSSG had no effect on *P. tricornutum* eROS production (Fig 5.12, one-way ANOVA, P>0.05), suggesting that GR activity is not primarily responsible for eROS production in *P. tricornutum*.

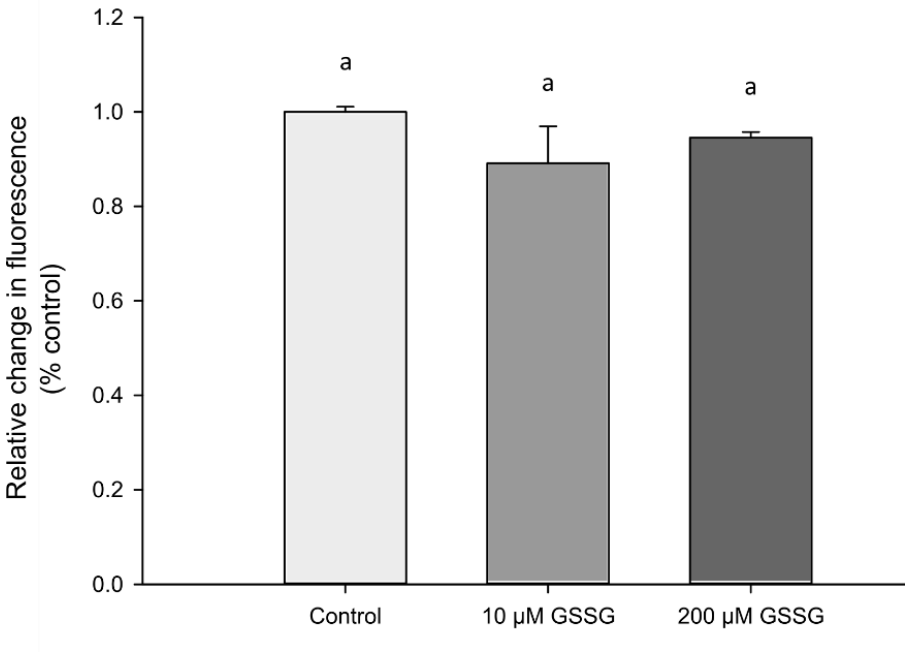

Figure 5.12 GSSG has no effect on *P. tricornutum* eROS production.
Using OxyBURST Green, *P. tricornutum* eROS production was measured over two hours following incubation with differing concentrations of GSSG at medium light intensity (45 µmol photons m^{-2} s^{-1}). Cell density = $3x10^6$ cells mL^{-1}. Different letters indicate significant difference within each light intensity (one-way ANOVA, Tukey post hoc test). Error bars show standard deviation for three biological replicates with three technical replicates.

5.3.6 Redox state-altering chemicals affect iROS and eROS production in P. tricornutum

Metabolic inhibitors were added to *roGFP2-Orp1* cells and cytosolic H_2O_2 levels were monitored. Salicylhydroxamic acid (SHAM) inhibits alternative oxidase (AOX), a mitochondrial electron dissipation enzyme (Murik *et al.*, 2019) while DCMU inhibits chloroplast PSII electron transport. 1 mM SHAM caused an immediate, significant, sustained increase in cytosolic H_2O_2 within 5 min (two-way ANOVA, P<0.001) that slowly declined over 180 min (Fig 5.13). 1 µM DPI caused a slower increase of cytosolic H_2O_2, becoming significant after 30 min (two-way ANOVA, P<0.05). In the DPI treatment, cytosolic H_2O_2 continued to increase throughout the experiment so that after

180 min, SHAM and DPI treatments had similar levels of cytosolic H_2O_2. In contrast, 10 µM DCMU had no significant on cytosolic H_2O_2 throughout the experiment (two-way ANOVA, P>0.05).

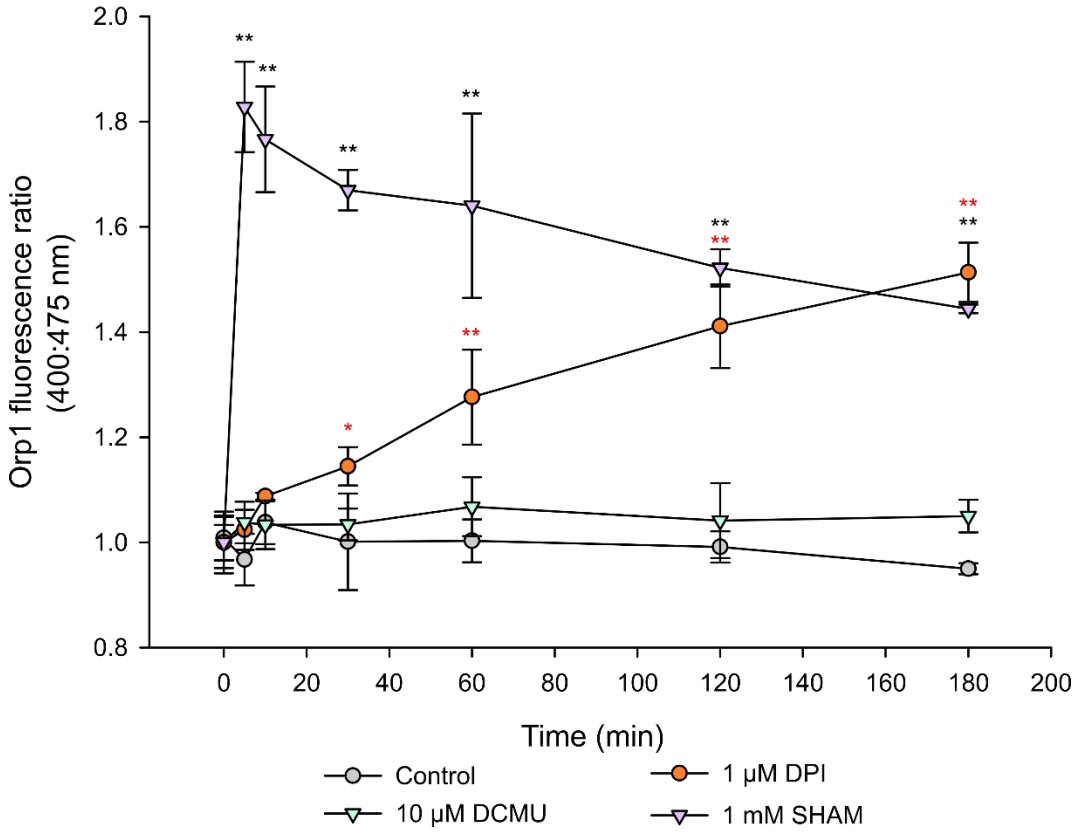

Figure 5.13 Metabolic inhibitors affect *P. tricornutum* cytosolic H_2O_2 levels. Inhibitors were added to *roGFP2-Orp1* cells at medium light intensity (40 µmol photons m^{-2} s^{-1} light intensity). Cytosolic H_2O_2 was tracked with roGFP2-Orp1 fluorescence in a plate reader assay. Cell density = $2.5x10^6$ cells mL^{-1}. Error bars show standard deviation for three biological replicates with two technical replicates. A two-way ANOVA tested statistical significance between control values and added chemical at each time point. * P=<0.05 ** P=<0.001. Black asterisk indicates test between control and 1 mM SHAM and red asterisk indicates test between control and 1 µM DPI.

eROS production and Fv/Fm following AOX and PSII inhibition was monitored. 1 mM SHAM (one-way ANOVA, P<0.001) and 10 µM DCMU (one-way ANOVA, P=0.004) significantly increased eROS production in *P. tricornutum* (Fig 5.14A, 5.15A). 0.5-1 mM SHAM had no effect on Fv/Fm up to 24 hours post addition (Fig 5.14B). In contrast, 10 µM DCMU significantly reduced Fv/Fm within 30 min, decreasing by 57% after 180 min (Fig 5.15B).

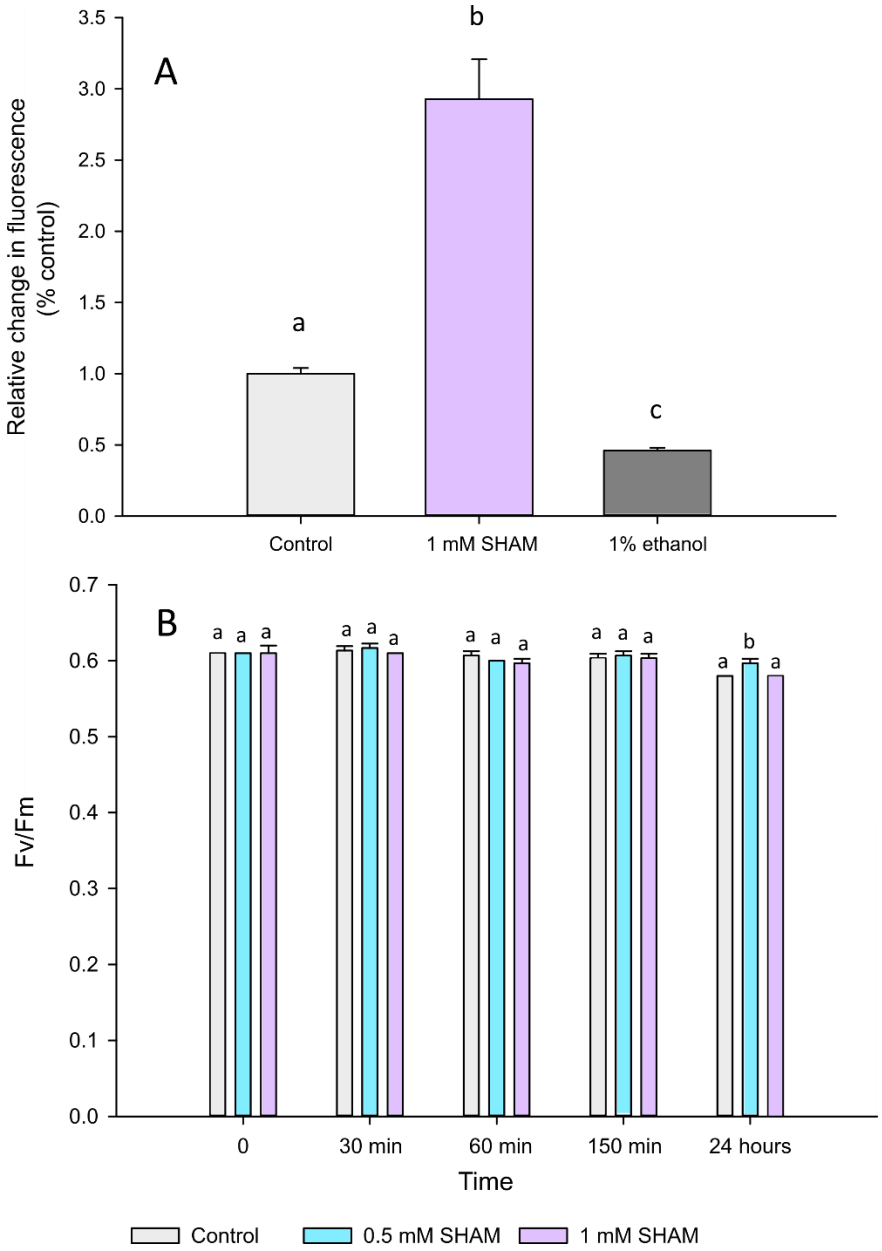

Figure 5.14 AOX inhibition increases *P. tricornutum* eROS production but does not affect Fv/Fm.

A) Using OxyBURST-Green the change in fluorescence was monitored for two hours at medium light intensity (40-50 µmol photons m^{-2} s^{-1}) in wild type *P. tricornutum* ($3.5x10^6$ cells mL^{-1}). B) Changes in Fv/Fm with different concentrations of SHAM ($5.5x10^6$ cells mL^{-1}). Statistical analysis on Fv/Fm compared the effect of time within each dataset. Different letters indicate significantly different treatments (one-way ANOVA for eROS production, two-way repeated measures ANOVA for Fv/Fm, $P<0.05$). Error bars indicate standard deviation for three biological replicates.

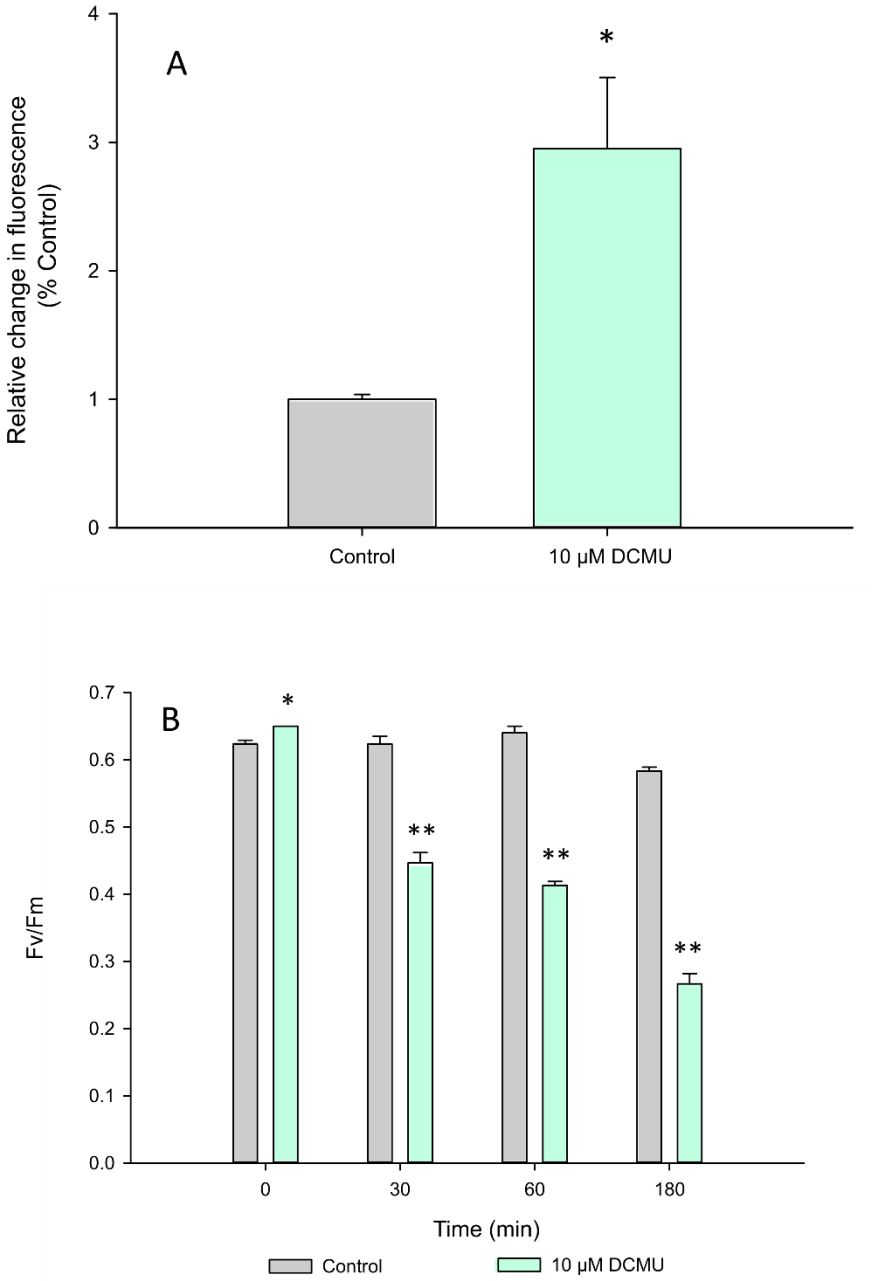

Figure 5.15 PSII inhibition increases eROS production and reduces Fv/Fm in *P. tricornutum.*

A) Measurement of eROS production over two hours using OxyBURST Green following addition of 10 µM DCMU to *P. tricornutum* cells ($3.2x10^6$ cells/ mL) at 45 µmol photons m^{-2} s^{-1}. B) Changes in Fv/Fm with 10 µM DCMU addition ($3.7x10^6$ cells mL^{-1}), also at 45 µmol photons m^{-2} s^{-1}. No ethanol was added to control. One-way ANOVA tested eROS production and two-way repeated measures ANOVA compared difference of DCMU with control at each time point. Asterisks indicate significant differences between control and DPI at each time point. *P<0.05 ** P<0.001. Error bars indicate standard deviation for three biological replicates.

5.4 Discussion

5.4.1 NOX activity can affect P. tricornutum redox state

Microalgal studies using DPI have typically focused on measuring its effect on eROS production (Kustka *et al.*, 2005; Laohavisit *et al.*, 2015; Diaz *et al.*, 2019) or electron transport (Eckhardt & Buckhout, 1998; Davey *et al.*, 2003). This study shows that chemical inhibition of NOX affects *P. tricornutum* redox state by generating cytosolic H_2O_2 (Fig 5.6). In addition, PtNOX1 localises to the plasma membrane (Fig 5.4). As *PtNOX1* is more highly expressed than *PtNOX2* and its gene expression is affected by the light regime (Laohavisit *et al.*, 2015), it is likely the predominant source of plasma membrane electron transport to produce eROS in *P. tricornutum*. Inhibiting NOX likely prevents the dissipation of intracellular electrons, resulting in over-reduction of the photosynthetic ETC and subsequent electron leakage and ROS production in the chloroplast. The steady increase of cytosolic H_2O_2 during NOX inhibition suggests NOX is continually dissipating intracellular electrons. Eventually the electron leakage and ROS generation may overwhelm antioxidant defences. This suggests that NOX activity could regulate redox signalling pathways in *P. tricornutum* in a different manner to multicellular organisms. NOX-derived redox signalling in multicellular organisms predominantly occurs by eROS re-entering the cell to alter redox state (Coelho *et al.*, 2002; Ross *et al.*, 2005; Miller *et al.*, 2009; Niethammer *et al.*, 2009). In contrast, NOX activity in *P. tricornutum* predominantly prevents increases in cytosolic H_2O_2 levels and a subsequent shift in redox state, though NOX-derived eROS may be involved in redox signalling in diatoms (Chapter 4, Bilcke *et al.*, 2020). Light intensity significantly affects diatom eROS production and trans-membrane electron transport (Lomas *et al.*, 2000; Davey *et al.*, 2003; Milne *et al.*, 2009; Laohavisit *et al.*, 2015; Schneider *et al.*, 2016; Diaz *et al.*, 2019), but other factors such as cell morphotype (Chapter 2, Ovide *et al.*, 2018) can alter NOX expression. Further research into how other environmental stresses affect NOX activity may indicate other NOX redox signalling roles in *P. tricornutum*.

5.4.2 Is DPI a suitable inhibitor for P. tricornutum NOX proteins?

DPI is an irreversible flavoprotein inhibitor capable of affecting non-NOX proteins. For example, DPI can inhibit oxidative pentose phosphate (OPP) proteins in mouse glial cells (Riganti *et al.*, 2004). Thus, caution was required to assess whether results obtained in the present study arose from NOX inhibition or non-specific inhibition of other flavoproteins. Dose-dependent effects of DPI are infrequently reported in microalgae (Kim *et al.*, 2000; Roháček *et al.*, 2014) but, as demonstrated here, can determine the extent of cellular physiology decline (Fig 5, Riganti *et al.*, 2004; Roháček *et al.*, 2014). Previous studies using diatoms and DPI have used 2-50 µM DPI

(Davey *et al.*, 2003; Kustka *et al.*, 2005; Laohavisit *et al.*, 2015; Diaz *et al.*, 2019) and incubation periods of up to 1 hour (Laohavisit *et al.*, 2015). Based on the effects of >5 µM DPI on *P. tricornutum* (Fig 5.5), there may have been significant oxidative stress in previously tested *P. tricornutum* cells (Laohavisit *et al.*, 2015) that may have contributed to reduced eROS production. 3-5 µM DPI can cause significant reduction in chlorophyll fluorescence and NPQ in *P. tricornutum*, though it is unclear whether this is due to inhibition of NOX or other flavoproteins (Roháček *et al.*, 2014). However, 1 µM DPI significantly reduces eROS production (see Chapter 3) and generates less cytosolic H_2O_2 than higher concentrations of DPI, minimising the risk of non-specific effects.

There are also species-specific effects of DPI that strongly suggests that NOX inhibition underlies the increase in cytosolic H_2O_2 and decline in photosynthetic parameters. For example, 50 µM DPI increased cytosolic H_2O_2 over five hours in *Arabidopsis thaliana* leaves (Nietzel *et al.*, 2019), but 100 µM DPI had no effect on cytosolic H_2O_2 in zebrafish larvae or *Brassica napus* leaf protoplasts (Niethammer *et al.*, 2009; Tewari *et al.*, 2012; Tao *et al.*, 2017). Similarly in algae, 2 µM DPI reduced Fv/Fm after 30 min in *T. weissflogii* but had no effect in the NOX-lacking green alga *Dunaliella tertiolecta* (Davey *et al.*, 2003). Thus, the absence of a DPI effect on Fv/Fm in *A. glacialis* is important. *P. tricornutum* and *A. glacialis* are both pennate diatoms so their cellular machinery should possess similar flavoenzymes. However, they possess different NOX proteins (Chapter 2) and differing cellular mechanics for eROS production (Chapter 3). The differing effects of DPI on Fv/Fm in marine diatoms suggests non-specific inhibition is not the cause of the reduction in *P. tricornutum*. Thus, the concentration used is suitable and *P. tricornutum* NOX inhibition is likely responsible for the other physiological effects reported.

5.4.3 NOX activity in P. tricornutum is coupled with photosynthesis

If eROS production is a strategy to dissipate excess photosynthetically-derived reductant as previously suggested (Hansel *et al.*, 2016; Diaz *et al.*, 2019), it follows that photosynthetic parameters would be strongly affected by NOX inhibition. This was confirmed, with DPI treated cells having significantly reduced measures of photosynthetic efficiency. Notably, qP dropped to 0 in all light conditions within 30 min (Fig 5.8D) and NPQ was significantly compromised (Fig 5.8C, 5.9). This suggests that PSII reaction centres were closed and electron flow was strongly inhibited, leading to photosystem over-reduction. This supports NOX function to dissipate excess reductant. Inhibiting NOX would prevent dissipation of excess NADPH and the regeneration of $NADP^+$, leading to reduced availability of electron acceptors and reaction centre closure. qP recovery increased with time, which may suggest adaptation to NOX absence. In addition, qP recovery was greatest in HL cells (Fig 5.8D) and O_2 evolution was slightly less affected in HL after 30 min (Fig 5.10). Potentially, upregulation of other electron dissipation mechanisms such as AOX (Bailleul *et*

al., 2015; Broddrick *et al.*, 2019) may allow greater electron flow, reducing NOX inhibitory effects. However, as overall chlorophyll fluorescence concurrently decreased with qP (Fig 5.9) and Ft increased, there may be extensive photosystem damage, which could affect the reliability of qP recovery values.

This photosystem damage likely occurs from increased chloroplast ROS generation. The over-reduction of the photosystem and reduced availability of $NADP^+$ would increase electron leakage or Mehler reactions (Asada, 2006; Waring *et al.*, 2010), generating damaging ROS. Hence, increasing light with DPI results in greater decline of Fv/Fm (Fig 5.8B). This decline matches observations in *T. oceanica* (Diaz *et al.*, 2019). However, the decline in Fv/Fm in *P. tricornutum* occurred at lower light intensities than those tested by Diaz et al. (HL= 200 µmol photons m^{-2} s^{-1} here vs 2000 µmol photons m^{-2} s^{-1}) which suggests NOX activity is consistently required and not just a response to extremely high light intensities.

The suppression of NPQ in DPI treatments matches previous findings in *P. tricornutum* (Roháček *et al.*, 2014). As NPQ is frequently upregulated in stress conditions such as nutrient depletion or high light (Allen *et al.*, 2008; Lepetit *et al.*, 2013), this suppression may also contribute to the ROS increase by preventing dissipation of excess energy. This may suggest NOX activity can affect NPQ, but the underlying mechanisms are unclear. DPI can inhibit the xanthophyll cycle in plants (Büch *et al.*, 1995), thus Roháček et al (2014) proposed >3 µM DPI also inhibits NPQ by inhibiting the diatom xanthophyll cycle and closing reaction centres. However, DPI inhibition of diatom photophysiology is not universal (Fig 5.10) and diatoms have different xanthophyll pigments to plants (Goss & Lepetit, 2015). Thus, the suppression of *P. tricornutum* NPQ may also relate to its NOX inhibition and consequent photophysiology effects. As H_2O_2 can also supress diatom NPQ (Chapter 4), increased ROS resulting from NOX inhibition may also act to inhibit NPQ.

5.4.4 NOX interactions with non-photosynthetic pathways

Although NOX strongly affected photosynthetic parameters, there is also evidence for interactions with other metabolic pathways. The greatest increase in cytosolic H_2O_2 occurred during Darkness + DPI treatment (Fig 5.8A) but photosynthetic parameters were least affected. This suggests an alternate source of electrons are shuttled to NOX. As several phytoplankton have substantial eROS production or electron transfer rates in darkness (Chapter 3, Xue *et al.*, 1998; Davey *et al.*, 2003; Diaz *et al.*, 2018), NOX may also dissipate excess dark-derived electrons. For example, NOX may dissipate excess mitochondrial-derived electrons and therefore inhibition of NOX may reduce mitochondria efficiency, consistent with reduced respiration rate (Fig 5.10). However, diatom photosynthesis and respiration rate are tightly coupled (Bailleul *et al.*, 2015; Broddrick *et al.*,

2019), so the observed reduction in respiration rate may be indirectly linked to photoinhibition. Alternatively, DPI may interfere with the diatom OPP either directly or via NOX inhibition (Riganti *et al.*, 2004), preventing NADPH generation. Diatom OPP is localised to the cytosol (Kroth *et al.*, 2008; Gruber *et al.*, 2009) and thus is more likely to be inhibited than plastid proteins (Riganti *et al.*, 2004). Diatoms would be unable to regenerate NADPH for antioxidant use, resulting in reduced ROS detoxification. Assessing how products of the OPP change in darkness + DPI treatment (Xue *et al.*, 1998; Riganti *et al.*, 2004) would reveal if the OPP is affected by NOX inhibition or DPI application.

5.4.5 Evidence for NOX interactions with other metabolic pathways: AOX and PSII

In plants and *P. tricornutum*, AOX activity prevents photosystem over-reduction by dissipating excess reductant, normally during stress situations such as high light (Yoshida *et al.*, 2007; Cvetkovska *et al.*, 2014; Bailleul *et al.*, 2015; Murik *et al.*, 2019). In the present study, SHAM inhibition of AOX increased both cytosolic H_2O_2 and eROS production (Fig 5.13, 5.14). Notably, these effects occurred under normal light conditions, further supporting diatom metabolic coupling as a consistent strategy to dissipate reductant (Bailleul *et al.*, 2015), rather than a stress response as in plants (Yoshida *et al.*, 2007; Cvetkovska & Vanlerberghe, 2012; Cvetkovska *et al.*, 2014). The rapid increase of cytosolic H_2O_2 during AOX inhibition suggests AOX is vital for preventing oxidative stress. AOX inhibition prevents dissipation of excess reductant to heat and by removing an alternate electron pathway, it is likely that more mitochondrial electrons are channelled through Complex III. As Complex III is a major source of mitochondrial ROS (Murphy, 2009), the increased electron flow and increased likelihood for ETC over-reduction may explain the rapid increase in cytosolic H_2O_2 following SHAM application (Fig 5.13). AOX is therefore likely to be an important redox state-influencing protein in *P. tricornutum*.

RNAi *AOX* mutants in *P. tricornutum* have lower Fv/Fm than wild-type cells (Murik *et al.*, 2019). Thus, the lack of effect of SHAM on Fv/Fm was surprising, though this has also been reported in several plants under non-stressful conditions (Bartoli *et al.*, 2005; Hu *et al.*, 2017). It is possible that significant decline in Fv/Fm in RNAi mutants may only occur following long-term inhibition of AOX and the subsequent sustained oxidative stress. Prioritisation of other electron dissipation mechanisms strategies, such as NOX, may potentially alleviate AOX absence in the short term. The increase in eROS production can be explained by excess reductant being channelled to NOX instead of AOX. Hence, eROS production increases and cytosolic H_2O_2 slowly declines from its peak level. Thus, NOX and AOX may interact together with metabolic coupling to ensure efficient dissipation of reductant.

The DCMU effect on eROS and cytosolic H_2O_2 production is more difficult to explain (Fig 5.15). While DCMU had no significant effect on cytosolic H_2O_2, eROS production increased. This does support suggestions from Chapter 3 that the eROS produced is from an enzymatic source and not due to diffusion of cytosolic H_2O_2. Dark production of phytoplankton eROS has shown photosynthesis is not the sole source of electrons (Saragosti *et al.*, 2010; Diaz *et al.*, 2018) and diatom metabolic coupling proposes efficient exchange of reductant and ATP (Bailleul *et al.*, 2015). As PSII is inhibited, this may reduce the efficiency of other electron dissipation mechanisms such as NPQ, Mehler reaction or metabolic coupling. Thus, NOX dissipates excess electrons from other sources. However, this is highly speculative, requiring greater experimental validation.

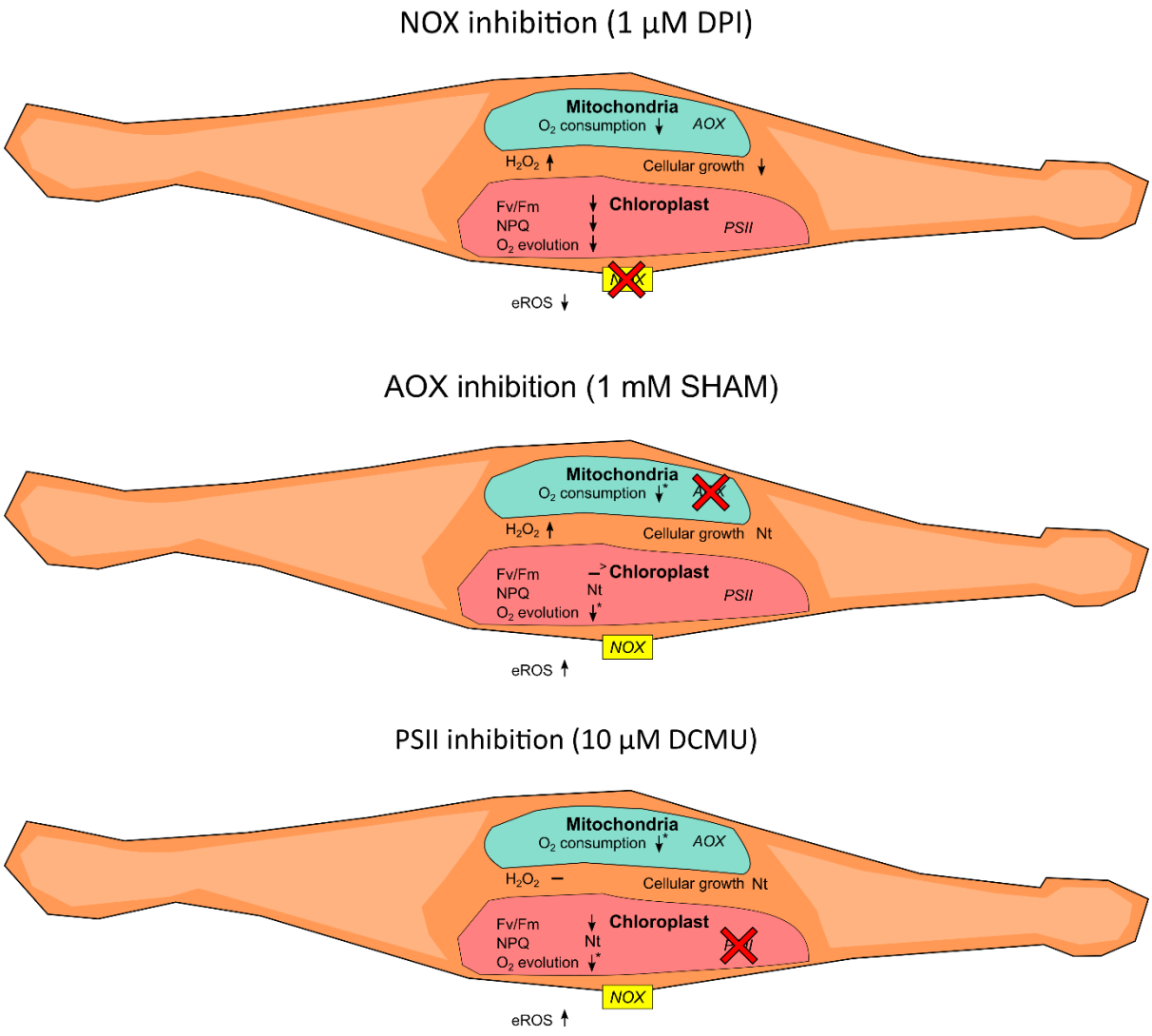

Figure 5.16 Comparing the effects of different metabolic inhibitors on cellular parameters in *P. tricornutum*.

Using the results acquired in this chapter and selected papers, a summary of the effects of DPI, SHAM and DCMU to *P. tricornutum* cellular parameters is presented. Nt not tested. * reported by Bailleul et al. (2015). > lower Fv/Fm was reported in downregulated AOX mutants by Murik et al. (2019).

5.4.6 Enzymatic and functional differences in eROS production between diatoms

While NOX proteins are the best characterised enzymatic source of eROS production, recent work has shown they are not the sole source in marine diatoms (Diaz *et al.*, 2019) and so caution is required when assigning an enzymatic source for eROS production. However, in *P. tricornutum*, there is significant support for NOX being the source (Table 5.3). As discussed in Chapter 2, *P. tricornutum* GR proteins lack a TMD, contrasting with *T. oceanica*. The current chapter shows *P. tricornutum* eROS production is GSSG-insensitive, also contrasting with *T. oceanica* (Diaz *et al.*, 2019). In addition, *T. weissflogii* Fv/Fm and eROS production are reduced with DPI application (Chapter 3, Davey *et al.*, 2003; Kustka *et al.*, 2005). This suggests that three different enzymatic sources of eROS (NOX, NOX-like, GR) are used to dissipate excess photosynthetic reductant in three different diatoms (Table 5.3). Similarly, metabolic coupling has been described in five ecologically diverse diatoms (*P. tricornutum*, *T. weissflogii*, *T. pseudonana*, *Ditylum brightwellii* and *Fragilaria pinnata)* (Bailleul *et al.*, 2015). Four of these species possess NOX/NOX-like proteins (*F. pinnata* is not sequenced) (Chapter 2). eROS production may interact with metabolic coupling to maximise efficient electron dissipation. However, the limited effect of DPI on eROS production (Chapter 3) and Fv/Fm in *A. glacialis* suggests that different diatoms may prioritise different strategies for electron dissipation. Differences in eROS production rate may reflect electron dissipation strategies. For example, *T. oceanica* has greater eROS production rates than *P. tricornutum* (Schneider *et al.*, 2016; Diaz & Plummer, 2018) but lower NPQ activity (Lavaud *et al.*, 2007), which may reflect their pelagic and benthic environments respectively. It is also notable that though *T. weissflogii* and *T. oceanica* have greater eROS production rates than *P. tricornutum*, NOX proteins are more abundant than *T. oceanica*-like GR and NOX-like proteins (Chapter 2). NOX proteins may represent the default enzymatic mechanism for diatom eROS production.

Table 5.3 Comparison of diatom eROS production and potential enzymatic sources.

Nt = not tested. * Results from Diaz et al. 2019.

Species	**NOX Class**	**GR group (TMD Y/N)**	**DPI reduced eROS**	**GSSG reduced eROS**	**DPI affected photosynthetic parameters**
P. tricornutum	Class 2	Group 1 (N)	Y	N	Y
T. oceanica	Class 3	Group 2 (Y)	Y*	Y*	Y*
T. weissflogii	NOX-like	Group 1, (N), Group 2, (N)	Y	Nt	Y
A. glacialis	Class 1, Class 3	Group 1, (N), Group 2, (N)	N	Nt	N

5.4.7 Conclusions

This study presents various ways in which NOX proteins in *P. tricornutum* can affect cellular function. The following model is proposed for how plasma membrane-localised NOX interacts with photosynthesis. Following NOX inhibition, chloroplast electron flow in light decreases, due to prevention of NOX-derived $NADP^+$ regeneration. Consequently, photosystem reaction centres become over-reduced, leading to greater electron leakage and chloroplast ROS generation. Some of this ROS dismutates to H_2O_2 and enters the cytoplasm. ROS generation overwhelms antioxidant defence, resulting in increased damage to photosynthetic components and photoinhibition. The results indicate that NOX activity is an important electron dissipation strategy, working alongside other metabolic components involving mitochondria and AOX as part of metabolic coupling. While this use for NOX may not be universal in diatoms, it further highlights the diversity of mechanisms diatoms possess for dissipating excess electrons. In particular, this work has highlighted the importance of species comparisons for understanding how different electron dissipation mechanisms are used. In this instance, NOX proteins in *P. tricornutum* have a comparable role to GR in *T. oceanica* for redox balance and eROS production.

Chapter 6 General Discussion

6.1 Summary of key findings

Though studies into marine phytoplankton eROS production are increasing, the functional characterisation of NOX proteins in specific microalgal lineages is very limited (Anderson *et al.*, 2011; Laohavisit *et al.*, 2015; Diaz *et al.*, 2019). This thesis set out to address this knowledge gap by characterising the diversity of NOX proteins and eROS production in marine diatoms. In Chapter 2, diatom NOX proteins were shown to have greater phylogenetic and structural diversity than any other previously screened group, with three distinct NOX Classes and one NOX-like group present. In combination with unusual diatom transmembrane GR proteins (Diaz *et al.*, 2019), these findings illustrate that diatoms possess diverse enzymatic mechanisms for eROS production. Chapter 3 demonstrated that there are significant differences in eROS production and FCR activity between diatom species. Increasing light intensities increased eROS production in 2/3 species tested, while high light inhibited FCR activity in all species. Similarly, eROS production in 2/3 species tested was susceptible to DPI application, suggesting a significant contribution from a flavoprotein source. In Chapter 4, roGFP2-Orp1 was expressed in *P. tricornutum* and demonstrated how exogenous H_2O_2 impacts *P. tricornutum* physiology. Though *P. tricornutum* is effective at removing H_2O_2 from the cytosol, H_2O_2 has significant long-term effects on growth and photosynthesis, indicating a potentially important role in redox signalling and regulation. In Chapter 5, it was proposed that NOX proteins have a photoprotection function in *P. tricornutum* by removing excess photosynthetic reductant (Fig 6.1), similar to metabolic coupling (Bailleul *et al.*, 2015). The importance of NOX proteins was demonstrated, as inhibiting NOX activity under non-stressful conditions had serious consequences, affecting photophysiology, redox state and growth. This discussion will highlight three key themes of this thesis, discuss these findings and propose future research directions.

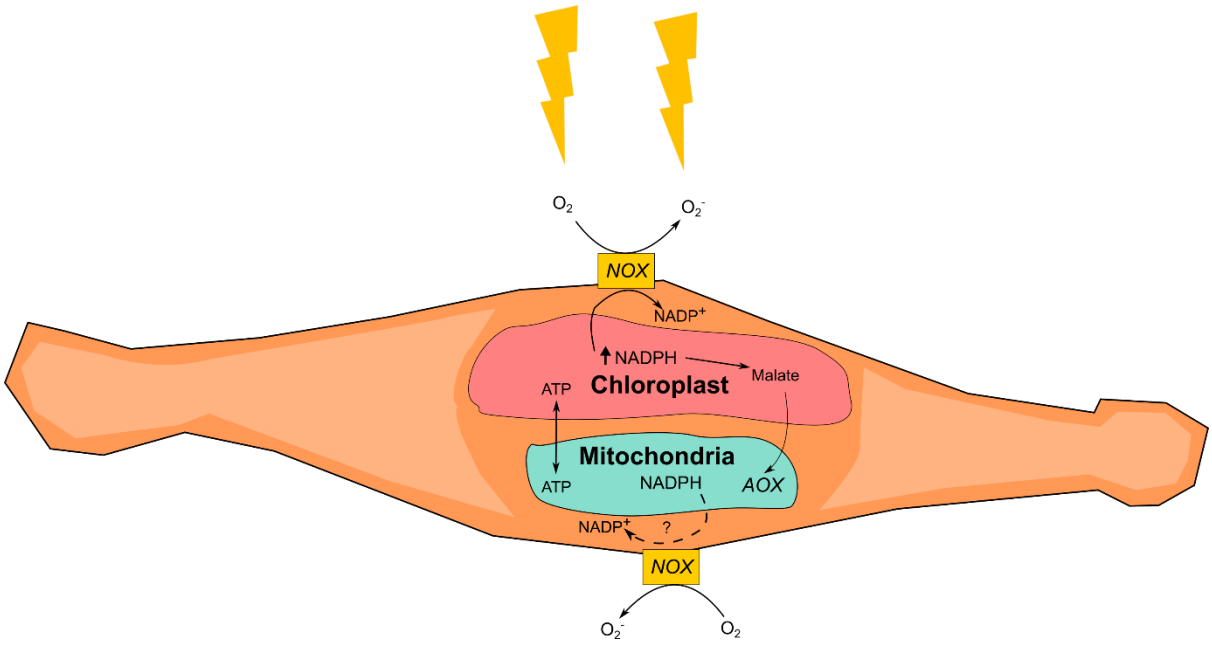

Figure 6.1 NOX as an electron dissipation mechanism.

A basic model demonstrating how NOX interacts with metabolic coupling to dissipate excess electrons. During high light, diatoms dissipate the excess NADPH produced in the chloroplast to prevent over-reduction of the photosystem. NADPH can be transferred to the mitochondria as part of metabolic coupling or to NOX for eROS production. NOX may dissipate excess mitochondrial NADPH, but further research is required to confirm this.

6.2 The structural diversity of diatom NOX proteins

6.2.1 What processes may have led to the diversity of diatom NOX proteins?

This thesis proposed a new Class system for classifying NOX proteins (Chapter 2). Class 1 NOX proteins are found in phylogenetically diverse lineages such as animals, plants, fungi and diatoms, suggesting Class 1 NOX proteins resemble the ancestral NOX protein and further supports NOX to be an ancient widespread enzyme (Sumimoto, 2008; Inupakutika *et al.*, 2016). However, diatom NOX proteins are structurally and phylogenetically diverse, displaying NOX Class similarity to plants, red algae and green algae. This diversity is most likely shaped by endosymbiosis events (Dorrell & Smith, 2011; Dorrell *et al.*, 2017), with diatoms retaining Class 2 and Class 3 NOX proteins originating in red and green algae. While diatoms as a lineage have retained all three Classes of NOX protein, gene loss is also prevalent, as 50% of screened diatoms did not possess a confirmed NOX protein. Finally, each diatom species has typically retained NOX proteins from a single Class, with only two exceptions (Chapter 2).

6.2.2 A functional explanation for diatom NOX diversity?

The absence of a clear pattern of conservation for NOX proteins between different diatom taxonomic groups (pennate vs centric) could suggest functional redundancy between different diatom NOX Class proteins. Alternatively, different NOX Classes may have different functions, with different diatoms retaining different NOX proteins. There is contrasting evidence of this in animals and plant NOX proteins. Within humans, different functions are ascribed to structurally different NOX1-4, NOX5 and DUOX (Sirokmany *et al.*, 2016) and these structural differences coincide with phylogenetic differences between these groups (Kawahara *et al.*, 2007). Meanwhile, plant Rboh proteins in *A. thaliana* are structurally and phylogenetically similar but possess diverse functions (Marino *et al.*, 2012). Due to a lack of data, only limited inferences can be made for diatom NOX proteins but there may be some functional diversity. *S. robusta* (Class 1) and *P. tricornutum* (Class 2) are likely to use NOX proteins for ROS signalling during sexual reproduction and electron dissipation respectively (Chapter 5, Laohavisit *et al.*, 2015; Bilcke *et al.*, 2020). Though less robustly tested, constitutive eROS production in *Coscinodiscus* sp. is unaffected by light (Hansel *et al.*, 2016) and *C. wailesii* has a Class 3 NOX protein (Chapter 2). Similarly, raphid pennate diatoms were predominantly associated with Class 2 NOX proteins (Chapter 2), which could suggest another specialised role for pennates. Further screening of diatom NOX functions is required to validate these ideas.

6.2.3 Why are there alternative enzymatic sources in diatoms?

Alongside diversity within NOX proteins, marine diatoms have at least three different enzymatic sources of eROS production: NOX, NOX-like and GR proteins. While GR and NOX-like proteins appear less common than NOX proteins (Chapter 2, Diaz *et al.*, 2019), it further highlights the importance of eROS production in marine diatoms. These non-NOX enzymatic sources may be more efficient than classic NOX proteins, resulting in evolutionary loss of NOX in these lineages. *T. oceanica* and *T. weissflogii* have relatively high rates of eROS production (Schneider *et al.*, 2016) and use eROS derived from GR and NOX-like proteins for electron dissipation (Chapter 5, Diaz *et al.*, 2019). Greater eROS production could indicate greater electron dissipation (Chapter 5, Diaz *et al.*, 2019), minimising the risk of electron leakage from electron transport chains. There may be other specialised eROS producing enzymes in microalgae. Diverse enzymatic sources for eROS production could explain eROS production in organisms lacking a classic NOX protein such as *Ectocarpus* (Kupper *et al.*, 2002; Cock *et al.*, 2010) or species whose eROS production is relatively insensitive to DPI, such as *A. glacialis* (Chapter 3).

The presence of NOX, NOX-like and GR proteins make assessing the source of eROS production in marine microalgae more difficult. DPI is commonly used to inhibit NOX proteins and reduce eROS in marine algae (Kupper *et al.*, 2002; Saragosti *et al.*, 2010; Laohavisit *et al.*, 2015). As DPI targets flavoproteins, it can target and inhibit GR, NOX and NOX-like proteins. Future studies should be cautious when using DPI to screen for NOX protein activity, especially if sequences are not available. Rather than label eROS production as NOX-derived, the source should be described as an oxidoreductase protein, unless protein sequences are available to support assessment.

6.2.4 Future steps to identify NOX proteins

The predictions made for the NOX Class diversity are supported by structural and phylogenetic evidence but remain putative until characterised accurately for eROS production. NOX proteins display significant structural similarity to FRE proteins, which can lead to mis-annotation (Chapter 2, Zhang *et al.*, 2013; Hajjar *et al.*, 2017; Rossi *et al.*, 2017). Realistically, molecular tools such as gene knockout are required to accurately assess the functions of putative proteins. *P. tricornutum* and *T. pseudonana* are increasingly being studied using gene editing tools (Hopes *et al.*, 2017; Serif *et al.*, 2017). With the exception of *C. reinharditii*, other algal groups are more limited by gene editing availability, though this is steadily improving (Tirichine *et al.*, 2017; Faktorová *et al.*, 2020).

In the absence of universally applied molecular tools, greater screening of diverse algal groups may assist NOX identification. Genetic databases are increasing for different algal lineages (*Phaeoexplorer*, Keeling *et al.*, 2014; Cheng *et al.*, 2018) and analysing these datasets will facilitate NOX identification and understanding NOX evolution. Given the structural diversity of algal NOX proteins, wider screening of NOX proteins in more algal lineages could test if Thr178 is a reliable identification motif to separate NOX proteins from FRE (Chapter 2). Wider screening may also reveal other well-conserved amino acid residues or motifs to identify NOX.

In addition, the endosymbiotic explanation for diatom NOX diversity could be tested. With a wide screen of algae, Class 1 NOX proteins, as the most conserved NOX protein, should be the most abundant Class. Stramenopile algae such as brown algae and raphidophytes should have the same level of NOX diversity as diatoms (Class 1-3). In contrast, Class 2 NOX proteins should not appear in green algae and vice versa with Class 3 NOX proteins and red algae, as these lineages are the proposed origin for Class 2 and 3 NOX proteins respectively.

6.3 The importance of H_2O_2 in diatom tolerance and signalling

6.3.1 How does H_2O_2 affect P. tricornutum signalling?

Expressing roGFP2-Orp1 in *P. tricornutum* further demonstrated that H_2O_2 can significantly alter cellular physiology in *P. tricornutum*. In line with previous work, the concentration of ROS affects the signalling response (Nakamura *et al.*, 2003; Murik & Kaplan, 2009; Graff van Creveld *et al.*, 2015). In this study, 100 µM H_2O_2 represented an important threshold for exogenous addition, with significant effects on Fv/Fm, NPQ, and cell growth. This aligns with previous work showing how >100 µM H_2O_2 can trigger PCD in *P. tricornutum* (Graff van Creveld *et al.*, 2015; Mizrachi *et al.*, 2019). Interestingly, though 50 µM H_2O_2 had limited effect in the present study, 50 µM H_2O_2 increases *AOX* expression in *P. tricornutum* (Murik *et al.*, 2019). Thus, ranges of concentration thresholds exist in *P. tricornutum* and affect different cellular pathways.

Furthermore, redox signalling is not a uniform population response in *P. tricornutum*. Variations in cytosolic Ca^{2+} elevations following H_2O_2 addition and heterogeneous responses following high light demonstrate that even in a clonal line of *P. tricornutum* cells, phenotype variability exists. As highlighted by Mizrachi *et al.*, (2019), assessment of population responses can hide single cell specific trends. These intercellular differences may contribute to microalgae success by having multiple responses to stimuli to enhance cell survival.

6.3.2 How do diatom tolerances to H_2O_2 compare?

Exposure to 200 µM H_2O_2 severely reduced growth rate and Fv/Fm in *P. tricornutum*, suggesting 200 µM H_2O_2 is close to its maximum tolerance. This is comparable to the tolerance of other diatoms, based on cell death and decline in Fv/Fm, of 200-300 µM H_2O_2 (Drábková *et al.*, 2007a; Thamatrakoln *et al.*, 2012). Diatom H_2O_2 tolerance is greater than cyanobacteria (nanomolar to micromolar) (Drábková *et al.*, 2007a,b; Ma *et al.*, 2018), comparable to dinoflagellates (Ganini *et al.*, 2013) but lower than the millimolar tolerance of green algae (Darehshouri *et al.*, 2008; Murik & Kaplan, 2009; Murik *et al.*, 2014). A screen of H_2O_2 tolerance has not been carried out in diatoms but some factors could be used to predict the different species tolerances. For example, diatoms that are frequently exposed to oxidative stress-inducing conditions would be expected to have greater tolerance to H_2O_2. In intertidal diatoms, salt stress and increased light are frequent stressors that trigger oxidative stress and strong antioxidant responses (Rijstenbil, 2003, 2005; Roncarati *et al.*, 2005, 2008). Therefore, intertidal diatoms likely have greater tolerance to exogenous H_2O_2 (Rijstenbil, 2003, 2005; Roncarati *et al.*, 2005, 2008). Similarly, polar diatoms would also be expected to have a high tolerance as they are exposed to rapid changes in light,

salinity and temperature that would generate oxidative stress (Lyon & Mock, 2014; Yoshida *et al.*, 2020). Finally, diatoms with high constitutive production of eROS such as *T. weissflogii* or *Pseudo-nitzschia* sp. (Schneider *et al.*, 2016; Diaz *et al.*, 2018) may have greater tolerance. High production rates may increase localised levels of exogenous H_2O_2, resulting in increased diffusion into the cell to be detoxified. However, this may only be comparable for similar species that exist in the same ecological environmental rather than between lineages. For example, *C. reinharditii* has lower eROS production than diatoms but greater tolerance to H_2O_2 (Murik & Kaplan, 2009; Anderson *et al.*, 2016; Schneider *et al.*, 2016).

6.3.3 What sources of H_2O_2 could initiate redox signalling in diatoms?

This thesis has demonstrated three mechanisms that affect cytosolic H_2O_2 levels and potentially initiate redox signalling: exogenous H_2O_2 (Chapter 4), environmental stressors such as high light (Chapter 4) and activity of electron dissipation enzymes (Chapter 5). In the natural environment, exogenous H_2O_2 is unlikely to trigger the severe effects in photophysiology seen in Chapter 4 as oceanic steady state levels of H_2O_2 typically only reach low nanomolar concentrations (Zinser, 2018) rather than the micromolar concentrations used in the laboratory. However, nanomolar concentrations of H_2O_2 could affect H_2O_2 sensitive species such as cyanobacteria, resulting in changes to community composition (Xenopoulos & Bird, 1997; Hunken *et al.*, 2008; Morris *et al.*, 2011; Matthijs *et al.*, 2012). Moreover, H_2O_2 toxicity can be exacerbated by interactions with increased light and temperature (Drábková *et al.*, 2007a; Ma *et al.*, 2018) and steady state ROS can be affected by factors such as water-column depth, time of day and cell concentration (Rose *et al.*, 2008; Matthijs *et al.*, 2012; Roach *et al.*, 2015; Sutherland *et al.*, 2020). Thus, spatial and temporal variations in oceanic ROS concentrations could affect diatoms. Environmental stressors such as light, salinity, nutrient limitation or heavy metal pollution can generate increased cellular ROS in diatoms (Rijstenbil *et al.*, 1994; Rijstenbil, 2003; Roncarati *et al.*, 2005; Allen *et al.*, 2008; Graff van Creveld *et al.*, 2016; Mizrachi *et al.*, 2019) and it is likely this is the most common form of ROS signalling, with the resultant increase in cellular ROS acting as a stress signal. Finally, the activity of electron dissipation enzymes such as AOX, GR or NOX can influence cellular redox state. AOX and NOX activity dissipates excess electrons that may be generated following stressful conditions, minimising ROS generation (Chapter 5, Murik *et al.*, 2019). Therefore, environmental stressors and electron dissipation enzymes can interact together as part of a ROS signalling response. As inhibiting AOX and NOX resulted in different dynamics for H_2O_2 generation (Chapter 5), they may partake in different redox signalling pathways.

6.3.4 What steps should be taken to further understand H_2O_2 signalling in P. tricornutum?

As H_2O_2 strongly affected photophysiology parameters, roGFP2-Orp1 and roGFP2-ChlOrp1 can be used to further explore the role of H_2O_2 in photo-oxidative stress and cell signalling. Under high light, it would be expected that chloroplast H_2O_2 would increase more rapidly than cytosolic levels and that recovery of photosynthetic parameters would correlate strongly with chloroplast H_2O_2 levels. In plants, chloroplast production of H_2O_2 interacts with other cellular compartments, altering gene expression (Exposito-Rodriguez *et al.*, 2017; Nietzel *et al.*, 2019). As *P. tricornutum* is increasingly demonstrated to display localised compartment signalling and interactions (this thesis, Bailleul *et al.*, 2015; Flori *et al.*, 2017; Helliwell *et al.*, 2019; Mizrachi *et al.*, 2019), differences between chloroplast and cytoplasm H_2O_2 dynamics could be investigated, such as comparing how localised H_2O_2 dynamics differ with redox state dynamics (Mizrachi *et al.*, 2019). Alongside this, measuring gene expression of key photosynthetic enzymes following H_2O_2 addition could infer which enzymes are susceptible to H_2O_2. Finally, confocal microscopy on roGFP2-Orp1 cells could investigate localised increases in H_2O_2 under stress conditions. In particular, this could be combined with research into Ca^{2+} dynamics. *P. tricornutum* exhibit tip-localised increases following osmotic shock (Helliwell *et al.*, 2019) while in brown algae embryos, Ca^{2+}: ROS gradients can co-localise during osmotic shock response and during growth development (Coelho *et al.*, 2002, 2008).

6.4 NOX proteins as an electron dissipation mechanism in P. tricornutum

This thesis provides evidence supporting a role for eROS production as a mechanism for dissipating excess photosynthetically-derived reductant (Hansel *et al.*, 2016; Sutherland *et al.*, 2019). NOX is a vital component for functioning *P. tricornutum* physiology as chemical inhibition of NOX causes significant reduction of photosynthetic parameters. In addition, disruption to respiration from NOX inhibition suggests NOX may dissipate excess electrons from other sources, such as the mitochondria. This could explain eROS production in the absence of photosynthesis (Chapter 3, 5). NOX activity likely works in combination with metabolic coupling, involving both chloroplast and mitochondria (Bailleul *et al.*, 2015) to ensure efficient electron use (Fig 6.1).

6.4.1 How do NOX proteins enhance diatom fitness?

The work presented in this thesis supports a role for NOX as a photoprotection mechanism to minimise light stress, alongside NPQ, AOX, the Mehler reaction and specialised light harvesting

proteins (Ruban *et al.*, 2004; Bailleul *et al.*, 2010; Waring *et al.*, 2010; Murik *et al.*, 2019). Having a variety of photoprotective mechanisms likely gives diatoms greater flexibility to respond to changing electron requirements under different environmental conditions. As well as dissipating electrons, NOX activity may promote efficient electron use to help balance the ATP:NADPH ratio under non-stressful conditions (Bailleul *et al.*, 2015). Diatoms display intricate control of their cellular machinery by regulating different pathways in response to high light (Broddrick *et al.*, 2019) and so more mechanisms may exist in diatoms to facilitate this. For example, it was previously reported that in nitrogen-replete diatoms, increasing light intensity results in greater NO_3^- reduction, which may represent another extracellular electron dissipation mechanism (Lomas *et al.*, 2000). If alternative substrates to oxygen are available, diatoms may use different pathways to remove excess electrons. However, oxygen represents an abundant default electron acceptor for cells.

6.4.2 eROS production for electron dissipation is a common microalgal strategy

Raphidophytes, dinoflagellates, haptophytes, green algae and cyanobacteria also increase eROS production with light intensity (Saragosti *et al.*, 2010; Li *et al.*, 2015; Anderson *et al.*, 2016; Hansel *et al.*, 2016; Plummer *et al.*, 2019), suggesting eROS production for electron dissipation is a common strategy in microalgae. The differences in per-cell production rates may reflect the relative importance of NOX for electron dissipation to different algal groups. For example, green algae have a lower per-cell production rate of eROS but are considered to utilise cyclic electron flow in a higher capacity than diatoms (Forti *et al.*, 2003; Lucker & Kramer, 2013; Bailleul *et al.*, 2015; Anderson *et al.*, 2016). As NOX proteins evolved very early (Inupakutika *et al.*, 2016), this electron dissipation function may be a very old strategy, explaining its use in both cyanobacteria and eukaryotic algae. The widespread use in microalgae as an electron dissipation mechanism is facilitated by direct contact of cells with the external medium, which prevents the build-up of harmful concentrations of ROS. This could explain the diversity of eROS producing enzymes in microalgae. In comparison, continual eROS production in terrestrial plants would result in a significant build-up of ROS which may explain why plants don't use NOX and eROS production for electron dissipation.

6.4.3 How can the risk of DPI toxicity be minimised in future NOX characterisation experiments?

Though efforts were taken to reduce non-specific DPI toxicity in this thesis, this frequently is not considered in other studies characterising NOX. NOX research is limited by the availability of specific inhibitors, as other inhibitors such as apocynin can also have nonspecific effects similar to

DPI (Riganti *et al.*, 2004, 2006). Thus, dose-dependent effects of DPI should be reported more frequently. Other steps may include minimising the risk of non-specific DPI toxicity. This may be achieved by washing cells after DPI incubation or using a flow through system for accurate per-second measurements of eROS (Kustka *et al.*, 2005; Milne *et al.*, 2009; Diaz *et al.*, 2019). Both of these methods would reduce exposure time to DPI and therefore reduce the chance of DPI targeting intracellular flavoproteins (Milne *et al.*, 2009; Diaz *et al.*, 2019). Genetic knockout of *P. tricornutum* NOX proteins is the ideal solution to characterise NOX function (Hopes *et al.*, 2017; Serif *et al.*, 2017). Seeing similar physiological effects in *NOX* mutants as that of DPI treated *P. tricornutum* (Chapter 5) would further validate NOX interactions with photophysiology and possibly the mitochondria. PtNOX1 should be preferentially targeted as it has greater gene expression and responds more strongly to light regime than PtNOX2 (Laohavisit *et al.*, 2015). However, there may be functional redundancy between the two *P. tricornutum* NOX proteins, thus requiring double mutants. It is possible that knockouts of either NOX protein would be lethal, given the strong negative effects on cellular physiology following DPI use. A possible solution is to use RNAi to reduce NOX expression as used recently to characterise AOX in *P. tricornutum* (Murik *et al.*, 2019). Phenotypes in RNAi mutants may be less prevalent compared to gene knockout mutants but would be more likely to permit growth of NOX-depleted cells for further experiments.

6.4.4 What other conditions may affect NOX activity in diatoms?

Inhibiting AOX results in increased eROS production, likely reflecting increased NOX activity to dissipate electrons that would otherwise be used by AOX (Chapter 5). Thus, conditions that affect AOX activity may also affect NOX activity. As increased temperature, light and nutrient depletion increase AOX expression (Murik *et al.*, 2019), comparing NOX expression under similar conditions may reveal a hierarchy of differing importance for different electron dissipation mechanisms in *P. tricornutum*.

There may be multiple functions for NOX in *P. tricornutum* and other diatoms. In *C. marina* and *C. reinharditii*, NOX proteins and eROS production are implicated for PCD signalling, electron dissipation, growth regulation, defence and iron uptake (Oda *et al.*, 1995; Garg *et al.*, 2007b; Pérez-Pérez *et al.*, 2012; Laohavisit *et al.*, 2015; Li *et al.*, 2015). *A. glacialis* may be an ideal species to test alternate NOX functions as it possesses Class 1 and Class 3 NOX proteins, and a role for electron dissipation is less clear than in *P. tricornutum* (Chapter 5). A defence role has yet to be tested in marine diatoms but oxidative bursts or increased NOX protein expression occur in several macroalgae following addition of bacterial peptides such as Flg22 (Kupper *et al.*, 2006; Luo *et al.*, 2015). Constitutive production of eROS may have a secondary role to inhibit growth of

neighbouring bacteria which typically have lower tolerances to H_2O_2 (Xenopoulos & Bird, 1997; Drábková *et al.*, 2007a). If diatoms can upregulate eROS production when electron dissipation mechanisms are compromised, they may upregulate eROS production to deal with increased presence of bacteria.

6.5 Concluding Remarks

Using a combination of bioinformatics, physiological assays and molecular techniques, NOX proteins are shown to be diverse and important components of diatom cell physiology. Using the model diatom *P. tricornutum*, NOX proteins represent an important electron dissipation mechanism. However, diatoms have multiple enzymatic sources for eROS production, suggesting eROS production is an important component. It is likely that NOX has other functions outside of electron dissipation, which could explain the structural diversity of diatom NOX proteins. As molecular tools develop, there will be greater opportunities to explore investigate ecologically diverse diatoms and test NOX distribution and function further (Hopes *et al.*, 2017; Tirichine *et al.*, 2017; Faktorová *et al.*, 2020). By increasing research into NOX and eROS production in microalgae, there are implications for diatom evolution, greater understanding of the dynamics of oceanic ROS steady state concentrations and how ROS may influence community composition.

Appendix A Chapter 1 Supplementary information

A.1 List of diatoms screened and distribution of NOX protein hits.

Green indicates the presence of a NOX protein following screening while red indicates no confirmed NOX protein.

Species Name	Group	Database sampled	Sequence hits	Likely NOX proteins	Class 1	Class 2	Class 3	NOX-like
Asterionellopsis glacialis	Araphid Pennate	MMETSP	4	2	1		1	
Grammatophora oceanica	Araphid Pennate	MMETSP	4	1			1	
Licmophora paradoxa	Araphid Pennate	MMETSP	3	1			1	
Staurosira complex	Araphid Pennate	MMETSP	2	1	1			
Striatella unipunctata	Araphid Pennate	MMETSP	8	2	2			
Synedropsis recta	Araphid Pennate	MMETSP	3	0				
Thalassionema frauenfeldii	Araphid Pennate	MMETSP	6	1			1	

Thalassionema nitzschioides	Araphid Pennate	MMETSP	3	2			2	
Thalassiothrix antarctica	Araphid Pennate	MMETSP	1	1				
Amphipora sp	Raphid Pennate	MMETSP	4	2	1		1	
Amphiprora paludosa	Raphid Pennate	MMETSP	2	1	1			
Amphora coffeaeformis	Raphid Pennate	MMETSP	1	0				
Cylindrotheca closterium	Raphid Pennate	MMETSP	11	1		1		
Entomoneis sp	Raphid Pennate	MMETSP	0	0				
Fistulera solaris	Raphid Pennate	NCBI-Genome	1	1			1	
Fragilariopsis cylindrus	Raphid Pennate	NCBI	4	2		2		
Fragilariopsis kerguelensis	Raphid Pennate	MMETSP	2	0				
Nitzschia punctata	Raphid Pennate	MMETSP	2	1	1			
Phaeodactylum tricornutum	Raphid Pennate	NCBI-Genome	2	2		2		
Pseudo-nitzschia arenysensis	Raphid Pennate	MMETSP	3	0				

Pseudo-nitzschia australis	Raphid Pennate	MMETSP	3	1		1		
Pseudo-nitzschia delicatissima	Raphid Pennate	MMETSP	3	2		2		
Pseudo-nitzschia fradulenta	Raphid Pennate	MMETSP	7	3	2	1		
Pseudo-nitzschia heimii	Raphid Pennate	MMETSP	2	2		2		
Pseudo-nitzschia multiseries	Raphid Pennate	JGI-Genome	2	2		2		
Pseudo-nitzschia multistriata	Raphid Pennate	NCBI-Genome	2	1		1		
Pseudo-nitzschia pungens cf. pungens	Raphid Pennate	NCBI	4	0				
Seminavis robusta	Raphid Pennate	*Seminavis robusta* genome, courtesy of Gust Bilke	6	5	5			
Chaetoceros sp.	Polar Centric	MMETSP	3	0				
Chaetoceros affinis	Polar Centric	MMETSP	1	0				
Chaetoceros curvisetus	Polar Centric	MMETSP	1	0				

Chaetoceros debilis	Polar Centric	MMETSP	1	0				
Chaetoceros neogracile	Polar Centric	MMETSP	1	1			1	
Cyclophora tenuis	Polar Centric	MMETSP	3	2			2	
Cyclotella meneghiniana	Polar Centric	MMETSP	2	0				
Detonula confervacea	Polar Centric	MMETSP	2	1	1			
Ditylum brightwellii	Polar Centric	MMETSP	2	0			1	
Eucampia antartica	Polar Centric	MMETSP	0	0				
Extubocellulus spinifer	Polar Centric	MMETSP	2	1		1		
Minutocellus polymorphus	Polar Centric	MMETSP	1	0				
Odontella aurita	Polar Centric	MMETSP	0	0				
Odontella sinensis	Polar Centric	MMETSP	2	1			1	
Skeletonema dohrnii	Polar Centric	MMETSP	1	0				
Skeletonema japonica	Polar Centric	MMETSP	2	0				
Skeletonema marinoi	Polar Centric	MMETSP	1	0				

Skeletonema menzelii	Polar Centric	MMETSP	1	0				
Thalassiosira antarctica	Polar Centric	MMETSP	3	1	1			
Thalassiosira gravida	Polar Centric	MMETSP	1	0				
Thalassiosira miniscula	Polar Centric	MMETSP	1	0				
Thalassiosira oceanica	Polar Centric	NCBI-Genome	1	1			1	
Thalassiosira pseudonana	Polar Centric	NCBI-Genome	2	2				2
Thalassiosira punctigera	Polar Centric	MMETSP	1	0				
Thalassiosira rotula (GSO102)	Polar Centric	MMETSP	3	0				
Thalassiosira weissflogii (CCMP1010)	Polar Centric	MMETSP	2	2				2
Aulacoseira subarctica	Radial Centric	MMETSP	1	0				
Coscinodiscus wailesi	Radial Centric	MMETSP	1	1			1	
Corethron pennatum	Radial Centric	MMETSP	0	0				
Corethron hystrix	Radial Centric	MMETSP	0	0				

Leptocylindrus danicus	Radial Centric	MMETSP	2	0				
Proboscia alata	Radial Centric	MMETSP	1	0				
Proboscia inermis	Radial Centric	MMETSP	0	0				
Rhizosolenia setigera	Radial Centric	MMETSP	0	0				
Stephanopyxis turris	Radial Centric	MMETSP	1	1	1			

Appendix B Chapter 4 Supplementary information

B.1 Biosensor sequences cloned into plasmid.

roGFP2	ATGGTCTCCAAGGGTGAAGAACTTTTTACGGGTGTCGTCCCGATCCTCGTCGAACTCGATGGTGATGTCAACGGCACAAGTTTTCCGTCTCCGGAGAAGGTGAAGGAGACG CCACCTACGGCAAGCTCACCCTCAAGTTCATCTCCACCACCGGAAAGCTCCCCGTCCCCTGGCCCACCCTCGTCACCACCCTCACCTACGGAGTCCAGTGCTTTTCCCGTTACC CCGACCACATGAAGCGTCACGACTTTTTCAAGTCCGCCATGCCCGAAGGCTACGTCCAGGAACGTACCATCTTCTTTAAGGACGACGGAAACTACAAGACCCGTGCCGAAG TCAAGTTCGAAGGAGACACCCTCGTCAACCGTATCGAACTCAAGGGAATCGACTTCAAGGAAGACGGAAACATCCTCGGACACAAGCTCGAATACAACTACAACTGCCACA ACGTCTACATCATGGCCGACAAGCAGAAGAACGGAATCAAGGTCAACTTCAAGATCCGTCACAACATCGAAGACGGTTCCGTCCAGCTCGCCGACCACTACCAGCAGAACA CCCCCATTGGTGACGGACCCGTCCTCCTCCCCGACAACCACTACCTCTCCACCTGCTCCGCCCTCTCCAAGGACCCCAACGAAAAGCGTGACCACATGGTCTTGCTCGAATTT GTCACCGCCGCCGGAATCACCCTCGGAATGGACGAACTTTACAAG
roGFP2- Orp1	ATGGCCGTCTCCAAGGGTGAAGAACTCTTTACGGGTGTCGTCCCGATCCTCGTCGAACTCGATGGTGATGTCAACGGTCACAAGTTTTCCGTCTCCGGTGAAGGAGAAGGT GACGCCACCTACGGAAAGCTCACCCTCAAGTTCATCTCCACCACCGGAAAGCTCCCCGTCCCCTGGCCCACCCTCGTCACCACCCTCACCTACGGTGTCCAGTGCTTCTCCCG TTACCCCGACCACATGAAGCAGCACGACTTTTTCAAGTCCGCCATGCCCGAAGGATACGTCCAGGAACGTACCATCTTTTTCAAGGACGACGGTAACTACAAGACCCGTGCC GAAGTCAAGTTCGAAGGCGACACCCTCGTCAACCGCATTGAACTCAAGGGTATCGACTTCAAGGAAGACGGTAACATCCTCGGTCACAAGCTCGAATACAACTACAACTGC CACAACGTCTACATCATGGCCGACAAGCAGAAGAACGGTATCAAGGTCAACTTCAAGATCCGCCACAACATTGAAGACGGTTCCGTCCAGCTCGCCGACCACTACCAGCAG AACACCCCCATTGGAGACGGTCCCGTCCTCCTCCCCGACAACCACTACCTCTCCACCTGCTCCGCCCTCTCCAAGGACCCCAACGAAAAGCGTGACCACATGGTCCTCCTCGA ATTTGTCACCGCCGCCGGTATTACCCTCGGAATGGACGAACTCTACAAGACCTCCGGTGGTTCCGGCGGAGGTGGTTCCGGTGGAGGCGGTTCCGGCGGAGGCGGTTCCG GAGGCGGAGGTTCCGGTGGTGGAGGCTCCGGTGGCGAATTTGACATCTCCGAATTTTACAAGCTCGCCCCCGTCGACAAGAAGGGTCAGCCCTTTCCCTTCGACCAGCTCA AGGGCAAGGTCGTCCTCATCGTCAACGTCGCCTCCAAGTGCGGATTTACCCCGCAGTACAAGGAACTCGAAGCCCTCTACAAGCGTTACAAGGACGAAGGTTTCACCATTA TCGGCTTCCCCTGCAACCAGTTCGGTCACCAGGAACCCGGTTCCGACGAAGAAATTGCCCAGTTCTGCCAGCTCAACTACGGCGTCACCTTTCCCATTATGAAGAAGATCGA

	CGTCAACGGTGGAAACGAAGACCCCGTCTACAAGTTCCTCAAGTCCCAGAAGTCCGGAATGCTCGGTCTCCGTGGCATCAAGTGGAACTTCGAAAAGTTTCTCGTCGACAA GAAGGGAAAGGTCTACGAACGTTACTCCTCCCTCACCAAGCCCTCGTCGCTCTCGGAAACCATTGAAGAATTGTTGAAGGAAGTCGAAGGTCGTGACTCGTCC
roGFP2-Grx	ATGGCCTCCGAATTTTCCAAGGGTGAAGAACTTTTTACGGGTGTCGTCCCGATCCTCGTCGAACTCGATGGTGATGTCAACGGTCACAAGTTTTCCGTCTCCGGCGAAGGTG AAGGAGACGCCACCTACGGAAAGCTCACCCTCAAGTTCATCTCCACCACCGGAAAGCTCCCCGTCCCCTGGCCCACCCTCGTCACCACCCTCACCTACGGCGTCCAGTGCTTT TCCCGCTACCCCGACCACATGAAGCAGCACGACTTTTTCAAGTCCGCCATGCCCGAAGGTTACGTCCAGGAACGTACCATCTTTTTCAAGGACGACGGTAACTACAAGACCC GTGCCGAAGTCAAGTTTGAAGGCGACACCCTCGTCAACCGTATTGAACTCAAGGGTATCGACTTCAAGGAAGACGGCAACATTCTCGGTCACAAGCTCGAATACAACTACA ACTGCCACAACGTCTACATTATGGCCGACAAGCAGAAGAACGGTATTAAGGTCAACTTTAAGATCCGTCACAACATCGAAGACGGTTCCGTCCAGCTCGCCGACCACTACCA GCAGAACACCCCCATTGGAGACGGTCCCGTCCTCCTCCCCGACAACCACTACCTCTCCACCTGCTCCGCCCTCTCCAAGGACCCCAACGAAAAGCGTGACCACATGGTCCTCC TCGAATTTGTCACCGCCGCCGGAATCACCCTCGGCATGGACGAACTCTACAAGACCTCCGGAGGTTCCGGTGGAGGTGGCTCCGGTGGTGGAGGCTCCGGTGGAGGTGGT TCCGGAGGTGGAGGTTCCGGAGGCGGAGGTTCCGGCGGTGAATTTACCATGGTCTCCCAGGAAACCATCAAGCACGTCAAGGACCTCATCGCCGAAAACGAAATCTTCGT CGCCTCCAAGACCTACTGCCCCTACTGCCACGCCGCCCTCAACACCCTCTTCGAAAAGCTCAAGGTCCCCCGTTCCAAGGTCCTCGTCCTCCAGCTCAACGACATGAAGGAAG GCGCCGACATTCAGGCCGCCCTCTACGAAATCAACGGACAGCGTACCGTCCCCAACATTTACATCAACGGCAAGCACATTGGTGGAAACGACGACCTCCAGGAACTTCGTG AAACGGGTGAACTTGAAGAATTGCTTGAACCGATTCTCGCCAAC
roGFP2-Tsa	ATGGCCTCCGAATTTTCCAAGGGTGAAGAACTTTTTACGGGTGTCGTCCCGATCCTCGTCGAACTCGATGGTGATGTCAACGGTCACAAGTTCTCCGTCTCCGGTGAAGGAG AAGGTGACGCCACCTACGGCAAGCTCACCCTCAAGTTTATCTCCACCACCGGAAAGCTCCCCGTCCCCTGGCCCACCCTCGTCACCACCCTCACCTACGGCGTCCAGTGCTTC TCCCGCTACCCCGACCACATGAAGCAGCACGACTTTTTCAAGTCCGCCATGCCCGAAGGATACGTCCAGGAACGTACCATCTTCTTTAAGGACGACGGTAACTACAAGACCC GTGCCGAAGTCAAGTTCGAAGGTGACACCCTCGTCAACCGTATTGAACTCAAGGGAATCGACTTCAAGGAAGACGGAAACATCCTCGGACACAAGCTCGAATACAACTACA ACTGCCACAACGTCTACATTATGGCCGACAAGCAGAAGAACGGAATCAAGGTCAACTTCAAGATCCGTCACAACATTGAAGACGGTTCCGTCCAGCTCGCCGACCACTACC AGCAGAACACCCCCATTGGTGACGGACCCGTCCTCCTCCCCGACAACCACTACCTCTCCACCTGCTCCGCCCTCTCCAAGGACCCCAACGAAAAGCGTGACCACATGGTCCTC CTCGAATTTGTCACCGCCGCCGGAATTACCCTCGGTATGGACGAACTCTACAAGACCTCCGGCGGTTCCGGTGGTGGAGGCTCCGGAGGTGGAGGCTCCGGTGGAGGCGG TTCCGGCGGTGGCGGTTCCGGAGGCGGAGGTTCCGGTGGCGAATTTGTCGCCGAAGTCCAGAAGCAGGCCCCGCCCTTCAAGAAGACCGCCGTCGTCGACGGAATCTTTG AAGAAATCTCCCTCGAAAAGTACAAGGGCAAGTACGTCGTCCTCGCCTTCGTCCCCCTCGCCTTTTCCTTCGTCTGCCCCACCGAAATTGTCGCCTTCTCCGACGCCGCCAAG AAGTTTGAAGACCAGGGTGCCCAGGTCCTCTTCGCCTCCACCGACTCCGAATACTCCCTCCTCGCCTGGACCAACCTCCCCCGTAAGGACGGTGGACTCGGTCCCGTCAAGG TCCCCCTCCTCGCCGACAAGAACCACTCCCTCTCCCGTGACTACGGCGTCCTCATCGAAAAGGAAGGAATCGCCCTCCGTGGACTCTTCATTATCGACCCCAAGGGAATTATC

	CGCCACATCACCATTAACGACCTCTCCGTCGGACGTAACGTCAACGAAGCCCTCCGCCTCGTCGAAGGTTTCCAGTGGACCGACAAGAACGGTACCGTCCTCCCCGCCAACT GGACCCCCGGAGCCGCCACGATTAAGCCCGATGTCAAGGACTCCAAGGAATACTTCAAGAACGCCAACAAC
roGFP2- ChlOrp1	TCTTGACCATGAAGTTCACTGCCGCCTGCTCTATTGCCCTCGCTGCTTCGGCTTCGGCCTTTGCCCCGATTCCCTCGGTTAGCGTGAGTTGATTTTGCAGTGGCCATGATAGG AAACGGTCGAGAGTTGCAGAGAACAAAAGCTGTTGAGCATTATGCCCTTTATTTCGTTCTTCGTCTGCGCTGTTTACGTCACAATGAATTTTATTGGCAGTAACTTTTTTGTT GTTGGCTGTAGTGATTTGTGTCTGACAAGTTTCGTTTTCGCCCTTATTGATACTGCAGCGTACCACCGATCTTAGCATGTCTTTGCAAAAGGATCTCGCTAATGTCGGCAAGG AATTCGCCAAGATGGCCGTCTCCAAGGGTGAAGAACTCTTTACGGGTGTCGTCCCGATCCTCGTCGAACTCGATGGTGATGTCAACGGTCACAAGTTTTCCGTCTCCGGTGA AGGAGAAGGTGACGCCACCTACGGAAAGCTCACCCTCAAGTTCATCTCCACCACCGGAAAGCTCCCCGTCCCCTGGCCCACCCTCGTCACCACCCTCACCTACGGTGTCCAG TGCTTCTCCCGTTACCCCGACCACATGAAGCAGCACGACTTTTTCAAGTCCGCCATGCCCGAAGGATACGTCCAGGAACGTACCATCTTTTTCAAGGACGACGGTAACTACA AGACCCGTGCCGAAGTCAAGTTCGAAGGCGACACCCTCGTCAACCGCATTGAACTCAAGGGTATCGACTTCAAGGAAGACGGTAACATCCTCGGTCACAAGCTCGAATACA ACTACAACTGCCACAACGTCTACATCATGGCCGACAAGCAGAAGAACGGTATCAAGGTCAACTTCAAGATCCGCCACAACATTGAAGACGGTTCCGTCCAGCTCGCCGACC ACTACCAGCAGAACACCCCCATTGGAGACGGTCCCGTCCTCCTCCCCGACAACCACTACCTCTCCACCTGCTCCGCCCTCTCCAAGGACCCCAACGAAAAGCGTGACCACAT GGTCCTCCTCGAATTTGTCACCGCCGCCGGTATTACCCTCGGAATGGACGAACTCTACAAGACCTCCGGTGGTTCCGGCGGAGGTGGTTCCGGTGGAGGCGGTTCCGGCGG AGGCGGTTCCGGAGGCGGAGGTTCCGGTGGTGGAGGCTCCGGTGGCGAATTTGACATCTCCGAATTTTACAAGCTCGCCCCCGTCGACAAGAAGGGTCAGCCCTTTCCCTT CGACCAGCTCAAGGGCAAGGTCGTCCTCATCGTCAACGTCGCCTCCAAGTGCGGATTTACCCCGCAGTACAAGGAACTCGAAGCCCTCTACAAGCGTTACAAGGACGAAGG TTTCACCATTATCGGCTTCCCCTGCAACCAGTTCGGTCACCAGGAACCCGGTTCCGACGAAGAAATTGCCCAGTTCTGCCAGCTCAACTACGGCGTCACCTTTCCCATTATGA AGAAGATCGACGTCAACGGTGGAAACGAAGACCCCGTCTACAAGTTCCTCAAGTCCCAGAAGTCCGGAATGCTCGGTCTCCGTGGCATCAAGTGGAACTTCGAAAAGTTTC TCGTCGACAAGAAGGGAAAGGTCTACGAACGTTACTCCTCCCTCACCAAGCCCTCGTCGCTCTCGGAAACCATTGAAGAATTGTTGAAGGAAGTCGAAGGTCGTGACTCGT CCTAA

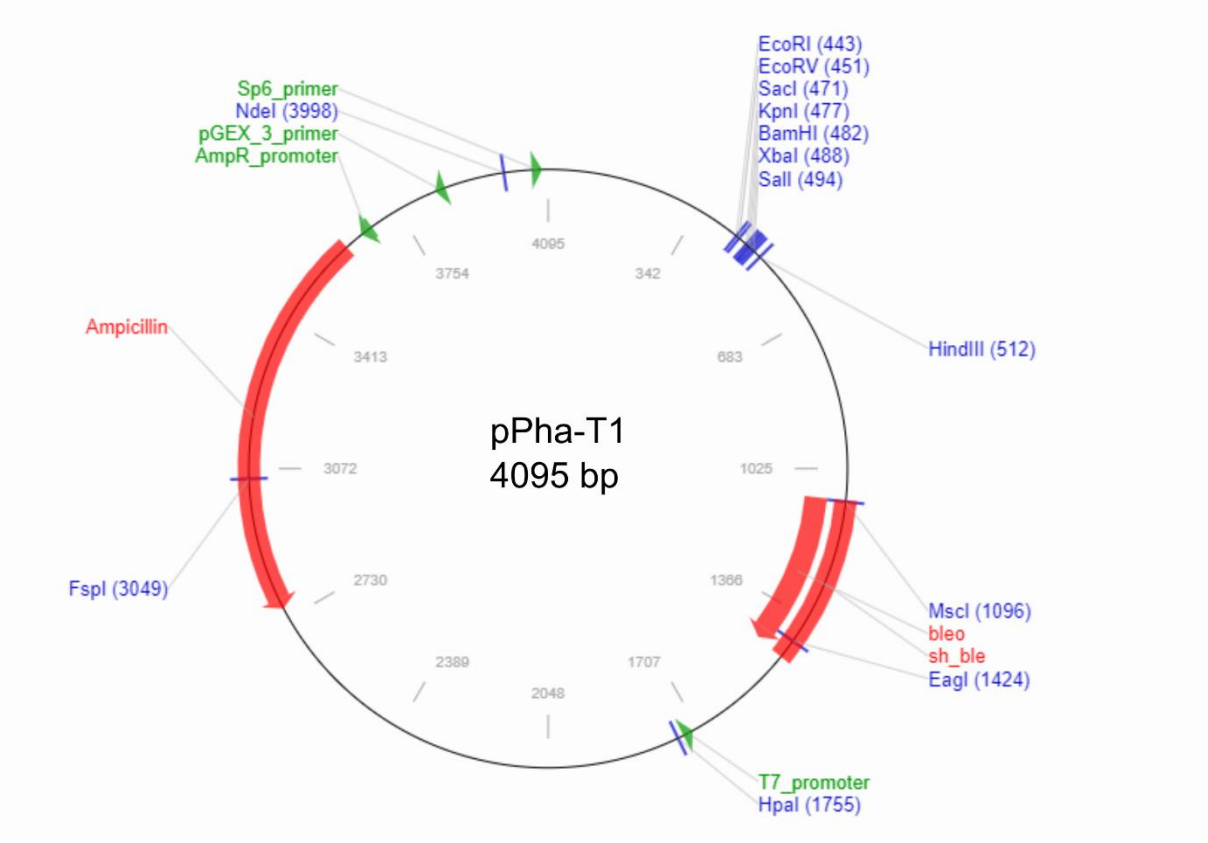

B.2 Plasmid map for shuttle vector pPhat-T1.

Antibiotic resistance for ampicillin, Zeocin (sh_ble) and bleomycin (bleo) indicated by red regions. Map made using Addgene (https://www.addgene.org/analyze-sequence/) and pPha-T1 gene sequence (GenBank accession no. AF219942).

Appendix C Chapter 5 Supplementary information

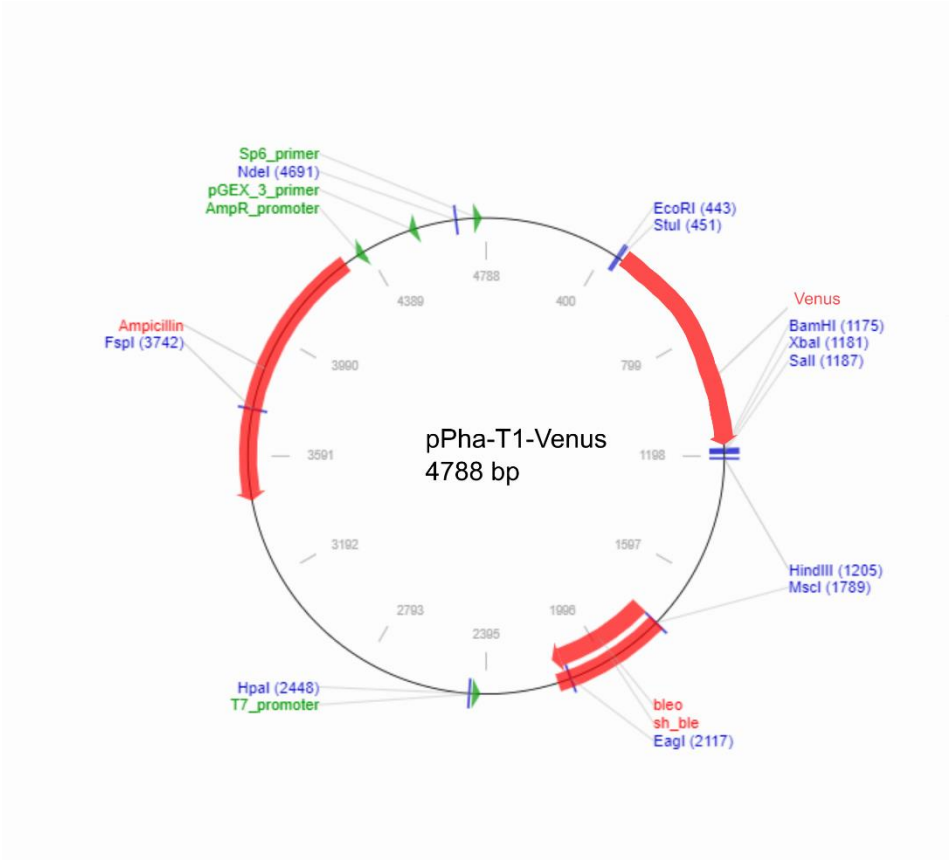

C.1 Plasmid map for pPha-T1-Venus shuttle vector.

Plasmid created through fusion of pPha-T1 (accession no. AF219942) and codon optimised Venus (accession AJN91098.1), from Helliwell *et al.* (2019). Antibiotic resistance for ampicillin, Zeocin (sh_ble) and bleomycin (bleo) indicated by red regions. Map made using Addgene (https://www.addgene.org/analyze-sequence/).

List of Accompanying Materials

Full dataset available in University of Southampton online repository (PURE)

https://doi.org/10.5258/SOTON/D1869

List of References

Aguirre J, Ríos-Momberg M, Hewitt D, Hansberg W. **2005**. Reactive oxygen species and development in microbial eukaryotes. *Trends in Microbiology* **13**: 111–118.

Allen AE, LaRoche J, Maheswari U, Lommer M, Schauer N, Lopez PJ, Finazzi G, Fernie AR, Bowler C. **2008**. Whole-cell response of the pennate diatom *Phaeodactylum tricornutum* to iron starvation. *Proceedings of the National Academy of Sciences of the United States of America* **105**: 10438–10443.

Amin SA, Hmelo LR, van Tol HM, Durham BP, Carlson LT, Heal KR, Morales RL, Berthiaume CT, Parker MS, Djunaedi B, *et al.* 2015. Interaction and signalling between a cosmopolitan phytoplankton and associated bacteria. *Nature* **522**: 98–101.

Anderson A, Bothwell JH, Laohavisit A, Smith AG, Davies JM. **2011**. NOX or not? Evidence for algal NADPH oxidases in algae. *Trends in Plant Science* **16**: 579–580.

Anderson A, Laohavisit A, Blaby IK, Bombelli P, Howe CJ, Merchant SS, Davies JM, Smith AG. **2016**. Exploiting algal NADPH oxidase for biophotovoltaic energy. *Plant Biotechnology Journal* **14**: 22–28.

Annunziata R, Ritter A, Fortunato AE, Manzotti A, Cheminant-Navarro S, Agier N, Huysman MJJ, Winge P, Bones AM, Bouget F-Y, *et al.* 2019. bHLH-PAS protein RITMO1 regulates diel biological rhythms in the marine diatom *Phaeodactylum tricornutum*. *Proceedings of the National Academy of Sciences*: 13137–13142.

Armbrust E V. **2009**. The life of diatoms in the world's oceans. *Nature* **459**: 185–192.

Armbrust E V, Berges JA, Bowler C, Green BR, Martinez D, Putnam NH, Zhou SG, Allen AE, Apt KE, Bechner M, *et al.* 2004. The genome of the diatom *Thalassiosira pseudonana*: Ecology, evolution, and metabolism. *Science* **306**: 79–86.

Asada K. **2006**. Production and scavenging of reactive oxygen species in chloroplasts and their functions. *Plant Physiology* **141**: 391–396.

Ashworth J, Coesel S, Lee A, Armbrust E V, Orellana M V, Baliga NS. **2013**. Genome-wide diel growth state transitions in the diatom *Thalassiosira pseudonana*. *Proceedings of the National Academy of Sciences of the United States of America* **110**: 7518–7523.

Bailleul B, Berne N, Murik O, Petroutsos D, Prihoda J, Tanaka A, Villanova V, Bligny R, Flori S, Falconet D, *et al.* 2015. Energetic coupling between plastids and mitochondria drives CO_2 assimilation in diatoms. *Nature* **524**: 366–369.

Bailleul B, Rogato A, de Martino A, Coesel S, Cardol P, Bowler C, Falciatore A, Finazzi G. **2010**. An atypical member of the light-harvesting complex stress-related protein family modulates diatom responses to light. *Proceedings of the National Academy of Sciences* **107**: 18214–18219.

Barrero-Gil J, Garciadeblás B, Benito B. **2005**. Sodium, potassium-ATPases in algae and oomycetes. *Journal of Bioenergetics and Biomembranes* **37**: 269–278.

Bartoli CG, Gomez F, Gergoff G, Guiamé JJ, Puntarulo S. **2005**. Up-regulation of the mitochondrial alternative oxidase pathway enhances photosynthetic electron transport under drought

conditions. *Journal of Experimental Botany* **56**: 1269–1276.

Beckman KB, Ames BN. **1997**. Oxidative decay of DNA. *Journal of Biological Chemistry* **272**: 19633–19636.

Bedoshvili YD, Popkova TP, Likhoshway Y V. 2009. Chloroplast structure of diatoms of different classes. *Cell and Tissue Biology* **3**: 297–310.

Bedard K, Krause KH. **2007**. The NOX family of ROS-generating NADPH oxidases: Physiology and pathophysiology. *Physiological Reviews* **87**: 245–313.

Bedard K, Lardy B, Krause K-H. **2007**. NOX family NADPH oxidases: Not just in mammals. *Biochimie* **89**: 1107–1112.

Belousov V V, Fradkov AF, Lukyanov KA, Staroverov DB, Shakhbazov KS, Terskikh A V, Lukyanov S. **2006**. Genetically encoded fluorescent indicator for intracellular hydrogen peroxide. *Nature Methods* **3**: 281–286.

Berlett BS, Stadtman ER. **1997**. Protein oxidation in aging, disease, and oxidative stress. *Journal of Biological Chemistry* **272**: 20313–20316.

Bertucci A, Tambutté É, Tambutté S, Allemand D, Zoccola D. **2010**. Symbiosis-dependent gene expression in coral-dinoflagellate association: Cloning and characterization of a P-type H^+-ATPase gene. *Proceedings of the Royal Society B: Biological Sciences* **277**: 87–95.

Bhattacharya D, Yoon HS, Hackett JD. **2004**. Photosynthetic eukaryotes unite: Endosymbiosis connects the dots. *BioEssays* **26**: 50–60.

Bhattacharyya P, Volcani BE. **1980**. Sodium-dependent silicate transport in the apochlorotic marine diatom Nitzschia alba. *Proceedings of the National Academy of Sciences* **77**: 6386–6390.

Białasek M, Górecka M, Mittler R, Karpiński S. **2017**. Evidence for the involvement of electrical, calcium and ROS signaling in the systemic regulation of non-photochemical quenching and photosynthesis. *Plant and Cell Physiology* **58**: 207–215.

Bidle KD, Bender SJ. **2008**. Iron starvation and culture age activate metacaspases and programmed cell death in the marine diatom *Thalassiosira pseudonana*. *Eukaryotic Cell* **7**: 223–236.

Bienert GP, Chaumont F. **2014**. Aquaporin-facilitated transmembrane diffusion of hydrogen peroxide. *Biochimica et Biophysica Acta (BBA) - General Subjects* **1840**: 1596–1604.

Bilcke G, Berge K Van den, Decker S De, Bonneure E, Poulsen N, Bulankova P, Osuna-Cruz CM, Dickenson J, Sabbe K, Pohnert G, *et al.* 2020. Mating type specific transcriptomic response to sex inducing pheromone in the pennate diatom *Seminavis robusta*. *bioRxiv*: 2020.03.16.987719.

Bolwell GP, Butt VS, Davies DR, Zimmerlin A. **1995**. The origin of the oxidative burst in plants. *Free Radical Research* **23**: 517–532.

Bombelli P, Bradley RW, Scott AM, Philips AJ, McCormick AJ, Cruz SM, Anderson A, Yunus K, Bendall DS, Cameron PJ, *et al.* 2011. Quantitative analysis of the factors limiting solar power transduction by *Synechocystis* sp. PCC 6803 in biological photovoltaic devices. *Energy & Environmental Science* **4**: 4690–4698.

Bouarab K, Potin P, Correa J, Kloareg B. **1999**. Sulfated oligosaccharides mediate the interaction between a marine red alga and its green algal pathogenic endophyte. *Plant Cell* **11**: 1635–1650.

Bouchard JN, Purdie DA. **2011**. Effect of elevated temperature, darkness and hydrogen peroxide treatment on oxidative stress and cell death in the bloom-forming cyanobacterium *Microcystis aeruginosa*. *Journal of Phycology* **47**: 1316–1325.

Bowler C, Allen AE, Badger JH, Grimwood J, Jabbari K, Kuo A, Maheswari U, Martens C, Maumus F, Otillar RP, *et al.* 2008. The *Phaeodactylum* genome reveals the evolutionary history of diatom genomes. *Nature* **456**: 239–244.

Boyd PW, Watson AJ, Law CS, Abraham ER, Trull T, Murdoch R, Bakker DCE, Bowie AR, Buesseler KO, Chang H, *et al.* 2000. A mesoscale phytoplankton bloom in the polar Southern Ocean stimulated by iron fertilization. *Nature* **407**: 695–702.

Broddrick JT, Du N, Smith SR, Tsuji Y, Jallet D, Ware MA, Peers G, Matsuda Y, Dupont CL, Mitchell BG, *et al.* 2019. Cross-compartment metabolic coupling enables flexible photoprotective mechanisms in the diatom *Phaeodactylum tricornutum*. *New Phytologist* **222**: 1364–1379.

Büch K, Stransky H, Hager A. **1995**. FAD is a further essential cofactor of the NAD(P)H and O2-dependent zeaxanthin-epoxidase. *FEBS Letters* **376**: 45–48.

Burki F. **2014**. The eukaryotic tree of life from a global phylogenomic perspective. *Cold Spring Harbor Perspectives in Biology* **6**.

Cachat J, Deffert C, Hugues S, Krause K-H. **2015**. Phagocyte NADPH oxidase and specific immunity. *Clinical Science* **128**: 635–648.

Cardol P, Forti G, Finazzi G. **2011**. Regulation of electron transport in microalgae. *Biochimica et Biophysica Acta - Bioenergetics* **1807**: 912–918.

Casotti R, Mazza S, Brunet C, Vantrepotte V, Ianora A, Miralto A. **2005**. Growth inhibition and toxicity of the diatom aldehyde 2-trans, 4-trans-decadienal on *Thalassiosira weissflogii* (Bacillariophyceae). *Journal of Phycology* **41**: 7–20.

Catalano A, Rodilossi S, Caprari P, Coppola V, Procopio A. **2005**. 5-Lipoxygenase regulates senescence-like growth arrest by promoting ROS-dependent p53 activation. *Embo Journal* **24**: 170–179.

Cavalier-Smith T. **2002**. Chloroplast evolution: Secondary symbiogenesis and multiple losses. *Current Biology* **12**: R62–R64.

Chan CX, Zäuner S, Wheeler G, Grossman AR, Prochnik SE, Blouin NA, Zhuang Y, Benning C, Berg GM, Yarish C, *et al.* 2012. Analysis of *Porphyra* membrane transporters demonstrates gene transfer among photosynthetic eukaryotes and numerous sodium-coupled transport systems. *Plant Physiology* **158**: 2001–2012.

Cheng S, Melkonian M, Smith SA, Brockington S, Archibald JM, Delaux P-M, Li F-W, Melkonian B, Mavrodiev E V, Sun W, *et al.* 2018. 10KP: A phylodiverse genome sequencing plan. *GigaScience* **7**: 9.

Chepurnov VA, Mann DG, Sabbe K, Vyverman W. **2004**. Experimental studies an sexual reproduction in diatoms. In: Jeon KW, ed. International Review of Cytology - a Survey of Cell

Biology. 91–143.

Choi WG, Miller G, Wallace I, Harper J, Mittler R, Gilroy S. **2017**. Orchestrating rapid long-distance signaling in plants with Ca^{2+}, ROS and electrical signals. *Plant Journal* **90**: 698–707.

Chrachri A, Hopkinson BM, Flynn K, Brownlee C, Wheeler GL. **2018**. Dynamic changes in carbonate chemistry in the microenvironment around single marine phytoplankton cells. *Nature Communications* **9**.

Cock JM, Sterck L, Rouze P, Scornet D, Allen AE, Amoutzias G, Anthouard V, Artiguenave F, Aury JM, Badger JH, *et al.* 2010. The *Ectocarpus* genome and the independent evolution of multicellularity in brown algae. *Nature* **465**: 617–621.

Coelho SMB, Brownlee C, Bothwell JHF. **2008**. A tip-high, Ca^{2+}-interdependent, reactive oxygen species gradient is associated with polarized growth in Fucus serratus zygotes. *Planta* **227**: 1037–1046.

Coelho SM, Taylor AR, Ryan KP, Sousa-Pinto I, Brown MT, Brownlee C. **2002**. Spatiotemporal patterning of reactive oxygen production and Ca^{2+} wave propagation in fucus rhizoid cells. *Plant Cell* **14**: 2369–2381.

Collen J, Pedersen M. **1994**. A stress-induced oxidative burst in *Eucheuma platycladum* (Rhodophyta). *Physiologia Plantarum* **92**: 417–422.

Cvetkovska M, Dahal K, Alber NA, Jin C, Cheung M, Vanlerberghe GC. **2014**. Knockdown of mitochondrial alternative oxidase induces the 'stress state' of signaling molecule pools in *Nicotiana tabacum,* with implications for stomatal function. *New Phytologist* **203**: 449–461.

Cvetkovska M, Vanlerberghe GC. **2012**. Alternative oxidase modulates leaf mitochondrial concentrations of superoxide and nitric oxide. *New Phytologist* **195**: 32–39.

D'Autréaux B, Toledano MB. **2007**. ROS as signalling molecules: mechanisms that generate specificity in ROS homeostasis. *Nature Reviews Molecular Cell Biology* **8**: 813.

Darehshouri A, Affenzeller M, Lütz-Meindl U. **2008**. Cell death upon H_2O_2 induction in the unicellular green alga Micrasterias. *Plant Biology* **10**: 732–745.

Das K, Roychoudhury A. **2014**. Reactive oxygen species (ROS) and response of antioxidants as ROS-scavengers during environmental stress in plants. *Frontiers in Environmental Science* **2**.

Davey MS, Suggett DJ, Geider RJ, Taylor AR. **2003**. Phytoplankton plasma membrane redox activity: Effect of iron limitation and interaction with photosynthesis. *Journal of Phycology* **39**: 1132–1144.

Deschamps P, Moreira D. **2012**. Reevaluating the green contribution to diatom genomes. *Genome Biology and Evolution* **4**: 683–688.

Desikan R, Cheung MK, Bright J, Henson D, Hancock JT, Neill SJ. **2004**. ABA, hydrogen peroxide and nitric oxide signalling in stomatal guard cells. *Journal of Experimental Botany* **55**: 205–212.

Diaz JM, Hansel CM, Apprill A, Brighi C, Zhang T, Weber L, McNally S, Xun L. **2016**. Species-specific control of external superoxide levels by the coral holobiont during a natural bleaching event. *Nature Communications* **7**: 1–10.

Diaz JM, Hansel CM, Voelker BM, Mendes CM, Andeer PF, Zhang T. **2013**. Widespread

production of extracellular superoxide by heterotrophic bacteria. *Science* **340**: 1223–1226.

Diaz JM, Plummer S. **2018**. Production of extracellular reactive oxygen species by phytoplankton: past and future directions. *Journal of Plankton Research* **40**: 655–666.

Diaz JM, Plummer S, Hansel CM, Andeer PF, Saito MA, McIlvin MR. **2019**. NADPH-dependent extracellular superoxide production is vital to photophysiology in the marine diatom *Thalassiosira oceanica*. *Proceedings of the National Academy of Sciences* **116**: 16448–16453.

Diaz JM, Plummer S, Tomas C, Alves-de-Souza C. **2018**. Production of extracellular superoxide and hydrogen peroxide by five marine species of harmful bloom-forming algae. *Journal of Plankton Research* **40**: 667–677.

Dickinson BC, Chang CJ. **2011**. Chemistry and biology of reactive oxygen species in signaling or stress responses. *Nature Chemical Biology* **7**: 504–511.

Dikalov SI, Harrison DG. **2012**. Methods for detection of mitochondrial and cellular reactive oxygen species. *Antioxidants & Redox Signaling* **20**: 372–382.

Doke N. **1983**. Generation of superoxide anion by potato tuber protoplasts during the hypersensitive response to hyphal wall components of *Phytophthora infestans* and specific inhibition of the reaction by suppressors of hypersensitivity. *Physiological Plant Pathology* **23**: 359–367.

Donkó Á, Péterfi Z, Sum A, Leto T, Geiszt M. **2005**. Dual oxidases. *Philos Trans R Soc Lond B Biol Sci* **360**: 2301–2308.

Dooley CT, Dore TM, Hanson GT, Jackson WC, Remington SJ, Tsien RY. **2004**. Imaging dynamic redox changes in mammalian cells with green fluorescent protein indicators. *Journal of Biological Chemistry* **279**: 22284–22293.

Dorrell RG, Gile G, McCallum G, Meheust R, Bapteste EP, Klinger CM, Brillet-Gueguen L, Freeman KD, Richter DJ, Bowler C. **2017**. Chimeric origins of ochrophytes and haptophytes revealed through an ancient plastid proteome. *Elife* **6**: e23717.

Dorrell RG, Smith AG. **2011**. Do Red and Green Make Brown?: Perspectives on Plastid Acquisitions within Chromalveolates. *Eukaryotic Cell* **10**: 856–868.

Drábková M, Admiraal W, Marsalek B. **2007a**. Combined exposure to hydrogen peroxide and light - Selective effects on cyanobacteria, green algae, and diatoms. *Environmental Science & Technology* **41**: 309–314.

Drábková M, Matthijs HCP, Admiraal W, Maršálek B. **2007b**. Selective effects of H_2O_2 on cyanobacterial photosynthesis. *Photosynthetica* **45**: 363–369.

Dring MJ. **2005**. Stress resistance and disease resistance in seaweeds: The role of reactive oxygen metabolism. In: Advances in Botanical Research. Academic Press, 175–207.

Dummermuth AL, Karsten U, Fisch KM, König GM, Wiencke C. **2003**. Responses of marine macroalgae to hydrogen-peroxide stress. *Journal of Experimental Marine Biology and Ecology* **289**: 103–121.

Eckhardt U, Buckhout TJ. **1998**. Iron assimilation in *Chlamydomonas reinhardtii* involves ferric reduction and is similar to Strategy I higher plants. *Journal of Experimental Botany* **49**: 1219–1226.

Edens WA, Sharling L, Cheng G, Shapira R, Kinkade JM, Lee T, Edens HA, Tang X, Sullards C, Flaherty DB, *et al.* 2001. Tyrosine cross-linking of extracellular matrix is catalyzed by Duox, a multidomain oxidase/peroxidase with homology to the phagocyte oxidase subunit gp91phox. *The Journal of Cell Biology* **154**: 879–892.

Edreva A. **2005**. Generation and scavenging of reactive oxygen species in chloroplasts: A submolecular approach. *Agriculture, Ecosystems and Environment* **106**: 119–133.

Egan MJ, Wang ZY, Jones MA, Smirnoff N, Talbot NJ. **2007**. Generation of reactive oxygen species by fungal NADPH oxidases is required for rice blast disease. *Proceedings of the National Academy of Sciences of the United States of America* **104**: 11772–11777.

Egge JK, Aksnes DL. **1992**. Silicate as regulating nutrient in phytoplankton competition. *Marine Ecology Progress Series* **83**: 281–289.

Evans MJ, Choi WG, Gilroy S, Morris RJ. **2016**. A ROS-assisted calcium wave dependent on the AtRBOHD NADPH oxidase and TPC1 cation channel propagates the systemic response to salt stress. *Plant Physiology* **171**: 1771–1784.

Evans C, Malin G, Mills GP, Wilson WH. **2006**. Viral infection of *Emiliania huxleyi* (Prymnesiophyceae) leads to elevated production of reactive oxygen species. *Journal of Phycology* **42**: 1040–1047.

Exposito-Rodriguez M, Laissue PP, Yvon-Durocher G, Smirnoff N, Mullineaux PM. **2017**. Photosynthesis-dependent H_2O_2 transfer from chloroplasts to nuclei provides a high-light signalling mechanism. *Nature Communications* **8**.

Faktorová D, Nisbet RER, Fernández Robledo JA, Casacuberta E, Sudek L, Allen AE, Ares M, Aresté C, Balestreri C, Barbrook AC, *et al.* 2020. Genetic tool development in marine protists: emerging model organisms for experimental cell biology. *Nature Methods* **17**: 481–494.

Falciatore A, d'Alcala MR, Croot P, Bowler C. **2000**. Perception of environmental signal by a marine diatom. *Science* **288**: 2363–2366.

Falciatore A, Jaubert M, Bouly J-P, Bailleul B, Mock T. **2019**. Diatom molecular research comes of age: model species for studying phytoplankton biology and diversity. *The Plant Cell*: tpc.00158.2019.

Fan X, Qiu H, Han W, Wang Y, Xu D, Zhang X, Bhattacharya D, Ye N. **2020**. Phytoplankton pangenome reveals extensive prokaryotic horizontal gene transfer of diverse functions. *Science Advances* **6**: eaba0111.

Farrugia G, Balzan R. **2012**. Oxidative stress and programmed cell death in yeast. *Frontiers in Oncology* **2**: 1–21.

Field CB, Behrenfeld MJ, Randerson JT, Falkowski P. **1998**. Primary production of the biosphere: Integrating terrestrial and oceanic components. *Science* **281**: 237–240.

Fleury C, Mignotte B, Vayssiere JL. **2002**. Mitochondrial reactive oxygen species in cell death signaling. *Biochimie* **84**: 131–141.

Flores MV, Crawford KC, Pullin LM, Hall CJ, Crosier KE, Crosier PS. **2010**. Dual oxidase in the intestinal epithelium of zebrafish larvae has anti-bacterial properties. *Biochemical and Biophysical Research Communications* **400**: 164–168.

Flori S, Jouneau P-H, Bailleul B, Gallet B, Estrozi LF, Moriscot C, Bastien O, Eicke S, Schober A, Bártulos CR, *et al.* 2017. Plastid thylakoid architecture optimizes photosynthesis in diatoms. *Nature Communications* **8**: 15885.

Foreman J, Demidchik V, Bothwell JHF, Mylona P, Miedema H, Torres MA, Linstead P, Costa S, Brownlee C, Jones JDG, *et al.* 2003. Reactive oxygen species produced by NADPH oxidase regulate plant cell growth. *Nature* **422**: 442–446.

Forti G, Furia A, Bombelli P, Finazzi G. **2003**. In vivo changes of the oxidation-reduction state of NADP and of the ATP/ADP cellular ratio linked to the photosynthetic activity in *Chlamydomonas reinhardtii*. *Plant Physiology* **132**: 1464–1474.

Fujita M, Harada E, Matsumoto T, Mizuta Y, Ikegame S, Ouchi H, Inoshima I, Yoshida S, Watanabe K, Nakanishi Y. **2010**. Impaired host defence against *Mycobacterium avium* in mice with chronic granulomatous disease. *Clinical & Experimental Immunology* **160**: 457–460.

Gallina AA, Brunet C, Palumbo A, Casotti R. **2014**. The effect of polyunsaturated aldehydes on *Skeletonema marinoi* (Bacillariophyceae): The involvement of reactive oxygen species and nitric oxide. *Marine Drugs* **12**: 4165–4187.

Gallina AA, Chung CC, Cassotti R. **2015**. Expression of death-related genes and reactive oxygen species production in *Skeletonema tropicum* upon exposure to the polyunsaturated aldehyde octadienal. *Advances in Oceanography and Limnology* **6**: 13–20.

Gallina AA, Palumbo A, Casotti R. **2016**. Oxidative pathways in response to polyunsaturated aldehydes in the marine diatom *Skeletonema marinoi* (Bacillariophyceae). *Journal of Phycology* **52**: 590–598.

Gandara ACP, Torres A, Bahia AC, Oliveira PL, Schama R. **2017**. Evolutionary origin and function of NOX4-art, an arthropod specific NADPH oxidase. *Bmc Evolutionary Biology* **17**: 92.

Ganini D, Hollnagel HC, Colepicolo P, Barros MP. **2013**. Hydrogen peroxide and nitric oxide trigger redox-related cyst formation in cultures of the dinoflagellate *Lingulodinium polyedrum*. *Harmful Algae* **27**: 121–129.

Garg S, Rose AL, Godrant A, Waite TD. **2007a**. Iron uptake by the ichthyotoxic *Chattonella marina* (Raphidophyceae): impact of superoxide generation. *Journal of Phycology* **43**: 978–991.

Garg S, Rose AL, Waite TD. **2007b**. Production of reactive oxygen species on photolysis of dilute aqueous quinone solutions. *Photochemistry and Photobiology* **83**: 904–913.

Gechev T, Gadjev I, Van Breusegem F, Inzé D, Dukiandjiev S, Toneva V, Minkov I. **2002**. Hydrogen peroxide protects tobacco from oxidative stress by inducing a set of antioxidant enzymes. *Cellular and Molecular Life Sciences* **59**: 708–714.

Giesbert S, Schürg T, Scheele S, Tudzynski P. **2008**. The NADPH oxidase Cpnox1 is required for full pathogenicity of the ergot fungus *Claviceps purpurea*. *Molecular Plant Pathology* **9**: 317–327.

Goss R, Lepetit B. **2015**. Biodiversity of NPQ. *Journal of Plant Physiology* **172**: 13–32.

Graff van Creveld S, Rosenwasser S, Levin Y, Vardi A. **2016**. Chronic iron limitation confers transient resistance to oxidative stress in marine diatoms. *Plant Physiology* **172**: 968–979.

Graff van Creveld S, Rosenwasser S, Schatz D, Koren I, Vardi A. **2015**. Early perturbation in mitochondria redox homeostasis in response to environmental stress predicts cell fate in diatoms.

Isme Journal **9**: 385–395.

Grissa I, Bidard F, Grognet P, Grossetete S, Silar P. **2010**. The Nox/Ferric reductase/Ferric reductase-like families of Eumycetes. *Fungal Biology* **114**: 766–777.

Grouneva I, Gollan PJ, Kangasjärvi S, Suorsa M, Tikkanen M, Aro EM. **2013**. Phylogenetic viewpoints on regulation of light harvesting and electron transport in eukaryotic photosynthetic organisms. *Planta* **237**: 399–412.

Gruber A, Vugrinec S, Hempel F, Gould SB, Maier U-G, Kroth PG. **2007**. Protein targeting into complex diatom plastids: functional characterisation of a specific targeting motif. *Plant Molecular Biology* **64**: 519–530.

Gruber A, Weber T, Bártulos CR, Vugrinec S, Kroth PG. **2009**. Intracellular distribution of the reductive and oxidative pentose phosphate pathways in two diatoms. *Journal of Basic Microbiology* **49**: 58–72.

Guillard RRL, Ryther JH. **1962**. Studies of marine planktonic diatoms. I. *Cyclotella nana* Hustedt and *Detonula confervacea* (Cleve) Gran. *Canadian Journal of Microbiology* **8**: 229–239.

Guiry MD. **2012**. How many species of algae are there? *Journal of Phycology* **48**: 1057–1063.

Gutscher M, Pauleau A-L, Marty L, Brach T, Wabnitz GH, Samstag Y, Meyer AJ, Dick TP. **2008**. Real-time imaging of the intracellular glutathione redox potential. *Nature Methods* **5**: 553–559.

Gutscher M, Sobotta MC, Wabnitz GH, Ballikaya S, Meyer AJ, Samstag Y, Dick TP. **2009**. Proximity-based protein thiol oxidation by H_2O_2-scavenging peroxidases. *Journal of Biological Chemistry* **284**: 31532–31540.

Guzik TJ, Chen W, Gongora MC, Guzik B, Lob HE, Mangalat D, Hoch N, Dikalov S, Rudzinski P, Kapelak B, *et al.* 2008. Calcium-dependent NOX5 nicotinamide adenine dinucleotide phosphate oxidase contributes to vascular oxidative stress in human coronary artery disease. *Journal of the American College of Cardiology* **52**: 1803–1809.

Ha EM, Oh CT, Bae YS, Lee WJ. **2005**. A direct role for dual oxidase in Drosophila gut immunity. *Science* **310**: 847–850.

Hajjar C, Cherrier M V, Mirandela GD, Petit-Hartlein I, Stasia MJ, Fontecilla-Camps JC, Fieschi F, Dupuy J. **2017**. The NOX family of proteins is also present in bacteria. *mBio* **8**: e01487-17.

Hamm CE, Merkel R, Springer O, Jurkojc P, Maiert C, Prechtelt K, Smetacek V. **2003**. Architecture and material properties of diatom shells provide effective mechanical protection. *Nature* **421**: 841–843.

Hansel CM, Buchwald C, Diaz JM, Ossolinski JE, Dyhrman ST, Van Mooy BAS, Polyviou D. **2016**. Dynamics of extracellular superoxide production by *Trichodesmium* colonies from the Sargasso Sea. *Limnology and Oceanography* **61**: 1188–1200.

Harman D. **1956**. Aging: A theory based on free radical and radiation chemistry. *Journal of Gerontology* **11**: 298–300.

Hawkins BJ, Madesh M, Kirkpatrick CJ, Fisher AB. **2007**. Superoxide flux in endothelial cells via the chloride channel-3 mediates intracellular signaling. *Molecular Biology of the Cell* **18**: 2002–2012.

Hefti MH, Vervoort J, van Berkel WJH. **2003**. Deflavination and reconstitution of flavoproteins. *European Journal of Biochemistry* **270**: 4227–4242.

Hekimi S, Lapointe J, Wen Y. **2011**. Taking a 'good' look at free radicals in the aging process. *Trends in Cell Biology* **21**: 569–576.

Helliwell KE, Chrachri A, Koester JA, Wharam S, Verret F, Taylor AR, Wheeler GL, Brownlee C. **2019**. Alternative mechanisms for fast Na^+/Ca^{2+} signaling in eukaryotes via a novel class of single-domain voltage-gated channels. *Current Biology* **29**: 1503-1511.e6.

Hernando M, Schloss IR, Malanga G, Almandoz GO, Ferreyra GA, Aguiar MB, Puntarulo S. **2015**. Effects of salinity changes on coastal Antarctic phytoplankton physiology and assemblage composition. *Journal of Experimental Marine Biology and Ecology* **466**: 110–119.

Herrera-Vásquez A, Salinas P, Holuigue L. **2015**. Salicylic acid and reactive oxygen species interplay in the transcriptional control of defense genes expression. *Frontiers in Plant Science* **6**.

Herve C, Tonon T, Collen J, Corre E, Boyen C. **2006**. NADPH oxidases in Eukaryotes: red algae provide new hints! *Current Genetics* **49**: 190–204.

Hideg É, Kós PB, Schreiber U. **2008**. Imaging of NPQ and ROS formation in tobacco leaves: heat inactivation of the water–water cycle prevents down-regulation of PSII. *Plant and Cell Physiology* **49**: 1879–1886.

Hildebrand M, Lerch SJL, Shrestha RP. **2018**. Understanding diatom cell wall silicification—Moving forward. *Frontiers in Marine Science* **5**: 125.

Van Der Hoeven R, Cruz MR, Chávez V, Garsin DA. **2015**. Localization of the dual oxidase BLI-3 and characterization of its NADPH oxidase domain during infection of *Caenorhabditis elegans*. *PLoS ONE* **10**.

Hopes A, Nekrasov V, Belshaw N, Grouneva I, Kamoun S, Mock T. **2017**. Genome Editing in Diatoms Using CRISPR-Cas to Induce Precise Bi-allelic Deletions. *BIO-PROTOCOL* **7**.

Hopkinson BM, Dupont CL, Allen AE, Morela FMM. **2011**. Efficiency of the CO_2-concentrating mechanism of diatoms. *Proceedings of the National Academy of Sciences of the United States of America* **108**: 3830–3837.

Hossain MA, Bhattacharjee S, Armin SM, Qian PP, Xin W, Li HY, Burritt DJ, Fujita M, Tran LSP. **2015**. Hydrogen peroxide priming modulates abiotic oxidative stress tolerance: insights from ROS detoxification and scavenging. *Frontiers in Plant Science* **6**.

Houée-Levin C, Bobrowski K. **2013**. The use of the methods of radiolysis to explore the mechanisms of free radical modifications in proteins. *Journal of Proteomics* **92**: 51–62.

Hu WH, Yan XH, Yu JQ. **2017**. Importance of the mitochondrial alternative oxidase (AOX) pathway in alleviating photoinhibition in cucumber leaves under chilling injury and subsequent recovery when leaves are subjected to high light intensity. *Journal of Horticultural Science and Biotechnology* **92**: 31–38.

Hunken M, Harder J, Kirst GO. **2008**. Epiphytic bacteria on the Antarctic ice diatom *Amphiprora kufferathii* Manguin cleave hydrogen peroxide produced during algal photosynthesis. *Plant Biology* **10**: 519–526.

Hurd TR, DeGennaro M, Lehmann R. **2012**. Redox regulation of cell migration and adhesion.

Trends in Cell Biology **22**: 107–115.

Ianora A, Miralto A, Poulet SA, Carotenuto Y, Buttino I, Romano G, Casotti R, Pohnert G, Wichard T, Colucci-D'Amato L, *et al.* 2004. Aldehyde suppression of copepod recruitment in blooms of a ubiquitous planktonic diatom. *Nature* **429**: 403–407.

Inupakutika MA, Sengupta S, Devireddy AR, Azad RK, Mittler R. **2016**. The evolution of reactive oxygen species metabolism. *Journal of Experimental Botany* **67**: 5933–5943.

Jain A, Wilson G, Connolly E. **2014**. The diverse roles of FRO family metalloreductases in iron and copper homeostasis. *Frontiers in Plant Science* **5**.

Jones GJ, Morel FMM. **1988**. Plasmalemma redox activity in the diatom *Thalassiosira*. *Plant Physiology* **87**: 143.

Juillan-Binard C, Picciocchi A, Andrieu J-P, Dupuy J, Petit-Hartlein I, Caux-Thang C, Vivès C, Nivière V, Fieschi F. **2016**. A two-component NOX-like system in bacteria is involved in the electron transfer chain to the methionine sulfoxide reductase MsrP. *Journal of Biological Chemistry* **292**: 2485–2494.

Kaiser W. **1976**. The effect of hydrogen peroxide on CO_2 fixation of isolated intact chloroplasts. *Biochimica et Biophysica Acta (BBA) - Bioenergetics* **440**: 476–482.

Kaiser WM. **1979**. Reversible inhibition of the calvin cycle and activation of oxidative pentose phosphate cycle in isolated intact chloroplasts by hydrogen peroxide. *Planta* **145**: 377–382.

Kalyanaraman B, Darley-Usmar V, Davies KJA, Dennery PA, Forman HJ, Grisham MB, Mann GE, Moore K, Roberts LJ, Ischiropoulos H. **2012**. Measuring reactive oxygen and nitrogen species with fluorescent probes: challenges and limitations. *Free Radical Biology and Medicine* **52**: 1–6.

Kaneko M, Kodama M, Inoue F. **1994**. Bimodal pattern of killing of chinese hamster V79 variant cells by hydrogen peroxide. *Free Radical Research* **20**: 229–239.

Karas BJ, Diner RE, Lefebvre SC, McQuaid J, Phillips APR, Noddings CM, Brunson JK, Valas RE, Deerinck TJ, Jablanovic J, *et al.* 2015. Designer diatom episomes delivered by bacterial conjugation. *Nature Communications* **6**.

Kaur G, Guruprasad K, Temple BRS, Shirvanyants DG, Dokholyan N V, Pati PK. **2018**. Structural complexity and functional diversity of plant NADPH oxidases. *Amino Acids* **50**: 79–94.

Kawahara T, Quinn MT, Lambeth JD. **2007**. Molecular evolution of the reactive oxygen-generating NADPH oxidase (Nox/Duox) family of enzymes. *Bmc Evolutionary Biology* **7**.

Kaya H, Nakajima R, Iwano M, Kanaoka MM, Kimura S, Takeda S, Kawarazaki T, Senzaki E, Hamamura Y, Higashiyama T, *et al.* 2014. Ca^{2+}-activated reactive oxygen species production by *Arabidopsis* RbohH and RbohJ is essential for proper pollen tube tip growth. *Plant Cell* **26**: 1069–1080.

Keeling PJ, Burki F, Wilcox HM, Allam B, Allen EE, Amaral-Zettler LA, Armbrust EV, Archibald JM, Bharti AK, Bell CJ, *et al.* 2014. The marine microbial eukaryote transcriptome sequencing project (MMETSP): Illuminating the functional diversity of eukaryotic life in the oceans through transcriptome sequencing. *Plos Biology* **12**: e1001889.

Kennedy F, Martin A, Bowman JP, Wilson R, McMinn A. **2019**. Dark metabolism: a molecular insight into how the Antarctic sea-ice diatom Fragilariopsis cylindrus survives long-term darkness.

New Phytologist **223**: 675–691.

Kim CS, Lee SG, Lee CK, Kim HG, Jung J. **1999**. Reactive oxygen species as causative agents in the ichthyotoxicity of the red tide dinoflagellate *Cochlodinium polykrikoides*. *Journal of Plankton Research* **21**: 2105–2115.

Kim D, Nakamura A, Okamoto T, Komatsu N, Oda T, Iida T, Ishimatsu A, Muramatsu T. **2000**. Mechanism of superoxide anion generation in the toxic red tide phytoplankton *Chattonella marina*: possible involvement of NAD(P)H oxidase. *Biochimica Et Biophysica Acta-General Subjects* **1524**: 220–227.

Kim D, Nakashima T, Matsuyama Y, Niwano Y, Yamaguchi K, Oda T. **2007**. Presence of the distinct systems responsible for superoxide anion and hydrogen peroxide generation in red tide phytoplankton *Chattonella marina* and *Chattonella ovata*. *Journal of Plankton Research* **29**: 241–247.

Kimura S, Kaya H, Kawarazaki T, Hiraoka G, Senzaki E, Michikawa M, Kuchitsu K. **2012**. Protein phosphorylation is a prerequisite for the Ca^{2+}-dependent activation of *Arabidopsis* NADPH oxidases and may function as a trigger for the positive feedback regulation of Ca^{2+} and reactive oxygen species. *Biochimica Et Biophysica Acta-Molecular Cell Research* **1823**: 398–405.

Knutson MD. **2008**. STEAP proteins: Implications for iron and copper metabolism. *Nutrition Reviews* **65**: 335–340.

Kramer DM, Evans JR. **2011**. The importance of energy balance in improving photosynthetic productivity. *Plant Physiology* **155**: 70–78.

Krause JW, Schulz IK, Rowe KA, Dobbins W, Winding MHS, Sejr MK, Duarte CM, Agustí S. **2019**. Silicic acid limitation drives bloom termination and potential carbon sequestration in an Arctic bloom. *Scientific Reports* **9**: 1–11.

Kroth PG. **2007**. Genetic transformation; a tool to study protein targeting in diatoms. In: van der Giezen M, ed. Methods in molecular biology. Totowa, NJ: Humana Press Inc, 257–267.

Kroth PG, Chiovitti A, Gruber A, Martin-Jezeque V, Mock T, Parker MS, Stanley MS, Kaplan A, Caron L, Weber T, *et al.* 2008. A model for carbohydrate metabolism in the diatom *Phaeodactylum tricornutum* deduced from comparative whole genome analysis. *PLoS ONE* **3**.

Kuczynska P, Jemiola-Rzeminska M, Strzalka K. **2015**. Photosynthetic pigments in diatoms. *Marine Drugs* **13**: 5847–5881.

Kumar S, Stecher G, Tamura K. **2016**. MEGA7: Molecular evolutionary genetics analysis version 7.0 for bigger datasets. *Molecular Biology and Evolution* **33**: 1870–1874.

Kumari J, Rathore MS. 2020. Na^+/K^+-ATPase a Primary Membrane Transporter: An Overview and Recent Advances with Special Reference to Algae. *Journal of Membrane Biology* 253: 191–204.

Kupper FC, Gaquerel E, Boneberg EM, Morath S, Salaun JP, Potin P. **2006**. Early events in the perception of lipopolysaccharides in the brown alga *Laminaria digitata* include an oxidative burst and activation of fatty acid oxidation cascades. *Journal of Experimental Botany* **57**: 1991–1999.

Kupper FC, Kloareg B, Guern J, Potin P. **2001**. Oligoguluronates elicit an oxidative burst in the brown algal kelp *Laminaria digitata*. *Plant Physiology* **125**: 278–291.

Kupper FC, Muller DG, Peters AF, Kloareg B, Potin P. **2002**. Oligoalginate recognition and

oxidative burst play a key role in natural and induced resistance of sporophytes of laminariales. *Journal of Chemical Ecology* **28**: 2057–2081.

Kurusu T, Kuchitsu K, Tada Y. **2015**. Plant signaling networks involving Ca^{2+} and Rboh/Nox-mediated ROS production under salinity stress. *Frontiers in Plant Science* **6**: 427.

Kustka AB, Shaked Y, Milligan AJ, King DW, Morel FMM. **2005**. Extracellular production of superoxide by marine diatoms: Contrasting effects on iron redox chemistry and bioavailability. *Limnology and Oceanography* **50**: 1172–1180.

Kwak JM, Mori IC, Pei ZM, Leonhardt N, Torres MA, Dangl JL, Bloom RE, Bodde S, Jones JDG, Schroeder JI. **2003**. NADPH oxidase AtrbohD and AtrbohF genes function in ROS-dependent ABA signaling in *Arabidopsis*. *Embo Journal* **22**: 2623–2633.

Lacaze I, Lalucque H, Siegmund U, Silar P, Brun S. **2015**. Identification of NoxD/Pro41 as the homologue of the p22phox NADPH oxidase subunit in fungi. *Molecular Microbiology* **95**: 1006–1024.

Van Laer K, Dick TP. **2016**. Utilizing natural and engineered peroxiredoxins as intracellular peroxide reporters. *Molecules and Cells* **39**: 46–52.

Lalucque H, Silar P. **2003**. NADPH oxidase: an enzyme for multicellularity? *Trends in Microbiology* **11**: 9–12.

Laohavisit A, Anderson A, Bombelli P, Jacobs M, Howe CJ, Davies JM, Smith AG. **2015**. Enhancing plasma membrane NADPH oxidase activity increases current output by diatoms in biophotovoltaic devices. *Algal Research-Biomass Biofuels and Bioproducts* **12**: 91–98.

Lara-Ortiz T, Riveros-Rosas H, Aguirre J. **2003**. Reactive oxygen species generated by microbial NADPH oxidase NoxA regulate sexual development in *Aspergillus nidulans*. *Molecular Microbiology* **50**: 1241–1255.

Lardy B, Bof M, Aubry L, Paclet MH, Morel F, Satre M, Klein G. **2005**. NADPH oxidase homologs are required for normal cell differentiation and morphogenesis in *Dictyostelium discoideum*. *Biochimica et Biophysica Acta (BBA) - Molecular Cell Research* **1744**: 199–212.

Lavaud J, Strzepek RF, Kroth PG. **2007**. Photoprotection capacity differs among diatoms: Possible consequences on the spatial distribution of diatoms related to fluctuations in the underwater light climate. *Limnology and Oceanography* **52**: 1188–1194.

Leblanc K, Arístegui J, Armand L, Assmy P, Beker B, Bode A, Breton E, Cornet V, Gibson J, Gosselin MP, *et al.* 2012. A global diatom database- A bundance, biovolume and biomass in the world ocean. *Earth System Science Data* **4**: 149–165.

Ledford HK, Niyogi KK. **2005**. Singlet oxygen and photo-oxidative stress management in plants and algae. *Plant, Cell & Environment* **28**: 1037–1045.

Lepetit B, Sturm S, Rogato A, Gruber A, Sachse M, Falciatore A, Kroth PG, Lavaud J. **2013**. High light acclimation in the secondary plastids containing diatom *Phaeodactylum tricornutum* is triggered by the redox state of the plastoquinone pool. *Plant Physiology* **161**: 853–865.

Levine A, Tenhaken R, Dixon R, Lamb C. **1994**. H_2O_2 from the oxidative burst orchestrates the plant hypersensitive disease resistance response. *Cell* **79**: 583–593.

Lewin JC, Lewin RA, Philpott DE. **1958**. Observations on *Phaeodactylum tricornutum*.

Microbiology **18**: 418–426.

Li X, Liu T, Wang K, Waite TD. **2015**. Light-induced extracellular electron transport by the marine raphidophyte *Chattonella marina*. *Environmental Science & Technology* **49**: 1392–1399.

Liu W, Au DWT, Anderson DM, Lam PKS, Wu RSS. **2007**. Effects of nutrients, salinity, pH and light:dark cycle on the production of reactive oxygen species in the alga *Chattonella marina*. *Journal of Experimental Marine Biology and Ecology* **346**: 76–86.

Liu X, Williams CE, Nemacheck JA, Wang H, Subramanyam S, Zheng C, Chen M-S. **2010**. Reactive oxygen species are involved in plant defense against a gall midge. *Plant Physiology* **152**: 985–999.

Lomas MW, Glibert PM. **2000**. Comparisons of nitrate uptake, storage, and reduction in marine diatoms and flagellates. *Journal of Phycology* **36**: 903–913.

Lomas MW, Rumbley CJ, Glibert PM. **2000**. Ammonium release by nitrogen sufficient diatoms in response to rapid increases in irradiance. *Journal of Plankton Research* **22**: 2351–2366.

Lommer M, Specht M, Roy AS, Kraemer L, Andreson R, Gutowska MA, Wolf J, Bergner S V, Schilhabel MB, Klostermeier UC, *et al.* 2012. Genome and low-iron response of an oceanic diatom adapted to chronic iron limitation. *Genome Biology* **13**.

Long SP, Humphries S, Falkowski PG. **1994**. Photoinhibition of photosynthesis in nature. *Annual Review of Plant Physiology and Plant Molecular Biology* **45**: 633–662.

Lopez PJ, Desclés J, Allen AE, Bowler C. **2005**. Prospects in diatom research. *Current Opinion in Biotechnology* **16**: 180–186.

Lucker B, Kramer DM. **2013**. Regulation of cyclic electron flow in *Chlamydomonas reinhardtii* under fluctuating carbon availability. *Photosynthesis Research* **117**: 449–459.

Luo QJ, Zhu ZJ, Yang R, Qian FJ, Yan XJ, Chen HM. **2015**. Characterization of a respiratory burst oxidase homologue from *Pyropia haitanensis* with unique molecular phylogeny and rapid stress response. *Journal of Applied Phycology* **27**: 945–955.

Lynnes JA, Derzaph TLM, Weger HG. **1998**. Iron limitation results in induction of ferricyanide reductase and ferric chelate reductase activities in *Chlamydomonas reinhardtii*. *Planta* **204**: 360–365.

Lyon B, Mock T. **2014**. Polar microalgae: New approaches towards understanding adaptations to an extreme and changing environment. *Biology* **3**: 56–80.

Ma L, Calfee BC, Morris JJ, Johnson ZI, Zinser ER. **2018**. Degradation of hydrogen peroxide at the ocean's surface: The influence of the microbial community on the realized thermal niche of *Prochlorococcus*. *ISME Journal* **12**: 473–484.

Magnani F, Nenci S, Fananas EM, Ceccon M, Romero E, Fraaije MW, Mattevi A. **2017**. Crystal structures and atomic model of NADPH oxidase. *Proceedings of the National Academy of Sciences of the United States of America* **114**: 6764–6769.

Maksimov N, Evmenyeva A, Breygina M, Yermakov I. **2018**. The role of reactive oxygen species in pollen germination in *Picea pungens* (blue spruce). *Plant Reproduction* **31**: 357–365.

Malagnac F, Lalucque H, Lepere G, Silar P. **2004**. Two NADPH oxidase isoforms are required for

sexual reproduction and ascospore germination in the filamentous fungus *Podospora anserina*. *Fungal Genetics and Biology* **41**: 982–997.

Maldonado MT, Price NM. **2001**. Reduction and transport of organically bound iron by *Thalassiosira oceanica* (Bacillariophyceae). *Journal of Phycology* **37**: 298–310.

Malviya S, Scalco E, Audic S, Vincenta F, Veluchamy A, Poulain J, Wincker P, Iudicone D, de Vargas C, Bittner L, *et al.* 2016. Insights into global diatom distribution and diversity in the world's ocean. *Proceedings of the National Academy of Sciences of the United States of America* **113**: E1516–E1525.

Mann DG. **1999**. The species concept in diatoms. *Phycologia* **38**: 437–495.

Mann DG, Droop SJM. **1996**. Biodiversity, biogeography and conservation of diatoms. In: Hydrobiologia. Kluwer Academic Publishers, 19–32.

Mardones JI, Dorantes-Aranda JJ, Nichols PD, Hallegraeff GM. **2015**. Fish gill damage by the dinoflagellate *Alexandrium catenella* from Chilean fjords: Synergistic action of ROS and PUFA. *Harmful Algae* **49**: 40–49.

Marino D, Dunand C, Puppo A, Pauly N. **2012**. A burst of plant NADPH oxidases. *Trends in Plant Science* **17**: 9–15.

Marschall R, Tudzynski P. **2016**. BcIqg1, a fungal IQGAP homolog, interacts with NADPH oxidase, MAP kinase and calcium signaling proteins and regulates virulence and development in *B otrytis cinerea*. *Molecular Microbiology* **101**: 281–298.

Marshall JA, Hovenden M, Oda T, Hallegraeff GM. **2002**. Photosynthesis does influence superoxide production in the ichthyotoxic alga *Chattonella marina* (Raphidophyceae). *Journal of Plankton Research* **24**: 1231–1236.

Marshall JA, Ross T, Pyecroft S, Hallegraeff G. **2005a**. Superoxide production by marine microalgae - II. Towards understanding ecological consequences and possible functions. *Marine Biology* **147**: 541–549.

Marshall J-A, de Salas M, Oda T, Hallegraeff G. **2005b**. Superoxide production by marine microalgae. *Marine Biology* **147**: 533–540.

Maruta T, Inoue T, Tamoi M, Yabuta Y, Yoshimura K, Ishikawa T, Shigeoka S. **2011**. Arabidopsis NADPH oxidases, AtrbohD and AtrbohF, are essential for jasmonic acid-induced expression of genes regulated by MYC2 transcription factor. *Plant Science* **180**: 655–660.

Massey V, Hemmerich P. **1980**. Active-site probes of flavoproteins*. *Biochemical Society Transactions* **8**: 246–257.

Matthijs HCP, Visser PM, Reeze B, Meeuse J, Slot PC, Wijn G, Talens R, Huisman J. **2012**. Selective suppression of harmful cyanobacteria in an entire lake with hydrogen peroxide. *Water Research* **46**: 1460–1472.

Maxwell K, Johnson GN. **2000**. Chlorophyll fluorescence-a practical guide. *Journal of Experimental Botany* **51**: 659–668.

McCormick AJ, Bombelli P, Bradley RW, Thorne R, Wenzel T, Howe CJ. **2015**. Biophotovoltaics: oxygenic photosynthetic organisms in the world of bioelectrochemical systems. *Energy & Environmental Science* **8**: 1092–1109.

Medlin LK, Kaczmarska I. **2004**. Evolution of the diatoms: V. Morphological and cytological support for the major clades and a taxonomic revision. *Phycologia* **43**: 245–270.

Micinski E, Ball LA, Zafiriou OC. **1993**. Photochemical oxygen activation: Superoxide radical detection and production rates in the eastern Caribbean. *Journal of Geophysical Research: Oceans* **98**: 2299–2306.

Miller A-F. **2012**. Superoxide dismutases: Ancient enzymes and new insights. *FEBS Letters* **586**: 585–595.

Miller G, Schlauch K, Tam R, Cortes D, Torres MA, Shulaev V, Dangl JL, Mittler R. **2009**. The plant NADPH oxidase RBOHD mediates rapid systemic signaling in response to diverse stimuli. *Science Signaling* **2**.

Milne A, Davey MS, Worsfold PJ, Achterberg EP, Taylor AR. **2009**. Real-time detection of reactive oxygen species generation by marine phytoplankton using flow injection-chemiluminescence. *Limnology and Oceanography-Methods* **7**: 706–715.

Miralto A, Barone G, Romano G, Poulet SA, Ianora A, Russo GL, Buttino I, Mazzarella G, Laablr M, Cabrini M, *et al.* 1999. The insidious effect of diatoms on copepod reproduction. *Nature* **402**: 173–176.

Mitchell AL, Sangrador-Vegas A, Luciani A, Madeira F, Nuka G, Salazar GA, Chang H-Y, Richardson LJ, Qureshi MA, Fraser MI, *et al.* 2018. InterPro in 2019: improving coverage, classification and access to protein sequence annotations. *Nucleic Acids Research* **47**: D351–D360.

Mittler R. **2017**. ROS are good. *Trends in Plant Science* **22**: 11–19.

Mittler R, Vanderauwera S, Suzuki N, Miller G, Tognetti VB, Vandepoele K, Gollery M, Shulaev V, Van Breusegem F. **2011**. ROS signaling: the new wave? *Trends in Plant Science* **16**: 300–309.

Miura Y, Nakano Y, Yagi K, Miyamoto K. **1981**. Regeneration of NADPH by frozen-thawed cells of a blue-green alga, *Synechococcus* sp. *Agricultural and Biological Chemistry* **45**: 845–850.

Miyake C, Asada K. **1992**. Thylakoid-bound ascorbate peroxidase in spinach chloroplasts and photoreduction of its primary oxidation product monodehydroascorbate radicals in thylakoids. *Plant and Cell Physiology* **33**: 541–553.

Miyake C, Michihata F, Asada K. **1991**. Scavenging of hydrogen peroxide in prokaryotic and eukaryotic algae: Acquisition of ascorbate peroxidase during the evolution of cyanobacteria. *Plant and Cell Physiology* **32**: 33–43.

Mizrachi A, Graff van Creveld S, Shapiro OH, Rosenwasser S, Vardi A. **2019**. Light-dependent single-cell heterogeneity in the chloroplast redox state regulates cell fate in a marine diatom (DK Newman, Ed.). *Elife* **8**: e47732.

Mock T, Otillar RP, Strauss J, McMullan M, Paajanen P, Schmutz J, Salamov A, Sanges R, Toseland A, Ward BJ, *et al.* 2017. Evolutionary genomics of the cold-adapted diatom Fragilariopsis cylindrus. *Nature* **541**: 536–540.

Moeys S, Frenkel J, Lembke C, Gillard JTF, Devos V, Van den Berge K, Bouillon B, Huysman MJJ, De Decker S, Scharf J, *et al.* 2016. A sex-inducing pheromone triggers cell cycle arrest and mate attraction in the diatom Seminavis robusta. *Scientific Reports* **6**.

Monshausen GB, Bibikova TN, Messerli MA, Shi C, Gilroy S. **2007**. Oscillations in extracellular pH

and reactive oxygen species modulate tip growth of Arabidopsis root haris. *Proceedings of the National Academy of Sciences of the United States of America* **104**: 20996–21001.

Monshausen GB, Bibikova TN, Weisenseel MH, Gilroy S. **2009**. Ca^{2+} regulates reactive oxygen species production and pH during mechanosensing in Arabidopsis roots. *The Plant Cell* **21**: 2341.

Morelli E, Scarano G. **2004**. Copper-induced changes of non-protein thiols and antioxidant enzymes in the marine microalga Phaeodactylum tricornutum. *Plant Science* **167**: 289–296.

Morris JJ, Johnson ZI, Szul MJ, Keller M, Zinser ER. **2011**. Dependence of the cyanobacterium *Prochlorococcus* on hydrogen peroxide scavenging microbes for growth at the ocean's surface. *Plos One* **6**: e16805.

Morth JP, Pedersen BP, Buch-Pedersen MJ, Andersen JP, Vilsen B, Palmgren MG, Nissen P. **2011**. A structural overview of the plasma membrane Na^+,K^+-ATPase and H^+-ATPase ion pumps. *Nature Reviews Molecular Cell Biology* **12**: 60–70.

Mumbengegwi DR, Li Q, Li C, Bear CE, Engelhardt JF. **2008**. Evidence for a superoxide permeability pathway in endosomal membranes. *Molecular and Cellular Biology* **28**: 3700–3712.

Murata N, Takahashi S, Nishiyama Y, Allakhverdiev SI. **2007**. Photoinhibition of photosystem II under environmental stress. *Biochimica et Biophysica Acta - Bioenergetics* **1767**: 414–421.

Murik O, Elboher A, Kaplan A. **2014**. Dehydroascorbate: a possible surveillance molecule of oxidative stress and programmed cell death in the green alga *Chlamydomonas reinhardtii*. *New Phytologist* **202**: 471–484.

Murik O, Kaplan A. **2009**. Paradoxically, prior acquisition of antioxidant activity enhances oxidative stress-induced cell death. *Environmental Microbiology* **11**: 2301–2309.

Murik O, Tirichine L, Prihoda J, Thomas Y, Araújo WL, Allen AE, Fernie AR, Bowler C. **2019**. Downregulation of mitochondrial alternative oxidase affects chloroplast function, redox status and stress response in a marine diatom. *New Phytologist* **221**: 1303–1316.

Murphy MP. **2009**. How mitochondria produce reactive oxygen species. *Biochemical Journal* **417**: 1–13.

Musset B, Clark RA, DeCoursey TE, Petheo GL, Geiszt M, Chen Y, Cornell JE, Eddy CA, Brzyski RG, El Jamali A. **2012**. NOX5 in human spermatozoa: Expression, function and regulation. *Journal of Biological Chemistry* **287**: 9376–9388.

Mydlarz LD, Jacobs RS. **2004**. Comparison of an inducible oxidative burst in free-living and symbiotic dinoflagellates reveals properties of the pseudopterosins. *Phytochemistry* **65**: 3231–3241.

Mydlarz LD, Jacobs RS. **2006**. An inducible release of reactive oxygen radicals in four species of gorgonian corals. *Marine and Freshwater Behaviour and Physiology* **39**: 143–152.

Nakamura A, Okamoto T, Komatsu N, Ooka S, Oda T, Ishimatsu A, Muramatsu T. **1998**. Fish mucus stimulates the generation of superoxide anion by *Chattonella marina* and *Heterosigma akashiwo*. *Fisheries Science* **64**: 866–869.

Nakamura J, Purvis ER, Swenberg JA. **2003**. Micromolar concentrations of hydrogen peroxide induce oxidative DNA lesions more efficiently than millimolar concentrations in mammalian cells.

Nucleic Acids Research **31**: 1790–1795.

Nelson DM, Treguer P, Brzezinski MA, Leynaert A, Queguiner B. **1995**. Production and dissolution of biogenic silica in the ocean-revised global estimates, comparison with regional data and relationship to biogenic sedimentation. *Global Biogeochemical Cycles* **9**: 359–372.

Neubauer C, Schreiber U. **1989**. Photochemical and non-photochemical quenching of chlorophyll fluorescence induced by hydrogen peroxide. *Zeitschrift fur Naturforschung - Section C Journal of Biosciences* **44**: 262–270.

Niethammer P, Grabher C, Look AT, Mitchison TJ. **2009**. A tissue-scale gradient of hydrogen peroxide mediates rapid wound detection in zebrafish. *Nature* **459**: 996–999.

Nietzel T, Elsässer M, Ruberti C, Steinbeck J, Ugalde JM, Fuchs P, Wagner S, Ostermann L, Moseler A, Lemke P, *et al.* 2019. The fluorescent protein sensor roGFP2-Orp1 monitors in vivo H_2O_2 and thiol redox integration and elucidates intracellular H_2O_2 dynamics during elicitor-induced oxidative burst in *Arabidopsis*. *New Phytologist* **221**: 1649–1664.

Nimer NA, Ling MX, Brownlee C, Merrett MJ. **1999**. Inorganic carbon limitation, exofacial carbonic anhydrase activity and plasma membrane redox activity in marine phytoplankton species. *Journal of Phycology* **35**: 1200–1205.

Nimer NA, Warren M, Merrett MJ. **1998**. The regulation of photosynthetic rate and activation of extracellular carbonic anhydrase under CO2-limiting conditions in the marine diatom *Skeletonema costatum*. *Plant, Cell & Environment* **21**: 805–812.

Niyogi KK. **2000**. Safety valves for photosynthesis. *Current Opinion in Plant Biology* **3**: 455–460.

Noctor G, Foyer CH. **1998**. Ascorbate and glutathione: Keeping active oxygen under control. *Annual Review of Plant Physiology and Plant Molecular Biology* **49**: 249–279.

Noguchi K, Yoshida K. **2008**. Interaction between photosynthesis and respiration in illuminated leaves. *Mitochondrion* **8**: 87–99.

Nymark M, Valle KC, Brembu T, Hancke K, Winge P, Andresen K, Johnsen G, Bones AM. **2009**. An integrated analysis of molecular acclimation to high light in the marine diatom Phaeodactylum tricornutum. *PLoS ONE* **4**: e7743.

Oda T, Ishimatsu A, Shimada M, Takeshita S, Muramatsu T. **1992**. Oxygen-radical-mediated toxic effects of the red tide flagellate *Chattonella marina* on *Vibrio alginolyticus*. *Marine Biology* **112**: 505–509.

Oda T, Ishimatsu A, Takeshita S, Muramatsu T. **1994**. Hydrogen peroxide production by the red tide flagellate *Chatonella marina*. *Bioscience Biotechnology and Biochemistry* **58**: 957–958.

Oda T, Moritomi J, Kawano I, Hamaguchi S, Ishimatsu A, Muramatsu T. **1995**. Catalase- and superoxide dismutase-induced morphological changes and growth inhibition in the red tide phytoplankton *Chattonella marina*. *Bioscience, Biotechnology, and Biochemistry* **59**: 2044–2048.

Oda T, Nakamura A, Okamoto T, Ishimatsu A, Muramatsu T. **1998**. Lectin-induced enhancement of superoxide anion production by red tide phytoplankton. *Marine Biology* **131**: 383–390.

de Oliveira LS, Tschoeke DA, Magalhães Lopes ACR, Sudatti DB, Meirelles PM, Thompson CC, Pereira RC, Thompson FL. **2017**. Molecular mechanisms for microbe recognition and defense by the red seaweed Laurencia dendroidea. *mSphere* **2**: e00094-17.

Osada K, Maeda Y, Yoshino T, Nojima D, Bowler C, Tanaka T. **2017**. Enhanced NADPH production in the pentose phosphate pathway accelerates lipid accumulation in the oleaginous diatom *Fistulifera solaris*. *Algal Research* **23**: 126–134.

Osuna-cruz CM, Bilcke G, Vancaester E, Decker S De, Poulsen N. **2020**. The *Seminavis robusta* genome provides insights into the evolutionary adaptations of benthic diatoms. *bioRxiv*: 1–29.

Ovide C, Kiefer-Meyer M-C, Bérard C, Vergne N, Lecroq T, Plasson C, Burel C, Bernard S, Driouich A, Lerouge P, *et al.* 2018. Comparative in depth RNA sequencing of *P. tricornutum*'s morphotypes reveals specific features of the oval morphotype. *Scientific Reports* **8**: 14340.

Ozgur R, Uzilday B, Sekmen AH, Turkan I. **2015**. The effects of induced production of reactive oxygen species in organelles on endoplasmic reticulum stress and on the unfolded protein response in arabidopsis. *Annals of Botany* **116**: 541–553.

Paffenholz R, Bergstrom RA, Pasutto F, Wabnitz P, Munroe RJ, Jagla W, Heinzmann U, Marquardt A, Bareiss A, Laufs J, *et al.* 2004. Vestibular defects in head-tilt mice result from mutations in Nox3, encoding an NADPH oxidase. *Genes & Development* **18**: 486–491.

Palenik B, Morel FMM. **1988**. Dark production of H_2O_2 in the Sargasso Sea. *Limnology and Oceanography* **33**: 1606–1611.

Palenik B, Zafiriou OC, Morel FMM. **1987**. Hydrogen peroxide production by a marine phytoplankter1. *Limnology and Oceanography* **32**: 1365–1369.

Panday A, Sahoo MK, Osorio D, Batra S. **2015**. NADPH oxidases: An overview from structure to innate immunity-associated pathologies. *Cellular and Molecular Immunology* **12**: 5–23.

Pengtao W, Chun-Peng S. **2008**. Guard-cell signalling for hydrogen peroxide and abscisic acid. *New Phytologist* **178**: 703–718.

Percy MJ, Lappin TR. **2008**. Recessive congenital methaemoglobinaemia: cytochrome b5 reductase deficiency. *British Journal of Haematology* **141**: 298–308.

Pérez-Pérez ME, Couso I, Crespo JL. **2012**. Carotenoid deficiency triggers autophagy in the model green alga *Chlamydomonas reinhardtii*. *Autophagy* **8**: 376–388.

Peskin A V, Labas YA, Tikhonov AN. **1998**. Superoxide radical production by sponges *Sycon* sp. *FEBS Letters* **434**: 201–204.

Petrov V, Hille J, Mueller-Roeber B, Gechev TS. **2015**. ROS-mediated abiotic stress-induced programmed cell death in plants. *Frontiers in Plant Science* **6**.

Pfannschmidt T. **2003**. Chloroplast redox signals: how photosynthesis controls its own genes. *Trends in Plant Science* **8**: 33–41.

Plummer S, Taylor AE, Harvey EL, Hansel CM, Diaz JM. **2019**. Dynamic regulation of extracellular superoxide production by the coccolithophore *Emiliania huxleyi* (CCMP 374). *Frontiers in Microbiology* **10**: 1546.

Poole LB. **2015**. The basics of thiols and cysteines in redox biology and chemistry. *Free Radical Biology and Medicine* **80**: 148–157.

Pospíšil P, Arató A, Krieger-Liszkay A, Rutherford AW. **2004**. Hydroxyl radical generation by photosystem II. *Biochemistry* **43**: 6783–6792.

Potocky M, Jones MA, Bezvoda R, Smirnoff N, Zarsky V. **2007**. Reactive oxygen species produced by NADPH oxidase are involved in pollen tube growth. *New Phytologist* **174**: 742–751.

Quéguiner B. **2013**. Iron fertilization and the structure of planktonic communities in high nutrient regions of the Southern Ocean. *Deep-Sea Research Part II: Topical Studies in Oceanography* **90**: 43–54.

Raven JA, Beardall J. **2020**. Energizing the plasmalemma of marine photosynthetic organisms: The role of primary active transport. *Journal of the Marine Biological Association of the United Kingdom* **100**: 333–346.

Ren W, Ai HW. **2013**. Genetically encoded fluorescent redox probes. *Sensors* **13**: 15422–15433.

Riganti C, Costamagna C, Bosia A, Ghigo D. **2006**. The NADPH oxidase inhibitor apocynin (acetovanillone) induces oxidative stress. *Toxicology and Applied Pharmacology* **212**: 179–187.

Riganti C, Gazzano E, Polimeni M, Costamagna C, Bosia A, Ghigo D. **2004**. Diphenyleneiodonium inhibits the cell redox metabolism and induces oxidative stress. *Journal of Biological Chemistry* **279**: 47726–47731.

Rijstenbil JW. **2003**. Effects of UVB radiation and salt stress on growth, pigments and antioxidative defence of the marine diatom *Cylindrotheca closterium*. *Marine Ecology Progress Series* **254**: 37–47.

Rijstenbil JW. **2005**. UV- and salinity-induced oxidative effects in the marine diatom *Cylindrotheca closterium* during simulated emersion. *Marine Biology* **147**: 1063–1073.

Rijstenbil JW, Derksen JWM, Gerringa LJA, Poortvliet TCW, Sandee A, Vandenberg M, Vandrie J, Wijnholds JA. **1994**. Oxidative stress-induced by copper - Defense and damage in the marine planktonic diatom *Ditylum brightwellii*, grown in continuous cultures with high and low zinc levels. *Marine Biology* **119**: 583–590.

Rinnerthaler M, Buttner S, Laun P, Heeren G, Felder TK, Klinger H, Weinberger M, Stolze K, Grousl T, Hasek J, *et al.* 2012. Yno1p/Aim14p, a NADPH-oxidase ortholog, controls extramitochondrial reactive oxygen species generation, apoptosis, and actin cable formation in yeast. *Proceedings of the National Academy of Sciences of the United States of America* **109**: 8658–8663.

Roach T, Miller R, Aigner S, Kranner I. **2015**. Diurnal changes in the xanthophyll cycle pigments of freshwater algae correlate with the environmental hydrogen peroxide concentration rather than non-photochemical quenching. *Annals of Botany* **116**: 519–527.

Roe KL, Barbeau KA. **2014**. Uptake mechanisms for inorganic iron and ferric citrate in Trichodesmium erythraeum IMS101. *Metallomics* **6**: 2042–2051.

Roháček K, Bertrand M, Moreau B, Jacquette B, Caplat C, Morant-Manceau A, Schoefs B. **2014**. Relaxation of the non-photochemical chlorophyll fluorescence quenching in diatoms: Kinetics, components and mechanisms. *Philosophical Transactions of the Royal Society B: Biological Sciences* **369**: 20130241.

Romann J, Valmalette JC, Chauton MS, Tranell G, Einarsrud MA, Vadstein O. **2015**. Wavelength and orientation dependent capture of light by diatom frustule nanostructures. *Scientific Reports* **5**: 17403.

Roncarati F, Rijstenbil JW, Pistocchi R. **2005**. UVB, Salts and metals-induced oxidative stress in the

diatom *Cylindrotheca closterium*: Damages and antioxidative defences. *Phycologia* **44**: 87.

Roncarati F, Rijstenbil JW, Pistocchi R. **2008**. Photosynthetic performance, oxidative damage and antioxidants in *Cylindrotheca closterium* in response to high irradiance, UVB radiation and salinity. *Marine Biology* **153**: 965–973.

Roos D. **2019**. Chronic granulomatous disease. In: Methods in Molecular Biology. Humana Press Inc., 531–542.

Rose A. **2012**. The influence of extracellular superoxide on iron redox chemistry and bioavailability to aquatic microorganisms. *Frontiers in Microbiology* **3**.

Rose AL, Godrant A, Godrant A, Furnas M, Waite TD. **2010**. Dynamics of nonphotochemical superoxide production in the Great Barrier Reef lagoon. *Limnology and Oceanography* **55**: 1521–1536.

Rose AL, Salmon TP, Lukondeh T, Neilan BA, Waite TD. **2005**. Use of superoxide as an electron shuttle for iron acquisition by the marine cyanobacterium *Lyngbya majuscula*. *Environmental Science & Technology* **39**: 3708–3715.

Rose AL, Webb EA, Waite TD, Moffett JW. **2008**. Measurement and implications of nonphotochemically generated superoxide in the equatorial Pacific Ocean. *Environmental Science & Technology* **42**: 2387–2393.

Rosenwasser S, van Creveld SG, Schatz D, Malitsky S, Tzfadia O, Aharoni A, Levin Y, Gabashvili A, Feldmesser E, Vardi A. **2014**. Mapping the diatom redox-sensitive proteome provides insight into response to nitrogen stress in the marine environment. *Proceedings of the National Academy of Sciences of the United States of America* **111**: 2740–2745.

Ross C, Kupper FC, Jacobs RS. **2006**. Involvement of reactive oxygen species and reactive nitrogen species in the wound response of *Dasycladus vermicularis*. *Chemistry & Biology* **13**: 353–364.

Ross C, Küpper FC, Vreeland V, Herbert Waite J, Jacobs RS. **2005**. Evidence of a latent oxidative burst in relation to wound repair in the giant unicellular chlorophyte *Dasycladus vermicularis*. *Journal of Phycology* **41**: 531–541.

Rossi DCP, Gleason JE, Sanchez H, Schatzman SS, Culbertson EM, Johnson CJ, McNees CA, Coelho C, Nett JE, Andes DR, *et al.* 2017. *Candida albicans* FRE8 encodes a member of the NADPH oxidase family that produces a burst of ROS during fungal morphogenesis. *Plos Pathogens* **13**.

Round FE, Crawford RM, Mann DG. **1990**. *The diatoms- Biology and morphology of the genera*. New York: Cambridge University Press.

Ruban A, Lavaud J, Rousseau B, Guglielmi G, Horton P, Etienne A-L. **2004**. The super-excess energy dissipation in diatom algae: comparative analysis with higher plants. *Photosynthesis Research* **82**.

Rusak SA, Peake BM, Richard LE, Nodder SD, Cooper WJ. **2011**. Distributions of hydrogen peroxide and superoxide in seawater east of New Zealand. *Marine Chemistry* **127**: 155–169.

Sagi M, Davydov O, Orazova S, Yesbergenova Z, Ophir R, Stratmann JW, Fluhr R. **2004**. Plant respiratory burst oxidase homologs impinge on wound responsiveness and development in *Lycopersicon esculentum*. *Plant Cell* **16**: 616–628.

Saikia S, Oliveira D, Hu G, Kronstad J. **2014**. Role of ferric reductases in iron acquisition and

virulence in the fungal pathogen *Cryptococcus neoformans* (GS Deepe, Ed.). *Infection and Immunity* **82**: 839–850.

Samhan-Arias AK, Gutierrez-Merino C. **2014**. Purified NADH-cytochrome b5 reductase is a novel superoxide anion source inhibited by apocynin: sensitivity to nitric oxide and peroxynitrite. *Free Radical Biology and Medicine* **73**: 174–189.

Sapriel G, Quinet M, Heijde M, Jourdren L, Tanty V, Luo GZ, Le Crom S, Lopez PJ. **2009**. Genome-wide transcriptome analyses of silicon metabolism in *Phaeodactylum tricornutum* reveal the multilevel regulation of silicic acid transporters. *Plos One* **4**.

Saragosti E, Tchernov D, Katsir A, Shaked Y. **2010**. Extracellular production and degradation of superoxide in the coral *Stylophora pistillata* and cultured *Symbiodinium*. *Plos One* **5**: e12508–e12508.

Scarsini M, Marchand J, Manoylov KM, Schoefs B. **2019**. Photosynthesis in Diatoms. In: Diatoms: Fundamentals and Applications. Wiley, 191–211.

Schneider RJ, Roe KL, Hansel CM, Voelker BM. **2016**. Species-level variability in extracellular production rates of reactive oxygen species by diatoms. *Frontiers in Chemistry* **4**.

Schober AF, Río Bártulos C, Bischoff A, Lepetit B, Gruber A, Kroth PG. **2019**. Organelle studies and proteome analyses of mitochondria and plastids fractions from the diatom *Thalassiosira pseudonana*. *Plant and Cell Physiology* **60**: 1811–1828.

Schrader M, Fahimi HD. **2006**. Peroxisomes and oxidative stress. *Biochimica et Biophysica Acta - Molecular Cell Research* **1763**: 1755–1766.

Schröder K. **2013**. NADPH oxidases in redox regulation of cell adhesion and migration. *Antioxidants & Redox Signaling* **20**: 2043–2058.

Schwarzlander M, Dick TP, Meyer AJ, Morgan B. **2016**. Dissecting redox biology using fluorescent protein sensors. *Antioxidants & Redox Signaling* **24**: 680–712.

Scuffi D, Nietzel T, Di Fino LM, Meyer AJ, Lamattina L, Schwarzlander M, Laxalt AM, Garcia-Mata C. **2018**. Hydrogen sulfide increases production of NADPH oxidase-dependent hydrogen peroxide and phospholipase D-derived phosphatidic acid in guard cell signaling. *Plant Physiology* **176**: 2532–2542.

Segmuller N, Kokkelink L, Giesbert S, Odinius D, van Kan J, Tudzynski P. **2008**. NADPH oxidases are involved in differentiation and pathogenicity in Botrytis cinerea. *Molecular Plant-Microbe Interactions* **21**: 808–819.

Serif M, Lepetit B, Weißert K, Kroth PG, Rio Bartulos C. **2017**. A fast and reliable strategy to generate TALEN-mediated gene knockouts in the diatom *Phaeodactylum tricornutum*. *Algal Research* **23**: 186–195.

Shaked Y, Harris R, Klein-Kedem N. **2010**. Hydrogen peroxide photocycling in the Gulf of Aqaba, Red Sea. *Environmental Science and Technology* **44**: 3238–3244.

Shikata T, Takahashi F, Nishide H, Shigenobu S, Kamei Y, Sakamoto S, Yuasa K, Nishiyama Y, Yamasaki Y, Uchiyama I. **2019**. RNA-seq analysis eveals genes related to photoreception, nutrient uptake, and toxicity in a noxious red-tide raphidophyte *Chattonella antiqua*. *Frontiers in Microbiology* **10**.

Shin MH, Moon YJ, Seo JE, Lee Y, Kim KH, Chung JH. **2008**. Reactive oxygen species produced by NADPH oxidase, xanthine oxidase, and mitochondrial electron transport system mediate heat shock-induced MMP-1 and MMP-9 expression. *Free Radical Biology and Medicine* **44**: 635–645.

Shono M, Wada M, Hara Y, Fujii T. **2001**. Molecular cloning of Na^+-ATPase cDNA from a marine alga, *Heterosigma akashiwo*. *Biochimica et Biophysica Acta - Biomembranes* **1511**: 193–199.

Siegmund U, Heller J, van Kann JAL, Tudzynski P. **2013**. The NADPH oxidase complexes in *Botrytis cinerea*: Evidence for a close association with the ER and the tetraspanin Pls1. *PLoS ONE* **8**: e55879.

Sims PA, Mann DG, Medlin LK. **2006**. Evolution of the diatoms: Insights from fossil, biological and molecular data. *Phycologia* **45**: 361–402.

Sirisha VL, Sinha M, D'Souza JS. **2014**. Menadione-induced caspase-dependent programmed cell death in the green chlorophyte *Chlamydomonas reinhardtii. Journal of Phycology* **50**: 587–601.

Sirokmany G, Donko A, Geiszt M. **2016**. Nox/Duox Family of NADPH Oxidases: Lessons from knockout mouse models. *Trends in Pharmacological Sciences* **37**: 318–327.

Smayda TJ, Trainer VL. **2010**. Dinoflagellate blooms in upwelling systems: Seeding, variability, and contrasts with diatom bloom behaviour. *Progress in Oceanography* **85**: 92–107.

Smirnoff N, Arnaud D. **2019**. Hydrogen peroxide metabolism and functions in plants. *New Phytologist* **221**: 1197–1214.

Sommer U, Lengfellner K. **2008**. Climate change and the timing, magnitude, and composition of the phytoplankton spring bloom. *Global Change Biology* **14**: 1199–1208.

Song YG, Liu B, Wang LF, Li MH, Liu Y. **2006**. Damage to the oxygen-evolving complex by superoxide anion, hydrogen peroxide, and hydroxyl radical in photoinhibition of photosystem II. *Photosynthesis Research* **90**: 67–78.

Strzepek RF, Harrison PJ. **2004**. Photosynthetic architecture differs in coastal and oceanic diatoms. *Nature* **431**: 689–692.

Suggett DJ, Warner ME, Smith DJ, Davey P, Hennige S, Baker NR. **2008**. Photosynthesis and production of hydrogen peroxide by *Symbiodinium* (Pyrrhophyta) phylotypes with different thermal tolerances. *Journal of Phycology* **44**: 948–956.

Sullivan CW, Volcani BE. **1974**. Synergistically stimulated (Na^+,K^+) adenosine triphosphate from plasma membrane of a marine diatom. *Proceedings of the National Academy of Sciences of the United States of America* **71**: 4376–4380.

Sumimoto H. **2008**. Structure, regulation and evolution of Nox-family NADPH oxidases that produce reactive oxygen species. *Febs Journal* **275**: 3249–3277.

Sutherland KM, Coe A, Gast RJ, Plummer S, Suffridge CP, Diaz JM, Bowman JS, Wankel SD, Hansel CM. **2019**. Extracellular superoxide production by key microbes in the global ocean. *Limnology and Oceanography* **64**: 2679-2693

Sutherland KM, Wankel SD, Hansel CM. **2020**. Dark biological superoxide production as a significant flux and sink of marine dissolved oxygen. *Proceedings of the National Academy of*

Sciences **117**: 3433–3439.

Sutton HC, Winterbourn CC. **1989**. On the participation of higher oxidation states of iron and copper in fenton reactions. *Free Radical Biology and Medicine* **6**: 53–60.

Suzuki N, Miller G, Salazar C, Mondal HA, Shulaev E, Cortes DF, Shuman JL, Luo XZ, Shah J, Schlauch K, *et al.* 2013. Temporal-spatial interaction between reactive oxygen species and abscisic acid regulates rapid systemic acclimation in plants. *Plant Cell* **25**: 3553–3569.

Takahashi S, Murata N. **2008**. How do environmental stresses accelerate photoinhibition? *Trends in Plant Science* **13**: 178–182.

Takemoto D, Kamakura S, Saikia S, Becker Y, Wrenn R, Tanaka A, Sumimoto H, Scott B. **2011**. Polarity proteins Bem1 and Cdc24 are components of the filamentous fungal NADPH oxidase complex. *Proceedings of the National Academy of Sciences of the United States of America* **108**: 2861–2866.

Takemoto D, Tanaka A, Scott B. **2007**. NADPH oxidases in fungi: Diverse roles of reactive oxygen species in fungal cellular differentiation. *Fungal Genetics and Biology* **44**: 1065–1076.

Tanaka A, Christensen MJ, Takemoto D, Park P, Scott B. **2006**. Reactive oxygen species play a role in regulating a fungus-perennial ryegrass mutualistic interaction. *Plant Cell* **18**: 1052–1066.

Tao R, Zhao Y, Chu H, Wang A, Zhu J, Chen X, Zou Y, Shi M, Liu R, Su N, *et al.* 2017. Genetically encoded fluorescent sensors reveal dynamic regulation of NADPH metabolism. *Nature Methods* **14**: 720.

Taylor AR. **2009**. A fast Na^+/Ca^{2+}-based action potential in a marine diatom. *Plos One* **4**: e4966.

Taylor AR, Brownlee C, Wheeler GL. **2012**. Proton channels in algae: reasons to be excited. *Trends in Plant Science* **17**: 675–684.

Taylor AR, Chrachri A, Wheeler G, Goddard H, Brownlee C. **2011**. A voltage-gated H^+ channel underlying pH homeostasis in calcifying coccolithophores (PG Falkowski, Ed.). *PLoS Biology* **9**: e1001085.

Tewari RK, Watanabe D, Watanabe M. **2012**. Chloroplastic NADPH oxidase-like activity-mediated perpetual hydrogen peroxide generation in the chloroplast induces apoptotic-like death of Brassica napus leaf protoplasts. *Planta* **235**: 99–110.

Thamatrakoln K, Korenovska O, Niheu AK, Bidle KD. **2012**. Whole-genome expression analysis reveals a role for death-related genes in stress acclimation of the diatom *Thalassiosira pseudonana*. *Environmental Microbiology* **14**: 67–81.

Tirichine L, Rastogi A, Bowler C. **2017**. Recent progress in diatom genomics and epigenomics. *Current Opinion in Plant Biology* **36**: 46–55.

van Tol HM, Amin SA, Armbrust E V. **2017**. Ubiquitous marine bacterium inhibits diatom cell division. *Isme Journal* **11**: 31–42.

Tommaso P, Moretti S, Xenarios I, Orobitg M, Montanyola A, Chang JM, Taly JF, Notredame C. **2011**. T-Coffee: a web server for the multiple sequence alignment of protein and RNA sequences using structural information and homology extension. *Nucleic Acids Research* **39**: W13–W17.

Torres MA, Dangl JL, Jones JDG. **2002**. *Arabidopsis* gp91(phox) homologues AtrbohD and AtrbohF

are required for accumulation of reactive oxygen intermediates in the plant defense response. *Proceedings of the National Academy of Sciences of the United States of America* **99**: 517–522.

Tréguer P, Nelson DM, Van Bennekom AJ, Demaster DJ, Leynaert A, Quéguiner B. **1995**. The silica balance in the world ocean: A reestimate. *Science* **268**: 375–379.

Tsuda A, Takeda S, Saito H, Nishioka J, Nojiri Y, Kudo I, Kiyosawa H, Shiomoto A, Imai K, Ono T, *et al.* 2003. A mesoscale iron enrichment in the western Subarctic Pacific induces a large centric diatom bloom. *Science* **300**: 958–961.

Uji T, Endo H, Mizuta H. **2020**. Sexual reproduction via a 1-aminocyclopropane-1-carboxylic acid-dependent pathway through redox modulation in the marine red alga *Pyropia yezoensis* (Rhodophyta). *Frontiers in Plant Science* **11**.

Vacca RA, de Pinto MC, Valenti D, Passarella S, Marra E, De Gara L. **2004**. Production of reactive oxygen species, alteration of cytosolic ascorbate peroxidase, and impairment of mitochondrial metabolism are early events in heat shock-induced programmed cell death in tobacco bright-yellow 2 cells. *Plant Physiology* **134**: 1100–1112.

Vanelslander B, Paul C, Grueneberg J, Prince EK, Gillard J, Sabbe K, Pohnert G, Vyverman W. **2012**. Daily bursts of biogenic cyanogen bromide (BrCN) control biofilm formation around a marine benthic diatom. *Proceedings of the National Academy of Sciences* **109**: 2412–2417.

Vardi A, Berman-Frank I, Rozenberg T, Hadas O, Kaplan A, Levine A. **1999**. Programmed cell death of the dinoflagellate *Peridinium gatunense* is mediated by CO_2 limitation and oxidative stress. *Current Biology* **9**: 1061–1064.

Vardi A, Bidie KD, Kwityn C, Hirsh DJ, Thompson SM, Callow JA, Falkowski P, Bowler C. **2008**. A diatom gene regulating nitric-oxide signaling and susceptibility to diatom-derived aldehydes. *Current Biology* **18**: 895–899.

Vardi A, Formiggini F, Casotti R, De Martino A, Ribalet F, Miralto A, Bowler C. **2006**. A stress surveillance system based on calcium and nitric oxide in marine diatoms. *Plos Biology* **4**: 411–419.

Vaughan NE, Lenton TM. **2011**. A review of climate geoengineering proposals. *Climatic Change* **109**: 745–790.

Verret F, Wheeler G, Taylor AR, Farnham G, Brownlee C. **2010**. Calcium channels in photosynthetic eukaryotes: implications for evolution of calcium-based signalling. *New Phytologist* **187**: 23–43.

Volpert A, Graff van Creveld S, Rosenwasser S, Vardi A. **2018**. Diurnal fluctuations in chloroplast GSH redox state regulate susceptibility to oxidative stress and cell fate in a bloom-forming diatom. *Journal of Phycology* **54**: 329–341.

Wang F, Chen Z-H, Liu X, Colmer TD, Shabala L, Salih A, Zhou M, Shabala S. **2016**. Revealing the roles of GORK channels and NADPH oxidase in acclimation to hypoxia in *Arabidopsis*. *Journal of Experimental Botany* **68**: 3191–3204.

Wang G-F, Li W-Q, Li W-Y, Wu G-L, Zhou C-Y, Chen K-M. **2013**. Characterization of rice NADPH oxidase genes and their expression under various environmental conditions. *International Journal of Molecular Sciences* **14**: 9440–9458.

Wang F, Lv Y, Lin L, Xu N, Lu K, Sun X. **2018**. Characterization of a respiratory burst oxidase homolog from *Gracilariopsis lemaneiformis* (Rhodophyta) during stress and phytohormone

treatments. *Botanica Marina* **61**: 511–519.

Waring J, Klenell M, Bechtold U, Underwood GJC, Baker NR. **2010**. Light-induced responses of oxygen photoreduction, reactive oxygen species production and scavenging in two diatom species. *Journal of Phycology* **46**: 1206–1217.

Waters BM, Blevins DG, Eide DJ. **2002**. Characterization of FRO1, a pea ferric-chelate reductase involved in root iron acquisition. *Plant Physiology* **129**: 85–94.

Weger HG, Espie GS. **2000**. Ferric reduction by iron-limited *Chlamydomonas* cells interacts with both photosynthesis and respiration. *Planta* **210**: 775–781.

Weinberger F, Friedlander M, Hoppe HG. **1999**. Oligoagars elicit a physiological response in *Gracilaria conferta* (Rhodophyta). *Journal of Phycology* **35**: 747–755.

Wirtz NL, Treble RG, Weger HG. **2010**. Siderophore-independent iron uptake by iron-limited cells of the cyanobacterium *Anabaena flos-aquae*. *Journal of Phycology* **46**: 947–957.

Wong JL, Créton R, Wessel GM. **2004**. The oxidative burst at fertilization is dependent upon activation of the dual oxidase Udx1. *Developmental Cell* **7**: 801–814.

Wu F, Chi Y, Jiang Z, Xu Y, Xie L, Huang F, Wan D, Ni J, Yuan F, Wu X, *et al.* 2020. Hydrogen peroxide sensor HPCA1 is an LRR receptor kinase in *Arabidopsis*. *Nature* **578**: 577–581.

Xenopoulos MA, Bird DF. **1997**. Effect of acute exposure to hydrogen peroxide on the production of phytoplankton and bacterioplankton in a mesohumic lake. *Photochemistry and Photobiology* **66**: 471–478.

Xie YJ, Xu S, Han B, Wu MZ, Yuan XX, Han Y, Gu QA, Xu DK, Yang Q, Shen WB. **2011**. Evidence of Arabidopsis salt acclimation induced by up-regulation of HY1 and the regulatory role of RbohD-derived reactive oxygen species synthesis. *Plant Journal* **66**: 280–292.

Xue X, Collins CM, Weger HG. **1998**. The energetics of extracellular Fe(III) reduction by iron-limited *Chlamydomonas reinhardtii* (Chlorophyta). *Journal of Phycology* **34**: 939–944.

Yamasaki Y, Kim DI, Matsuyama Y, Oda T, Honjo T. **2004**. Production of superoxide anion and hydrogen peroxide by the red tide dinoflagellate *Karenia mikimotoi*. *Journal of Bioscience and Bioengineering* **97**: 212–215.

Yee DP, Hildebrand M, Tresguerres M. **2020**. Dynamic subcellular translocation of V-type H^+-ATPase is essential for biomineralization of the diatom silica cell wall. *New Phytologist* **225**: 2411–2422.

Yoshida K, Seger A, Kennedy F, McMinn A, Suzuki K. **2020**. Freezing, melting, and light stress on the photophysiology of ice algae: Ex situ incubation of the ice algal diatom *Fragilariopsis cylindrus* (Bacillariophyceae) using an ice tank. *Journal of Phycology* **56**: 1323–1338.

Yoshida K, Terashima I, Noguchi K. **2007**. Up-regulation of mitochondrial alternative oxidase concomitant with chloroplast over-reduction by excess light. *Plant and Cell Physiology* **48**: 606–614.

Young JN, Heureux AMC, Sharwood RE, Rickaby REM, Morel FMM, Whitney SM. **2016**. Large variation in the Rubisco kinetics of diatoms reveals diversity among their carbon-concentrating mechanisms. *Journal of Experimental Botany* **67**: 3445–3456.

Zaslavskaia LA, Lippmeier JC, Kroth PG, Grossman AR, Apt KE. **2000**. Transformation of the diatom *Phaeodactylum tricornutum* (Bacillariophyceae) with a variety of selectable marker and reporter genes. *Journal of Phycology* **36**: 379–386.

Zhang X, Krause K-H, Xenarios I, Soldati T, Boeckmann B. **2013**. Evolution of the ferric reductase domain (FRD) superfamily: modularity, functional diversification, and signature motifs. *Plos One* **8**: e58126.

Zhang Y, Li Y, He Y, Hu W, Zhang Y, Wang X, Tang H. **2018**. Identification of NADPH oxidase family members associated with cold stress in strawberry. *FEBS open bio* **8**: 593–605.

Zinser ER. **2018**. The microbial contribution to reactive oxygen species dynamics in marine ecosystems. *Environmental Microbiology Reports* **10**: 412–427.

Zuckerkandl E, Pauling L. **1965**. Evolutionary divergence and convergence in proteins. In: Bryson V, Vogel HJ, eds. Evolving Genes and Proteins. New York: Academic Press, 97–166.